MECHANICS OF ROLLING TUBE ON A MANDREL THROUGH TWO GROOVED ROLLS

by

Osama Mostafa Labib

Submitted in fulfilment of the requirements
of the degree of Doctor of Philosophy

The University of Aston in Birmingham
Department of Production Technology and Production Management

January 1982

Supervisor : Professor D.H.Sansome

THE UNIVERSITY OF ASTON IN BIRMINGHAM
DEPARTMENT OF PRODUCTION TECHNOLOGY & PRODUCTION MANAGEMENT

MECHANICS OF ROLLING TUBE ON A MANDREL THROUGH TWO GROOVED ROLLS

Submitted in fulfilment of the requirements
for the degree of Doctor of Philosophy

Author: OSAMA MOSTAFA LABIB Year: 1982

SUMMARY

This project is an investigation into the process of tube rolling on a mandrel through two grooved rolls. The research was carried out to assist operating companies in setting-up multi-stand mills to operate efficiently, especially when rolling thin walled tubes.

Lead, which was used as an analogue material for hot steel, was formed into tubes and rolled on a mandrel in an experimental single-stand mill. Rolling trials were performed to establish the way in which roll separating force, rolling torque and pressure distribution round the groove, vary for different rolling conditions, e.g. reduction of area, tube diameter to thickness ratio, friction conditions on the mandrel surface and front and back tensions. The pressure distribution round the groove perimeter and along the arc of contact was measured by means of pin-loadcells situated in the top roll.

Results taken from pin-loadcell readings during rolling showed that the pressures round the groove were not uniformly distributed. Also, by the use of pin-loadcells, the existence of a free deformation zone, wherein deformation takes place prior to the contact zone was established.

Rolling loads and torques were greatly affected by the change in tube thickness and friction conditions on the mandrel surface. While front and back tensions helped in reducing the rolling loads, increasing the mandrel speed reduced significantly the rolling torques.

A new theoretical approach based on the principle of least work done was proposed and comparisons were made with other existing equilibrium approaches and the experimental results.

A computer programme was developed for the assessment of the total work required in the process and for the calculation of tube and mandrel velocities in a production multi-stand mill. It is shown that there is good agreement between the theoretical predictions and the experimental results.

Key words: Tube rolling, Continuous rolling, Pin-loadcells, Energy method

CONTENTS

LIST OF PLATES

LIST OF TABLES

LIST OF FIGURES

Page

Page

List of Symbols

A_o Cross-sectional area of tube at the entry plane

A_1 Cross-sectional area of tube at the exit plane

a Tube cross-section minor axis after rolling

q Tube cross-section major axis after rolling

e Actual roll gap

e_i Initial roll gap

e_g Groove eccentricity

H Groove height

J Reduction of area

L_g Calculated length of the arc of contact

L_m Measured length of the arc of contact corrected only for the finite width of pin

$L_{m.c}$ Measured length of the arc of contact corrected for the finite width of the pin and also for torque sharing

m Friction factor

M Mill springback

P The roll separating force (RSF)

p_m Mean roll pressure

r_o Tube outside radius at the entry plane

r_1 Mean tube radius at the exit plane

r_b Radius of the mandrel

r_g Radius of the groove

R_r Radius of the roll at the root of the groove

R_s Radius of the roll at the shroud

R Radius of the roll at any point on the groove surface

S Contact area between tube and roll

t Tube wall thickness

t_o Wall thickness of the tube at the entry plane

t_1 Mean tube wall thickness at the exit plane

U Tube velocity in the direction of rolling

V Volume of tube in the deformation zone

v Tangential roll velocity

v_h Horizontal component of roll velocity

v_r Relative velocity between tube and roll

V_b Mandrel speed

$\dot{V}$ Volume rolled per unit time

W_h Work of homogeneous deformation per unit volume

W_r Redundant work per unit volume

W_f Work done against friction per unit volume

W_t Total work done by the rolls per unit volume

W_e Work done by the roll pressure

$W_{a,b}$ Work done by the applied front and back tensions per unit volume

W_T Total work done per unit volume

$\dot{W}$ Rate of doing work

X_3 Half the tube cross-section major axis

Greek Symbols:

ε_r Radial strain

ε_l Longitudinal strain

ε_θ Tangential or circumferential strain

ε_h Generalized homogeneous strain

$\varepsilon_{red.}$ Redundant strain

$\bar{\varepsilon}_m$ Total generalized strain

ε_f Frictional strain

μ Coefficient of friction

Φ_m Maximum angle of contact

Φ Angle of contact at any point on the line corresponding to the root of the groove

γ_c Peripheral angle of contact between tube and mandrel

ψ_c Peripheral angle of contact between tube and roll

γ_{c1} Peripheral angle of contact between tube and mandrel at the exit plane

ψ_{c1} Peripheral angle of contact between tube and roll at the exit plane

Θ Groove angle

θ_c Groove angle of contact

$\bar{\sigma}_y$ Mean yield stress

τ Shear stress

$\bar{\lambda}$ Mean strain rate

ω Angular velocity of the roll

Subscripts:

o Entry plane condition

1 Exit plane condition

N.B

Other symbols used in this text are defined as they appear.

CHAPTER (1)

INTRODUCTION

Chapter (1) Introduction

Seamless tubes are used in a wide range of applications, such as in the high pressure transportation of fluids and gasses in the oil and chemical industries, high pressure and superheater tubes in boilers and in many other arduous and structural situations. Although the introduction of welded tubes decreased partially the demand for seamless tubes, they still retain a considerable share of the market.

There are several different methods for the manufacture of seamless tubes, but they all have three common stages for converting the billet into a tube:

1. Piercing the hot billet to produce a hollow body or 'bloom'
2. Elongating the bloom to a 'hollow'
3. Reducing or stretch-reducing the hollow to the final tube size.

The first stage inevitably is accomplished hot since it involves heavy deformations, and the second stage also is a hot process. Usually small diameter seamless tubes are elongated by a cold working process such as cold-drawing. This is because all primary hot working processes involve the use of some form of mandrel inside the tube during its manufacture and this internal tool makes it extremely difficult to hot work tubes of small diameter. Again, the third stage is usually a hot working process but elongated tubes can be cold drawn and such a cold working process gives better tolerances in the finished tube sizes.

Several different hot working processes can be employed in the elongation of the bloom; generally, the complete process of tube manufacture takes its name from the primary

elongator, e.g. the pilger mill or the Assel mill or the continuous mill.

The continuous mill, which sometimes is called the mandrel mill, is one of the oldest methods employed in the manufacture of seamless tubes. But in spite of this fact, the potential of the process in the field of seamless tube manufacture was not recognized until the nineteen fifties. This was due to the very narrow range of tube diameters and wall thicknesses that could be obtained since for each tube size a new set of rolls or mandrels had to be used making the process prohibitively expensive for short runs. The incorporation of the stretch-reducing mill in the finishing line of a continuous mill increased the range of finished tube sizes that could be manufactured from a single hollow diameter and a few hollow wall thicknesses. Consequently, the continuous mill gained popularity, especially because of its high productivity compared with other known processes. For economic reasons, the continuous mill is unsuitable for the manufacture of large tube sizes. Also, the range of tube sizes that can be produced in such a mill is limited. A general arrangement of the complete continuous mill is shown in Figure (1.1). The mill mainly consists of a furnace for heating the billets to the required temperature, a two- or three-roll piercer for producing the bloom, a mandrel or continuous mill for elongating the bloom, a mandrel extractor, a re-heating furnace and finally a stretch-reducing mill.

The mandrel mill usually has between 7 and 9 stands of two or three rolls each. In a two-roll per stand mill, the axes of adjacent pairs of rolls are set at an angle of 90^{o}.

Figure (1.1)

General lay-out of a
complete continuous mill

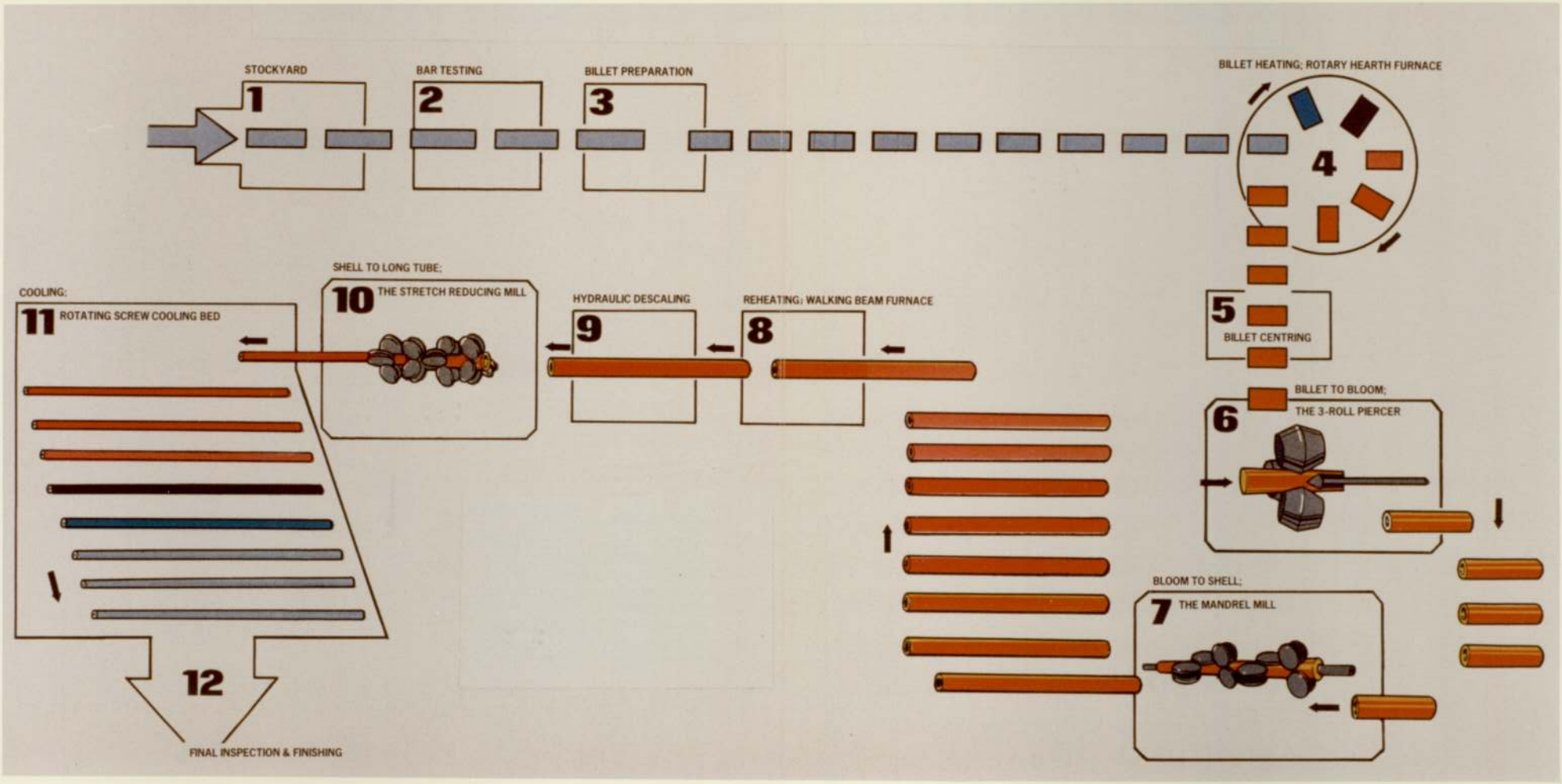
STOCKYARD
1
BAR TESTING
2
BILLET PREPARATION
3
BILLET HEATING; ROTARY HEARTH FURNACE
4
5
BILLET CENTRING
BILLET TO BLOOM;
THE 3-ROLL PIERCER
6
BLOOM TO SHELL;
7
THE MANDREL MILL
HYDRAULIC DESCALING
9
REHEATING; WALKING BEAM FURNACE
8
SHELL TO LONG TUBE;
10
THE STRETCH REDUCING MILL
COOLING;
11
ROTATING SCREW COOLING BED
12
FINAL INSPECTION & FINISHING

This arrangement of the rolls is adopted due to the shape of the roll groove in each stand, Figure (1.2), which produces an oval shaped tube. As the tube passes through a particular groove, it is reduced in the direction of the minor axis of the groove and will spread in the direction of the major axis. By a suitable choice of the reduction of area and since the groove shape is oval, the spread of the tube in the direction of the major axis of the groove will not reach the edge of the groove and hence no fins will be formed on the tube surface. If a simple semi-circular groove is used instead of an oval shape, the deformed material in the groove will flow into the gap between the two rolls causing the fin formation; hence the necessity for oval shaped grooves. To reduce the emerging tube from a particular stand in the direction of its major axis, the tube goes through the following pair of rolls with the tube major axis coinciding with the groove minor axis. This means that the axes of adjacent pairs of rolls are set at an angle of 90°. To obtain a round tube after the last stand, the ovality of the groove, which is defined as the distance between the centre of the circle forming the root of the groove and the pass centre, is reduced gradually until the last stand where the two centres coincide and the groove shape is circular. Due to the groove ovality in each stand, a clearance between the tube and mandrel is maintained at the groove sides. In the last stand this clearance is distributed over the whole circumference of the mandrel. This assists in stripping the mandrel from the tube. Since the mandrel is placed inside the tube, the tube wall thickness is reduced considerably during rolling. This is in contrast with the tube sinking

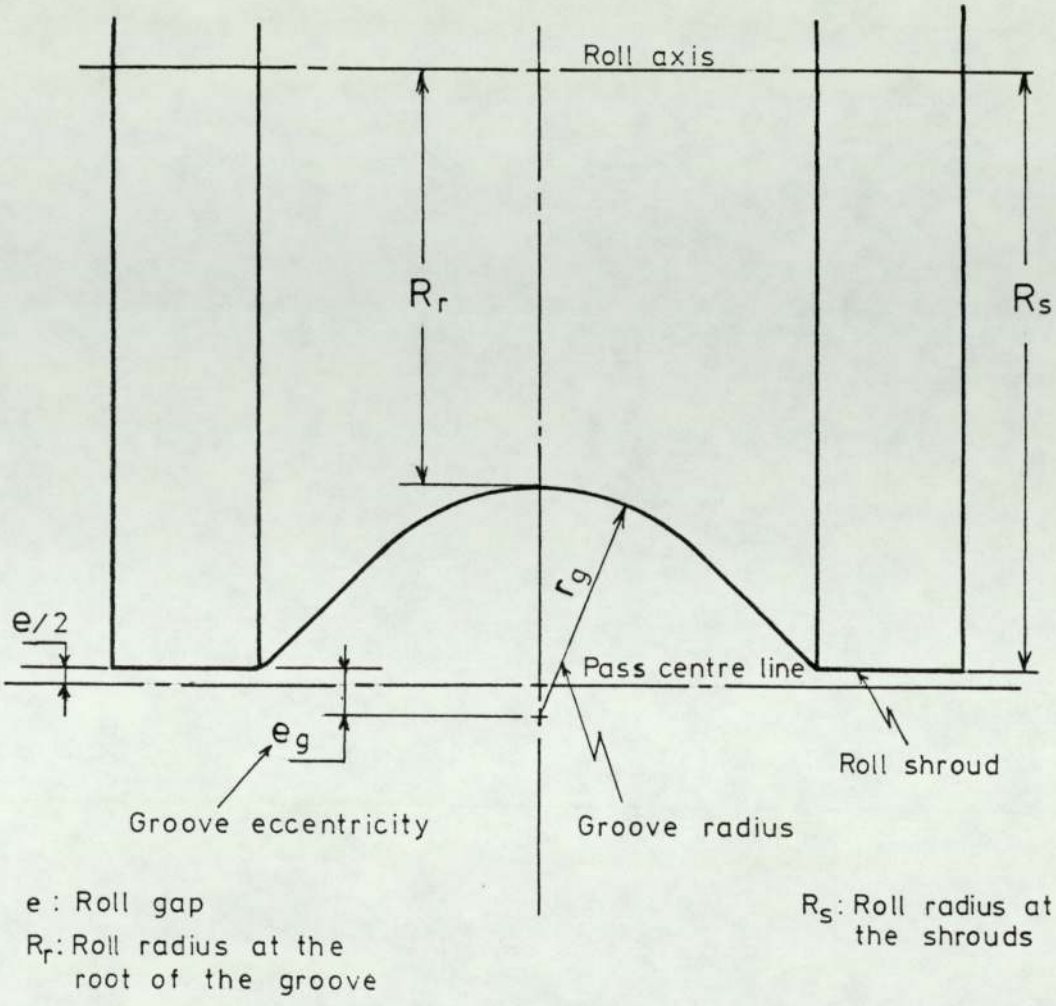

Fig.(1.2) General groove shape

process where the tube diameter, rather than the wall thickness, is reduced.

The mandrel rolling process constitutes an extremely important stage in the manufacture of seamless tubes. But, surprisingly, in spite of this fact, little attention has been given to the analysis of the process. The lack of attention is immediately apparent from the paucity of published work attributable to the rolling of tube on a mandrel by comparison, for example, with the amount of published work on flat rolling. As will be seen from the literature review chapter, few published papers could be found relating to the mandrel rolling process, and most of those are of a Russian origin.

In today's highly competitive market, the operating companies are always seeking new ways of improving the efficiency of existing continuous mills and extending the range of tube dimensions that can be obtained from such mills. Demand is also increasing for better quality tubes, and although the mandrel rolling process is an intermediate process in seamless tube manufacture, the quality of the finished tube is certainly affected by the quality of the tube from the mandrel mill. (Tube 'quality' may embody factors such as high tolerances, minimum eccentricity, minimum ovality and surface finish.) An increase in the efficiency of the mill and the manufacture of better quality tubes may best be achieved through a better understanding of the mechanics of the process. Hence the present research was carried out with a view to assisting operating companies to arrive at a better understanding of the factors affecting the process so that its efficiency could be increased.

The course of the experimental work involved rolling lead tubes on a mandrel through a two-roll single stand mill. The effect of such variables as the reduction of area, tube diameter to thickness ratio, groove shape and front and back tensions on the roll separating force, rolling torque and pressure distribution round the groove was examined. The pressure distribution round the perimeter of the groove and along the arc of contact was assessed by the use of pin-load-cells situated in the top roll of the experimental mill. Also, the use of pin-loadcells allowed an accurate measurement of the length of the arc of contact to be made. These measurements confirmed the existence of a free zone, i.e. the tube started to deform before contacting the rolls, and because of its importance this phenomenon was examined in some detail. The maximum rolling loads and torques are associated with the rolling of thin walled tubes. Therefore, in a production mill, the groove shapes and the amount of reduction assigned to each stand are determined with respect to the rolling of the thinnest wall. Thicker walled tubes can be rolled in the same groove shapes, but with smaller mandrel diameters. The majority of the rolling tests in the present investigation were devoted to the rolling of thin walled tubes.

The rolling of oval tubes through oval grooves was included in the rolling tests since this type of rolling is encountered in most stands of a production mill. The rolling of oval tubes has been neglected often in other investigations as it complicates the analysis.

Lead was used in the rolling tests as an analogue material for hot steel. Lead, which is hot worked at room

temperature, has the further advantage of being able to deform at lower stresses than hot steel and this enabled the mill loads to be low.

The course of the theoretical work on the mandrel rolling process is one of the most difficult metal forming processes to follow, and this may account for the small number of investigations which have been carried out on this process. Previous attempts to provide a theoretical treatment of the process resulted in the three theories which are presented in chapter (3) of this thesis. All three theories, two from the USSR and one from Japan, are based on equilibrium analyses. The equilibrium approach with its many assumptions and approximations has proved to be inadequate in providing reliable theoretical predictions. In an investigation by Cole (11) on tube rolling, he compared the theoretical predictions based on equlibrium approaches with his experimental results and found that the correlation was poor. Therefore, a new theoretical treatment of the process was attempted in this work. The theoretical analysis was based on an energy method which is now realising reliable results in many metal forming processes. To justify this assertion, comparisons were made between the theoretical predictions of the mean pressure and roll separating force , and the experimental results and other theoretical predictions. The theoretical analysis included also the estimation of the work done per unit volume in deforming the tube. The work done per unit volume, i.e. the specific work done,is of utmost importance since favourable rolling conditions can be selected on the basis of minimizing the specific work done. The complexity of deformation in the

mandrel rolling process and the analytical work involved in the energy method necessitated the use of a computer in the solution of the mathematical equations. All the computer programmes are given in the Appendix.

Finally, due to its importance, the tube and mandrel speed pattern in a multi-stand mill was examined theoretically and a computer programme was developed for the estimation of tube and mandrel speeds.

CHAPTER (2)

LITERATURE REVIEW

Chapter (2) Literature Review

It seems to be that the published work on tube rolling in general which originates from English language sources is very little. The situation is even worse when considering the mandrel rolling process in particular, and that was one of the reasons for carrying out the present investigation as further work in this field is still required.

Cole's work (11) was one of the few British references that could be found on the subject of tube rolling. Cole investigated experimentally the three types of tube rolling and he provided in his work an extensive review of the literature available at that time.

Haleem (12) continued Cole's work and although he investigated the processes of tube sinking and stretch-reducing, he reviewed some of the published work on tube rolling on a mandrel.

It is not intended here to review all the papers that have already been mentioned in Cole's and Haleem's work. Some of those papers which are of importance to the present work, were either briefly mentioned in their work or reviewed with different points of interest. Therefore it was felt necessary to include those papers among others in the present literature review.

Most of the published work on tube rolling on a mandrel is of a Russian origin, and of special interest to the present work is a paper by Matveev and Lavrov (1) (1964)

in which they investigated the effect of forward pressure and tension on the process. Lead, aluminium and steel tubes were rolled in oval and round grooves with straight outlets under various degrees of stretch, back tension and forward pressure. Test results showed that back tension substantially hampered groove filling, but at the same time roll pressure and roll force were reduced. Applying forward pressure increased roll force, reduced rolling torque and assisted in the complete filling of the groove. However, for values of forward pressure higher than $0.15\bar{\sigma}_y$, where $\bar{\sigma}_y$ is the yield stress of the material being rolled, the metal might encroach into the gap between the groove outlets.

One interesting feature of their work was the use of pin-loadcells to measure the pressure distribution in the groove. The pressure distribution curves were similar in shape to the curves obtained from the present investigation. The pressure was not uniformly distributed and the highest pressure occurred at the root of the groove. The actual length of the arc of contact obtained from pin-loadcell measurements was found to be higher than the theoretical one and the authors suggested that this was due to the elastic compression of the rolls. This explanation may not be completely correct especially in the case of a hot forming process such as mandrel rolling and it will be shown later from the current work that the increase in the length of the arc of contact can be attributed to the presence of a free zone, i.e. the tube may start to deform before contacting the rolls. No

theoretical treatment of the problem was given in their paper.

In a three-stand two-roll mill, Shevchenko and Chekmarev (2) in 1964 made a comprehensive experimental study of the variation of force and velocity parameters during rolling with different interstand tensions and compressions. Mild steel tubes were heated to a temperature of 1100°C and subsequently rolled on a mandrel in round grooves with straight outlets. Through the mismatch of roll speeds to tube speeds in the three stands, a state of tension or compression existed between the stands which affected roll forces and torques. While interstand tension helped in reducing rolling loads and torques, interstand compression increased roll force and reduced roll torque. The mandrel speed was shown to increase during entry to and exit from the mill.

Vatkin and Druyan (3) provided a detailed theoretical analysis of the mandrel tube rolling process based on an equilibrium approach. This is one of two Russian theories that will be examined in detail in the following chapter.

In their investigation, Vatkin and Druyan made some experimental tests using lead and steel tubes and were able to measure the pressure distribution in the groove by the use of three pin-loadcells situated at different angles in the circular groove. Their experimental work was intended to support the theoretical treatment of the problem.

The second Russian theory that will be dealt with in the next chapter is by Fomichev and Kirichenko (4). The theory again is based on an equilibrium approach and

Vatkin's (14) experimental results were used to check the theoretical work.

Neuhoff and Pfeiffer (5) of Germany provided an interesting study of the continuous tube rolling process in 1970. In a two-roll eight-stand mill, they measured the mandrel and tube speeds during the filling up, filled state, and emptying of the mill and the speed curves in figure(2.1) were obtained.

The mandrel moved at a constant speed only when the tube was situated in all stands. Otherwise, the mandrel accelerated on entry to and exit from the mill. The authors set down approximate equations for the calculation of mandrel and tube speeds at the various stands and indicated that at any stand the tube speed would take a mean value between the roll circumferential speed and the mandrel speed. Since the rolls rotated at a constant speed, any change in mandrel speed brought about a corresponding change in tube speed. The variation in tube dimensions over the front and rear ends of the tube, or what is known as the front and rear belly formation, was related to the change in mandrel speed on entry to and exit from the mill. However, in a later investigation, Pfeiffer (6) proved that only the origin of the rear belly formation was due to the change in mandrel speed. Neuhoff and Pfeiffer (5) suggested the following three measures to overcome the problem of belly formation:

1. a smaller coefficient of friction between mandrel and tube,
2. higher deformation in the first stands, and

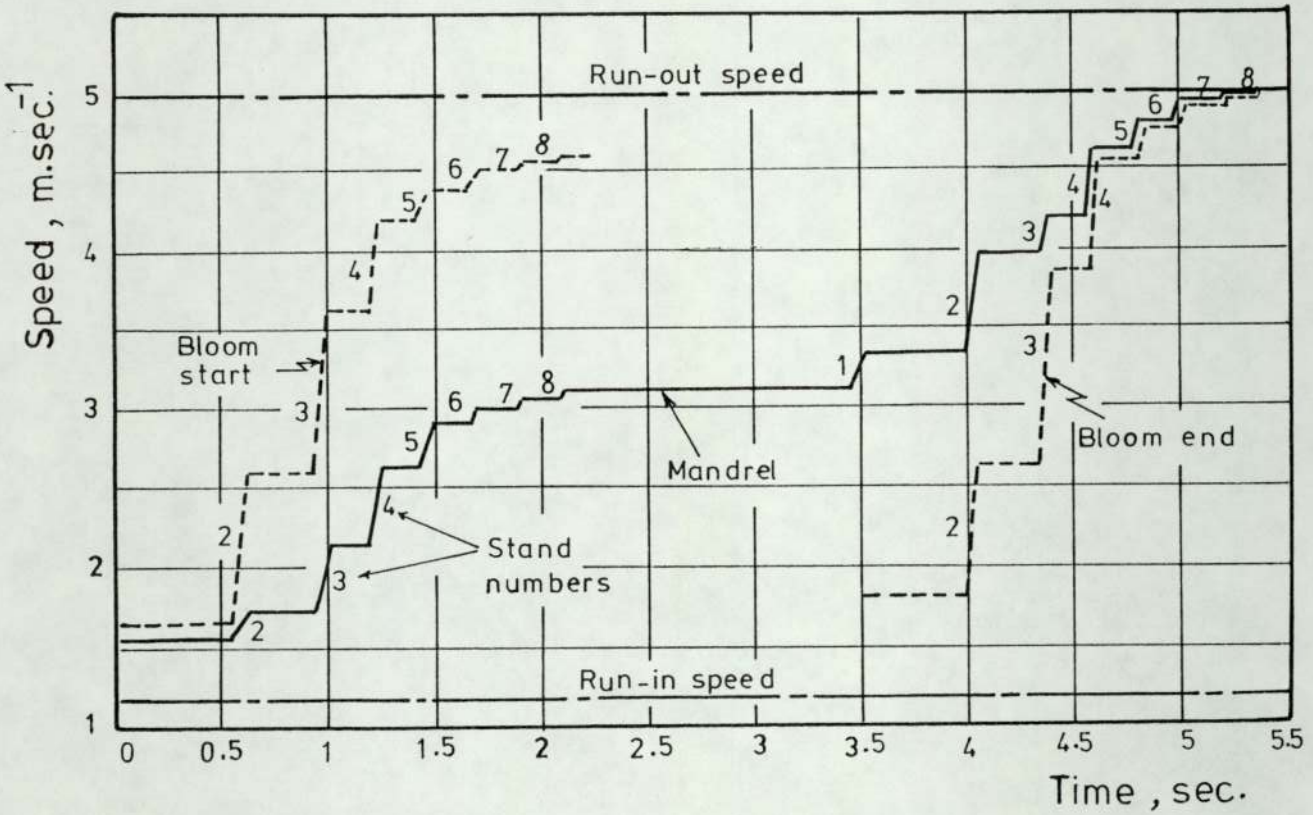

Fig.(2 . 1) Tube and mandrel speeds in a continuous mill
(From Neuhoff and Pfeiffer (5))

3. changing the roll speeds during the entry and exit of the tube from the mill so as to keep the tube speed at a constant level all the time.

The reasons behind points 1 and 3 can be understood, but the authors were not clear about the second measure and how higher deformations in the first stands could reduce belly formation.

Rolling loads were measured and a simplified theoretical calculation of roll pressure was provided based on the work by Karman (7) and Hoffmann and Sachs (8). Finally, the problem of thermal loading of the mandrel was treated since it affected the service life of the mandrel. The heat transferred to the mandrel through conduction and radiation from the tube as well as through friction between tube and mandrel was calculated.

In 1973, Pfeiffer (6) continued his research into the causes of irregularities of material flow in the continuous tube rolling process and carried out experiments on two 8-stand continuous mills. By the irregularities of material flow, the author was referring to the heavy deviations from nominal dimensions which can be detected in tube diameter and wall thickness over some parts of a continuous tube. Pfeiffer confirmed both experimentally and theoretically the fact that the formation of rear belly could be attributed to the acceleration of the mandrel on exit from the mill. However, a similar explanation could not be put for the cause of front belly as experiments showed that when only three stands were engaged in the rolling process, the front belly was not evident although the mandrel was accelerating on entry to the mill. Therefore another

explanation was suggested for the origin of front belly as being due to the shrinking of the tube onto the mandrel which increased the material resistance to flow in the forward direction. In support of this view, it was found that the front belly disappeared when hot mandrels were used instead of cold ones and this lowered the rate of tube cooling. Since the front belly occurred only in the rear stands, altering the groove shape in those stands to produce a larger diameter rolled product could be a measure against front belly formation. The author did not clarify this measure against front belly formation and it can only be suggested here that increasing the tube diameter or wall thickness will make the tube less susceptible to shrinking due to the lower rate of cooling from a thicker tube.

Pfeiffer indicated that the roll forces changed on entry to and exit from the mill due to the acceleration of the mandrel which altered the stress distribution in every stand. But he discarded the old idea that the discontinuities in material flow could be explained by the change in roll force and the corresponding spring back of the roll stand. His reason for discarding that old assumption is not clear as he referred to a previous investigation (5) where measurements of roll force were given. No mention was made of why the change in roll forces did or did not affect the material flow.

Pfeiffer measured the coefficient of friction between the tube and mandrel during the rolling process by holding the mandrel in a fixed position at the entry side. From measurements of roll force and the longitudinal force necessary to hold the mandrel in its fixed position, the

following equation was applied to evaluate the coefficient of friction μ_2 at any stand:

$$Z = 2P_w \cdot \mu_2$$

$$\mu_2 = \frac{Z}{2P_w}$$

where P_w is the roll force, and

Z is the mandrel force.

The advantage of that method is that it takes into account all the actual rolling conditions.

The author was able to measure the coefficient of friction between tube and mandrel in stands 1, 2 and 3 but unfortunately there was a great deal of scatter in his results. He corrected the values of the coefficient of friction to take into account the difference between the roll force P_w, and the normal forces which act perpendicularly to the friction surface. Also, corrections were made to include the fact that part of the measured roll force is responsible for sinking the tube onto the mandrel and this part does not contribute to the frictional forces between tube and mandrel.

Okamoto (9) introduced a deformation factor ν into the theoretical calculations of stresses in the three dimensional plastic deformation of tubes. This deformation factor ν, was defined as:

$$\varepsilon_2 = -(0.5 - \nu)\varepsilon_1$$

where ε_1 and ε_2 are the maximum and intermediate principal strains respectively.

Because the radial strain ε_r, and the tangential strain ε_t, were not constant over the tube section, the author introduced a "mean deformation factor", ν_m which was defined as:

$$\nu = \frac{r_a\, r_b}{r^2} \cdot \nu_m$$

where r_a and r_b are the outside and inside radii of the tube

r is the radius corresponding to ν at any position in the tube section.

Using the stress-strain relationships, in conjunction with the von-Mises yield criterion, equations were provided for the calculations of principal stresses in terms of the deformation factor . These equations were as follows:

$$\sigma_1 = \frac{K_f}{\sqrt{3}} \cdot \frac{1.5 + \nu}{\sqrt{\nu^2 + 0.75}} + \sigma_3$$, where K_f is the tensile yield stress.

$$\sigma_2 = \frac{K_f}{\sqrt{3}} \frac{2\ \nu}{\sqrt{\nu^2 + 0.75}} + \sigma_3$$

$$\sigma_3 = \frac{K_f}{\sqrt{3}} \ln\left(\nu + \sqrt{\nu^2 + 0.75}\right) + \frac{K_f}{\sqrt{3}} \ln\sqrt{0.75} - C$$

where C is an integration constant determined from the conditions of deformation in each case.

Two cases were considered in the calculations of stresses, namely the deformation of a tube under axial tension and outside pressure only, i.e. tube sinking and the deformation of a tube under axial tension and inside and outside pressure, i.e. tube plug drawing. Friction was not taken into consideration or the redundant deformation.

Okamoto and Hayashi (10) published a paper in 1970 on the theory of plasticity applied to the mandrel rolling process. Their main objective was to use the three dimensional theory of plasticity to make a judgement of

overfilling or underfilling of the roll groove. Excessive overfilling produces fins in the tube being rolled which can cause the mill to stop. Underfilling affects the tube roundness and can cause the tube to stick to the mandrel resulting in difficulty in extracting the mandrel from the tube.

The deformation zone was divided into two parts, the groove side where the tube inside was in contact with the mandrel, and the flange side where the tube inside was free. Fundamental equations were set up for both sides respectively based on the volume constancy condition, the stress-strain relationships, the von-Mises yield criterion and Okamoto's deformation factor ν which was used in another paper (9). Since the material in the groove side was subjected to axial compression and the material in the flange side was subjected to axial tension, the compatability equation for the axial stress was taken as a measure for the overfilling or underfilling of the groove. This compatability equation took the form:

$$f = \bar{\sigma}_1 A + \bar{\sigma}_1' A'$$

where $\bar{\sigma}_1$ and $\bar{\sigma}_1'$ are the axial stresses in the groove side and flange side respectively, and

A and A' are the cross-sectional areas of the groove side and flange side respectively.

If $f>0$ the material overfills, while if $f<0$, the material underfills. If $f=0$, the material flows in the shape of the groove.

Friction was not taken into account on the assumption that the forward slip regions were balanced with the backward slip regions of the tube outside and inside. This

assumption is, in most cases, not valid especially in a continuous mill where friction conditions vary from stand to stand according to whether the mandrel speed is higher, lower or equal to the tube speed. Also, friction conditions change with respect to the change in mandrel speed on entry to and exit from the mill.

As an example of calculations, the authors provided the distribution of deformations and stresses in an 8-stand mill designed on the condition of f=o. But no mention was made of the groove shapes, mandrel size, tube dimensions, rolling conditions, etc, so that it was impossible to check the method of calculations used by the authors.

Cole (11), (1969), investigated experimentally the three types of longitudinal tube rolling namely, tube sinking, stretch-reducing and mandrel rolling. The experimental results were compared with theoretical predictions based on equilibrium approaches emanating from Russian sources. Two theories concerning the mandrel rolling process were considered, the first by Vatkin and Druyan (3), and the second by Fomichev and Kirichenko (4). Both of these theories will be discussed in the next chapter.

Lead tubes were rolled in a circular groove representing the finishing stand in a production mill. Pressure distribution round the groove perimeter and along the arc of contact was measured by means of four pin-loadcells in the lower roll groove. Calibration curves revealed the presence of hysteresis and non-linearity in the operation of the pin-loadcells. Because the

calibration lines under conditions of increasing load were reproducible, Cole indicated that truly valid results from pin-loadcell measurements could only be obtained from the increasing side of the pressure variation curves and the peak pressure which was important.

In his mandrel rolling work, Cole's original intention was to compare the results with the deformation process of tube drawing on a mandrel and since in the latter process, the relationship between the internal diameter of the undrawn tube and the diameter of the mandrel is an important variable, different mandrel sizes were used for the same tube dimensions to assess the effect of varying the sink/draft ratio for the rolling process. Unfortunately Cole did not achieve his objective because the circular shape of the groove caused the rolled tube to possess heavy lateral finning and it was impossible to relate the results to the sink/draft ratio. Also due to the circular shape of the groove, the thickness of the tube varied, being least at the shrouds and greatest at the root of the groove which is opposite to the normal case of rolling a tube in an oval groove where the minimum tube thickness is found at the root of the groove. The results from the pin-loadcells were in agreement with the variation of wall thickness across the tube cross-section since the maximum pressure was found at the roll shroud where the tube thickness was minimum.

Due to the formation of fins, the experimental results could not be compared with theoretical predictions related to normal rolling conditions.

The yield stress of lead was obtained by plane strain compression testing but the effect of strain rate on the yield stress was not taken into account.

Cole provided a very extensive study of literature on tube sinking, stretch-reducing and mandrel rolling. Many Russian papers were covered in his literature review. Also included in his work was a review of the methods of measurement of contact stresses.

Haleem's work (12),from which the present investigation is an extension, was a continuation to Cole's work. Haleem investigated further the process of tube sinking and stretch-reducing. A new theoretical approach based on the strain energy principle was presented and applied to the tube sinking process to predict the average roll pressure, roll separating force and rolling torque. The theory was compared with other existing equilibrium approaches and it was shown that the energy approach was better than the equilibrium method in predicting the average roll pressure. A constant shear stress concept was used in the calculation of frictional work, and this took the form:

$$\tau = m \frac{\sigma_y}{\sqrt{3}}$$

where τ is the shear stress at the tube surface,

σ_y is the yield stress of the material being rolled,

m is the friction factor which is taken as constant for a particular set of conditions and can take a value between zero for frictionless conditions and unity for complete sticking.

Tests to determine the value of friction factor m showed that complete sticking did not take place during rolling, i.e. m was less than one. In applying his theory, Haleem assigned two values to the friction factor m, namely zero to give a lower value for the roll pressure and one to give an upper value. Redundant work was neglected in the theory on

the assumption that the maximum angle of bite was small.

Lead tubes of circular and oval sections were rolled in an oval groove generated from a circle having an eccentricity of 4.5 mm from the roll shrouds. This groove shape can be considered as representing one of the later stands in a production mill.

A new pin-loadcell design was developed to measure the pressure distribution in the roll groove and consisted of 4 pin-loadcells. (The same pin-loadcells were used also in the present investigation.) The use of pin loadcells allowed an accurate measurement of the length of arc of contact to be made and this showed that the measured length was less than the theoretical one calculated from the geometry of the tube and the groove. The author showed that this was due to the presence of a free zone, i.e. the tube started to deform before the contact zone between tube and rolls. The actual arc of contact was found to be about $1/\sqrt{2}$ of the calculated value in the absence of the free zone.

The yield stress of lead was determined by plane strain compression testing and again, cf. Cole, strain rate effects were discounted.

Finally, the paper by Pfeiffer (13), (1981) describes, among other aspects of seamless tube manufacture, recent developments in the continuous tube rolling process. A new method, called the MRK*, has been developed in which the mandrel is controlled to move at a constant speed which is equal to the rolling speed in the first stand. The new method was described in general without any experimental work or theoretical analysis to justify its advantages or

* MRK stands for Mannesmann Rohrkonti

disadvantages over the conventional continuous tube rolling process.

By a constant mandrel speed, Pfeiffer claimed that all the previous irregularities in material flow caused by the change in mandrel speed have been eliminated.

Although it can be understood that the causes of rear belly formation may be eliminated by the new method, it is suspected that there are some disadvantages which were not mentioned in the paper. One apparent disadvantage is that due to the reduced mandrel speed,friction between tube and mandrel in most stands may increase and its direction in all stands except stand 1 will be against the material flow leading to higher power requirements in the stands.

CHAPTER (3)

THEORETICAL TREATMENT OF THE MANDREL ROLLING PROCESS

3.1 Previous theories

Three theories will be examined here, two emanating from Russian sources and the third is of Japanese origin. The two Russian theories by Vatkin and Druyan (3) 1966, and Fomichev and Kirichenko (4) (1968) were discussed in detail in Cole's work (11). Therefore only a brief description of those two theories will be given in this chapter, while the third theory by Okamoto and Hayashi (10) will be examined in some detail.

3.1.1 Vatkin and Druyan (3) (1966)

Vatkin and Druyan examined the general case of rolling a tube on a circular mandrel in a non-circular groove. They considered the equilibrium of forces in the longitudinal direction acting on an element of tube in the deformation zone, Figure (3.1), and the following differential equation was obtained:

$$\frac{\partial \sigma_x}{\partial x} + (\sigma_x - p)\frac{1}{t}\frac{\partial t}{\partial x} + \frac{1}{t}(\tau + \tau_m) = 0 \qquad (3.1.1)$$

In this equation the tube thickness (t) was assumed to be small in comparison with $2r_m$, where r_m is the mandrel radius. Cole (11) indicated that this assumption was not justified since the mandrel rolling process is normally used industrially as a 'breaking-down' sequence, the ingoing material being a relatively thick pierced bloom.

The whole of the region of deformation was assumed to be subjected to the same stress system, i.e. homogeneous deformation. The authors applied a yield criterion in the form:

$$p - \sigma_x = \beta \sigma_y \qquad (3.1.2)$$

and the frictional conditions were:

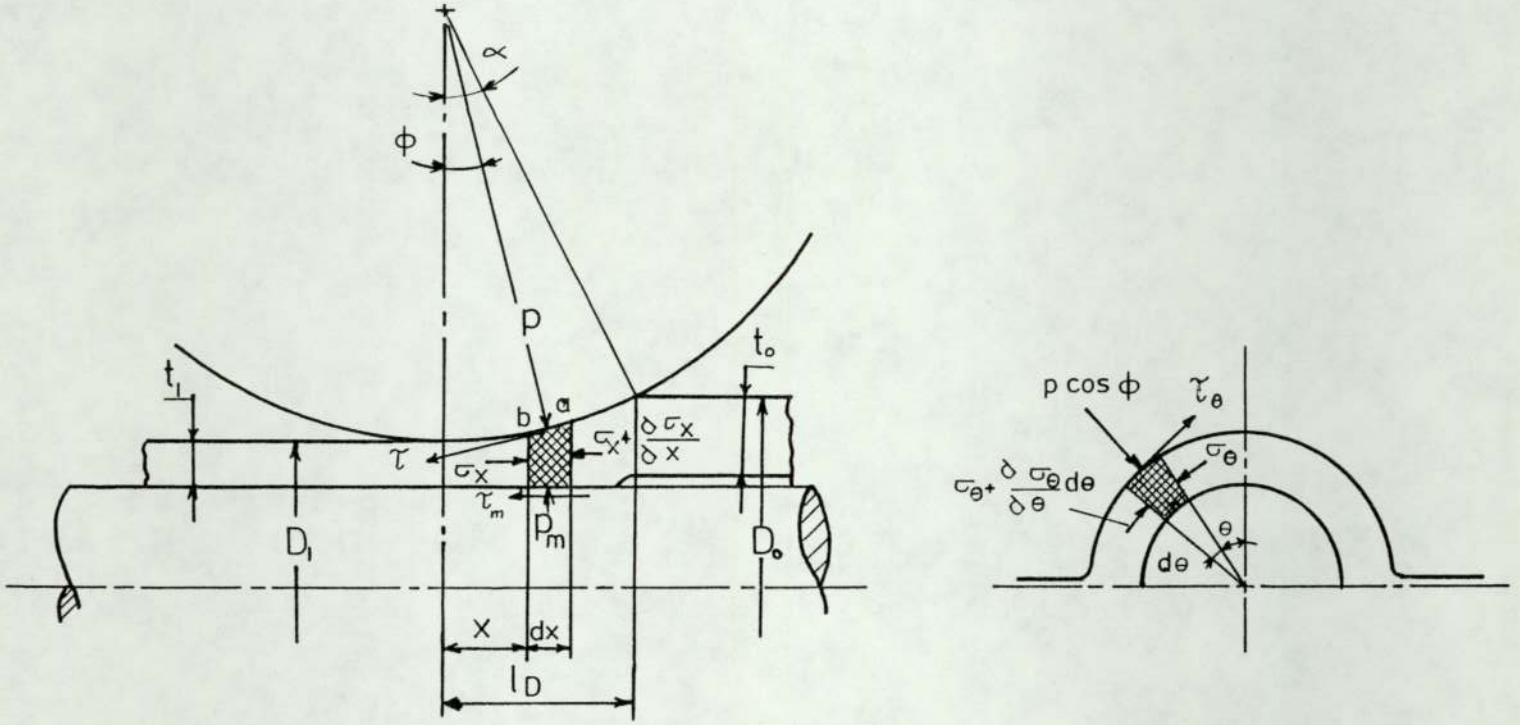

Fig.(3.1) Forces acting on an element in the deformation zone
(From Vatkin and Druyan (3))

$$\tau = \pm \mu \beta \sigma_y \qquad (3.1.3)$$

$$\tau_m = \pm \mu_m \beta \sigma_y \qquad (3.1.4)$$

If it is considered that the tube velocity is equal to the mandrel velocity at the neutral section, the positive sign in the above two expressions applies to the entry zone and the negative sign to the exit zone.

Substituting from equations (3.1.2),(3.1.3) and (3.1.4) into (3.1.1) gives:

$$\frac{\delta P}{\delta x} = \frac{\beta \sigma_y}{t} \cdot \frac{\delta t}{\delta x} \mp (\mu + \mu_m) \frac{\beta \sigma_y}{t} \qquad (3.1.5)$$

To solve the differential equation (3.1.5) the authors provided expressions for the thickness variation along the pass and around the groove. Also, by replacing the arc of contact by a chord and assuming that the distribution of normal pressure across the width of the groove was of parabolic form, which is a reasonable assumption, the authors were able to integrate equation (3.1.5) and obtained the following relationships:

For the entry zone:

$$P' = \beta \sigma_y \left\{ \left[1 - \left(\frac{2\theta}{\pi}\right)^2 \right] - \left(1 - \frac{\mu + \mu_m}{\Delta t} l_x\right) \ln \frac{t_{o,\theta}}{t_{x,\theta}} \right\} \qquad (3.1.6)$$

For the outlet zone:

$$P'' = \beta \sigma_y \left\{ \left[1 - \left(\frac{2\theta}{\pi}\right)^2 \right] + \left(1 + \frac{\mu + \mu_m}{\Delta t} l_x\right) \ln \frac{t_{x,\theta}}{t_{1,\theta}} \right\} \qquad (3.1.7)$$

μ and μ_m were assumed to be constant for a given set of conditions.

The mean specific pressure was obtained as:

$$P_{av} = \frac{\beta \sigma_y}{b_{av}} \left\{ \frac{\pi}{3} (t_o + W) - \left(1 - \frac{\mu + \mu_m}{t} l_D\right) \left[W \left(\ln t_o - \frac{t_o}{\Delta t} \ln t_o + \frac{t_1}{\Delta t} \ln t_1 \right) + t_{av} + d_m \right] \right\} \qquad (3.1.8)$$

where b_{a_v} is the average projected width of the region of contact

W = tube thickness at the exit plane + mandrel dia.

$t_{a_v} = \frac{1}{2}(t_o + t_1)$

l_D = length of the region of deformation

Vatkin and Druyan presented similar equations for conditions in which the velocity of the mandrel was either always greater or always less than the velocity of the tube.

The authors compared their theoretical predictions with experimental data and stated that good agreement between the two existed. However, Cole (11) mentioned that the yield stress figures quoted by Vatkin and Druyan appeared to be in error by a factor of 10.

The authors assumed that the peripheral angle of contact between tube and rolls was the same at any position along the pass, which is not the case in the mandrel rolling process where the peripheral angle of contact changes from a minimum at the entry plane to a maximum at the exit plane.

The peripheral angle of contact was taken to be $\pi/2$ throughout the deformation zone, i.e. full contact was assumed between tube and roll at all positions along the tube axis. This is far from the actual conditions since if complete filling of the groove is attempted, full contact occurs only at the exit plane. If complete filling of the groove occurs at a section before the exit plane, over-filling will surely take place in the following sections till the exit plane.

The assumption of a non-uniform pressure distribution round the groove was contradicted by assuming friction force to be constant, as can be seen from equations (3.1.3) and (3.1.4).

Throughout the paper, no definition was provided for the factor β which appears in the yield criterion $p - \sigma_x = \beta \sigma_y$, and the frictional conditions $\tau = \pm \beta \mu \sigma_y$ and $\tau_m = \pm \mu_m \beta \sigma_y$. Also μ and μ_m were not assigned any values although comparisons were made between the theoretical predictions and experimental data.

Finally, the derivation of equation (3.1.8) for the average specific pressure from the previous equations was not given and it is believed that equation (3.1.8) is in error since it includes the terms $\ln t_o$ and $\ln t_1$ where non-dimensional ratios are required.

3.1.2 Fomichev and Kirichenko (4) (1968)

Fomichev and Kirichenko also adopted the equilibrium approach in their analysis of the problem and the configuration for the mandrel pass is shown in Figure (3.2). They considered the equilibrium of forces in the longitudinal direction acting on an element in the deformation zone, Figure (3.2), and the following assumptions were made:

1. The groove shape was considered to be circular
2. The arc of contact was replaced by a chord
3. The elemental areas upon which the axial stress, σ_x and $(\sigma_x + d\sigma_x)$ acted were approximated to a rectangle of sides $\frac{1}{2}(D_x - d_m)$ and $\frac{1}{2}(\frac{1}{2} D_x d\theta + \frac{1}{2} d_m d\theta)$
4. The radial stress, σ_r, and the longitudinal stress, σ_x, were considered to be principal stresses. The yield criterion used was:

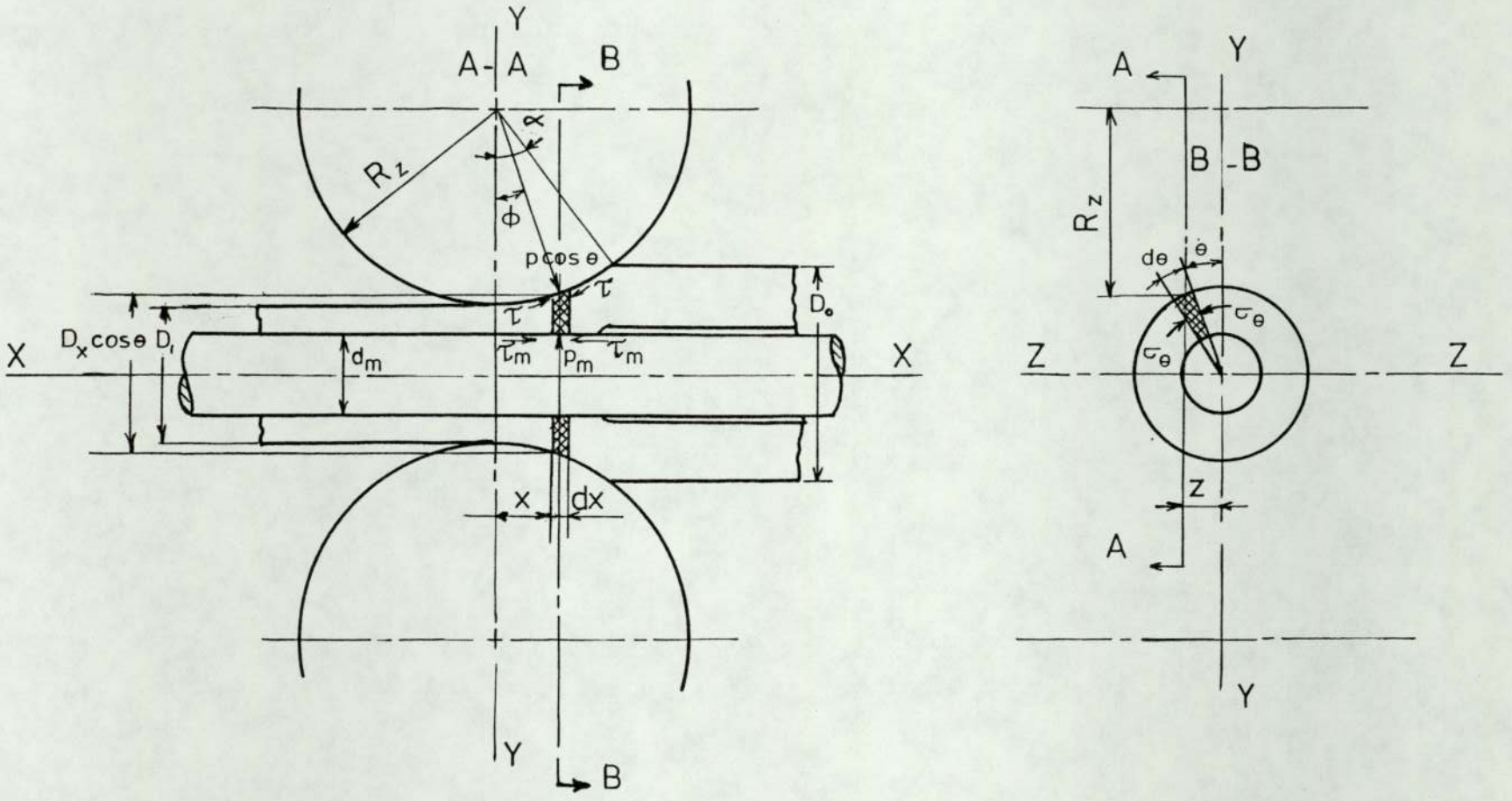

Fig.(3.2) Forces acting on an element in the deformation zone.
(From Fomichev and Kirichenko (4))

$$\sigma_r - \sigma_x = k'$$

where k' is a function of the yield stress σ_y in which $k' = \beta\ \sigma_y$ and $\frac{2}{\sqrt{3}} \geqslant \beta \geqslant 1$.

The differential equation of the equilibrium of forces in the longitudinal direction acting on an element becomes:

$$\frac{d\sigma_x}{dD_x} + \frac{2\sigma_x D_x}{(D_x^2 - d_m^2)} - \frac{2D_x}{(D_x^2 - d_m^2)} (p\cos\theta \tan\phi \mp \tau) \frac{\cos\theta}{\tan\phi}$$

$$\pm \frac{2\tau_m d_m}{(D_x^2 - d_m^2)} \frac{\cos\theta}{\tan\phi} = 0 \qquad (3.1.9)$$

Assuming a Coulomb type of friction and that the friction forces remain constant over the whole of the region of deformation, the solution of the above differential equation took the form: In the entry zone:

$$\sigma_x' = \frac{k'A}{1-A} + (q_o - \frac{k'A}{1-A})(\frac{D_o^2 - d_m^2}{D_x^2 - d_m^2})^{1-A} \qquad (3.1.10)$$

In the exit zone:

$$\sigma_x'' = \frac{k'A}{1-A} (q_1 - \frac{k'A}{1-A})(\frac{D_1^2 - d_m^2}{D_x^2 - d_m^2})^{1-A} \qquad (3.1.11)$$

where $A = \frac{\cos\theta}{\tan\phi} (\frac{\cos\theta \sin\phi \mp \mu\cos\phi}{\cos^2\theta \cos\phi \pm \sin^2\theta \pm \mu\cos\theta \sin\phi} \mp \mu_m)$

q_o is the axial stress at entry

q_1 is the axial stress at exit

If the differential equation is solved on the basis of the constancy of friction forces, i.e. a constant shear stress type of friction, the solution becomes:

$$\sigma_x' = \frac{N}{M} + (q_o - \frac{N}{M})(\frac{D_o^2 - d_m^2}{D_x^2 - d_m^2})^M \qquad (3.1.12)$$

and

$$\sigma_x'' = \frac{N}{M} + (q_1 - \frac{N}{M})(\frac{D_1^2 - d_m^2}{D_x^2 - d_m^2})^{2M} \qquad (3.1.13)$$

where $M = 1 - \dfrac{\cos^2\theta \cos\phi}{\cos^2\theta \cos\phi + \sin^2\theta}$

$$N = \frac{\cos\theta}{\tan\phi}\left(\frac{k' \cos\theta \sin\phi \mp \tau \cos^2\theta \sin\phi \tan\phi}{\cos^2\theta \cos\phi + \sin^2\theta} \mp \tau \mp \tau_m \frac{d_m}{D_{av}}\right)$$

D_{av} is the mean diameter of the tube in the region of deformation

The relationships for the distribution of normal pressure in the entry zone (p') and the exit zone (p'') for the condition of Coulomb friction are:

$$p' = \frac{k' \cos\phi}{\cos^2\theta \cos\phi + \sin^2\theta + \mu \cos\theta \sin\phi}\left[\frac{A}{1-A} + \left(\frac{q_o}{k'} - \frac{A}{1-A}\right)\left(\frac{D_o^2 - d_m^2}{D_x^2 - d_m^2}\right)^{1-A}\right] \qquad (3.1.14)$$

$$p'' = \frac{k' \cos\phi}{\cos^2\theta \cos\phi + \sin^2\theta - \mu \cos\theta \sin\phi}\left[\frac{A}{1-A} + \left(\frac{q_1}{k'} - \frac{A}{1-A}\right)\left(\frac{D_1^2 - d_m^2}{D_x^2 - d_m^2}\right)^{1-A}\right] \qquad (3.1.15)$$

On the basis of constancy of friction forces, the pressure distribution becomes:

$$p' = \frac{\cos\phi}{\cos^2\theta\cos\phi + \sin^2\theta}\left[k' - \tau\cos\theta\tan\phi + \frac{N}{M} - \left(\frac{q_o}{k'} - \frac{N}{M}\right)\left(\frac{D_o^2 - d_m^2}{D_x^2 - d_m^2}\right)^M\right] \qquad (3.1.16)$$

$$p'' = \frac{\cos\phi}{\cos^2\theta\cos\phi + \sin^2\theta}\left[k' + \tau\cos\theta\tan\phi + \frac{N}{M} - \left(\frac{q_1}{k'} - \frac{N}{M}\right)\left(\frac{D_1^2 - d_m^2}{D_x^2 - d_m^2}\right)^M\right] \qquad (3.1.17)$$

The theoretical predictions of Fomichev and Kirichenko compared well with the experimental results of Vatkin (14). Cole (11) stated that it was difficult to believe that the Fomichev and Kirichenko's prediction of the normal pressure distribution based on Coulomb friction should generally show higher values than that based on constancy of friction force.

The assumption of a Coulomb type of friction is a significant one and although the authors considered also the case of a constant shear stress type of friction in the form τ = constant, no definition was provided for the constant in the equation.

The geometry was greatly simplified by the assumption of a circular groove and replacing the arc of contact by a chord. This meant that the variation of tube wall thickness round the groove was not accounted for, which is hard to accept in the mandrel rolling process where the thickness varies considerably round the groove.

No mention was made of the peripheral angle of contact between tube and roll at any position along the pass. Also,

the contact area between tube and rolls was not considered.

3.1.3 T.Okamoto and C.Hayashi (10)

Okamoto and Hayashi applied the theory of plasticity to the problem of tube rolling on a mandrel. Their aim was to make a judgement of overfilling or underfilling of a given groove shape.

In Figure (3.3) the deformation zone is divided into two parts, the groove side where the tube inner surface is in contact with the mandrel, and the flange side, which is near the shrouds, where the tube inner surface is free. The material in the groove side is deformed under outside pressure, inside pressure and axial compression while the material in the flange side is deformed under outside pressure and axial tension. It was assumed that the stresses in the groove and flange sides were uniform and mean values of thickness were used in the calculations.

The authors used Okamoto's deformation factor ν in their theoretical treatment of the mandrel rolling process. The deformation factor ν gives an indication of the changes in shape that occurs in a body undergoing deformation and therefore it is sometimes called the shape factor. From the condition of volume constancy, i.e. $\Phi_1 + \Phi_r + \Phi_\theta = 0$, the deformation factor ν is defined as:

$$\nu = 0.5 + \frac{\Phi_\theta}{\Phi_1}$$

where $\Phi_1, \Phi_r, \Phi_\theta$ are the longitudinal, radial and circumferential natural strains respectively.

The constant in the above definition is chosen so that in simple tension, or compression, where $\nu = 0$, $\Phi_\theta = -0.5\Phi_1$.

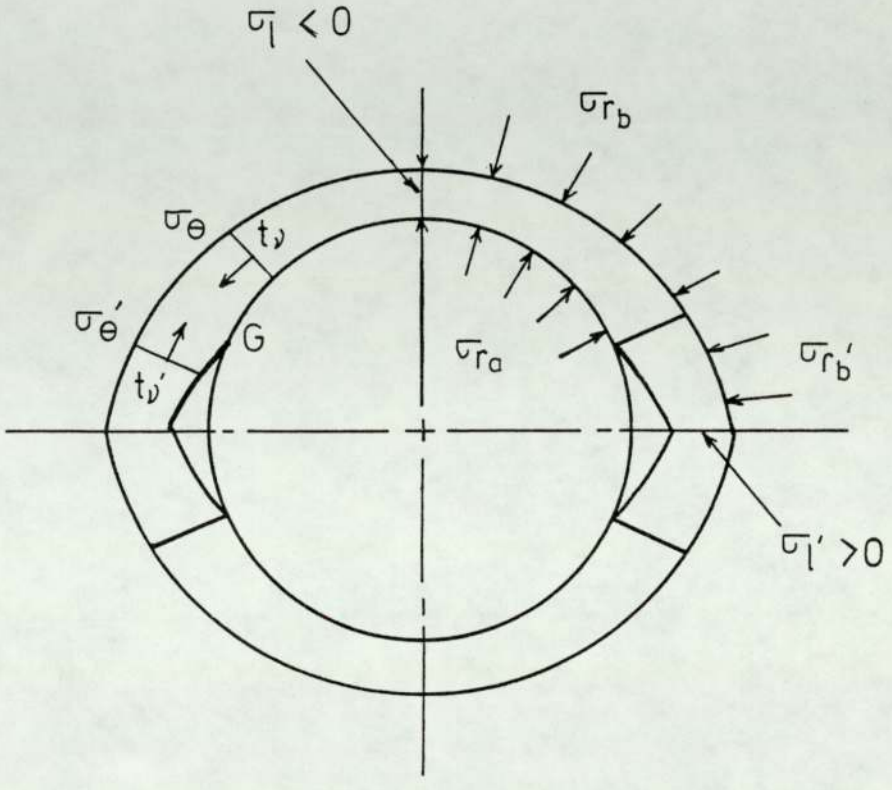

Fig.(3.3) Stress distribution in the deformation zone (From Okamoto and Hayashi (10))

It should be emphasized that the deformation factor ν does not contribute to the solution of any deformation problem since its value is determined from the strains occurring in the process under investigation. Its usefulness comes from the fact that it simplifies the mathematical expressions concerning the calculations of stresses. The authors set up fundamental equations for the groove and flange sides as follows:

For the groove side:

- the deformation factor ν is defined as:

$$\nu = 0.5 + \frac{\Phi_\theta}{\Phi_1} \qquad (3.1.18)$$

- the volume constancy condition is:

$$\Phi_1 + \Phi_\theta + \Phi_r = 0 \qquad (3.1.19)$$

where Φ_1, Φ_θ and Φ_r are the longitudinal, tangential and radial strains respectively.

- stress-strain relationships:

$$\frac{\sigma_1 - \sigma_\theta}{\Phi_1 - \Phi_\theta} = \frac{\sigma_\theta - \sigma_r}{\Phi_\theta - \Phi_r} \left(= \frac{\sigma_r - \sigma_1}{\Phi_r - \Phi_1} \right) \qquad (3.1.20)$$

- von-Mises flow condition:

$$(\sigma_1 - \sigma_\theta)^2 + (\sigma_\theta - \sigma_r)^2 + (\sigma_r - \sigma_1)^2 = 2k_f^2 \qquad (3.1.21)$$

From the above basic relationships, the following equations can be obtained:

- Equilibrium equation in the radial direction:

$$\sigma_{r_b} - \sigma_{r_a} = \int_{r_a}^{r_b} (\sigma_\theta - \sigma_r) \frac{dr}{r}$$

$$= \frac{k_f}{\sqrt{3}} \frac{2\nu}{\sqrt{\nu^2 + 0.75}} \ln \frac{r_b}{r_a} \qquad (3.1.22)$$

- Equation of the tangential stress:

$$\sigma_\theta = \frac{k_f}{\sqrt{3}} \frac{2\nu}{\sqrt{\nu^2+0.75}} + \sigma_r \qquad (3.1.23)$$

- Equation of the axial stress:

$$\sigma_l = \frac{k_f}{\sqrt{3}} \frac{1.5+\nu}{\sqrt{\nu^2+0.75}} + \sigma_r \qquad (3.1.24)$$

- Approximate equation for the mean radial stress:

$$\sigma_r = \tfrac{1}{2}(\sigma_{r_b} + \sigma_{r_a}) \qquad (3.1.25)$$

Similarly for the flange side:

$$\nu' = 0.5 + \frac{\Phi_\theta'}{\Phi_l'} \qquad (3.1.26)$$

$$\Phi_l' + \Phi_\theta' + \Phi_r' = 0 \qquad (3.1.27)$$

$$\sigma_{r_b}' = \frac{k_f}{\sqrt{3}} \frac{2\nu'}{\sqrt{\nu'^2+0.75}} \cdot \ln \frac{r_b'}{r_a'} \qquad (3.1.28)$$

$$\sigma_\theta' = \frac{k_f}{\sqrt{3}} \frac{2\nu'}{\sqrt{\nu'^2+0.75}} + \sigma_r' \qquad (3.1.29)$$

$$\sigma_l' = \frac{k_f}{\sqrt{3}} \frac{1.5+\nu'}{\sqrt{\nu'^2+0.75}} + \sigma_r' \qquad (3.1.30)$$

$$\sigma_r' = \tfrac{1}{2}\sigma_{r_b}' \qquad (3.1.31)$$

The compatibility equations between the groove side and the flange side are:

For the axial elongation:

$$\Phi_l = \Phi_l' \qquad (3.1.32)$$

For the tangential stress:

$$\sigma_\theta = \xi \sigma_\theta' \qquad \xi = (t_\nu'/t_\nu) \qquad (3.1.33)$$

For the axial stress:

$$f = \sigma_1 A + \sigma_1' A' = 0 \qquad (3.1.34)$$

where A and A' are the cross-sectional areas of the groove and flange sides respectively.

The above 15 equations in 17 unknowns can be solved by trial and error by assuming any two unknowns and solving the 15 simultaneous equations.

A judgement of overfilling or underfilling can be made by first assuming that the material flows in the shape of the groove. Assuming Φ_θ' and that $\Phi_r' = 0$, Φ_1' and Φ_1 are calculated. The value of Φ_θ' is then readjusted until the condition Φ_1' equals Φ_1 is satisfied. After performing the rest of the calculations, the balance of the longitudinal tension, σ_1', and longitudinal compression, σ_1, is examined by equation (3.1.34).

$$f = \sigma_1 A + \sigma_1' A'$$

If $f > 0$, the material overfills the groove, while if $f < 0$ the material underfills. If $f = 0$ the material flows in the shape of the groove.

Friction was not taken into account at all in the above calculations which is a serious drawback of the proposed theory.

3.2 The proposed theory

As opposed to the more widely used equilibrium approaches in the theoretical treatment of tube rolling processes, the present theory is based on an energy method which is believed to give more satisfactory predictions of rolling loads.

The drawbacks of any equilibrium approach result from

the fact that a yield criterion must be used and that the directions of principal stresses must be assigned before any solution to the problem is obtained. In tube rolling the principal directions are assumed to be longitudinal, radial and tangential. This system of principal stresses does not hold true if the friction forces are high and hence the shear stress contribution is large. Therefore it can be stated that while the yield criterion can be used with small error in the case of cold forming operations, where the friction forces contribution is small, it cannot be applied successfully to hot forming processes, such as hot rolling, where sticking friction is believed to occur. The inaccuracy of the equilibrium approach in dealing with the hot rolling process, led to the adoption of the energy method in the present investigation. Although the energy method gives only the average roll pressure and not the pressure distribution round the groove or along the arc of contact, which is useful in understanding the mechanics of the process, it is sufficient for practical considerations to predict the average pressure and total roll separating force.

In this method, the work done per unit volume of the rolled tube is divided into the following components:

1. Work of homogeneous deformation, W_h, which represents the minimum possible work required to change the tube shape. The homogeneous work can be visualized as the work needed in the absence of frictional and physical tool constraints.

2. Redundant work which is the work lost due to unnecessary internal shearing of the material caused by the constraints imposed on the material flow. This type of work does not contribute towards the required change of tube shape. In the mandrel rolling process two types of redundant deformation can be distinguished:
   a) Redundant deformation which is due to the shearing of the material as it enters the deformation zone,
   b) Redundant deformation which is due to the longitudinal shearing of the material caused by difference in the longitudinal velocities of the inner and outer tube surfaces. This component of the redundant work will be neglected since it was shown experimentally, by drilling holes in the tube wall before rolling and examining the longitudinal distortion of the holes after rolling, that the longitudinal shear was too small to justify the very complex calculations of that type of redundant deformation.
3. Frictional work which is the work done to overcome friction between tube and rolls and between tube and mandrel.
4. External work supplied by the applied front and back tensions.

The total work done by the rolls per unit volume, w_t, can be written as:

$$W_t = W_h + W_r + W_f$$

where W_h is the homogeneous work per unit volume,

W_r is the redundant work per unit volume,

W_f is the work done against friction per unit volume

In the case of rolling with applied front and back tensions, the total work per unit volume, W_T is:

$$W_T = W_t + W_{a,b}$$

where $W_{a,b}$ is the work done by the applied front and back tensions. Before attempting to calculate each component of the total work separately, the peripheral angle of contact, ψ_c, at any angle of contact, ϕ, and the contact area between tube and rolls will be determined since they will be used in the work calculations. To obtain the roll separating force, the horizontal projection of the area of contact will be evaluated first.

The calculations in the next sections will be performed for the groove shape shown in Figure (3.4), and later in this chapter two other groove shapes will be examined.

3.2.1 Peripheral angle of contact, ψ_c, at any angle of contact ϕ.

It will be assumed that contact between tube and groove surface starts when the instantaneous groove radius, r_ψ, at any angle of contact ϕ, equals the tube radius r_o, Figure (3.4). This assumption is intended as a first approximation since it does not take into account the lateral spread of the tube material that can occur during rolling.

By taking any vertical section in the YOZ plane at a distance Z from the line joining the two centres of the rolls, axis OY, Figure (3.4), the following equation can be written for the contact point C:

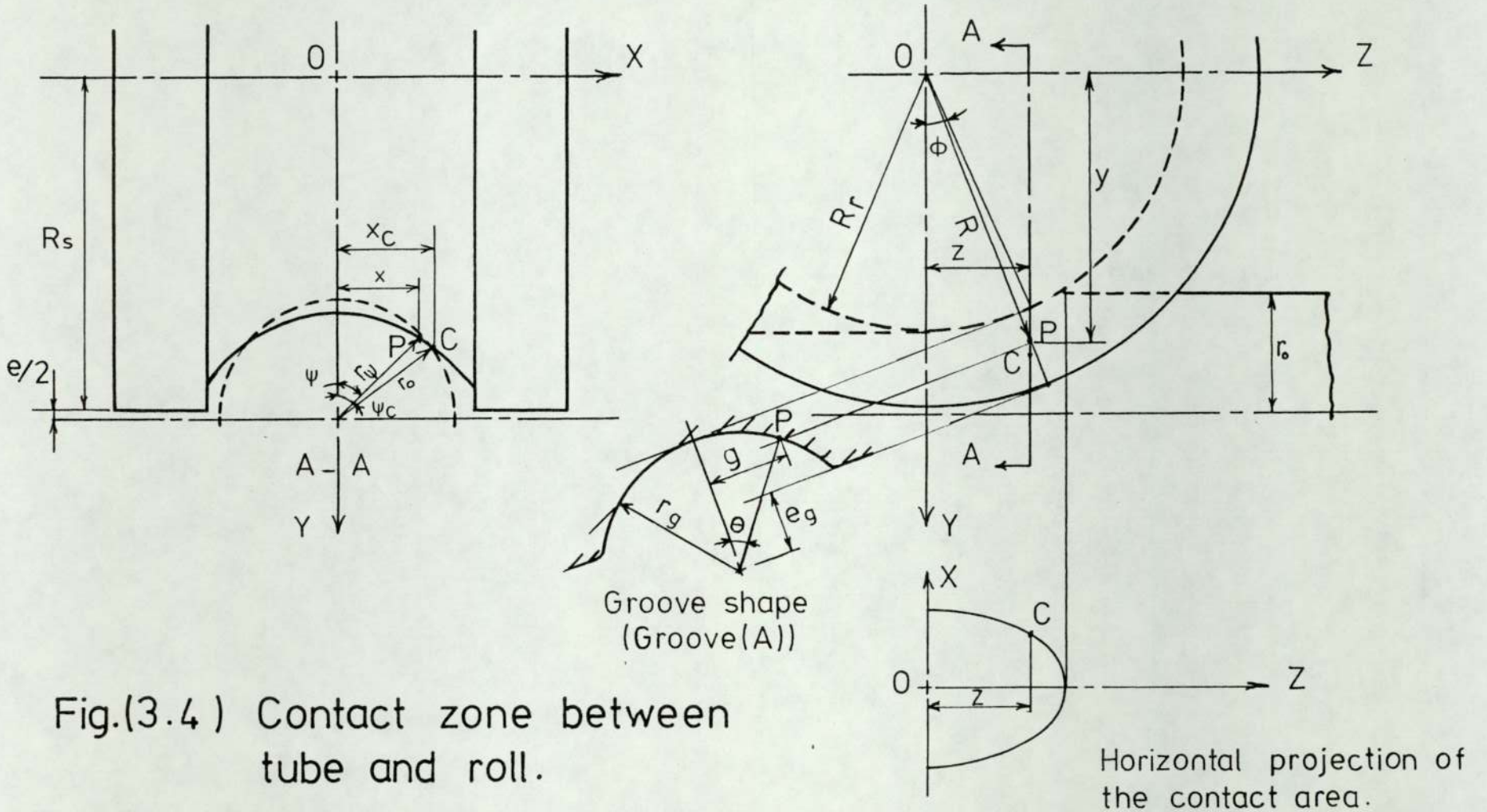

Fig.(3.4) Contact zone between tube and roll.

$$\cos\theta_c = \frac{1}{r_g}(R_s - R_c + e_g)$$

where R_c is the distance of point C from the roll centre O.

Rearranging the above equation:

$$R_c = R_s + e_g - r_g \cos\theta_c \qquad (3.2.1)$$

At the point of contact, the instantaneous groove radius r_ψ is equal to the tube radius r_o and,

$$g = r_g \sin\theta_c = r_o \sin\psi_c \qquad (3.2.2)$$

$$y_c = (R_s + \frac{e}{2}) - r_o \cos\psi_c \qquad (3.2.3)$$

$$R_c^2 = z_c^2 + y_c^2$$

Since $z = R_r \sin\Phi$

then $R_c^2 = R_r^2 \sin^2\Phi + y_c^2 \qquad (3.2.4)$

To get the relationship between Φ and ψ_c, equations (3.2.1) and (3.2.3) are substituted in equation (3.2.4).

$$R_r^2 \sin^2\Phi + \left[(R_s + \frac{e}{2}) - r_o \cos\psi_c\right]^2 = \left[(R_s + e_g) - r_g\cos\theta_c\right]^2$$

$$R_r^2\sin^2\Phi = \left[(R_s + e_g)^2 - 2\, r_g(R_s + e_g)\cos\theta_c + r_g^2\cos^2\theta_c - (R_s + \frac{e}{2})^2 + 2r_o(R_s + \frac{e}{2})\cos\psi_c - r_o^2\cos^2\psi_c\right]$$

Putting $r_g^2\cos^2\theta_c = r_g^2(1 - \sin^2\theta_c)$

$$= r_g^2 - r_g^2\sin^2\theta_c$$

$$= r_g^2 - r_o^2\sin^2\psi_c$$

$$R_r^2\sin^2\Phi = \left[(R_s + e_g)^2 - (R_s + \frac{e}{2})^2 + r_g^2 - r_o^2\right] - 2r_g(R_s + e_g)\cos\theta_c + 2r_o(R_s + \frac{e}{2})\cos\psi_c$$

$$R_r^2 \sin^2\Phi = \left[(R_s + e_g)^2 - (R_s + \tfrac{e}{2})^2 + r_g^2 - r_o^2\right] + 2r_o(R_s + \tfrac{e}{2}) \cos\psi_c - 2(R_s + e_g)(r_g^2 - r_o^2 \sin^2\psi_c)^{\frac{1}{2}}$$

Putting $A = R_r^2 \sin^2\Phi$

$$B = \left[(R_s + e_g)^2 - (R_s + \tfrac{e}{2})^2 + r_g^2 - r_o^2\right]$$

$$C = 2r_o (R_s + \tfrac{e}{2})$$

and rearranging:

$$A - B - C\cos\psi_c = -2(R_s + e_g)(r_g^2 - r_o^2 \sin^2\psi_c)^{\frac{1}{2}}$$

squaring both sides:

$$[A - B - C\cos\psi_c]^2 = 4(R_s + e_g)^2 (r_g^2 - r_o^2 \sin^2\psi_c)$$

Putting $F = 4(R_s + e_g)^2$

$$D = A - B$$

$$[D - C\cos\psi_c]^2 = r_g^2 F - r_o^2 F \sin^2\psi_c$$

$$D^2 - 2D.C.\cos\psi_c + C^2\cos^2\psi_c = r_g^2 F - r_o^2 F(1 - \cos^2\psi_c)$$

$$(C^2 - r_o^2 F)\cos^2\psi_c - 2D.C.\cos\psi_c + (D^2 - r_g^2.F + r_o^2.F) = 0 \qquad (3.2.5)$$

Equation (3.2.5) is a second degree equation in $\cos\psi_c$ which can be solved to give the peripheral contact angle ψ_c at the corresponding contact angle Φ.

3.2.2 Contact area between tube and rolls

To find the equation of the roll groove surface, an arbitrary point P (x,y,z) is chosen on that surface, Figure (3.4).

In the YOZ plane, it can be written that:

$$y^2 + z^2 = R^2 \text{ or } R = (y^2 + z^2)^{\frac{1}{2}} \qquad (3.2.6)$$

where R is the distance of point P from the roll centre O. From figure (3.4):

$$\cos\theta = \frac{1}{r_g}(R_s - R + e_g)$$

$$x = g = r_g \sin\theta$$

$$x^2 = r_g^2 \sin^2\theta$$

$$= r_g^2(1 - \cos^2\theta)$$

$$= r_g^2\left[1 - \frac{1}{r_g^2}(R_s - R + e_g)^2\right]$$

$$= r_g^2 - (R_s - R + e_g)^2 \qquad (3.2.7)$$

Substituting from (3.2.6) in (3.2.7):

$$x^2 = r_g^2 - \left[(R_s + e_g) - (y^2 + z^2)^{\frac{1}{2}}\right]^2$$

Putting $R_s + e_g = b$ and rearranging:

$$x^2 + \left[b - (y^2 + z^2)^{\frac{1}{2}}\right]^2 = r_g^2 \qquad (3.2.8)$$

where $z = R_r \sin\phi$

Equation (3.2.8) is the three dimensional equation of the roll groove surface.

At any angle ϕ, the elemental length, dL, of the contact curve between tube and rolls is:

$$dL = (dx^2 + dy^2)^{\frac{1}{2}} \qquad (3.2.9)$$

By differentiating equation (3.2.8) with respect to x and y while keeping z constant:

$$2x\,dx + 2\left[b-(y^2+z^2)^{\frac{1}{2}}\right]\left[-\tfrac{1}{2}(y^2+z^2)^{-\frac{1}{2}}(2ydy)\right] = 0$$

$$x\,dx + \left[b - (y^2+z^2)^{\frac{1}{2}}\right]\frac{-ydy}{(y^2+z^2)^{\frac{1}{2}}} = 0$$

$$x\,dx = \left[\frac{b}{(y^2+z^2)^{\frac{1}{2}}} - 1\right] y\,dy$$

$$dy = \frac{x}{y}\,\frac{1}{\left[\frac{b}{(y^2+z^2)^{\frac{1}{2}}} - 1\right]}\,dx$$

$$= \frac{x}{y}\,\frac{(y^2 + z^2)^{\frac{1}{2}}}{\left[b-(y^2+z^2)^{\frac{1}{2}}\right]}\,dx$$

$$dy^2 = \frac{x^2}{y^2} \frac{(y^2+z^2)}{\left[b-(y^2+z^2)^{\frac{1}{2}}\right]^2} \, dx^2$$

From equation (3.2.8):

$$\left[b - (y^2+z^2)^{\frac{1}{2}}\right]^2 = r_g^2 - x^2 \qquad (3.2.10)$$

$$\therefore dy^2 = \frac{x^2}{y^2(r_g^2-x^2)} \frac{(y^2+z^2)}{} \, dx^2 \qquad (3.2.11)$$

Taking the square root of both sides of equation (3.2.10)

$$b - (y^2+z^2)^{\frac{1}{2}} = (r_g^2 - x^2)^{\frac{1}{2}}$$

$$(y^2 + z^2)^{\frac{1}{2}} = b - (r_g^2-x^2)^{\frac{1}{2}}$$

squaring both sides:

$$y^2+z^2 = \left[b - (r_g^2-x^2)^{\frac{1}{2}}\right]^2$$

$$y^2 = \left[b - (r_g^2-x^2)^{\frac{1}{2}}\right]^2 - z^2 \qquad (3.2.12)$$

Substituting from (3.2.11) and (3.2.12) in 3.2.9):

$$\therefore dL = \left\{ dx^2 + \frac{x^2\left(1 + \frac{z^2}{\left[b-(r_g^2-x^2)^{\frac{1}{2}}\right]^2 - z^2}\right)}{(r_g^2 - x^2)} dx^2 \right\}^{1/2}$$

$$dL = \left\{ \frac{x^2\left[1 + \frac{z^2}{\left[b-(r_g^2-x^2)^{\frac{1}{2}}\right]^2 - z^2}\right]}{(r_g^2 - x^2)} + 1 \right\}^{\frac{1}{2}} dx \qquad (3.2.13)$$

To obtain the contact area between tube and roll, equation (3.2.13) is integrated twice, first with respect to x between limits x = 0 and $x_c = r_o \sin\psi_c$, and secondly with respect to z between limits z = 0 and $z = R_r \sin\Phi_m$, where Φ_m is the maximum angle of contact which can be found from the geometry of tube and groove as:

$$\cos \phi_m = 1 - \frac{r_o - (r_g - e_g) - e/2}{R_r} \qquad (3.2.14)$$

Due to the complex nature of the function in equation (3.2.13) and also to the fact that x_c is in itself a complex function of z, approximate numerical methods had to be adopted in solving the double integration of equation (3.2.13). A computer programme has been developed for the calculation of contact area between tube and rolls and this can be found in Appendix (A-1).

3.2.3 Horizontal projection of the contact area

The horizontal projection of the contact area can be determined by finding the equation of the contact curve in the XOZ plane, Figure (3.4). The co-ordinates of any point lying on that curve can be written as:

$$z = R_r \sin\phi \quad \text{and} \quad x = g = r_o \sin\psi_c$$

The relationship between ϕ and ψ_c and hence the relationship between x and z can be obtained from the solution of equation (3.2.5). . It is clear that this relationship will be too difficult to integrate using the normal methods of integration. Therefore numerical methods were again used in the calculation of the horizontal projection of the contact area by the use of a computer.

3.2.4 Work of homogeneous deformation W_h

Considering the true stress-strain curve shown in Figure (3.5), the increment of plastic work per unit volume required to deform the material is:

$$dW = \sigma_y \, d\varepsilon \qquad (3.2.15)$$

where $d\varepsilon$ is the change in strain occurring in the material,

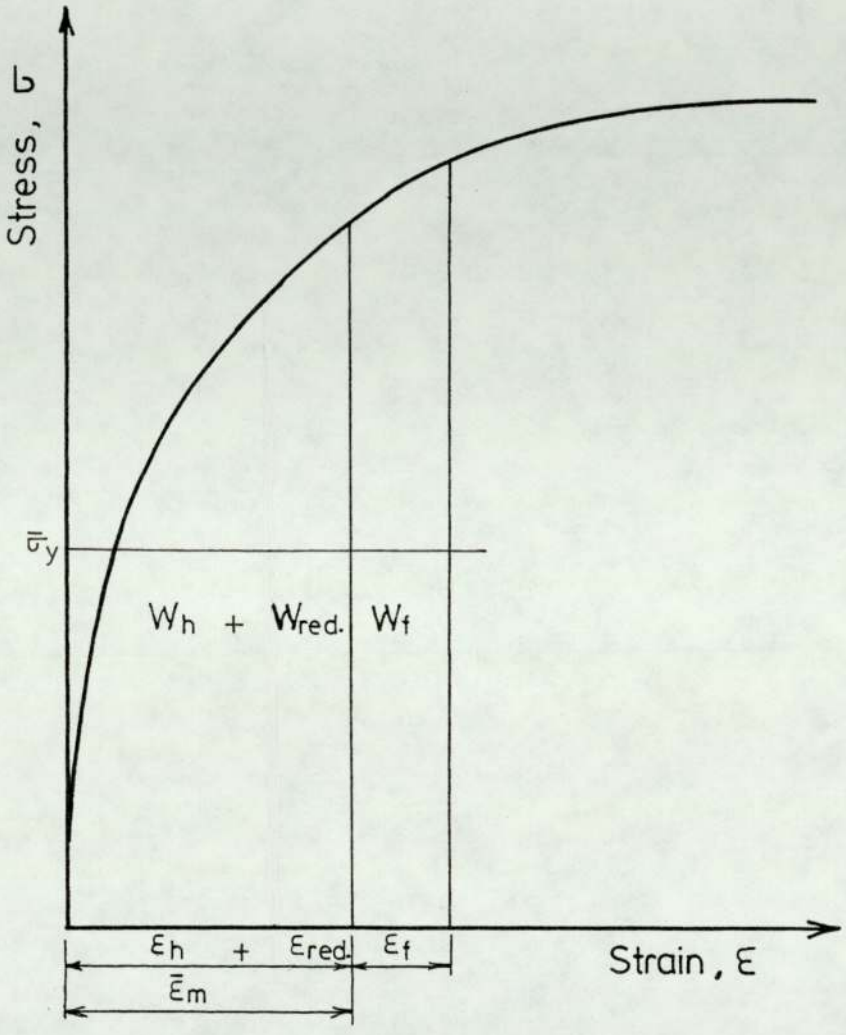

Fig.(3.5) Total work of deformation.

σ_y is the yield stress of the material.

The total work per unit volume is equal to the area under the true stress-strain curve for the appropriate strain ε,

$$W = \int_0^{\varepsilon} \sigma_y \, d\varepsilon \qquad (3.2.16)$$

Due to the variation of yield stress with ε, the concept of a mean yield stress is employed in the present investigation to be able to integrate equation (3.2.16). The mean yield stress for a given strain ε can be defined as the yield stress which when multiplied by ε will give the same area under the stress-strain curve.

Since the value of the mean yield stress depends on the combined effect of all the strains imposed on the tube, the notion of a generalized strain (15), (16), (17), suffered by the material can be introduced into the calculations. The generalized strain has the same effect as that of the complex actual strain pattern imposed. It should be emphasized that the generalized strain does not exist in reality and that it is only a convenient measure of the total deformation actually imposed.

The generalized homogeneous strain increment can be written in the form (16), (17):

$$d\varepsilon_h = \sqrt{\frac{2}{9}\left[(d\varepsilon_1 - d\varepsilon_r)^2 + (d\varepsilon_r - d\varepsilon_c)^2 + (d\varepsilon_c - d\varepsilon_1)^2\right]} \qquad (3.2.17)$$

where $d\varepsilon_1$ is the longitudinal strain increment

$d\varepsilon_r$ is the radial strain increment

$d\varepsilon_c$ is the circumferential strain increment

It will be assumed that the rotation of the axes of strain increments in mandrel tube rolling is negligibly small. In that case equation (3.2.17) can be integrated directly to give:

$$\varepsilon_h = \sqrt{\frac{2}{3}\left[\varepsilon_1^2 + \varepsilon_r^2 + \varepsilon_c^2\right]} \qquad (3.2.18)$$

and the work of homogeneous deformation can be written as:

$$W_h = \bar{\sigma}_y \ \varepsilon_h \qquad (3.2.19)$$

where $\bar{\sigma}_y$ is the mean yield stress of the material corresponding to strain ε_h.

3.2.5 Redundant work

Only the redundant work caused by the shearing of the material as it enters the deformation zone will be considered here. In dealing with that type of redundant deformation the following assumptions are made when steady state conditions have been attained:

1. The tube longitudinal velocity U at any point on the surface of contact making an angle ϕ with the line connecting the centres of the two rolls, Figure (3.6), will be assumed constant across the vertical plane passing through this point. This assumption is justified for the case of thin walled tubes.
2. As the tube mean linear velocity U changes from U_o at the entry plane to U_1 at the exit plane, the change in U with the angle of contact ϕ is assumed to be linear. This assumption takes the form:

$$U = U_1 - a\phi \qquad (3.2.20)$$

where a is a constant determined from the conditions at the entry plane.

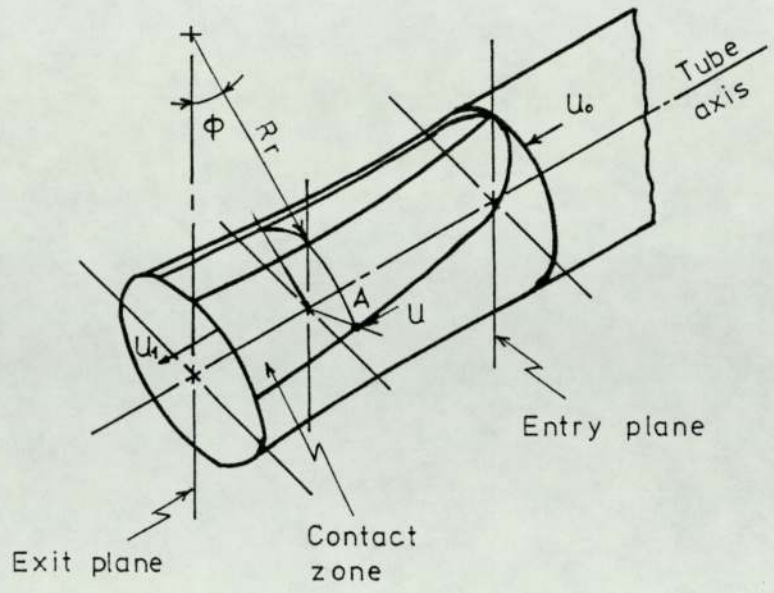

(a) Contact zone between tube and roll.

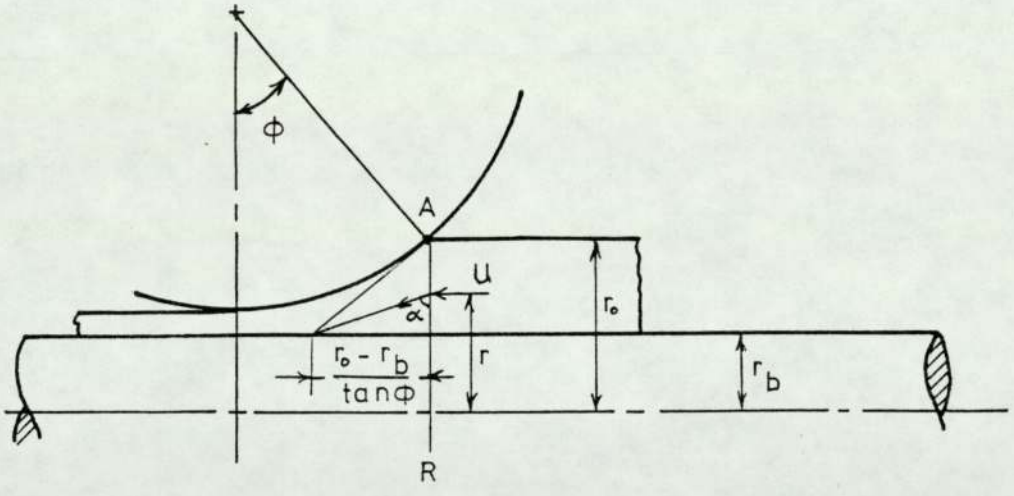

(b) Section passing through point A and tube axis.

Fig.(3 . 6) Determination of redundant work.

At entry, $\Phi = \Phi_m$, $\quad U = U_o$

$$U_o = U_1 - a\Phi_m \qquad \therefore\ a = \frac{U_1 - U_o}{\Phi_m} \tag{3.2.21}$$

From the volume constancy condition:

$$A_o U_o = A_1 U_1 = AU$$

or $$\frac{A_1}{A_o} = \frac{U_o}{U_1}$$

$$J = \text{reduction ratio} = \frac{A_o - A_1}{A_o}$$

$$= 1 - \frac{A_1}{Ao}$$

$$= 1 - \frac{U_o}{U_1}$$

$$U_1 = \frac{U_o}{1-J} \tag{3.2.22}$$

Substituting from (3.2.21) and (3.2.22) in (3.2.20):

$$U = \frac{U_o}{1-J} - \left[\frac{U_o}{1-J} - U_o\right] \frac{\Phi}{\Phi_m}$$

$$= \frac{U_o}{1-J} - \frac{U_o}{1-J}\,[J]\,\frac{\Phi}{\Phi_m}$$

$$U = \frac{U_o}{1-J}\left[1 - \frac{J\Phi}{\Phi_m}\right] \tag{3.2.23}$$

By taking a section passing through any contact point A lying on the curve at the edge of the deformation zone, and the tube axis, Figure (3.6), it can be put that the radial line AR is a line of velocity discontinuity. At any point on that line the velocity discontinuity ΔV is:

$$\Delta V = V \cos \alpha \tag{3.2.24}$$

Because of the volume constancy condition, the normal component of the velocity V must equal U.

$$V \sin\alpha = U \qquad \text{or} \qquad V = \frac{U}{\sin\alpha} \tag{3.2.25}$$

Substituting from (3.2.23) in (3.2.25)

$$V = \frac{U_o}{(1-J)\sin\alpha} \left[1 - \frac{J\phi}{\phi_m}\right] \tag{3.2.26}$$

The velocity discontinuity ΔV gives rise to shear within the deformed material. The maximum resistance to shear, τ, that the material can develop is found from von-Mises' yield criterion:

$$\tau = \frac{\sigma_y}{\sqrt{3}} \tag{3.2.27}$$

The redundant work per unit time is found by first integrating the shear stress times the velocity discontinuity over the line R and subsequently integrating from $\phi = 0$ to $\phi = \phi_m$ as follows:

$$\dot{W}_{r/\substack{\text{unit}\\\text{length}}} = \int_R \tau . \Delta V . dr \tag{3.2.28}$$

where $\dot{W}_r$ is the redundant work per unit time.

$$\dot{W}_{r/\substack{\text{unit}\\\text{length}}} = \int_{r_b}^{r_o} \frac{\sigma_y}{\sqrt{3}} \frac{U_o}{(1-J)\sin\alpha} \left[1 - \frac{J\phi}{\phi_m}\right] \cos\alpha . dr$$

where r_b is the radius of the mandrel.

Adopting the concept of a constant mean yield stress:

$$\dot{W}_{r/\substack{\text{unit}\\\text{length}}} = \frac{\bar{\sigma}_y}{\sqrt{3}} \cdot \frac{U_o}{1-J} \left[1 - \frac{J\phi}{\phi_m}\right] \int_{r_b}^{r_o} \frac{dr}{\tan\alpha}$$

From Figure (3.6):

$$\tan\alpha = \frac{r_o - r_b}{\tan\phi\,(r - r_b)}$$

$$\dot{\bar{W}}_{r/\substack{\text{unit}\\\text{length}}} = \frac{\bar{\sigma}_y}{\sqrt{3}} \frac{U_o}{1-J}\left[1 - \frac{J\phi}{\phi_m}\right] \int_{r_b}^{r_o} \frac{\tan\phi\,(r-r_b)}{r_o - r_b}\, dr$$

$$= \frac{\bar{\sigma}_y}{\sqrt{3}} \cdot \frac{U_o}{1-J}\left[1 - \frac{J\phi}{\phi_m}\right] \frac{\tan\phi}{(r_o-r_b)} \int_{r_b}^{r_o} (r-r_b)\,dr$$

$$= \frac{\bar{\sigma}_y}{\sqrt{3}} \cdot \frac{U_o}{1-J}\left[1 - \frac{J\phi}{\phi_m}\right] \frac{\tan\phi}{(r_o-r_b)} \left[\frac{r^2}{2} - r\, r_b\right]_{r_b}^{r_o}$$

$$= \frac{\bar{\sigma}_y}{\sqrt{3}} \cdot \frac{U_o}{1-J}\left[1 - \frac{J\phi}{\phi_m}\right] \frac{\tan\phi}{(r_o-r_b)} \left[\frac{r_o^2}{2} - r_o r_b - \frac{r_b^2}{2} + r_b^2\right]$$

$$= \frac{\bar{\sigma}_y}{\sqrt{3}} \frac{U_o}{1-J}\left[1 - \frac{J\phi}{\phi_m}\right] \frac{\tan\phi}{(r_o-r_b)} \left[\frac{r_o - r_b}{\sqrt{2}}\right]^2$$

$$= \frac{\bar{\sigma}_y}{\sqrt{3}} \frac{U_o}{1-J}\left[1 - \frac{J\phi}{\phi_m}\right] \frac{\tan\phi}{2}\,(r_o-r_b)$$

$$\dot{\bar{W}}_r = \int_o^{\phi_m} \frac{\bar{\sigma}_y}{\sqrt{3}} \frac{U_o}{1-J}\left[1 - \frac{J\phi}{\phi_m}\right] \frac{\tan\phi}{2}\,(r_o - r_b)\, R_r \cdot d\phi$$

$$\dot{\bar{W}}_r = \frac{\bar{\sigma}_y}{2\sqrt{3}} \frac{U_o}{1-J}\,(r_o-r_b).R_r \int_o^{\phi_m}\left[1 - \frac{J\phi}{\phi_m}\right]\tan\phi \cdot\, d\phi$$

If ϕ is considered to be small, then $\tan\phi \simeq \phi$

$$\dot{\bar{W}}_r = \frac{\bar{\sigma}_y}{2\sqrt{3}} \frac{U_o}{1-J}\,(r_o-r_b)\, R_r \int_o^{\phi_m} \left(\phi - \phi^2 \cdot \frac{J}{\phi_m}\right) d\phi$$

$$= \frac{\bar{\sigma}_y}{2\sqrt{3}} \cdot \frac{U_o}{1-J}\,(r_o-r_b) R_r \left[\frac{\phi^2}{2} - \frac{\phi^3}{3}\frac{J}{\phi_m}\right]_o^{\phi_m}$$

$$= \frac{\bar{\sigma}_y}{2\sqrt{3}} \frac{U_o}{1-J} (r_o - r_b) R_r \left[\frac{\Phi_m^2}{2} - \frac{\Phi_m^2}{3} J \right]$$

$$= \frac{\bar{\sigma}_y}{2\sqrt{3}} \frac{U_o}{1-J} (r_o - r_b) R_r \frac{\Phi_m^2}{6} [3 - 2J]$$

To obtain the redundant work per unit volume, the above expression is divided by the volume rolled per unit time $A_o U_o$:

$$\therefore \quad W_r = \frac{\bar{\sigma}_y}{12\sqrt{3}} \frac{(r_o - r_b)}{A_o(1-J)} \cdot R_r \cdot \Phi_m^2 (3-2J) \qquad (3.2.29)$$

Also it can be written that:

$$W_r = \varepsilon_{red.} \bar{\sigma}_y \qquad (3.2.30)$$

where $\varepsilon_{red.}$ is the redundant strain.

From equations (3.2.29) and (3.2.20)

$$\varepsilon_{red.} = \frac{(r_o - r_b)}{12\sqrt{3} A_o(1-J)} R_r \cdot \Phi_m^2 (3-2J) \qquad (3.2.31)$$

3.2.6 Work done against friction

It is found that, due to the complexity of the calculation of friction losses in any process, no exact mathematical relationships have yet been established between the shear stress τ at the surface of contact and the other variables in the process. However, two types of friction have been widely used for the approximate determination of friction losses in any process:

1. Coulomb friction in which the shear stress τ at the interface between two bodies is proportional to the pressure p between them. It is written in the form:

   $\tau = \mu p$

where μ is the coefficient of friction which is assumed in most cases to be constant for a given set of conditions between the two surfaces in contact.

2. Constant shear. The shear stress, in that case, at the surface of contact is assumed to be constant irrespective of the pressure on that surface and is related to the shear yield stress of the deformed material by:

$\tau = mk$

where k is the shear yield stress of the material at the surface of contact,

$k = \frac{\sigma_y}{\sqrt{3}}$ according to von-Mises yield criterion,

m is a friction factor which is taken as constant for a given set of conditions. For frictionless conditions, m = 0. For sticking friction, m = 1 since the maximum shear a material can withstand according to von-Mises yield criterion is $\sigma_y / \sqrt{3}$.

The second type of shear is particularly useful in the case of hot working of metals where sticking friction is known to exist and the assumption of Coulomb friction is thus not valid since it leads to an overestimation of the friction losses.

The concept of a constant shear stress at the surface of contact is adopted in the present calculations of friction losses. It should be emphasized that this concept of a constant shear stress is not realized in the actual rolling process since sticking friction does not prevail over the whole of the arc of contact and even in the case

of rolling lead tubes it has been reported previously (12) that sticking friction does not occur. This finding coupled with the fact that the pressure distribution round the groove is far from being uniform, makes the assumption of a constant shear stress unrealistic. However, since the energy method requires average pressures and not the actual distribution, the assumption of a uniform pressure and hence a constant shear stress at the contact surface is justified (also, the calculations of friction losses are made much easier by the adoption of a constant shear stress).

The work done against friction per unit time, $\dot{\bar{W}}_f$, is found by integration over the surface of contact S of the shear stress times the relative velocity between the two surfaces in contact:

$$\dot{\bar{W}}_f = \int_S \tau . V_r . dS \qquad (3.2.32)$$

where V_r is the relative velocity between the two surfaces in contact. The work done per unit volume of the deformed material is:

$$W_f = \frac{\dot{\bar{W}}_f}{A_o U_o} \qquad (3.2.33)$$

3.2.6.1 Work done against friction between tube and rolls W_{f_a}

From Figure (3.7), and at any angle of contact ϕ, the equation of the contact surface was obtained previously as:

$$x^2 + \left[b - (y^2 + z^2)^{\frac{1}{2}} \right]^2 = r_g^2 \qquad (3.2.8)$$

and $z = R_r \sin\phi$

The tube velocity at any angle ϕ is:

$$U = \frac{U_o}{1-J}\left[1 - \frac{J\phi}{\phi_m} \right] \qquad (3.2.23)$$

The tangential roll velocity $V = \omega R$, where ω is the angular velocity of the rolls.

The horizontal component of the tangential roll velocity is:

$$V_h = \omega y \qquad (3.2.34)$$

The relative velocity V_r between tube and roll is:

$$V_r = V_h - U$$
$$= \omega y - \frac{U_o}{1-J}\left[1 - \frac{J\phi}{\phi_m} \right] \qquad (3.2.35)$$

From (3.2.8), $y = \sqrt{\left[b - (r_g^2 - x^2)^{1/2} \right]^2 - z^2}$

From equation (3.2.13) the elemental length dL of the contact curve between tube and rolls is:

$$dL = \left\{ \frac{x^2 \left[1 + \frac{z^2}{\left[b - (r_g^2 - x^2)^{\frac{1}{2}} \right]^2 - z^2} \right]}{(r_g^2 - x^2)} + 1 \right\}^{\frac{1}{2}} dx \qquad (3.2.13)$$

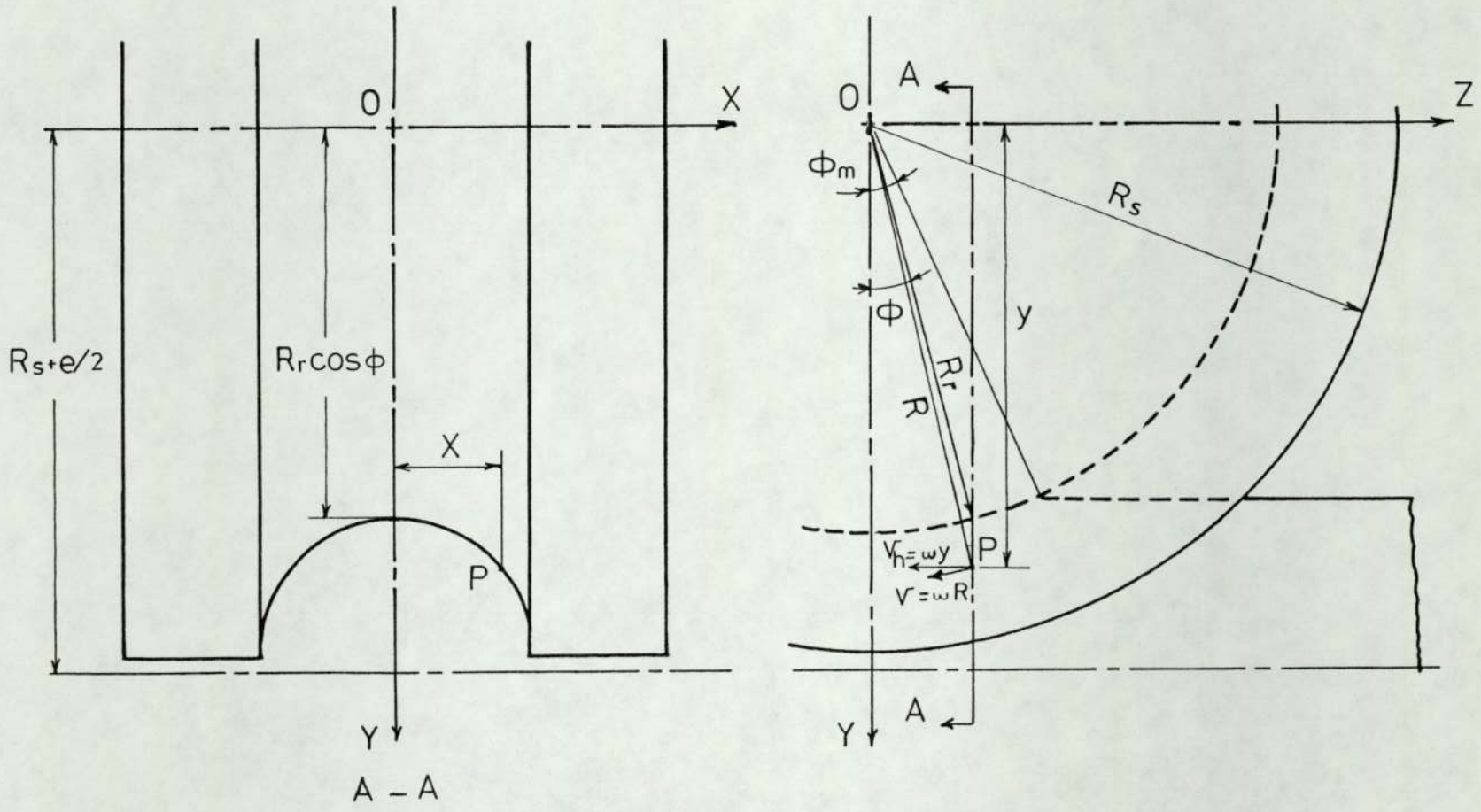

Fig.(3.7) Roll speed at any point on the groove surface

$$\dot{\bar{W}}_{f_a} = \int_S \tau . V_r . dS$$

where dS is the elemental surface area

$$dS = dL . R_r d\phi$$

$$\dot{\bar{W}}_{f_a} = \int_0^{\Phi_m} \int_0^{x_c} \left[\omega \sqrt{\left[b - (r_g^2 - x^2)^{\frac{1}{2}} \right]^2 - z^2} - \frac{U_o}{1-J}\left(1 - \frac{J\phi}{\Phi_m}\right) \right]$$

$$\left\{ \frac{x^2 \left[1 + \frac{z^2}{\left[b-(r_g^2 - x^2)^{\frac{1}{2}} \right]^2 - z^2} \right]}{r_g^2 - x^2} + 1 \right\}^{\frac{1}{2}} dx \, R_r d\phi \quad (3.2.36)$$

where x_c is the distance in the X-direction which corresponds to ψ_c.

The double integration in equation (3.2.36) is solved by numerical methods using a computer, see Appendix (A-1).

3.2.6.2 Work done against friction between tube and mandrel W_{f_b}

It will be assumed that the same peripheral contact angles ψ_c suspended between tube and rolls will apply also between tube and mandrel.

The work done against friction between tube and mandrel per unit time can be written as:

$$\dot{\bar{W}}_{f_b} = \int_S \tau . V_r . dS$$

where τ is the shear stress at the surface of contact, and is equal to $m \cdot \frac{\sigma_y}{\sqrt{3}}$ from von-Mises yield criterion,

V_r is the relative velocity between tube and mandrel.

Tube velocity at any angle of contact ϕ :

$$U = \frac{U_o}{1-J} \left(1 - \frac{J\Phi}{\Phi_m}\right)$$

Mandrel speed is constant throughout the whole of the deformation zone and is equal to V_b.

$$V_r = V_b - \frac{U_o}{1-J}\left[1 - \frac{J\Phi}{\Phi_m}\right] \qquad (3.2.37)$$

The elemental surface area is:

$$dS = r_b \cdot d\psi \cdot R_r \, d\phi$$

$$\dot{W}_{f_b} = \int_0^{\Phi_m} \int_0^{\psi_c} \tau \left[V_b - \frac{U_o}{1-J}\left(1 - \frac{J\Phi}{\Phi_m}\right)\right] r_b \cdot d\psi \cdot R_r \, d\phi \qquad (3.2.38)$$

The solution to that integration is obtained by approximate numerical methods using a computer, see Appendix (A-1).

The work done per unit volume, $W_{f_b} = \frac{\dot{W}_{f_b}}{A_o U_o}$ (3.2.39)

3.2.7 Work done by the applied front and back tensions

In a production mill where the tube is fed through several stands, tension is sometimes maintained in the tube between stands by changing the roll speeds. Such tension

has the advantage of reducing the pressure on the rolls and controlling the gauge size and uniformity. If front tension is applied, some power to help the rolls is associated with this tension. On the other hand, if back tension is appied, the roll power must increase to overcome the added resistance. Work done by the front tension per unit volume, W_a is:

$$W_a = \sigma_a \qquad (3.2.40)$$

Work done by the back tension per unit volume W_b is:

$$W_b = \sigma_b \qquad (3.2.41)$$

where σ_a and σ_b are the front and back applied stresses respectively.

3.2.8 Mean roll pressure p_m

Having estimated the total work done in deforming the tube, W_t, the mean roll pressure p_m can be calculated by equating W_t to the work done by the externally applied roll pressure.

The pressure distribution round the groove and along the arc of contact is assumed to be uniform.

Although this assumption does not describe the actual situation in the roll groove, it allows an easy assessment of the mean roll pressure p_m to be made without the need for very complicated mathematical expressions which render any obtainable solution to be impractical.

Since the tube inner surface is in contact with the mandrel during rolling, the inside pressure does not do

any work. For a close pass rolling, i.e. no gap between the tube inside and the mandrel before rolling, the outer uniform pressure p_m is responsible for changing the tube wall thickness from t_o before rolling to a mean thickness of t_1 after rolling.

The increment of work done by the mean uniform pressure p_m is equal to:

$$dW_e = p_m.S.dt$$

where S is the surface area of contact (or the contact area) and, dt is the change in tube wall thickness.
The total work done by the external roll pressure per unit volume is:

$$W_e = \int_{t_1}^{t_o} p_m.S.dt/V$$

where V is the volume of the rolled material

$$V = A_o.U_o.\frac{\Phi_m}{\omega}$$

$$W_e = p_m.S.\left[t\right]_{t_1}^{t_o} / V$$

$$= p_m.S.(t_o-t_1) \quad / V \qquad (3.2.42)$$

The surface area, S, has been determined in section (3.2.2).

$$W_e = W_h + W_r + W_f$$

3.2.9 Roll separating force, RSF

Multiplying the mean roll pressure p_m by the horizontal projection of the area of contact on each roll will give the roll separating force.

3.2.10 Rolling torque

The rolling torque can be estimated by considering the moment of the resultant vertical force , i.e. the RSF, about the roll axis. If the roll separating force is assumed to act at a distance (a) from the roll axis, the total rolling torque T_t can be written as:

$$T_t = 2Pa \qquad (3.2.43)$$

where P is the roll separating force.
This method, which is called the lever arm method, is an approximate method since it neglects the contribution of horizontal forces which deflect the resultant force slightly from the vertical. The distance (a) is determined by a method which will be mentioned in section (7.12), chapter (7).

3.2.11 New groove shapes

Two new groove shapes, Figure (3.8), are examined in the present investigation apart from the groove shape shown in Figure (3.4). It is not intended here to repeat the previous steps in determining the different components of the total work done per unit volume since it is sufficient to derive the equation of the groove surface and to

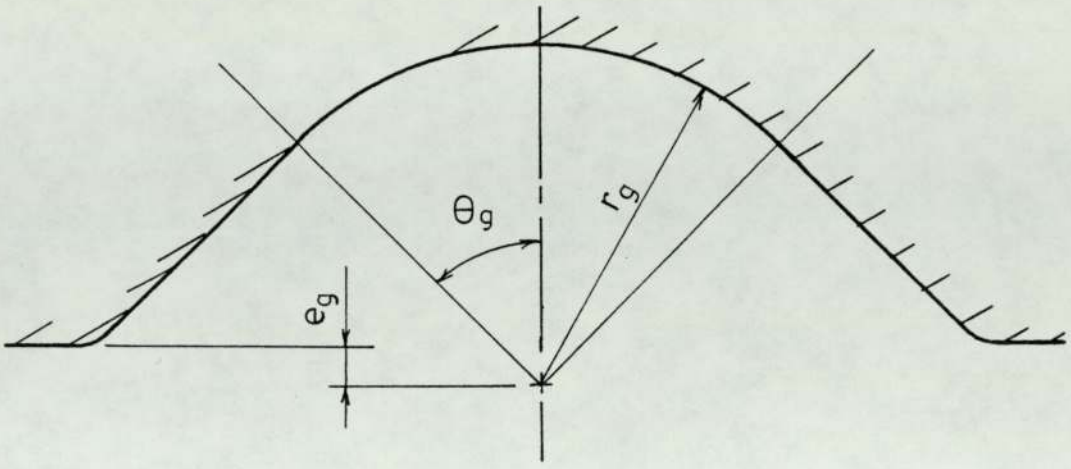

Groove (B)

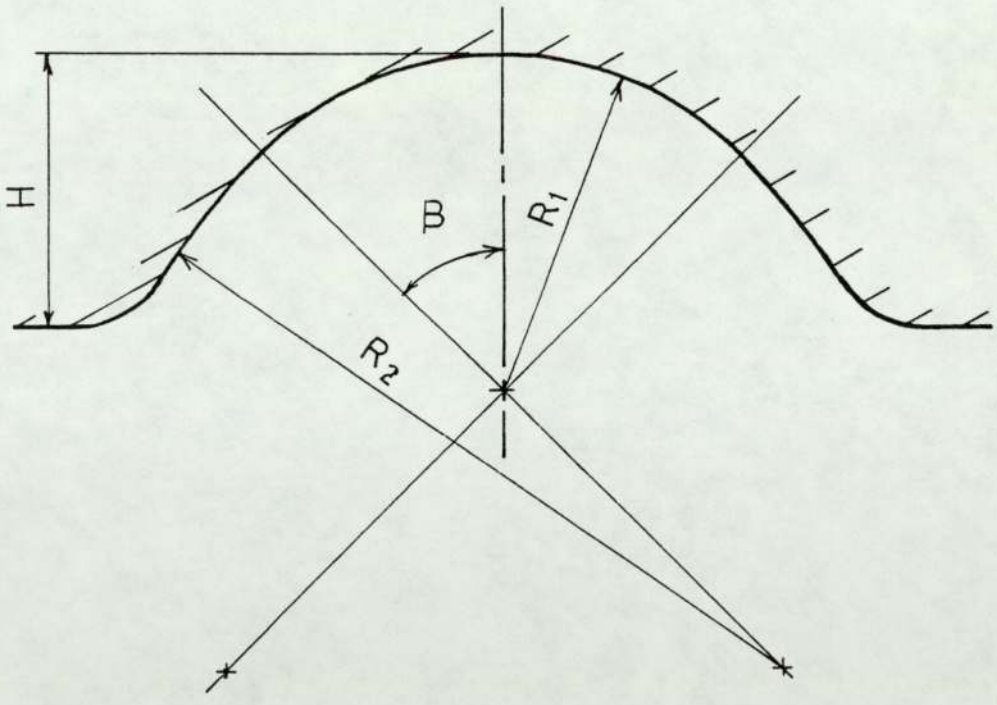

Groove (C)

Fig. (3.8) Groove shapes

obtain the peripheral angle of contact ψ_c at any contact angle ϕ. The rest of the calculations are included in a computer programme which can be found in Appendix (A).

3.2.11.1 Groove (B)

At any contact angle ϕ, the groove can be divided into two parts; a circular part from $\theta = 0$ to $\theta = \theta_g$ and a straight part for $\theta \geqslant \theta_g$. Or it can be written that the circular part extends from $X = 0$ to $X = r_g \sin\theta_g$ and the straight part extends for $X \geqslant r_g \sin\theta_g$, Figure (3.9).

For the circular part, the equation of the groove surface is the same as the equation for the previous groove shape, i.e.,

$$x^2 + [b - (y^2+z^2)^{\frac{1}{2}}]^2 = r_g^2 \qquad 0 \leqslant x \leqslant r_g \sin\theta_g \qquad (3.2.8)$$

$$z = R_r \sin\phi$$

$$y^2 + z^2 = R^2$$

Contact is assumed to start when the instantaneous groove radius is equal to the tube outer radius.

The peripheral angle of contact ψ_c at any angle of contact ϕ was obtained previously from equation (3.2.5),

$$(C^2 - r_o^2.F)\cos^2\psi_c - 2D.C.\cos\psi_c + (D^2 - r_g^2.F + r_o^2.F) = 0$$

$$x_c = r_o \sin\psi_c$$

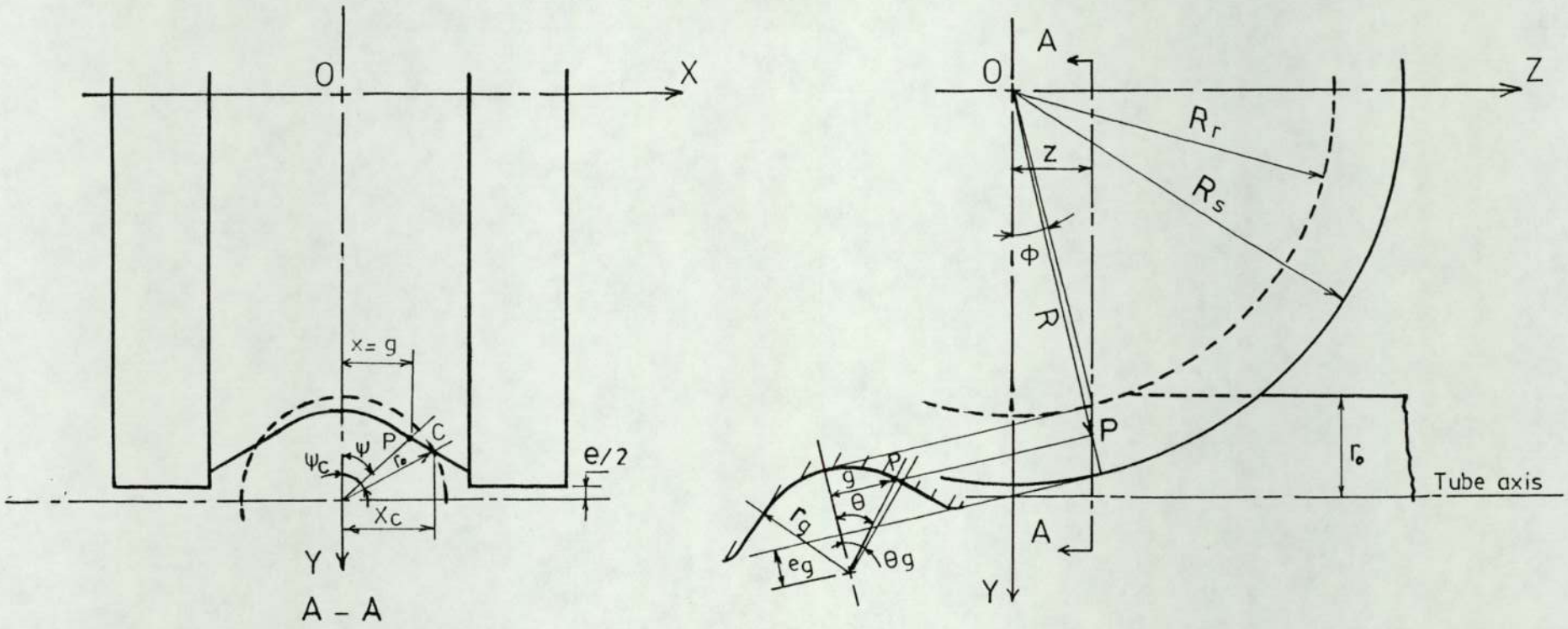

Fig.(3.9) Pass geometry in groove (B)

If $x_c > r_g \sin\theta_g$, the contact point must lie on the straight part of the groove and the calculation of the peripheral angle of contact has to be made using the equation of the groove surface for the straight part.

For the straight part, Figure (3.9):

$$y^2 + z^2 = R^2$$

$$z = R_r \sin\phi$$

$$g = x = r_g \sin\theta_g + [r_g \cos\theta_g - (R_s - R + e_g)] \tan\left(\frac{\pi}{2} - \theta_g\right)$$

$$x + [((R_s + e_g) - r_g \cos\theta_g) \tan\left(\frac{\pi}{2} - \theta_g\right) - r_g \sin\theta_g] =$$

$$R \tan\left(\frac{\pi}{2} - \theta_g\right)$$

putting $A = [((R_s + e_g) - r_g \cos\theta_g) \tan\left(\frac{\pi}{2} - \theta_g\right) - r_g \sin\theta_g]$

and $B = \tan\left(\frac{\pi}{2} - \theta_g\right)$

$$x + A = BR$$

$$x + A = B(y^2 + z^2)^{\frac{1}{2}} \qquad x \geq r_g \sin\theta_g \qquad (3.2.44)$$

Equation (3.2.44) is the equation of the groove surface for the straight part.

The contact point C is determined from the following equations:

$$x_c + A = BR_c$$

$$y_c^2 + z^2 = R_c^2$$

$$x_c^2 + (B_1 - y_c)^2 = r_o^2$$

where $B_1 = R_s + e/2$

The above three equations are solved simultaneously to

obtain the three unknowns x_c, y_c and R_c. Arranging the three equations in one equation containing any of the three variables will result in an equation of the fourth degree which can be solved using a computer.

3.2.11.2 Groove (C)

This type of groove corresponds to the actual shape found in a production mill. It is of the same shape as groove (B), but the straight outlet is substituted by a circular curve of radius R_2, Figure (3.10).

The groove is divided into two parts, a circular part of radius R_1 and another circular part of radius R_2.

For the first circular part, the equation of the groove surface is:

$$x^2 + \left[b - (y^2 + z^2)^{\frac{1}{2}} \right]^2 = R_1^2 \qquad 0 \leqslant x \leqslant R_1 \sin\beta \qquad (3.2.8)$$

$$z = R_r \sin\phi$$

$$y^2 + z^2 = R^2$$

$$b = R_s + e_g$$

The peripheral angle of contact ψ_c at any angle of contact ϕ is determined from equation (3.2.5),

$$(C^2 - r_o^2.F)\cos^2\psi_c - 2D.C.\cos\psi_c + (D^2 - r_g^2.F + r_o^2.F) = 0$$

$$x_c = r_o \sin\psi_c$$

If $x_c > R_1 \sin\beta$, the contact point must lie on the second circular part.

For the second circular part, Figure (3.10), it can be written:

$$g = x = R_2 \sin(\theta_1 + \beta) - (R_2 - R_1)\sin\beta$$

$$x + (R_2 - R_1)\sin\beta = R_2 \sin(\theta_1 + \beta)$$

$$[x + (R_2 - R_1)\sin\beta]^2 = R_2^2 \sin^2(\theta_1 + \beta)$$

$$= R_2^2[1 - \cos^2(\theta_1 + \beta)] \qquad (3.2.45)$$

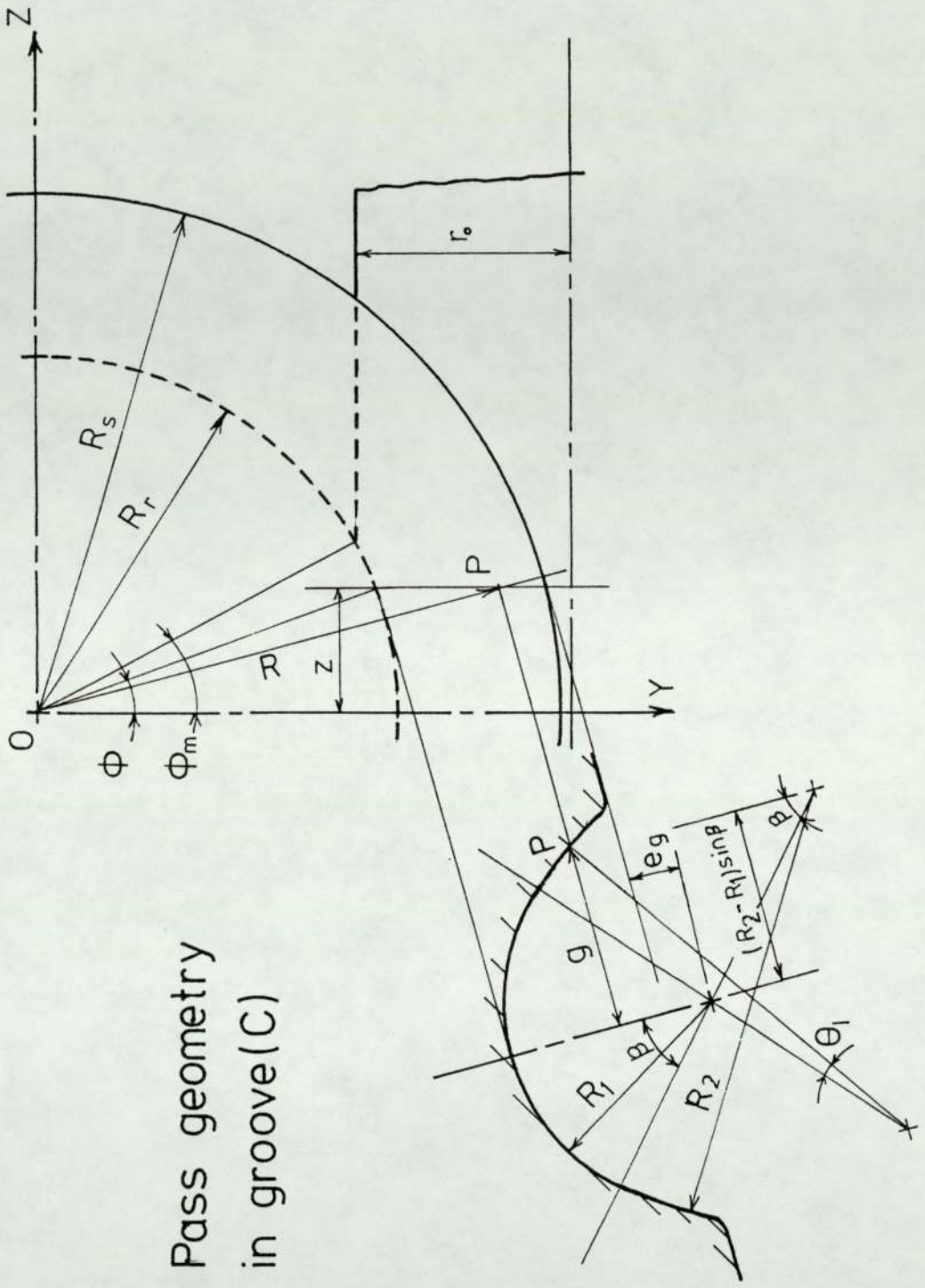

Fig.(3.10) Pass geometry in groove(C)

$$\cos(\theta_1 + \beta) = \frac{1}{R_2}[R_s + e_g - R + (R_2 - R_1)\cos\beta]$$

$$\cos^2(\theta_1 + \beta) = \frac{1}{R_2^2}[R_s + e_g + (R_2 - R_1)\cos\beta - R]^2$$

putting $A = (R_2 - R_1)\sin\beta$

and $B = R_s + e_g + (R_2 - R_1)\cos\beta$

$$\therefore \cos^2(\theta_1 + \beta) = \frac{(B - R)^2}{R_2^2} \qquad (3.2.46)$$

Substituting from (3.2.46) in (3.2.45):

$$(x + A)^2 = R_2^2\left[1 - \frac{(B-R)^2}{R_2^2}\right]$$

$$(x + A)^2 = R_2^2 - (B-R)^2$$

but $R^2 = y^2 + z^2$

$$\therefore (x + A)^2 + [B - (y^2 + z^2)^{\frac{1}{2}}]^2 = R_2^2 \qquad X \geqslant R_1 \sin \qquad (3.2.47)$$

Equation (3.2.47) is the equation of the groove surface for the second part of the groove.

The groove contact point C is determined from the following equations:

$$(x_c + A)^2 + (B - R_c)^2 = R_2^2$$

$$y_c^2 + z^2 = R_2^2$$

$$x_c^2 + (B_1 - y_c)^2 = r_o^2$$

where $B_1 = R_s + e/2$

Arranging the above three equations in one equation which contains any of the three variables x_c, y_c and R_c will result in an equation of the fourth degree which is solved by a computer, to obtain the contact point C at any angle of contact Φ .

3.3 Theoretical predictions of tube and mandrel speeds in a multi-stand mill

The calculations of tube and mandrel speeds follow closely the work by Pfeiffer (6). The presence of the mandrel inside the tube makes the velocity pattern in a multi-stand mill more difficult to analyse due to the interaction between roll, tube and mandrel speeds in any stand and to the fact that changing the velocity pattern in any stand affects the tube and mandrel speeds in all the stands. To understand clearly the velocity pattern which exists in a multi-stand production mill, only two stands are considered here, since the results from two stands can be generalized to include any number of stands.

From Figure (3.11), it is assumed that the tube velocity, U, in any stand adapts itself to a mean value between the peripheral roll speed, V_w, and the mandrel speed, V_b, according to the relationship.

$$U = \frac{V_w \mu_1 + V_b \mu_2}{\mu_1 + \mu_2} \qquad (3.3.1)$$

where V_w is the peripheral roll speed which corresponds to the roll working diameter.

μ_1 and μ_2 are the coefficients of friction between tube and rolls and between tube and mandrel respectively.

Since the mandrel is free to move in the horizontal direction, its velocity can be assumed to be a function of the forces acting upon it which are transmitted from the tube, the coefficients of friction between tube and mandrel in the various stands, and the tube speeds.

When the tube and mandrel enter stand 1, the outgoing tube and mandrel speeds can be assumed to be the same. On

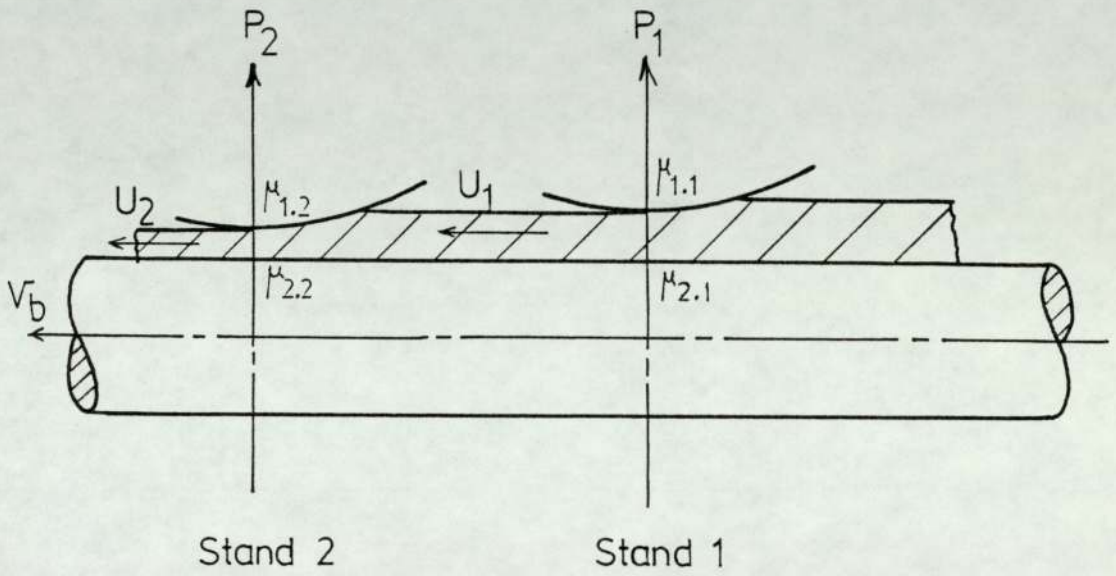

Fig.(3.11) Tube and mandrel speeds

entering stand 2, the mandrel speed is increased which affects the tube speed in stand 1. The change in tube speed in stand 1 causes a corresponding change in mandrel speed which in turn changes the tube speed in stand 2. This chain interaction between tube and mandrel speeds continues until steady state conditions have been attained and the mandrel moves at a speed which lies between the final tube speeds U_1 and U_2. At any instant, both stands will contribute to the mandrel velocity by amounts proportional to the roll force and coefficient of friction in each stand. The contribution of stand 1 to the mandrel speed, V_b, can be written as:

$$\frac{P_1 \mu_{2.1}}{P_1 \mu_{2.1} + P_2 \mu_{2.2}} U_1 ,$$

and the contribution of stand 2 is:

$$\frac{P_2 \mu_{2.2}}{P_1 \mu_{2.1} + P_2 \mu_{2.2}} U_2$$

where P_1 and P_2 are the roll forces in stands 1 and 2 respectively. The mandrel speed can be written as:

$$V_b = \frac{P_1 \mu_{2.1}}{P_1 \mu_{2.1} + P_2 \mu_{2.2}} U_1 + \frac{P_2 \mu_{2.2}}{P_1 \mu_{2.1} + P_2 \mu_{2.2}} U_2 \qquad (3.3.2)$$

If only stand 1 is gripping the tube, it is seen from equation (3.3.2) that the outgoing tube velocity equals the mandrel speed which conforms to the assumption made earlier in this section. Also, if the conditions in stands 1 and 2 are identical, i.e. the roll forces and coefficients of friction are the same in both stands, the mandrel speed takes a mean value between U_1 and U_2. To determine the final tube and mandrel speeds, successive calculations are carried out as follows:

First, V_b is calculated from equation (3.3.2) using the peripheral roll speeds V_{w_1} and V_{w_2} instead of U_1 and U_2 as a first approximation. Having calculated V_b, the tube speeds U_1 and U_2 can be determined from equation (3.3.1) and then substituted in equation (3.3.2) to obtain V_b again. The calculations are carried out until there is practically no change in tube and mandrel speeds. The calculations of tube and mandrel speeds in a multi-stand mill are made using a computer. The computer programme can be found in Appendix (A-7).

3.4 Rolling oval tubes in oval grooves

So far only the rolling of round tubes in oval grooves has been considered. Since in a production mill that situation is met only in the first stand while the remaining stands are rolling oval tubes, it is felt necessary to include the rolling of oval tubes in the theoretical treatment of the mandrel tube rolling process. The treatment of that subject is neglected in other works on tube rolling.

Only the groove shape shown in Figure (3.12) will be examined here and the other two shapes are included in the computer programmes found in Appendix (A).

The equation of the tube outer surface before rolling should be known from a knowledge of the previous groove shape which it had passed through. The tube outer surface can be divided into two parts; the part which was in contact with the previous groove surface and a free part which is assumed to be circular of radius r_1 and extends from $\psi = 0$ to $\psi = \alpha$, Figure (3.12).

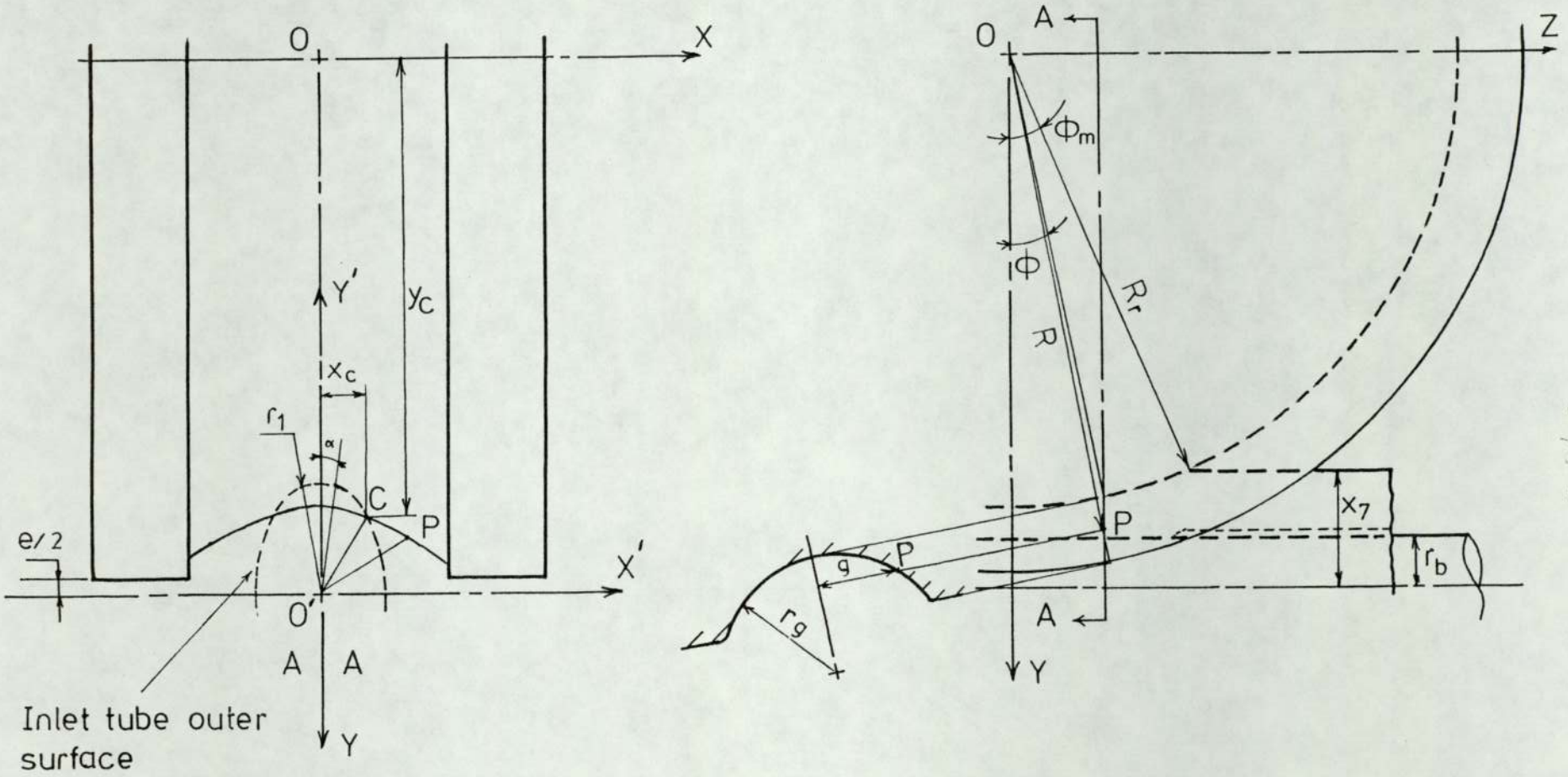

Fig.(3.12) Rolling oval tubes

With respect to the OX and OY axes, the equation of the circular part can be written as:

$$x^2 + (B_2 - y)^2 = r_1^2 \qquad 0 \leqslant x \leqslant r_1 \sin\alpha \qquad (3.4.1)$$

where $B_2 = R_s + e/2$

It should be noted that the axes of the present groove are set at right angles to the previous groove axes, or it can be said that the tube is rotated through a 90° angle. Since the tube axes are not transferred but are rotated, it is better to write the equation of the part, which was in contact with the previous groove surface, with respect to the tube axes O'X' and O'Y' and then change the old X' dimension with the new Y' dimension and visa versa to account for the rotation of the tube axes. Finally, the O'X' and O'Y' axes are transferred back to the new OX and OY axes as shown in Figure (3.12), since the equation of the groove surface is written with respect to the OX and OY axes.

The equation of the tube outer surface as it emerges from the previous groove is:

$$x^2 + (b-y)^2 = r_g^2 \qquad (3.4.2)$$

where $b = R_s + e_g$

Transferring the axes to O'X' and O'Y', equation (3.4.2) becomes:

$$x'^2 + [b - (R_s + e_1/2 - y')]^2 = r_g^2$$

where $y = (R_s + e_1/2 - y')$

and e_1 is the roll gap in the previous groove.

$$x'^2 + [R_s + e_g - R_s - e_1/2 + y']^2 = r_g^2$$

putting $B_1 = e_g - e_1/2$

$\therefore\ x'^2 + [y' + B_1]^2 = r_g^2$

Changing the X' dimension to the Y' dimension and vice versa,

$$y'^2 + [x' + B_1]^2 = r_g^2$$

Transferring the axes to OX and OY:

$$[R_s + e/2 - y]^2 + [x + B_1]^2 = r_g^2$$

Putting $B_2 = R_s + e/2$, the equation of the tube outer surface becomes:

$$[x + B_1]^2 + [B_2 - y]^2 = r_g^2 \qquad x \geqslant r_1 \sin\alpha \qquad (3.4.3)$$

The equation of the groove surface remains as:

$$x^2 + \left[b - (y^2 + z^2)^{\frac{1}{2}}\right]^2 = r_g^2 \qquad (3.2.8)$$

where $z = R_r \sin\phi$

From Figure (3.12) at any angle of contact ϕ, the contact point C between the groove and tube surface is determined by solving simultaneously either equations (3.4.1) and (3.2.8) or equations (3.4.3) and (3.2.8) Using equation (3.4.3) or equation (3.4.1) depends on whether X_c is greater than or less than $r_1 \sin\alpha$. Having calculated the coordinates of the contact point C, the corresponding peripheral angle of contact ψ_c at any angle of contact ϕ can be obtained. The angle of contact, ϕ, at which contact starts between the tube inside and the mandrel can be found from the following equation:

$$R_r \cos\phi = R_r \cos\phi_m + (X_7 - r_b) \qquad (3.4.4)$$

After the start of contact between the tube inside and the mandrel, the peripheral angle of contact ψ_c suspended between the tube and rolls at any contact angle ϕ, will be

assumed to apply also between the internal tube surface and the mandrel.

The deformation of the tube from the start of contact between the tube and rolls until the tube inside touches the mandrel will be considered as a sinking process followed by the mandrel rolling process.

Once the surfaces of contact between tube and rolls and between tube and mandrel are determined, the rest of the calculations of the total work done per unit volume can be performed as previously outlined.

CHAPTER (4)

EXPERIMENTAL ARRANGEMENT AND MEASURING EQUIPMENT

4.1 Experimental roll stand

The rolling trials were performed in a single stand experimental mill which was used previously in the investigations by Cole (11) and Haleem (12). The rolling stand was made by modifying an old milling machine for the purpose of rolling tubes, as shown in Figure (4.1) and plate (4.1). A removable upper shaft, for reasons of facilitating the calibration of pin-loadcells which were situated in the top roll, was connected to the original milling machine arbor by a cylindrical coupling. The coupling served also as the upper torquemeter. Since the lower shaft was suspended from the upper shaft by two loadcells, the roll gap could be altered by the adjustment of the screws holding the loadcells to the upper shaft. The lower shaft was driven by the upper shaft at the same rotational speed through a pair of helical gears, and in order not to affect the distance between the two gears when altering the roll gap, the lower shaft was made of two parts connected together by a flexible coupling. The coupling permitted the part of the shaft supporting the bottom roll to be moved in the vertical direction, to alter the roll gap, without changing the distance between the driving and driven gears.

4.2 Rolls and groove shapes

The same rolls used by Haleem in his investigation (12) were used also in the first part of the present work. The rolls were manufactured from steel EN24, but were not heat treated due to the relatively small rolling loads encountered in rolling lead tubes. The radius of the roll at the root of the groove was 94.55mm while at the shroud it was 113.45mm.

Two groove shapes were examined. The first shape was of the single radius oval type, Figure (4.2a) , and can be

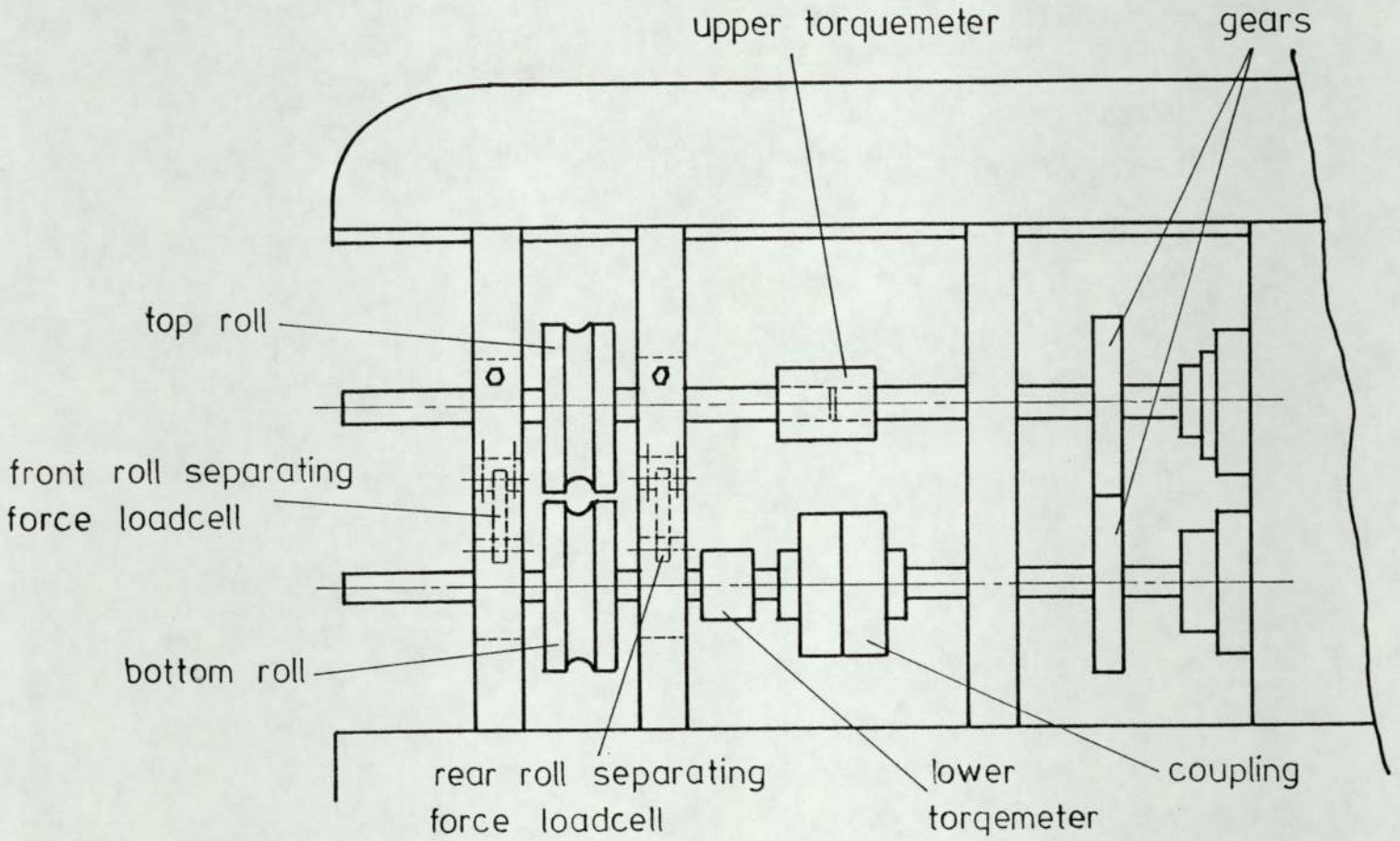

Fig.(4.1) General Assembly of the Rolling Stand

Plate (4.1)

General view of
the rolling stand

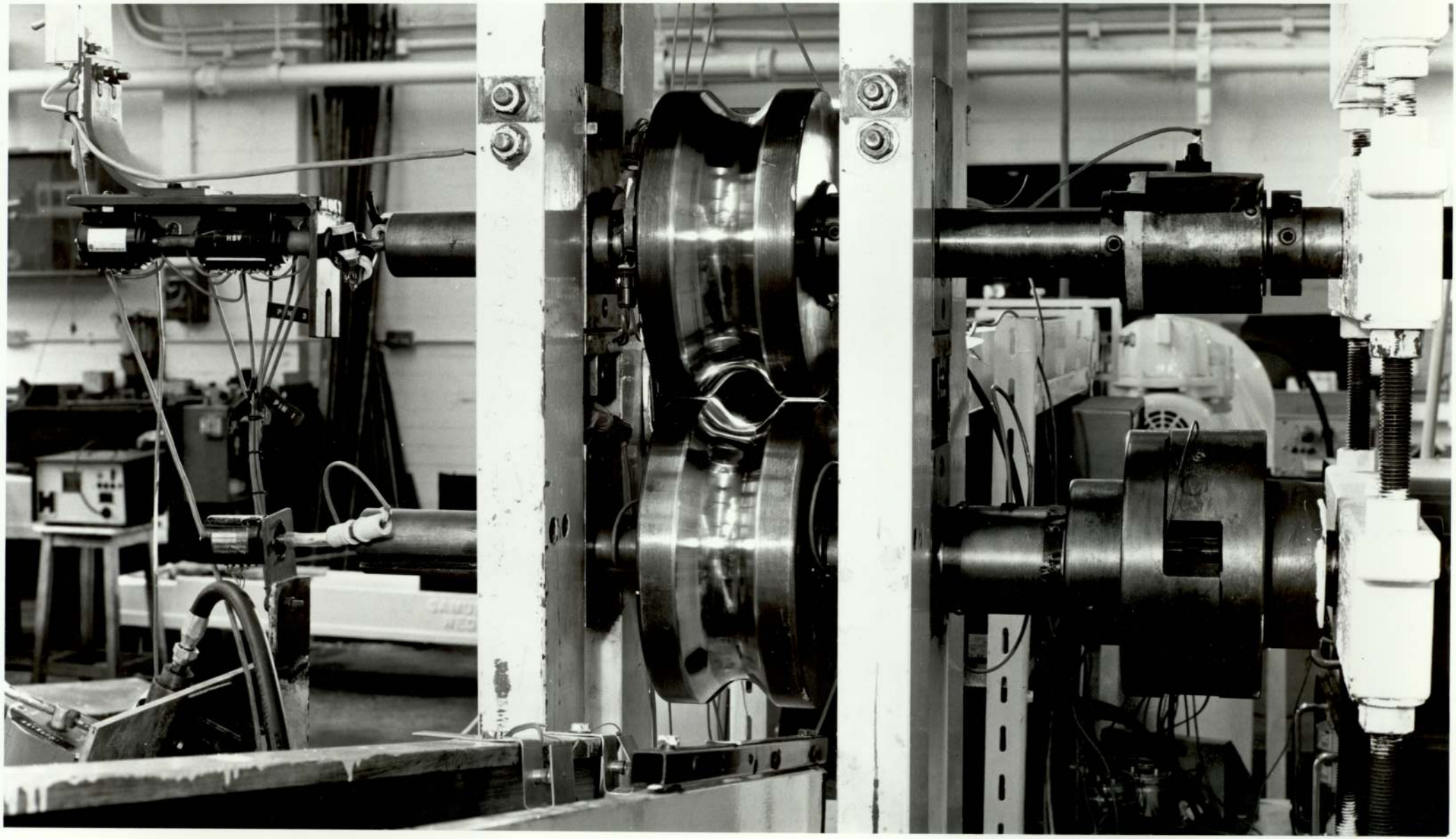

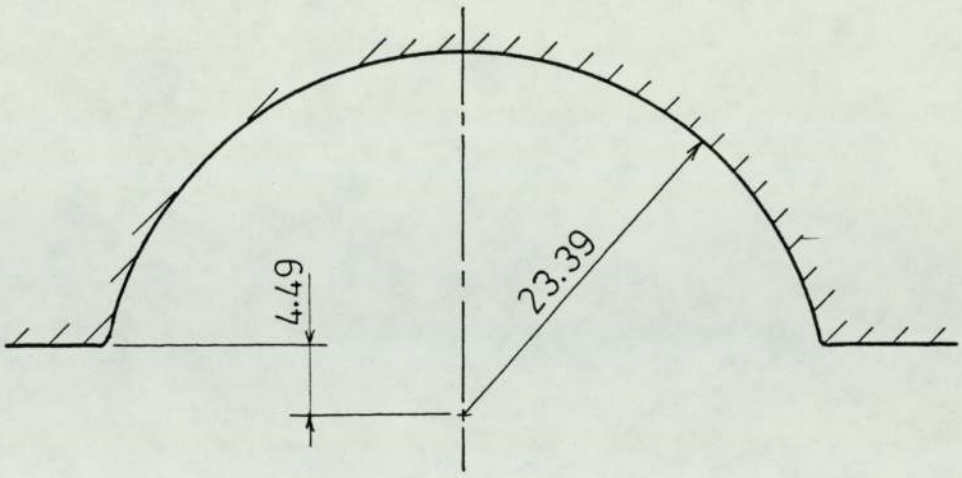

(a) Geometry of groove(A)

All dimensions in mm

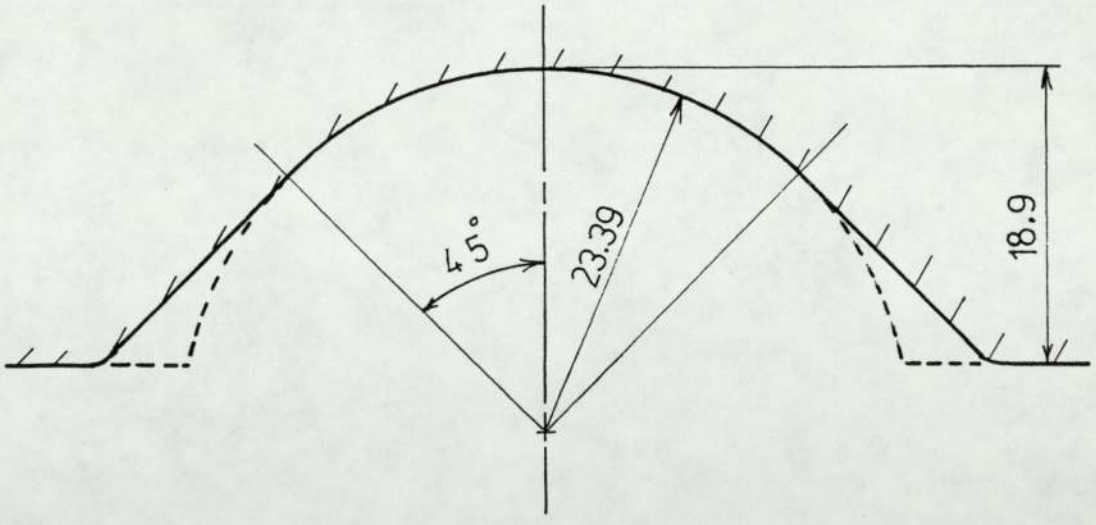

(b) Geometry of groove(B)

Fig.(4.2) Groove dimensions

considered as representing one of the later stands in a production mill. The second groove had the shape shown in Figure (4.2b) and was formed by machining the original rolls to that shape. The diameter of the roll at the root of the groove and at the shroud was kept similar to the first groove. Impressions using Plasticine¥ were made of the groove at different positions in the two rolls to check the groove dimensions and ensure that the groove shapes in the top and bottom rolls were similar.

4.3 Front and back tension devices

The front tension device, plate (4.2) consisted of a drum connected to an electric motor through a variable speed gearbox. One end of a wire rope was attached to the drum, while the other end was connected to a carriage which could slide inside two channel sections. The front end of the tube, after passing through the roll groove, was fixed to the carriage through a tension loadcell. By the adjustment of the rotational speed of the gearbox shaft so that the drum peripheral speed, and hence the rope speed was higher than the tube exit speed, front tension could be generated in the tube. The front tension could be altered by changing the rotational speed of the gearbox shaft. A helical slot was machined on the drum surface to keep the

¥ Plasticine is formed by mixing together Acrulite-Microtech powder and liquid. At first the mixture is in the liquid state so that it can be poured to take the shape of the groove. After a short time, the mixture solidifies giving an impression of the groove shape.

Plate (4.2)

View of the rolling stand showing
the front tension device

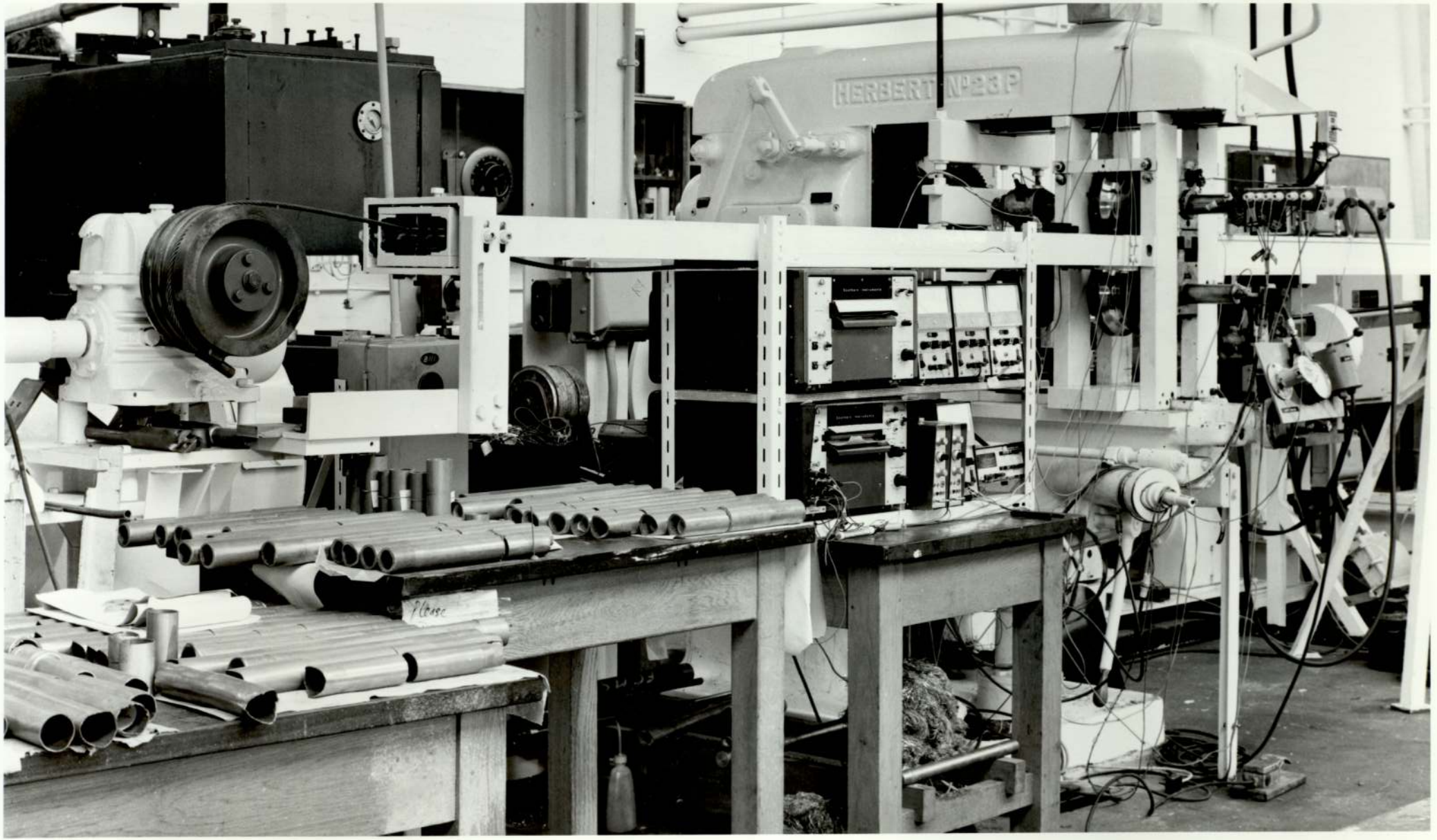
HERBERT N°23 P

peripheral rope speed constant. Both the motor on/off foot switch and the gearbox speed regulator knob were conveniently situated in front of the roll stand. The back tension was applied by creating a braking force between a moving carriage connected to the end of the tube and a stationary surface. The carriage carried an automobile brake cylinder with two friction pads fixed to the two pistons in the brake cylinder. The carriage could move in a channel section which acted at the same time as the stationary surface against which the braking force was applied. The oil pressure acting on the two slave pistons was supplied by a piston in the master cylinder which in turn was acted upon by an L-shaped lever carrying a weight. By changing the position of the weight on the lever arm, the force on the piston in the master cylinder can be altered and this consequently varied the pressure on the friction pads and the value of the braking force between the carriage and the stationary channel section surface. To change the position of the weight smoothly on the lever, an electric motor was used to rotate a threaded rod passing through the weight. The tube ends were fixed to the front and back tension devices through two similar gripping attachments. Each gripping attachment consisted of a collar with two serrated jaws which were screwed down on to the outside of the tube. The two attachments were connected to the front and back tension loadcells.

4.4 Measuring equipment

During the rolling trials, measurements were made of the roll separating force, rolling torque, pressure

distribution round the groove, front and back tensions and tube and mandrel velocities.

The loadcells used in the previous investigation (12) were checked and when found to be in good working order were used in the present work.

The roll separating force was measured by means of the two loadcells which held the bottom shaft to the top shaft. The design of the loadcell can be seen in Figure (4.3). Eight foil strain gauges connected in a bridge circuit were mounted on the two faces of the loadcell.

The torques on the top and bottom shafts were measured by means of four standard 45^{o} electrical resistance torque gauges connected in a bridge circuit. In the case of the top torquemeter, the torque gauges were bonded round the cylindrical coupling which connected the removable part of the top shaft to the fixed part, Figure (4.1). The torque gauges in the bottom torquemeter were bonded directly to the shaft itself, Figure (4.1).

The design of the front and back tension loadcells can be seen in Figure (4.4). Eight linear foil strain gauges were mounted on each loadcell and connected in a bridge circuit to give the maximum sensitivity to the axial load together with temperature correction and insensitivity to bending stresses.

Four pin-loadcells in the top roll were used to measure the pressure distribution round the groove perimeter and along the arc of contact. Four pins were used to transmit the radial pressure exerted by the tube on the roll to four cantilever type transducers [5], Figure (4.5). The pins were located radially in the top roll at planes making 0^{o},

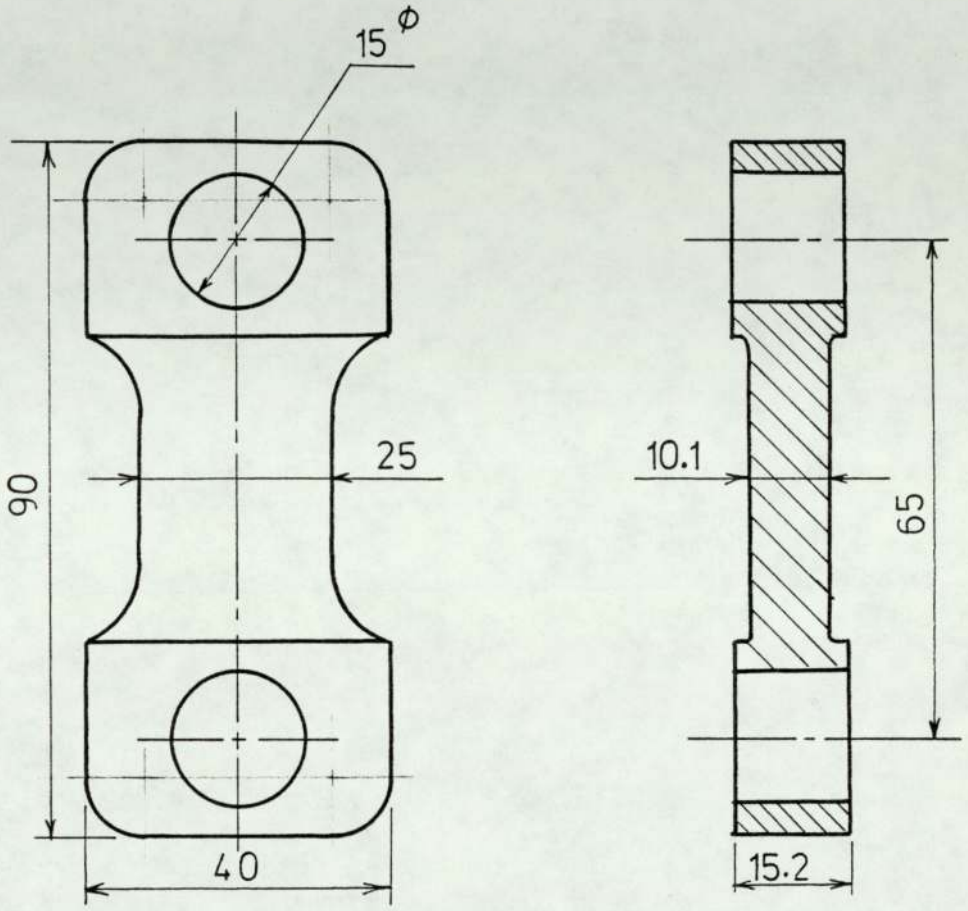

All dimensions in mm

Fig.(4.3) RSF loadcell

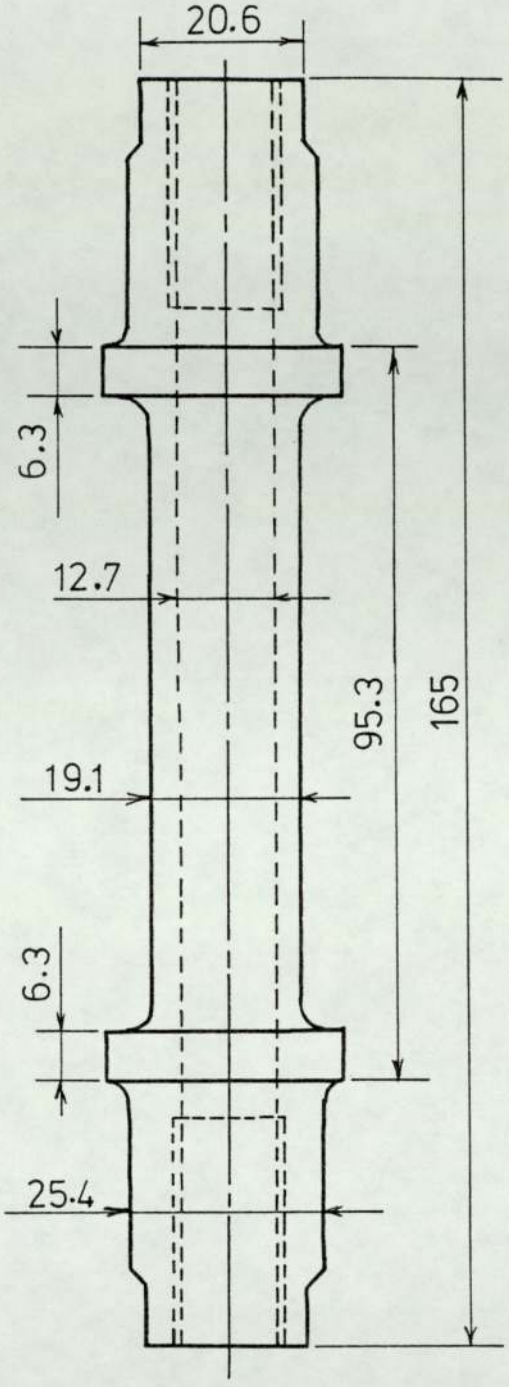

All dimensions in mm

Fig.(4 . 4) Tension loadcell

Figure (4.5)

Pin-loadcells

(From Haleem and Sansome (21))

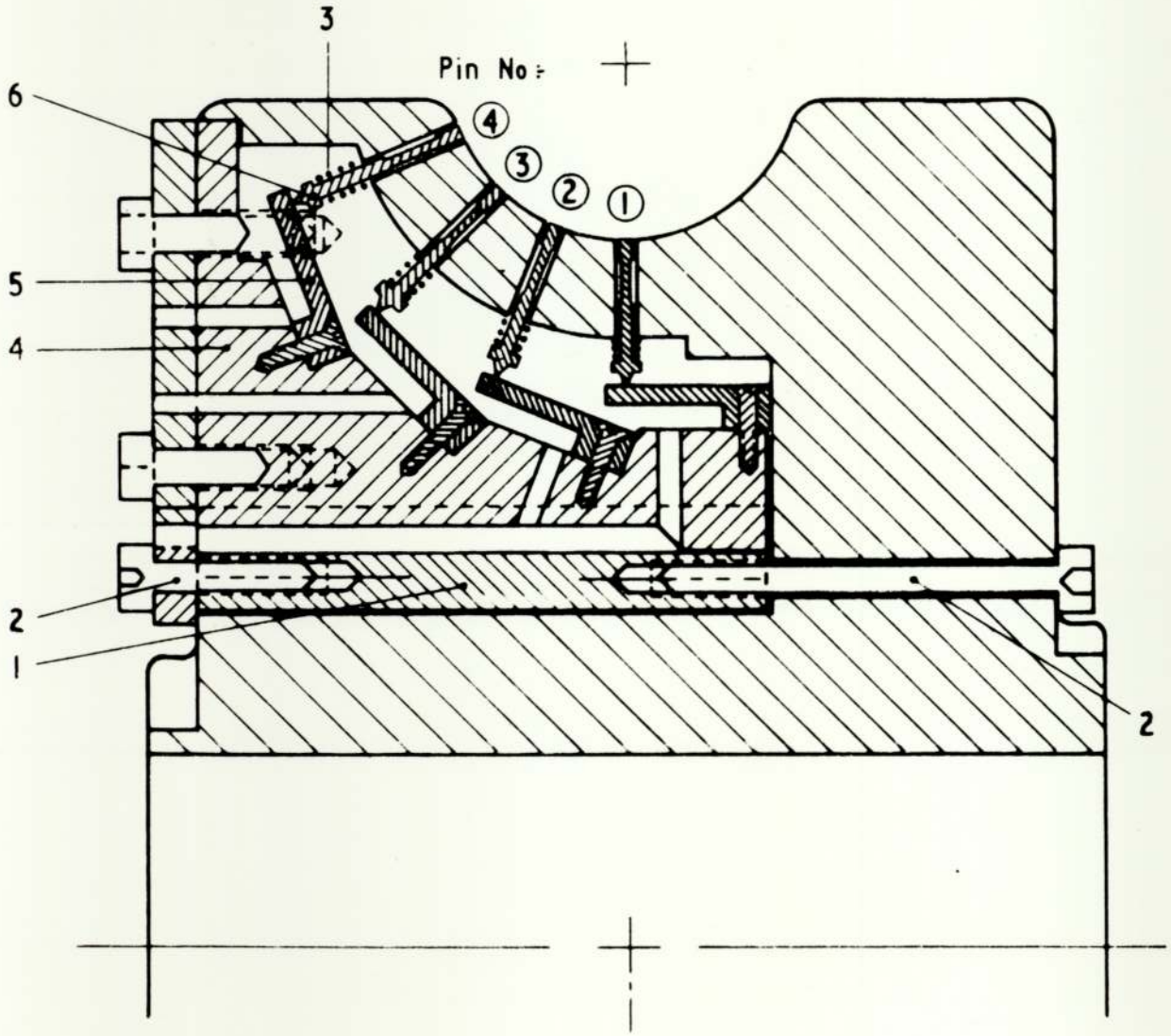

a) Assembly

b) Pressure Transmitting Pin

22.5°, 45° and 67.5° with the root of the groove. Four strain gauges connected in a bridge circuit were mounted on each cantilever.

The transducer assembly for the four loadcells was made as one unit, as shown in Figure (4.5), which facilitated removal of the loadcells for inspection without removing the upper roll. This facility is essential since in rolling, metal is extruded in the annular clearance between the pin and the orifice which necessitates regular removal and inspection of the loadcells in order not to affect the pin loadcells results. The pin itself was designed to accommodate provisionally any back-extruded fragments of metal. This was achieved by designing the pin with a relief which provided an enlarged clearance between the pin and the orifice. Any burr could be accommodated in that clearance without disturbing the performance of the pin-loadcell.

Although making the transducer assembly for the four loadcells as one unit facilitated removal of the loadcells, difficulty was experienced in adjusting the individual pin heights above the roll surface since the pins were acting against one assembly for the loadcells. It took some time to adjust each pin protrusion by the system made for that purpose. The system consisted of two tapered bolts [2] and a supporting block [1] with split ends, see Figure (4.5). By turning either or both of the two tapered bolts [2], together with the adjustment of the tightness of the fixing bolts [10], it was found possible, after some effort, to adjust one pin height without disturbing the setting of the other pins significantly. Tests carried out by Smith et al (18) and Haleem (12) showed that pin protrusion of up to 25 μm did not affect the pin-loadcells results significantly.

But the results were affected if the pin was recessed below the roll surface.

The inlet and outlet tube speeds as well as the mandrel speed were determined by means of photo-electric cells. Two photo-electric cells at a known distance from each other were employed on the entry side and another two on the exit side of the roll stand. In the first rolling tests, only the tube inlet and outlet speeds were measured. Light falling on the exit side photo-electric cells was intersected by the tube front end so that two signals were provided on the UV recorder sensitive paper. By measuring the distance between the two signals, and from a knowledge of the UV recorder paper speed, which was constant, and the actual distance between the two photo-electric cells, the speed of the front end of the tube, or the outlet speed, could be determined. The two photo-electric cells on the entry side of the roll stand were activated by the rear edge of the tube, so that the tube inlet speed could be determined by the above mentioned method. However, the presence of the mandrel inside the tube meant that only the top part of the tube rear edge could be used to intersect the light falling on the photo-electric cells. This presented a problem as the tube did not remain completely horizontal as it travelled through the roll gap and consequently the tube rear end moved up and down by very small amounts. The intersection of light falling on the photo-electric cells by the tube rear edge was spoiled by such small movements and the tube inlet speed could not be measured by this method.

In later rolling tests, tube and mandrel speeds were determined using a slightly different method. Light falling on the photo-electric cells was intersected by three small pins fixed by adhesives on the tube start, tube end and the mandrel. When any of the three pins intersected the light falling on one photo-electric cell, a signal was provided on the UV recorder sensitive paper. By measuring the distance between two consecutive signals provided by the same pin and from a knowledge of the UV recorder paper speed and the actual distance between the two photo-electric cells, the velocity of the pin, and hence the velocity of the part to which it was fixed, could be determined. The use of the small pins did not have any effect on the tube or mandrel speed or on any of the rolling conditions.

When front or back tension was applied to the tube, the light source was fixed to the carriage to which the tube start or end was attached. The light source activated the two photo-electric cells as it travelled with the carriage and provided two signals on the UV recorder paper. Following the previous procedure, the carriage speed could be determined.

4.5 Mandrel sizes

Two mandrel sizes were used throughout the experiments, 31.38 mm and 37.6 mm. The mandrels were machined from mild steel bars and finally were ground finished to the required size, all parallel. In the same mandrel size group, one mandrel was used for all the experiments which ensured that the same frictional conditions existed between the mandrel and tube throughout the tests.

To achieve higher friction forces between tube and mandrel in some of the experiments, a 3.76 mm diameter mandrel was prepared with a groove machined along its surface.

4.6 Tube Preparation

Lead was selected in the rolling tests as an analogue material for hot steel. Lead, which is hot worked at room temperature, has the further advantage of being able to deform at lower stresses than hot steel and this assisted in reducing the mill loads. The use of lead as a model material will be discussed in more detail later on.

From the start of the present investigation, it was difficult to obtain lead tubes, especially thin walled tubes which were used in the rolling tests. Since the introduction of copper tubes for domestic plumbing, demand for lead tubes has decreased considerably so that fewer companies are manufacturing lead tubes and they tend to manufacture thick walled tubes. The quality of the tubes was not good enough for research work; by quality is meant tube straightness, dimensional accuracy and eccentricity. The poor quality of the tubes was demonstrated when a small quantity of tubes, 1.75 in. outer diameter and 1.25 in. inner diameter, was ordered from a company. It was found that the tubes supplied, apart from possessing a certain degree of eccentricity, were not straight and it was extremely difficult to place the mandrel inside the tube without first straightening it.

Due to the difficulty experienced in obtaining thin walled tubes and the fact that the quality of the available tubes was poor for research work, it was decided to

manufacture lead tubes in the laboratory. This also ensured the homogeneity of the test tubes before rolling.

Pure lead was melted to form a billet which was extruded over a long mandrel to produce a tube of about one metre in length. The extrusion unit, which was designed and manufactured in the university, is shown in Figure (4.6). The unit was attached to the fixed and moving heads of a Denison testing machine which provided the pressing force necessary for extrusion.

Two tube sizes were extruded, 44.45 mm outer diameter and 31.75 mm inner diameter tube, and 44.45 mm and 38.1 mm outer and inner diameter tube.

It was inevitable that the extruded tubes would possess some degree of eccentricity since it was impossible to position the mandrel, which was fixed to the ram, and the die so that their centres coincided exactly with each other during extrusion. To overcome the problem of eccentricity in the unrolled tubes, the following procedure was adopted. Lead tubes, in the as-extruded form, were drawn on a mandrel through a ring die and then turned in a lathe to the required size. Plate (4.3) shows a lead billet and two tubes after the drawing process. The mandrel which was used in drawing was used also in rolling and this procedure therefore eliminated eccentricity and ensured a close pass tube rolling process. Lead tubes with diameter to thickness ratios, (d/t), of 7.9, 8.5, 9 & 10 were rolled on the same mandrel having a diameter of 31.38 mm. Thinner walled tubes with d/t ratios of 24 and 30.4, were rolled on a 37.6 mm mandrel.

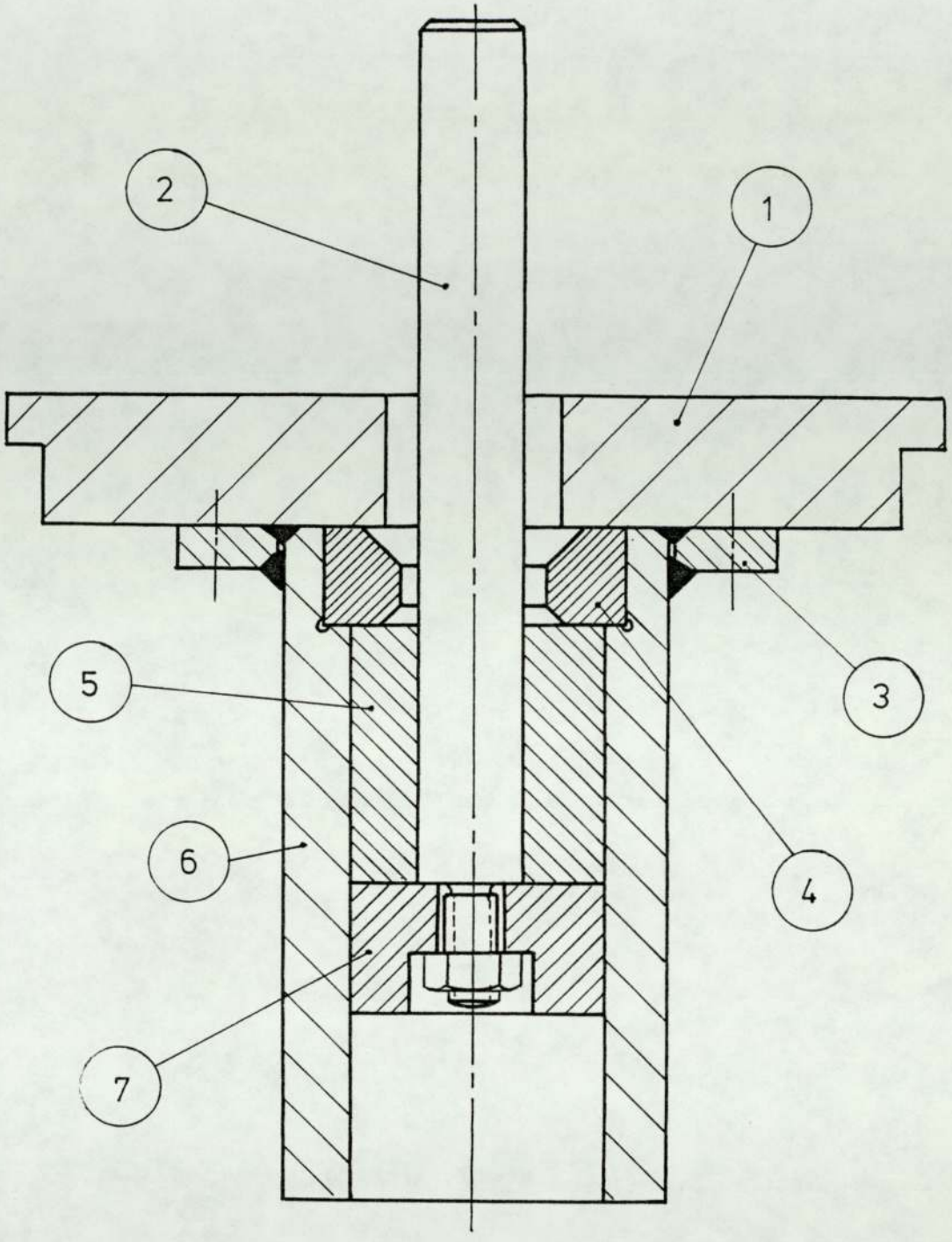

Fig.(4 . 6) Tube extrusion attachment

No.	Description
1	Press plate
2	Mandrel
3	Flange
4	Die
5	Lead billet
6	Container
7	Ram

Plate (4.3)

Lead billet and tubes
after the drawing process

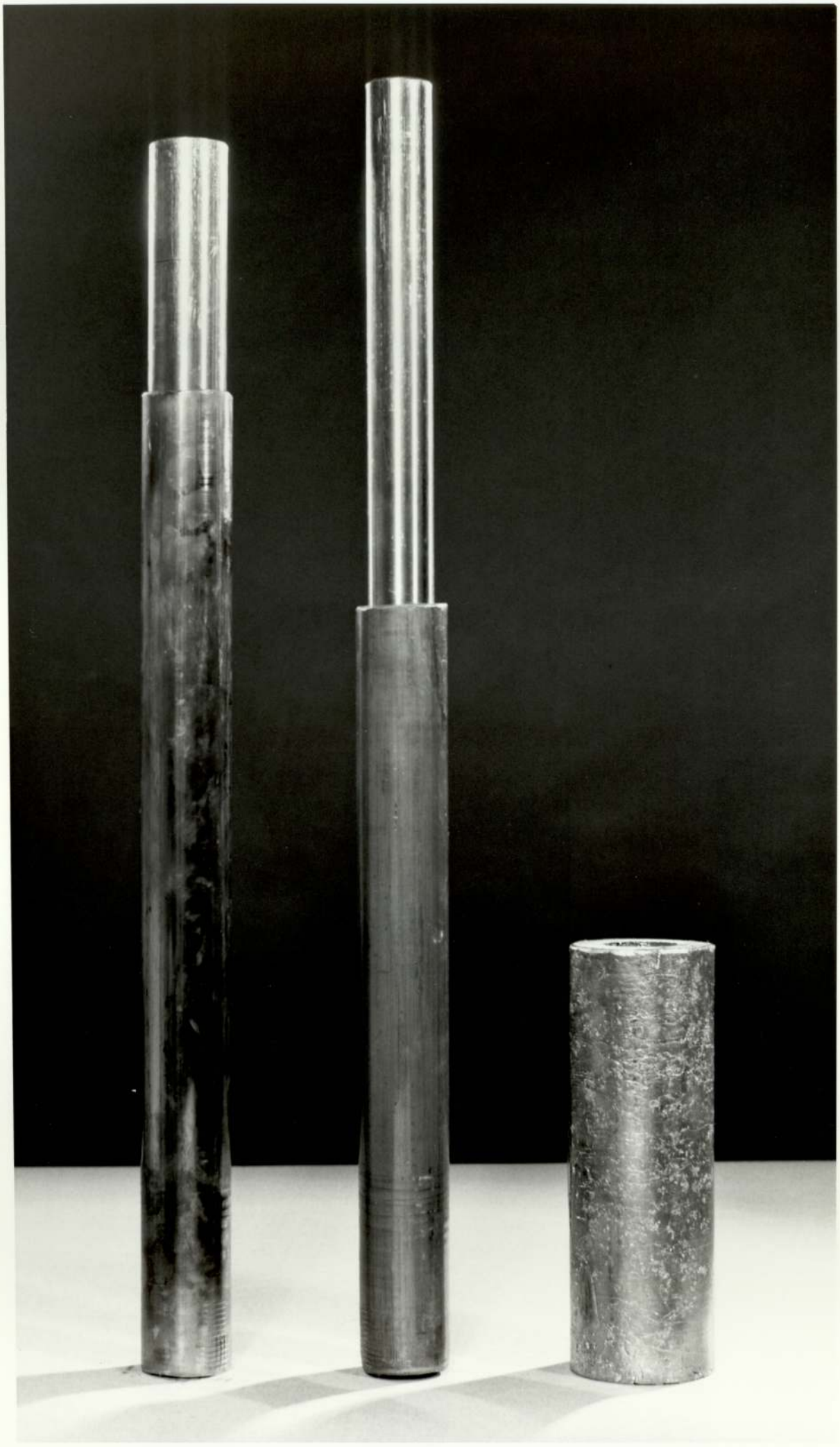

4.7 The use of lead as a model material

It was impossible to use hot steel in the present rolling tests due to the limited capacity of the experimental mill and it was difficult to heat and maintain the tube temperature at a constant level during rolling. Therefore a model material was required which should satisfy the following conditions:

1. simulates as closely as possible the stress-strain characteristics of the hot steel used in the production mill, i.e. a material which has a stress-strain curve of the same shape as steel,
2. deforms under lower stresses than hot steel - to minimize the rolling loads.

Lead is a typical model material which has been frequently used to simulate the behaviour of hot steel since it is hot worked at room temperature and deforms at low stresses.

Loizou and Sims (19) carried out a full experimental investigation of the properties of pure lead as a model material. They determined the yield stress of pure lead in uniaxial compression under different conditions and their experiments led to the now well known conclusions that the yield stress of lead depends on the temperature, strain rate and magnitude of the current strain especially at high strain rates. All those features are representative of the behaviour of hot steels. The susceptibility of lead to strain rate is indicated by Figure (4.7).

Ingham (20) obtained the yield stress of the same pure lead as that used in the present tests at different strain rates and his results will be used later in this work.

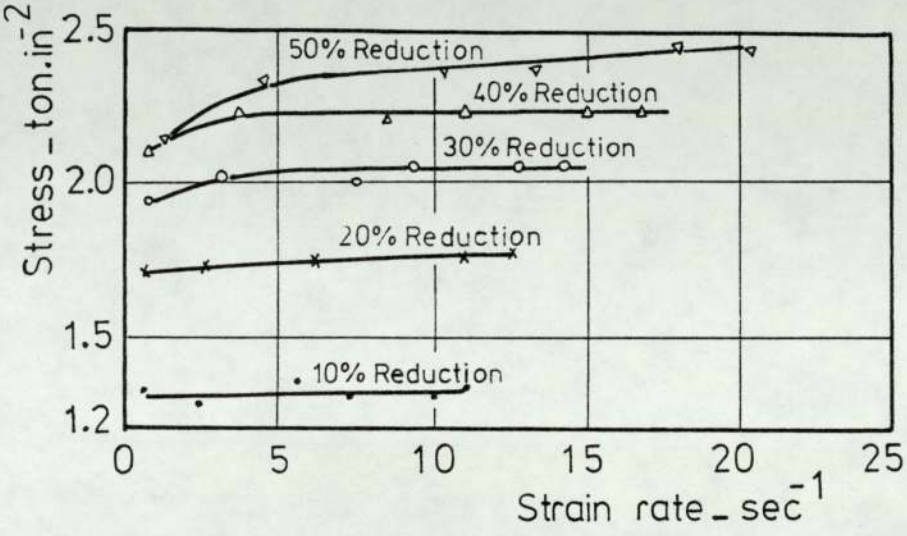

Fig (4.7) Yield stress v. strain rate of pure lead at 20°C. (From Sims and Loizou(19))

It should be mentioned here that lead has a low coefficient of friction as compared with hot steel. But this problem can be overcome as long as the difference in the frictional conditions is taken into account when comparing the experimental results using lead with hot steel. In applying the proposed theory to either the rolling of lead tubes or hot steel tubes, the appropriate values of the coefficient of friction or the friction factor, m, should be substituted in the equations.

4.8 Instrumentation

Recordings of signals from the two roll separating force (RSF) loadcells, the upper and lower torquemeters, the four pin-loadcells, front and back tension loadcells, and photo-electric cells were made using two ultra-violet, or UV in short, recorders. Both recorders were Southern Instruments type M1300 and each can record up to ten signals from ten different sources.

The requirements for any loadcell or torquemeter circuit were, a D.C. voltage supply, a bridge balancing circuit and a galvanometer, and they were all connected together in the fundamental Wheatstone bridge circuit shown in Figure (4.8).

The galvanometers, which were placed inside the UV recorder were of the mirror type, suspended coil, torsion filament. Ultra-violet light from a point source was reflected by the galvanometer mirror onto a photo-sensitive paper which provided the tracing of the applied signal to the galvanometer.

The sensitivity of each measuring circuit depends on the magnitude of the applied D.C. voltage to the Wheatstone

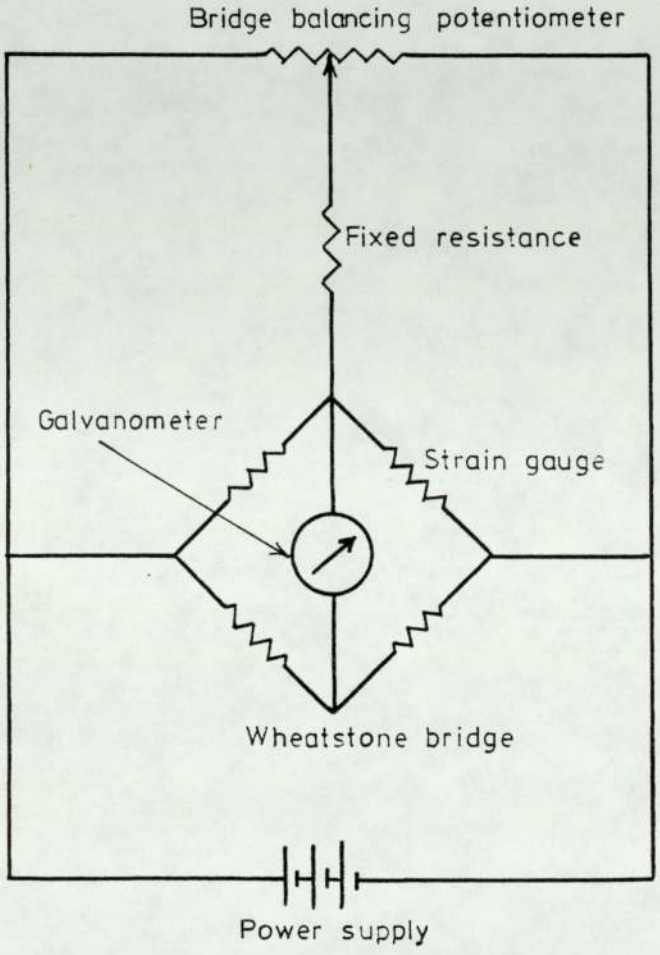

Fig.(4.8) Electrical connections to each loadcell

bridge circuit and the natural frequency characteristic of the galvanometer. The values of the applied voltage and the galvanometer natural frequency required for each individual circuit were determined from preliminary measurements and tests on the basis that maximum sensitivity was achieved while at the same time the galvanometer deflection was kept within the width of the recording paper. Table (4.1) shows the values of the applied voltage and the natural frequency of the galvanometer for each circuit. Since the applied voltage affected the sensitivity of the bridge circuit, its value was kept constant during the tests by using a stabilised D.C. power supply for every circuit. The voltage was checked frequently by a digital voltmeter.

Initial balancing of all bridge circuits was very important to obtain accurate measurements. The balancing for each circuit was carried out by means of a variable potentiometer and a fixed resistance connected as shown in Figure (4.8). The potentiometers and fixed resistances for all the circuits were put together in one balancing box.

The signals from the upper and lower torquemeters were too weak to give an adequate galvanometer deflection, even when using the most sensitive galvanometer and applying the maximum allowable supply voltage. Therefore two amplifiers were used to amplify the signals from the upper and lower torquemeters. The power supply and balancing circuit were built into each amplifier.

The wires from the front and rear RSF loadcells and from the front and back tension loadcells were connected

Table (4.1) Supply Voltage and Galvanometer Natural Frequency for the Different Loadcells

Loadcell	Supply Voltage, Volts	Galvanometer type and number	Galvanometer natural frequency, Hz
Front RSF	3 or 4	9074 M20	20
Rear RSF	3 or 4	9072 M20	20
Upper Torquemeter	6 or 7.5	SMI M711	1000
Lower Torquemeter	5	9544 M400	400
Front Tension	7.5	SMI A2404	60
Back Tension	7.5	SMI A2411	60
Pin-Loadcell 1	0.5	9005 M20	20
Pin-Loadcell 2	0.5	9172 M20	20
Pin-Loadcell 3	0.5	9192 M20	20
Pin-Loadcell 4	0.5	9034 M20	20

directly to the balancing box which in turn was connected to the different power supplies and the UV recorder.

Since the upper and lower torquemeters and the four pin-loadcells rotated with the shafts, it was impossible to make the wire connections to them without using slip-rings on the upper and lower shafts. The four-lead screened wire from the bottom torquemeter passed through an axial hole in the roll and then through a central hole in the shaft which ran from its free end to a point between the roll and the front bearing. The wire was connected to a slip-ring which was axially attached to the end of the shaft through a flexible tubing. Finally, screened wires were used between the slip-ring unit and the amplifier.

For the upper shaft, the number of wires that had to be accommodated inside a central hole in the shaft was great due to the presence of four pin-loadcells as well as the upper torquemeter. However, it was possible to cut down the number of wires needed by using the same value of supply voltage for all the four pin-loadcells. This meant that five twin-lead screened wires for the four pin-loadcells and one four-lead wire for the upper torquemeter passed through the central hole in the upper shaft to the free end of the shaft. The leads were connected to two slip-ring units which were coupled together to accommodate 14 leads. Screened wires were used between the slip-ring units and the remaining circuits.

The photo-electric cell circuit is shown in Figure (4.9). When light falls on the photo-electric cell, electric current flows in the circuit and the reed relay is activated so that current flows to the bridge circuit.

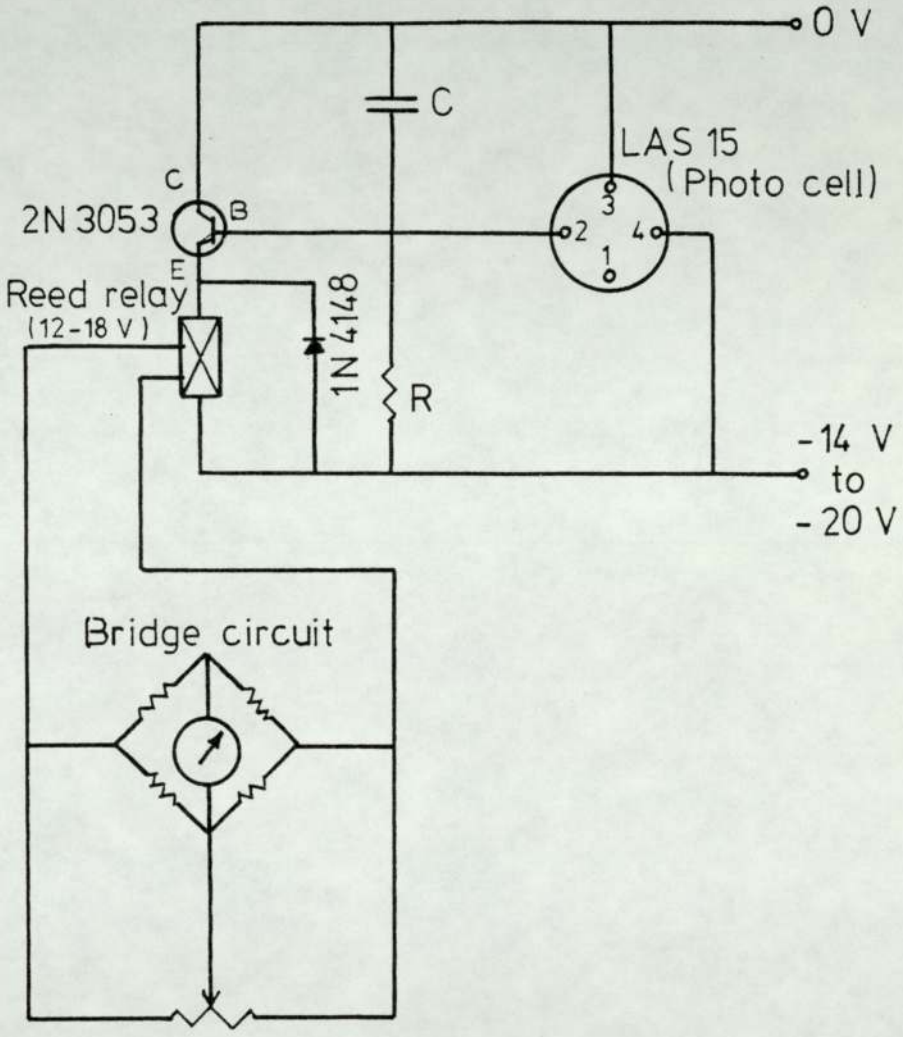

Fig.(4 . 9) Circuit diagram of the photo-electric cell

Since the bridge circuit is intentionally out of balance by a small amount, current also flows to the galvanometer causing it to deflect. If light falling on the photo-electric cell is interrupted, the galvanometer will return to its normal position providing a signal on the UV recorder paper.

The four photo-electric cells were connected to one UV recorder together with the signals from the four pin-loadcells. The signals from the RSF loadcells, upper and lower torquemeters, and front and back tension loadcells were connected to the other UV recorder.

4.9 Calibration

4.9.1 Calibration of front and rear RSF loadcells

Due to the difficulty in calibrating the RSF loadcells in situ, calibration was performed on a Denison testing machine. Simulation of the actual conditions on the testing machine was easily achieved since the loadcells were always subjected to a tensile force and the end fixing of the loadcells could be reproduced. Also, to simulate the actual conditions, the same leads were used for calibration.

The range of loads expected during rolling was determined from preliminary tests and calibration was carried out up to the maximum expected load. The RSF loadcells were calibrated first at a supply voltage of 4 volts. But unfortunately, when rolling thinner walled tubes, the galvanometer deflection was outside the width of the recording paper. Calibration had to be repeated using a smaller supply voltage of 3 volts to reduce the sensitivity of the measuring circuit. During calibration,

readings from the loadcells were taken while increasing and decreasing the applied loads. The balancing of each loadcell was checked and rectified before calibration and also a warming up period of about 2 hours was allowed before calibration commenced. The calibration curves for the front and rear RSF loadcells at 3 and 4 volts supply voltages are shown in Figures (4.10) and (4.11). Both figures show straight lines through the origin with no hysteresis. Calibration was repeated once more toward the end of the rolling tests to check the accuracy of the calibration curves.

4.9.2 Calibration of upper and lower torquemeters

The upper and lower torquemeters were calibrated by the direct application of moments to the end of the upper and lower shafts. These moments were provided by the use of a lever arm and weights. The lever arm was fixed to the end of the shaft by means of split block end fixing and a key which transmitted the moment from the lever to the end of the shaft. To counter-balance the weight of the lever arm, another arm of the same weight was fixed to the end of the shaft but pointing in the opposite direction.

Torquemeter readings were taken during both increasing and decreasing values of torque. The gears of the milling machine were engaged to prevent the rotation of the shafts during calibration. The calibration graphs are shown in Figures (4.12) and (4.13) and both gave linear relationships between the load on the lever arm and the galvanometer deflection, but the straight lines did not pass through the origin. The deviation did not present any problem since it was very small and the measured torques were found by adding

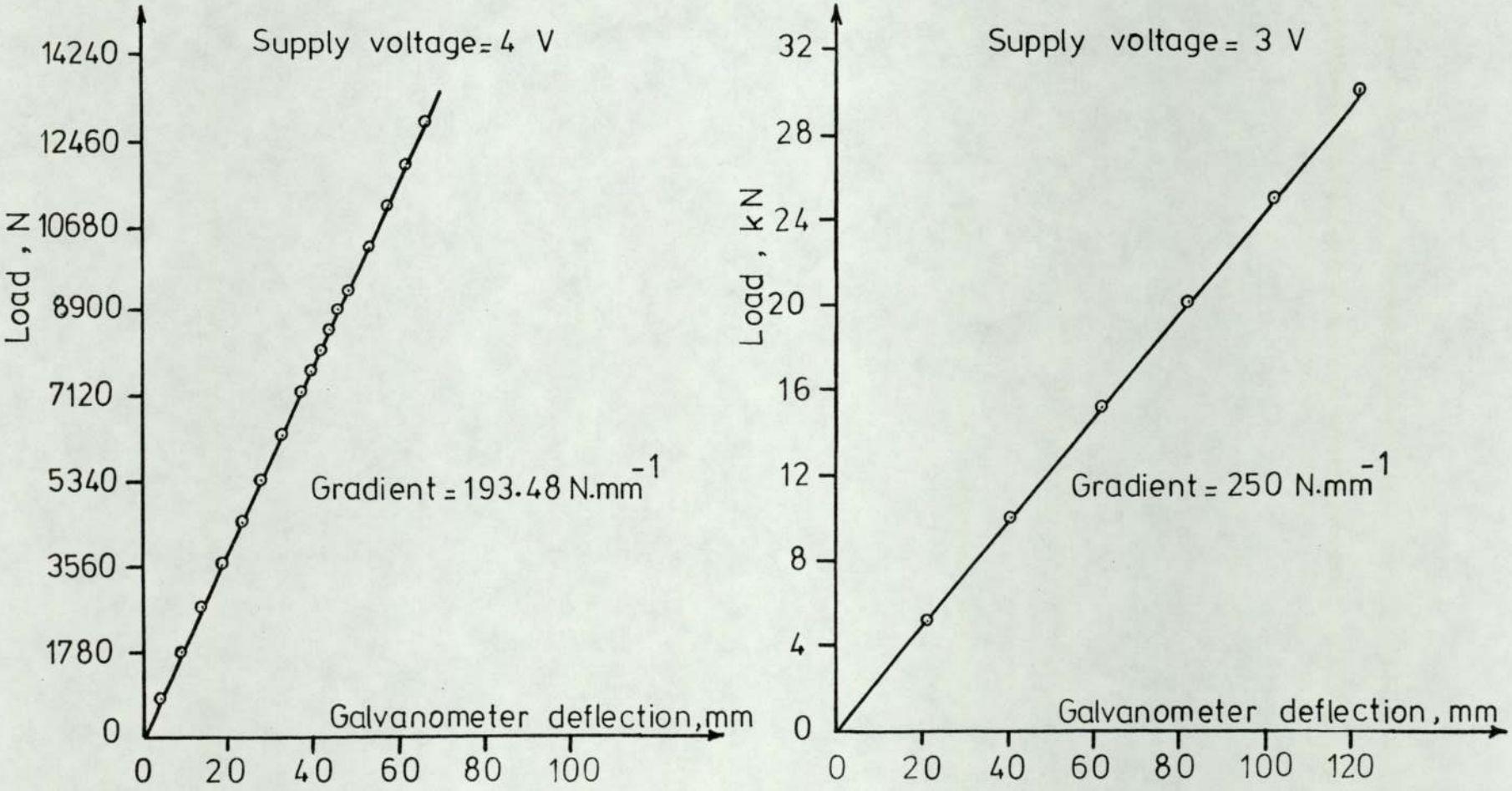

Fig (4.10) Calibration curves for the front RSF loadcell

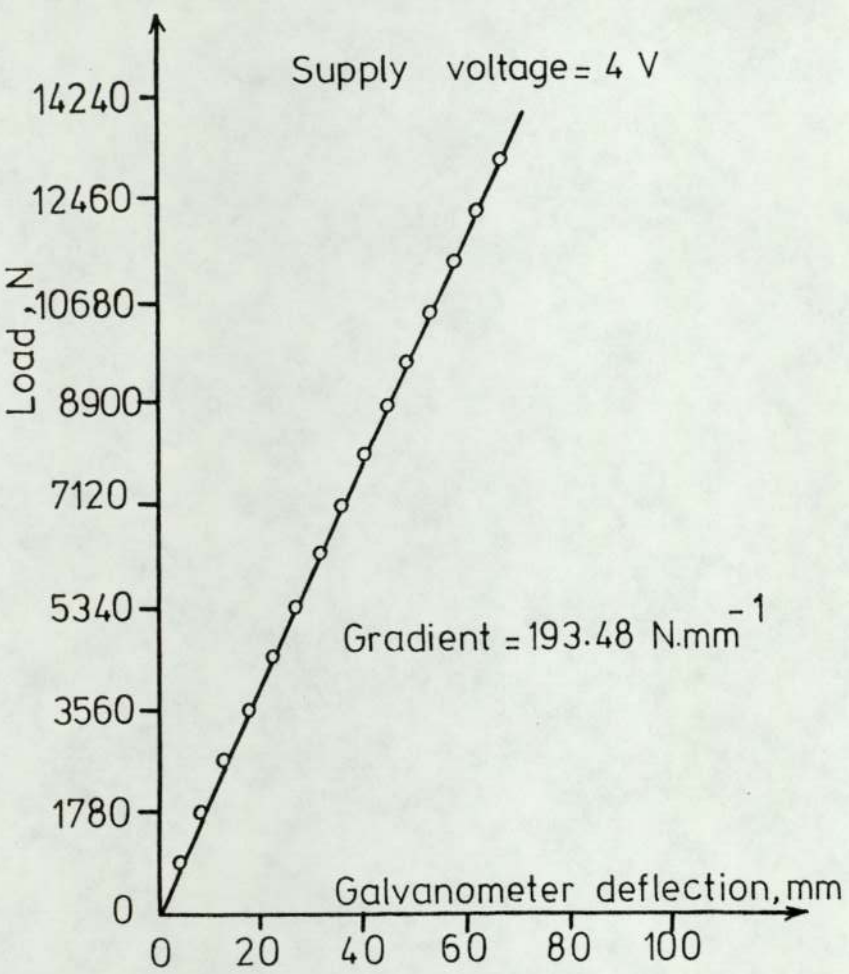

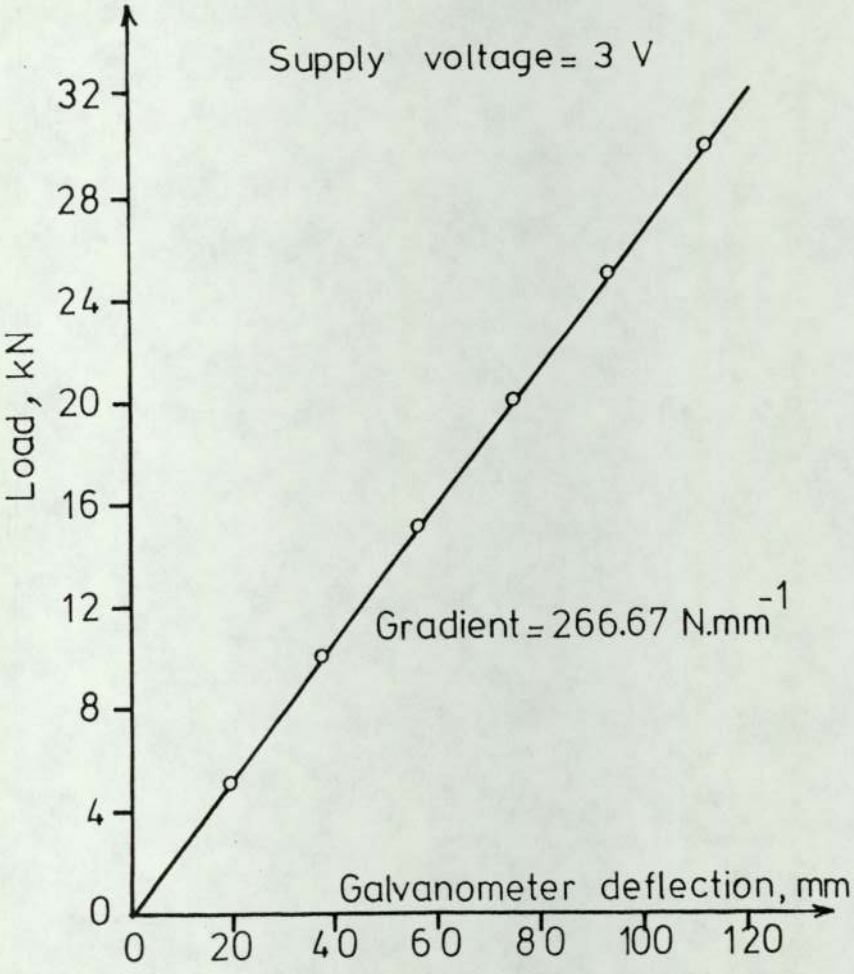

Fig.(4.11) Calibration curves for the rear RSF loadcell

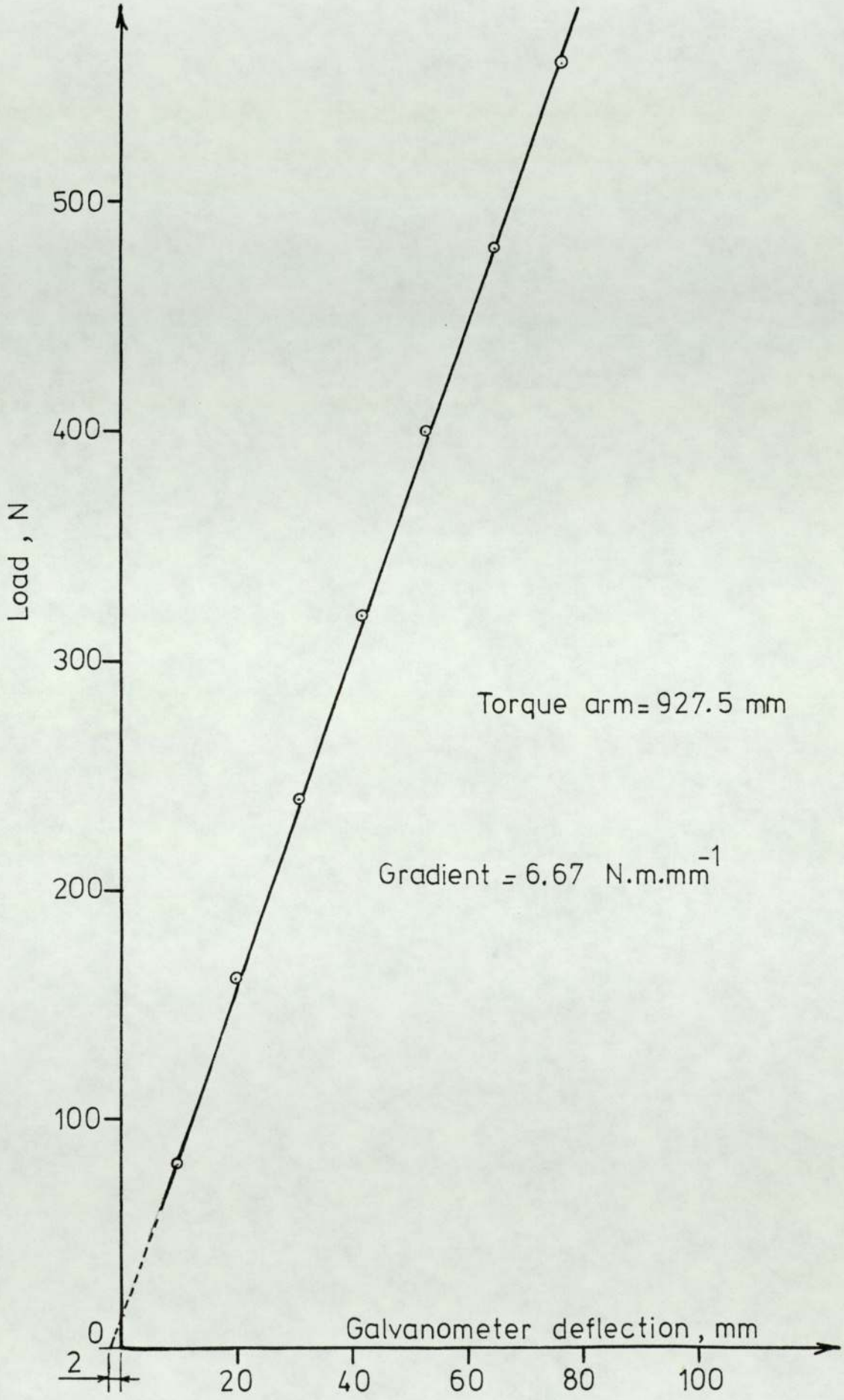

Fig.(4.12) Calibration curve for the lower torquemeter

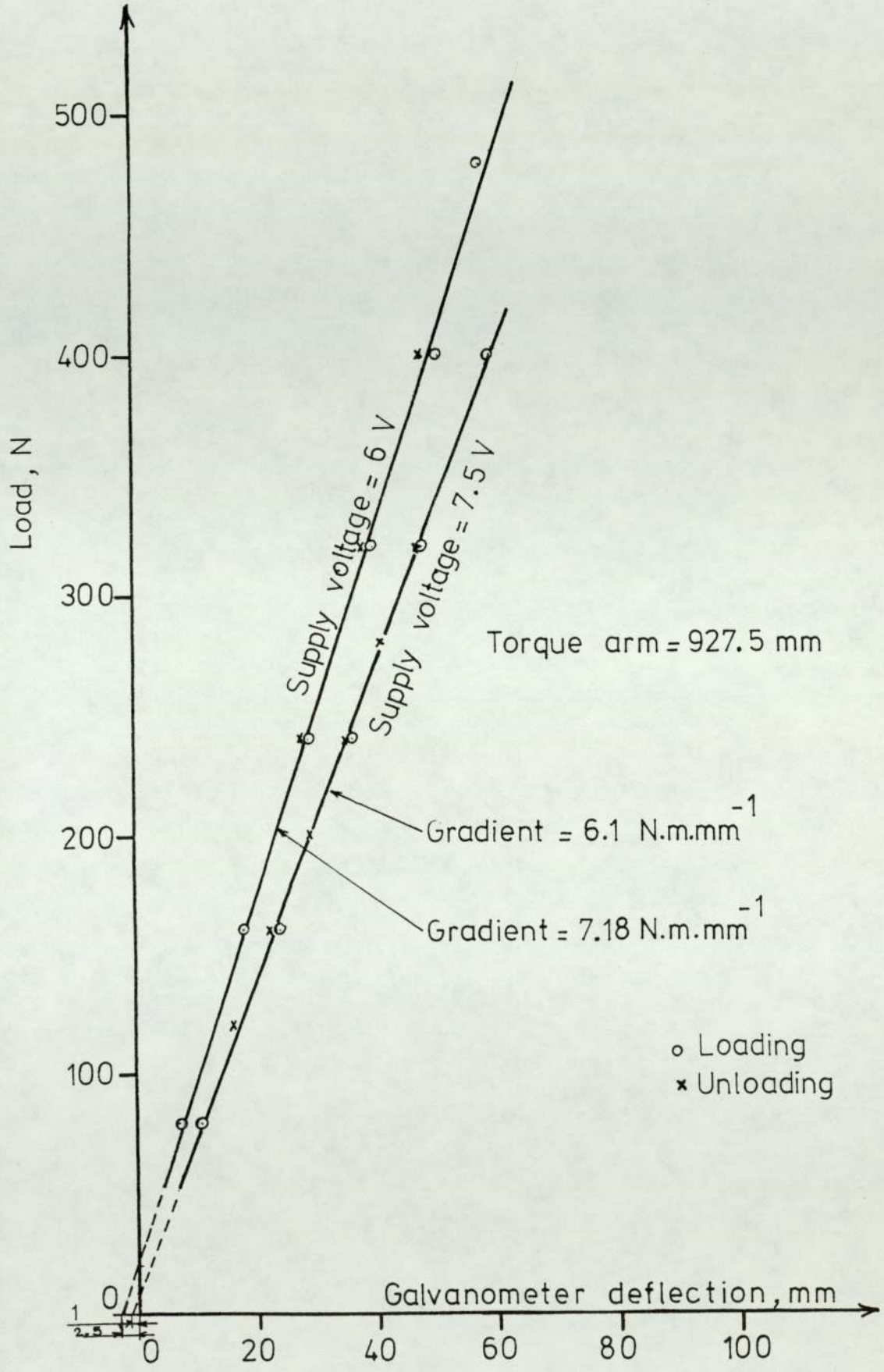

Fig.(4.13) Calibration curves for the upper torquemeter

the appropriate intersect with the X-axis to the galvanometer reading before multiplying by the gradient.

4.9.3 Calibration of front and back tension loadcells

The front and back tension loadcells were calibrated in exactly the same manner as the front and rear RSF loadcells except that instead of using a large capacity Denison testing machine, a smaller Denison, type T16, 2000 lb capacity, lever testing machine was used. This machine was selected since the values of the applied front and back tensions were low to ensure that the yield stress of lead was not exceeded.

Figures (4.14) and (4.15) show the calibration curves for the back and front tension loadcells respectively. Both curves show straight lines through the origin with no hysteresis.

4.9.4 Calibration of the pin-loadcells

The pin-loadcells were calibrated in situ by the direct application of load to each pin by means of dead weights. This method necessitated the removal of the upper shaft together with the top roll from the test rig. The slip-rings and all the wiring remained connected when the upper shaft and roll were removed. The shaft and roll were fixed as shown in figure (4.16) and were able to rotate about pivot (o) in a vertical plane, so that by the use of a spirit level with angle indicator, each pin could be located vertically where the load was applied through the loading pin. Calibration was performed several times at different supply voltages and every time the calibration curves showed straight lines passing through the origin with negligible scatter and hysteresis.

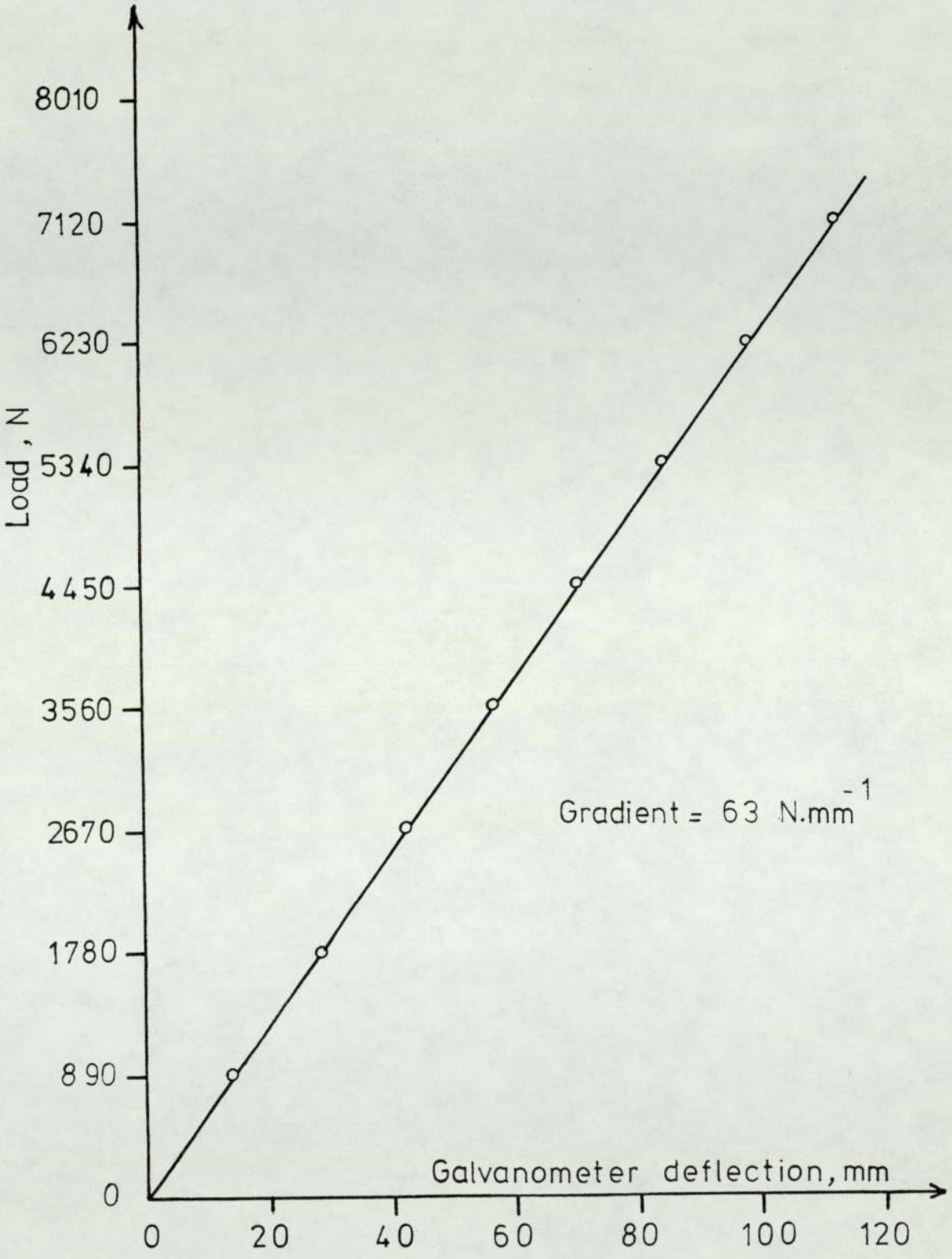

Fig.(4.14) Calibration curve for the back tension loadcell

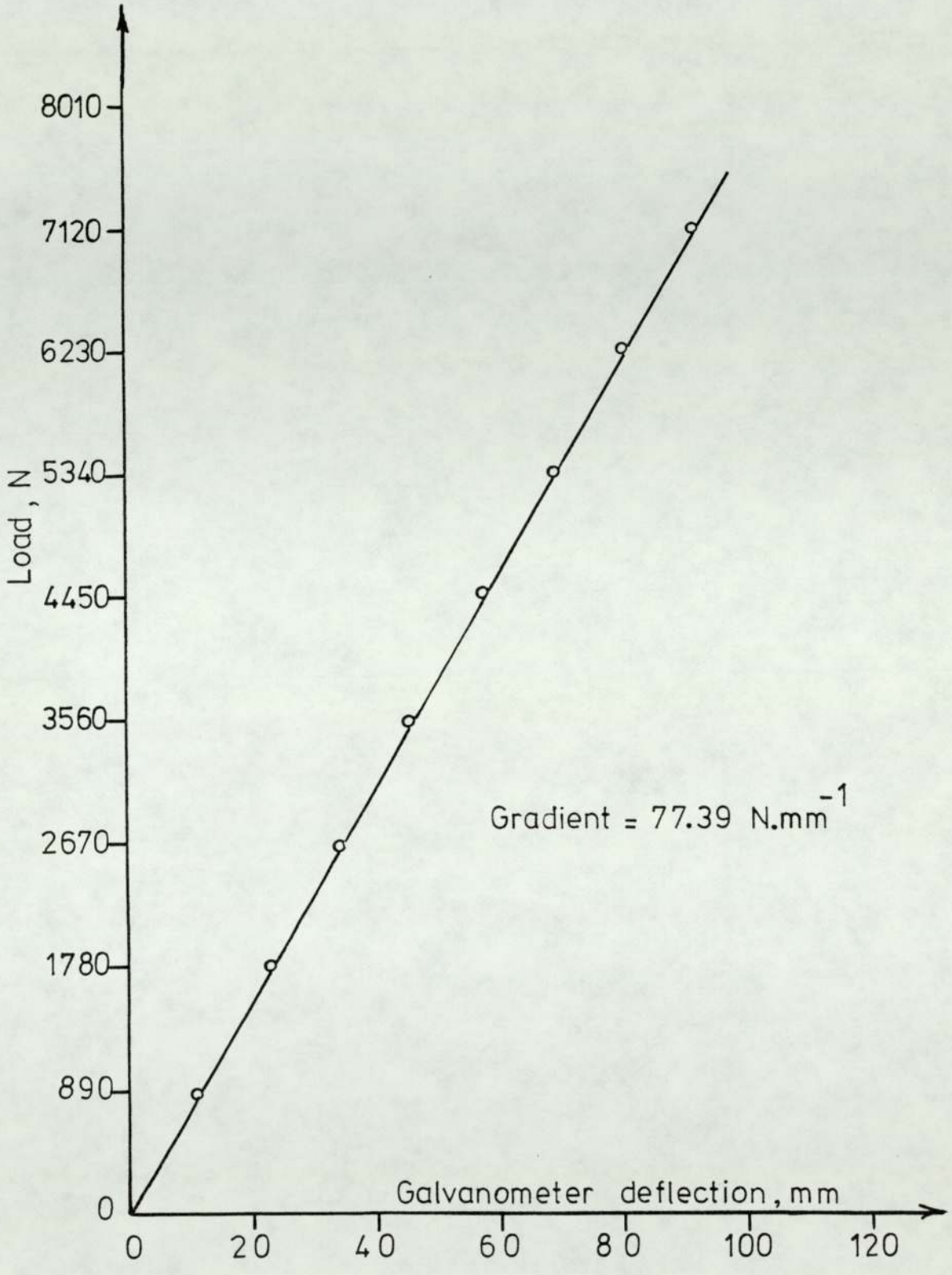

Fig.(4.15) Calibration curve for the front tension loadcell

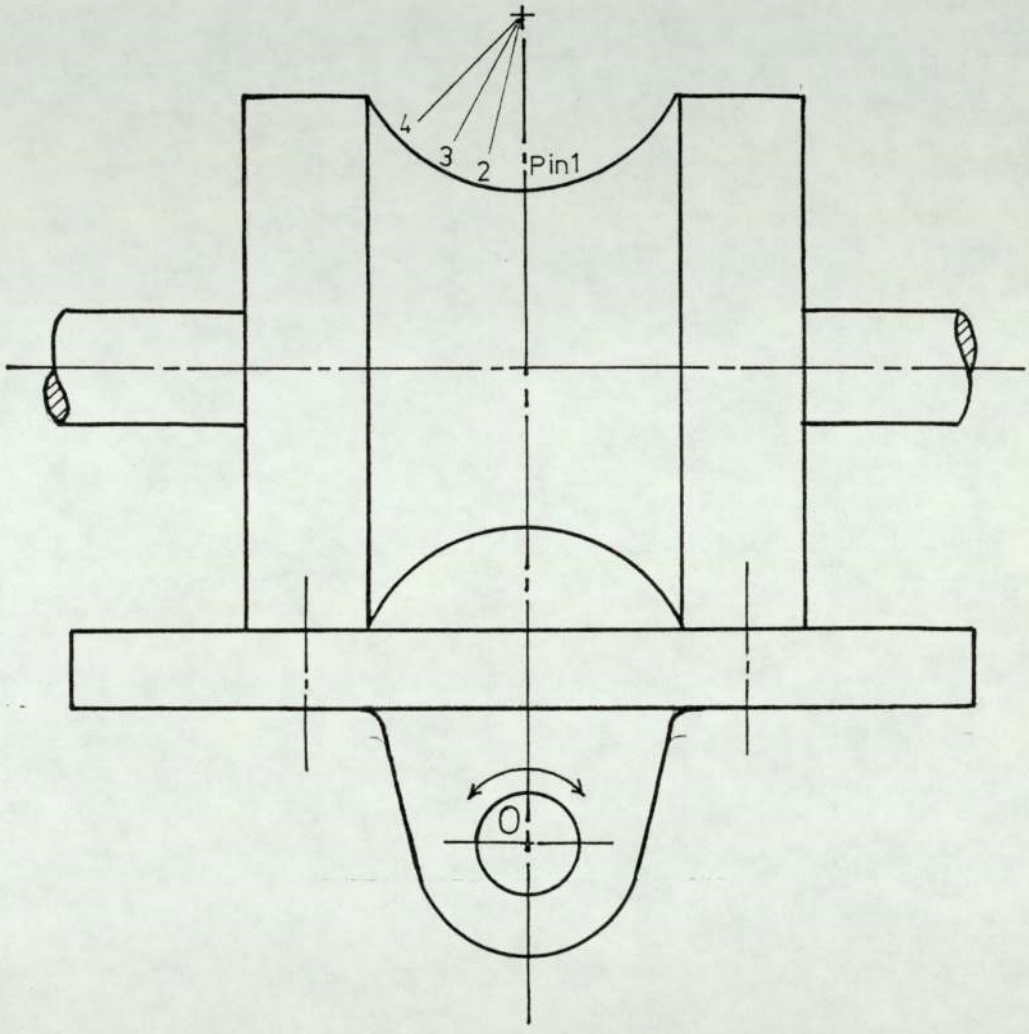

Fig.(4.16) Fixing the top roll on a rotating table

Although this method of calibration involved the removal of the upper shaft and roll, it was preferred to the proving ring device, Figure (4.17), used by Cole (11) in his calibration of pin-loadcells. As shown in Figure (4.17), the load-applying pin is connected to a proving ring which can deflect by a small amount when subjected to load. Those small deflections are detected by a dial gauge which is mounted across the diameter of the proving ring. The use of the proving ring involves double calibration which means that the dial gauge itself has to be calibrated by dead weights.

In the present investigation, since the loads on the pins during rolling were high, especially the loads on pins 1 and 2, a dead-weight lever system was used to apply the loads. The effective load on the pin was calculated by proportion. The calibration of the pin-loadcells was checked during the rolling tests and there were negligible changes in the calibration curves.

The calibration curves for the four loadcells are shown in Figures (4.18) to (4.21) and all show straight lines with negligible scatter of points.

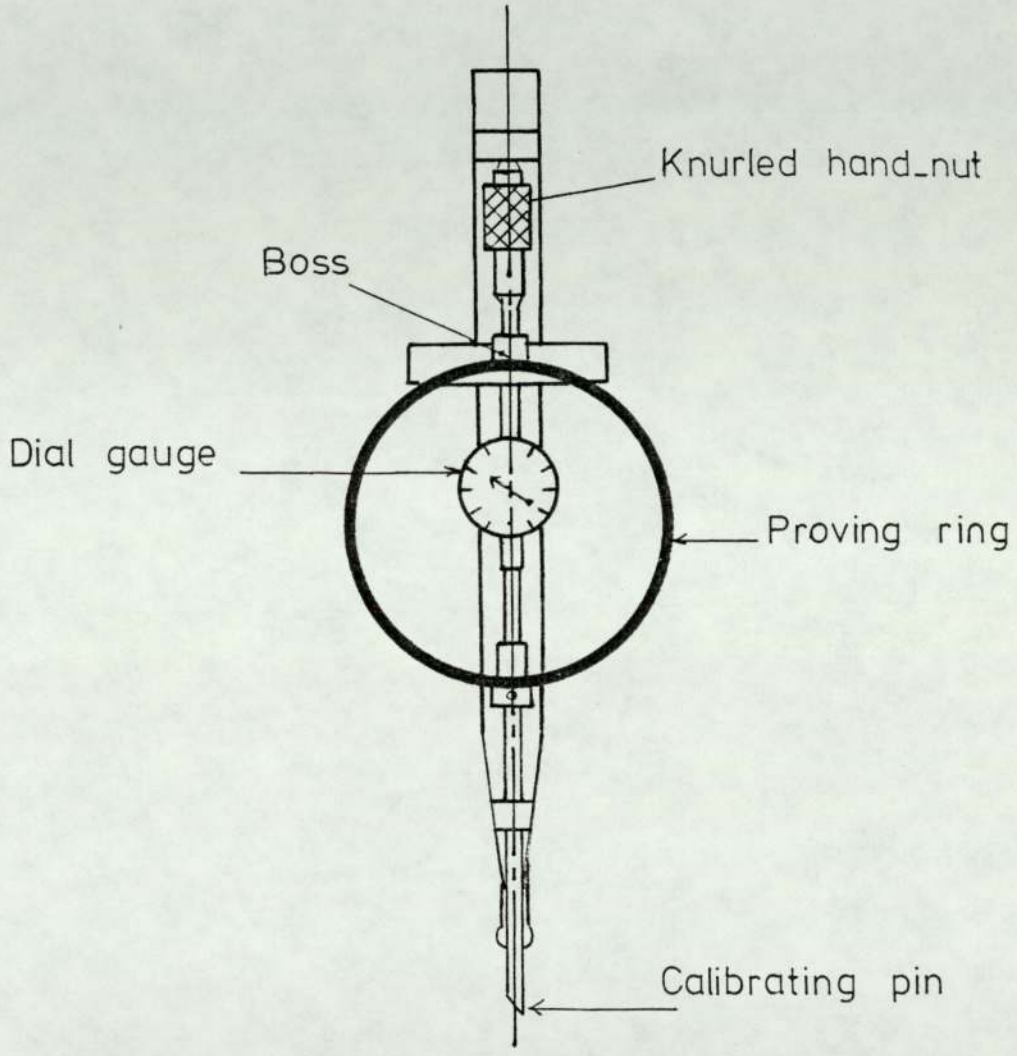

Fig.(4.17) Proving ring
[used by Cole(11)]

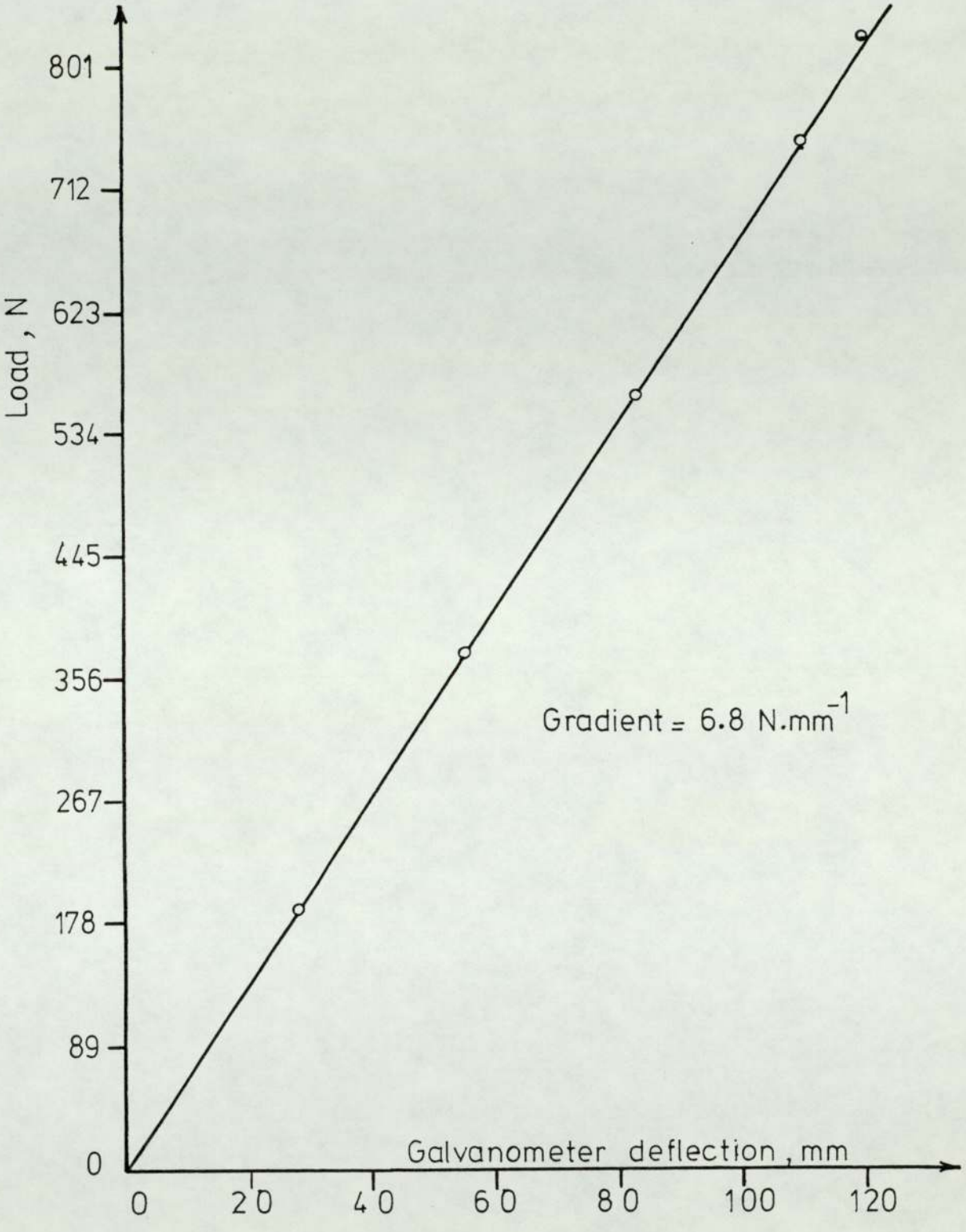

Fig.(4.18) Calibration of pin-loadcell 1

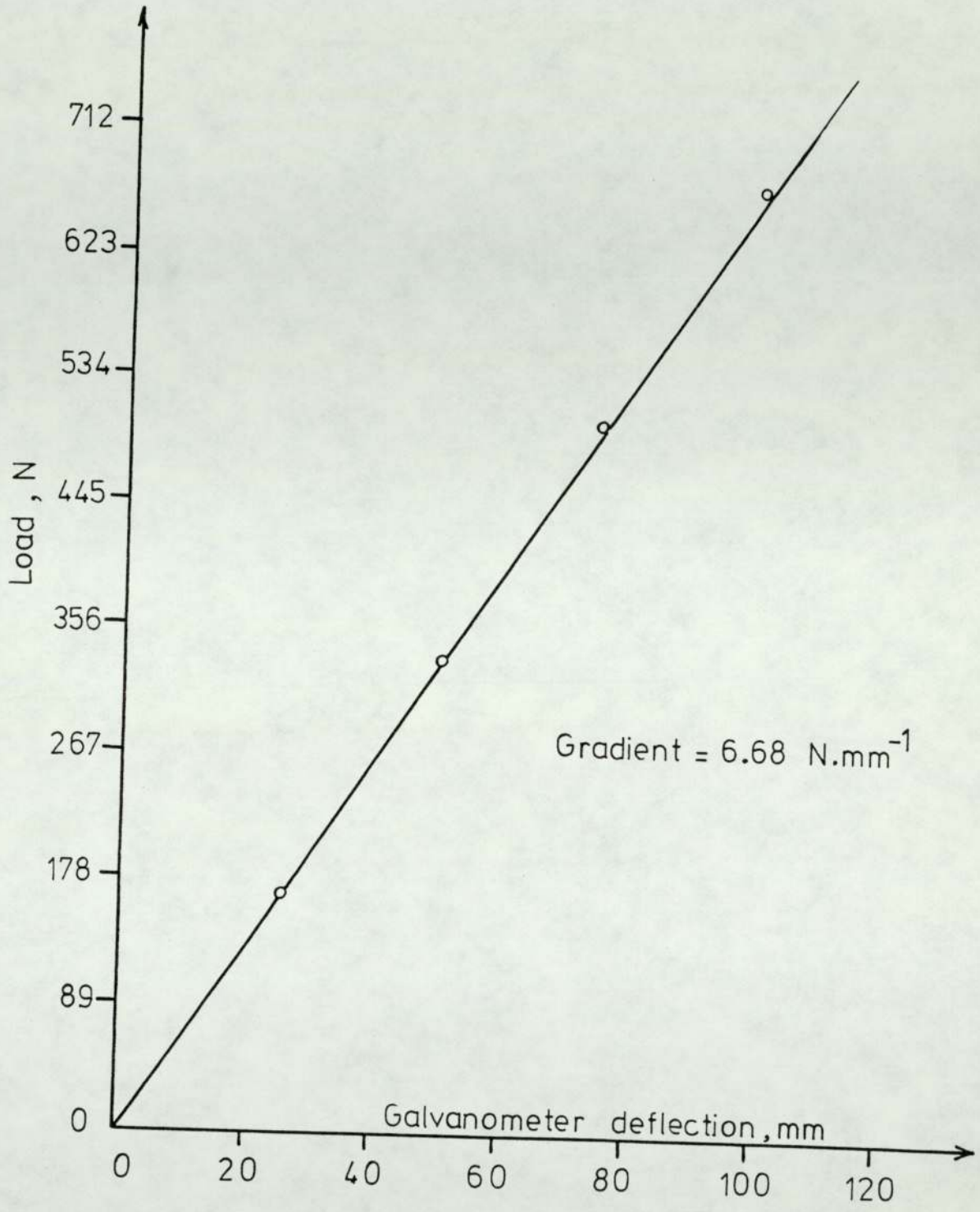

Fig.(4.19) Calibration of pin-loadcell 2

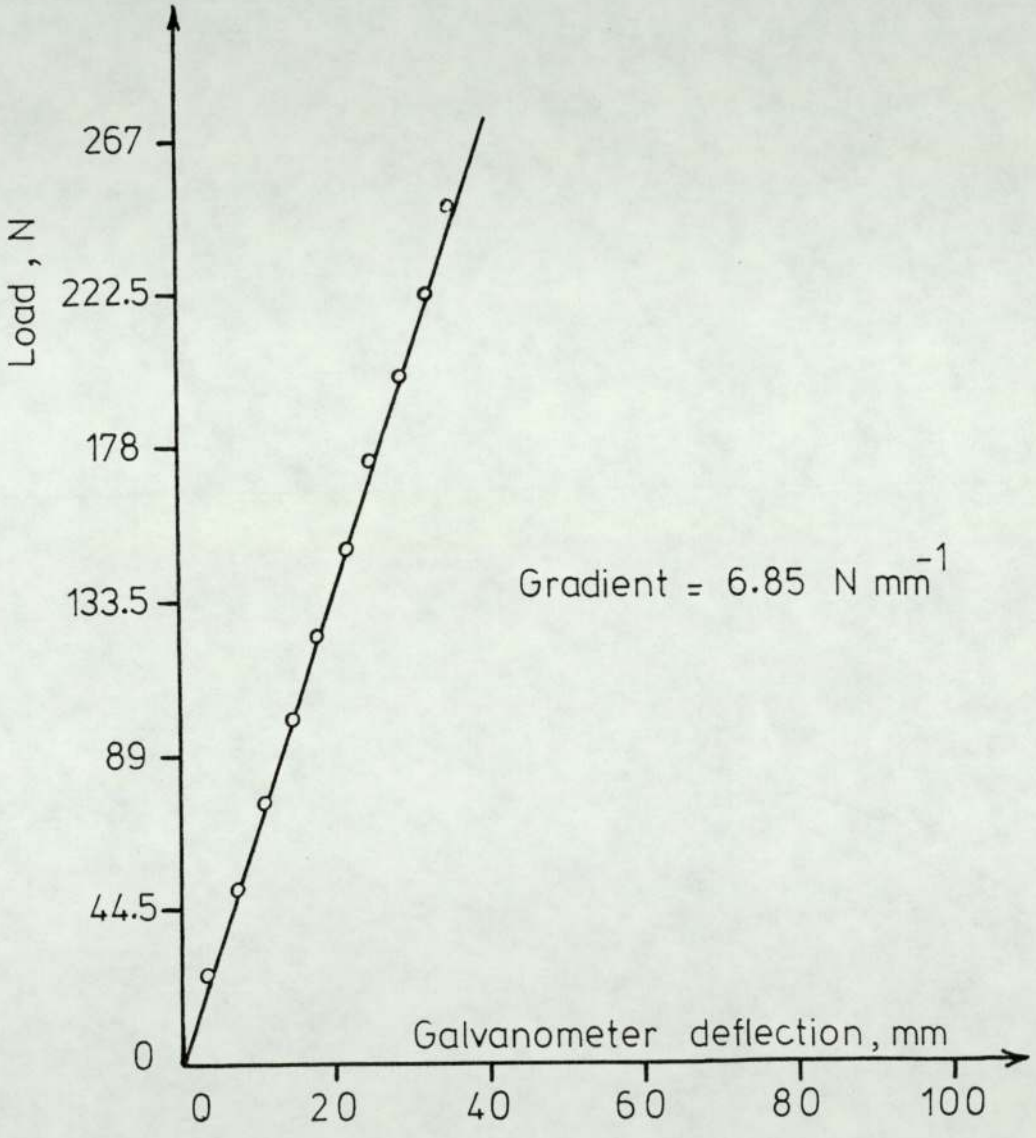

Fig.(4.20) Calibration of pin-loadcell 3

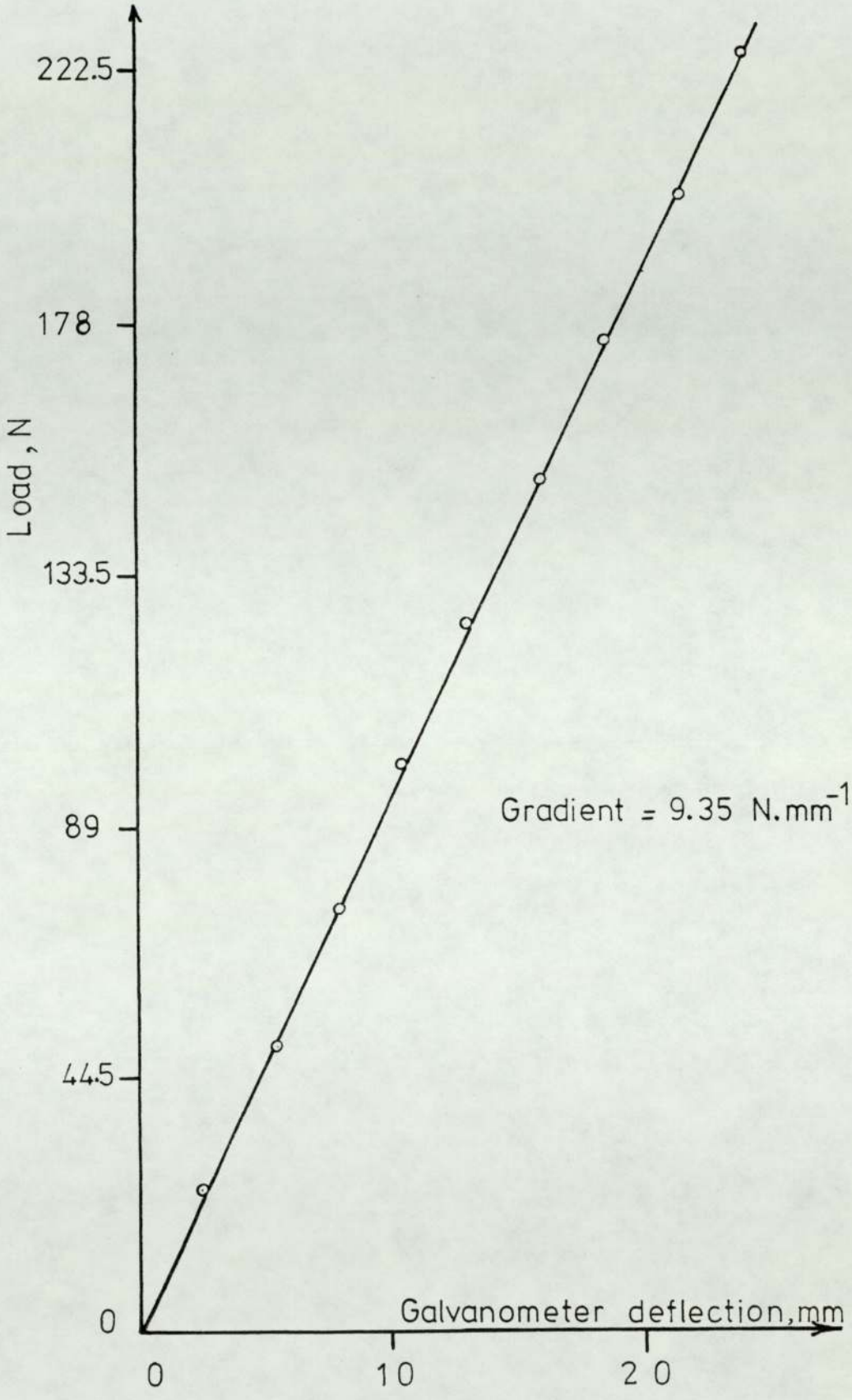

Fig.(4.21) Calibration of pin-loadcell 4

CHAPTER (5)

EXPERIMENTAL PROCEDURE

Chapter (5) Experimental Procedure

The objective of the experiments was to examine the way in which roll separating force, rolling torque and pressure distribution round the groove varied with the different rolling parameters, e.g. reduction of area, tube diameter to thickness ratio, front and back tensions.

In the following sections, the experimental procedure will be described starting with tube preparation and ending with the methods used for determining the tube cross-sectional area after rolling and the yield stress of lead which was used in the rolling tests as an analogue material for hot steel.

5.1 Preparation of test tubes

Great care was taken in preparing the tubes for rolling in order to provide homogeneity of the tube wall thickness in all the test tubes. The method used for preparing the tubes was described in the previous chapter and due to the long time taken in the preparations, every effort was made to minimize any waste during the rolling tests. This included making the tubes just long enough to reach steady state conditions. The required tube length was determined from preliminary tests which showed that a length of about 350 mm was sufficient to reach steady state conditions. The tubes were longer when applying front and back tensions to allow for the gripping of the tube ends in the front and back tension devices. Tests showed that small differences in tube lengths had very little effect on the rolling forces and torques.

Care was taken also in machining the tubes to the required outer diameter to ensure that all tubes had as closely as possible the same surface finish. This was achieved by

using two similar cutting tools and the same turning speed, depth of cut, and feed when turning the different tubes. Two mandrels were used in all the experiments and both were ground in the same manner to ensure identical conditions on the two mandrel surfaces. The surface finish of the two mandrels was measured by the Talysurf and both mandrels nearly had the same surface finish. Before inserting the mandrel inside the tube, both the tube inside and the mandrel were cleaned with trichlorethylene to remove any dirt or grease that might affect the surface conditions between tube and mandrel. The tube was drawn on the mandrel through a ring die and then turned in a lathe to the required size. For each mandrel size, the tube diameter to thickness ratio, d/t, was changed by varying the outer diameter. This method of varying the d/t ratio meant that for each mandrel size, the d/t ratios chosen were close to each other since the tube outer diameter could not be varied much. The tube inside was in contact with the mandrel during the whole process of tube rolling, i.e. close pass rolling, and this meant that before rolling, the tube inner diameter was the same as the mandrel diameter which was either 31.38 mm or 37.6 mm.

5.2 Preparations before each test

Before each test session, the balancing of all the load-cells bridge circuits was checked by a highly sensitive optical galvanometer and any out of balance was rectified using the potentiometers in the balancing circuits. Also, the supply voltage for each loadcell was checked by a digital voltmeter. The rolls were cleaned and degreased with trichlorethylene before each test.

Due to the high loads encountered in the mandrel rolling process, the roll rotational speed was set at its lowest value. The roll rotational speed was the same throughout the tests at 0.33 rev/min. A warming up period of about 2 hours was allowed before the commencement of each test session to ensure the stability of all the strain gauge circuits.

5.3 Process Parameters

The following parameters were examined in the present investigation:

1. Reduction of area

   The reduction of area was altered by changing the roll gap. The maximum reduction of area was restricted to 15%, due to the limited capacity of the experimental mill and the fact that rolling loads in the mandrel rolling process are high, especially when rolling thin walled tubes. The maximum angle of bite and the prevention of fin formation were other reasons behind the low values of reduction of area.

   Although the roll stand was rigid, some spring back of the rolls was observed during rolling. This meant that the measured roll gap before rolling was not the actual roll gap during rolling. To overcome this problem, the actual roll gap was determined from the measurement of the rolled tube minor axis, which was the tube dimension corresponding to the root of the groove, and from the geometry of the groove as shown in Figure (5.1).

2. Tube diameter to thickness ratio, d/t

   Two different mandrel sizes were used throughout the

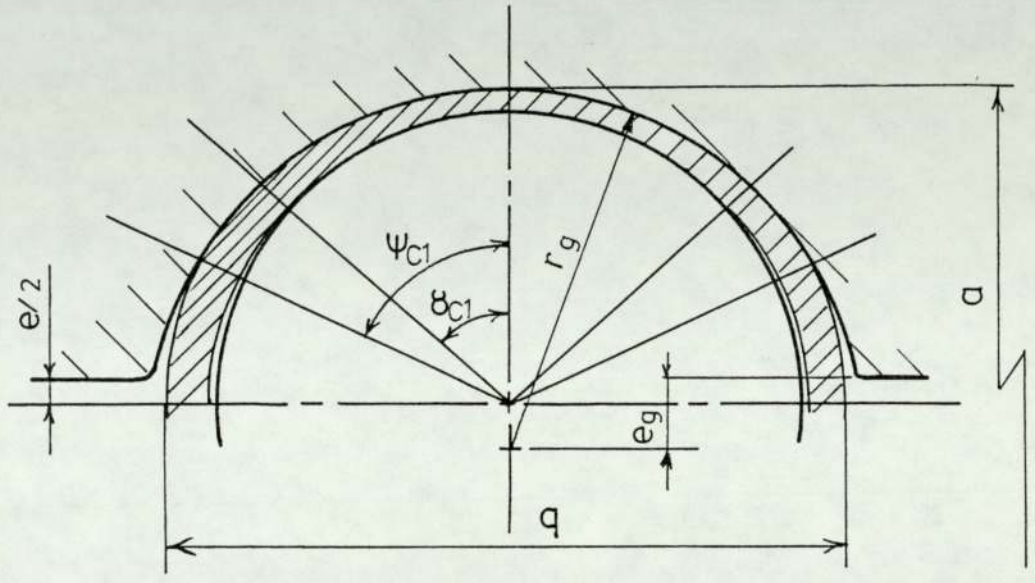

$$e = a - 2(r_g - e_g)$$

Fig.(5 .1) Geometry of tube and groove at the exit plane

experiments. Lead tubes with diameter to thickness ratios of 7.9, 8.5, 9 & 10 were rolled on the same mandrel having a diameter of 31.38 mm. Thinner walled tubes, with d/t ratios of 24 and 30.4 were rolled on a 37.6 mm mandrel.

For each d/t ratio, a series of experiments was carried out, by changing the roll gap, to determine the effect of varying the reduction of area, J, on the roll separating force, the rolling torque and the pressure distribution. Graphs could be drawn for the effect of varying both the reduction of area, J, and d/t ratio.

3. Mandrel surface conditions

Thin walled tubes with d/t ratios of 24 and 30.4 were rolled, at different reductions of area, on a 37.6 mm mandrel having the following surface conditions:

a. Dry conditions. The mandrel surface was smooth but dry.

b. Lubricated conditions. The same mandrel used in (a) was lubricated by Duckham's graphite grease type ADMAX LM2. Owing to the method adopted in preparing the tubes for rolling, some lubricant was squeezed out when the tube was drawn on the lubricated mandrel through a ring die. This reduced the effect of lubrication on the rolling loads and torques.

c. Rough conditions. A 37.6 mm mandrel with a groove machined along its surface was used to provide the rough conditions between the tube inside and the mandrel.

4. Front and back tensions

The front and back tensions were applied through the front and back tension devices described in the previous chapter.

Tubes with a d/t ratio of 24 were rolled on the 37.6 mm mandrel under various degrees of reduction of area. The rolling tests involving front and back tensions were divided into three groups. Tubes in the first group were rolled with only back tension applied to them, while tubes in the second group were rolled with front tension applied to them. Both front and back tensions were applied to the tubes in the third group.

The presence of the mandrel inside the tube presented a problem in fixing the tube ends to either the front or back gripping attachment since the mandrel should be free at both its ends. The method adopted here for fixing the tube end to the back gripping attachment involved taking the tube off the mandrel and re-inserting the mandrel again inside the tube but leaving a short length of tube at one end to be free from the inside. A short steel plug was pushed into that end of tube and the back gripping attachment was clamped onto the tube end. The same method was carried out when only front tension was applied to the tube, with the exception that the front gripping attachment was clamped onto the tube front end after it had passed through the roll groove.

Applying both front and back tensions at the same time required that the tube should be longer than the

mandrel. This was achieved by welding a piece of tube to the original tube so that the tube became longer than the mandrel. Attaching the tube ends to the front and back tension devices was carried out as described previously.

From the above description, it is clear that in all the tests which involved applying front and back tensions to the tube, the tube was first taken off the mandrel and then the mandrel was inserted back again inside the tube. So that the same conditions should apply when comparing the rolling tests using front and back tensions with the free rolling tests, i.e. without front and back tensions, the tube was taken off the mandrel and then the mandrel was inserted back into the tube for some of the free rolling tests.

The mandrel speed could not be measured during the application of front and back tensions to the tube due to the attachment of the front and back tension devices to the tube ends.

5. Mandrel speed

To simulate the actual conditions existing in a production mill where the mandrel speed exceeds the tube speed in some of the stands, the mandrel in the experimental mill was pulled through the roll groove at a higher speed than that occurring in free rolling. This was accomplished by connecting the front end of the mandrel to the front tension device through the front tension loadcell. By varying the rotational speed of the drum, the speed of the mandrel could be altered.

Tubes with a d/t ratio of 24 were rolled on a 37.6 mm mandrel under various degrees of reduction of area and with an increase in the mandrel speed.

6. Groove shape

Two groove shapes were examined in the present investigation and these are shown in Figure (4.2). The results of rolling tubes with a d/t ratio of 24 through the two grooves were compared with each other.

7. Rolling oval tubes

Some thin walled tubes which were rolled once on a 37.6 mm mandrel, were rotated 90^{o} about their axes and rolled once more through the two grooved rolls.

5.4 Measurement of tube cross-sectional area

The tube cross-sectional area can be measured by any of the following methods:

1. The weighing method in which a specimen is cut from the tube and faced in a lathe. From measurements of specimen length and weight and from a knowledge of the density of lead, the cross-sectional area of the tube can be determined.
2. Tracing the image of the cross-section on a sheet of paper using a shadowgraph. The area of the image is determined by a planimeter.
3. The method used by Haleem (12) which consisted of photographing the cross-section of the specimen and projecting the image on a screen where it could be traced and measured.

   In fact this method could be considered as a version of the second method.

4. Making an impression of the cross-section on a piece of paper where it can be traced by a planimeter to determine the cross-sectional area.

In all the above methods, a specimen is cut from the tube and its ends machined. The weighing method was preferred in the present investigation since it is accurate and quicker and less expensive than the photographing method used by Haleem. Also, the weighing method is not subjected to any image distortion that can occur when using an optical system in determining the cross-sectional area. The disadvantage of the weighing method was that it provided information on the cross-sectional area only without any indication of the variation of tube wall thickness across the cross-section. However, this problem was solved when considering that most of the tube outer and inner surfaces were constrained by the groove and mandrel surfaces respectively. The tube outer and inner surfaces were clearly marked after rolling so that the contact angles between tube and rolls and between tube and mandrel could be measured. By measuring also the cross-section major and minor axes and from a knowledge of the groove geometry, the tube outer and inner surfaces could be drawn accurately to indicate the variation of tube wall thickness across the cross-section. This method was checked by tracing the image of some tubes cross-sections using a shadowgraph and both methods gave very close results.

It was impossible to hold very thin walled specimens in the lathe chuck to face the specimen ends without distorting the specimen shape. Therefore, a short mandrel

was turned down to the same dimension as the original mandrel and inserted inside the specimen so that one end of the short mandrel could be gripped inside the lathe chuck. A very small length of specimen was left free of the other end of the short mandrel.

By using a wide strip of adhesive tape to hold the specimen to the mandrel, the free end of the specimen could be faced without distorting the specimen shape.

The density of pure lead, which could be taken from any material reference, was checked in the present investigation to make sure that the published value was similar to the density of pure lead used in the rolling tests. Specimens were taken from rolled and unrolled tubes and weighed in air and water. By applying Archimedes principle, the density of lead could be found as:

$$\text{Density of lead} = \frac{\text{Specimen weight in air}}{\text{Specimen weight in air} - \text{Specimen weight in water}}$$

The density of lead was checked also by comparing it with the value obtained from a knowledge of an unrolled specimen length, cross sectional-area and weight.

From experiments, the density of lead was established at 11.36 grm.cm^{-3}. This value was very close to the density of lead found in several references.

5.5 Yield stress of lead

As mentioned in the previous chapter, the results of Ingham's (20) tests on the determination of yield stress of pure lead were used in this investigation.

Before Ingham, Loizou and Sims (19) obtained the yield stress of pure lead at different strain rates and

temperatures, but it was decided to use Ingham's results since he carried out his experiments on the same pure lead as that used in the present experiments, and at similar low strain rates. Uniaxial compression tests were performed on pure lead cylindrical specimens 20 mm diameter x 20 mm height. Three lubrication grooves were machined on each end face of the specimen to minimize friction between the compression machine platens and the specimen during compression. The compression tests were carried out with constant platen speed and the curves in Figure (5.2) were plotted between the true stress and true strain at different platen speeds. During the compression of each specimen, the strain rate increased as shown by the lower curve in Figure (5.2). The strain rate figures attached to each test curve were the initial values. Ingham stated that the results of compression tests conducted at constant platen speeds could be assumed to apply for compression tests at constant strain rates without any significant effect on the values of the yield stress. It was shown from the lower curve in Figure (5.2) that even at a reduction of 50% the strain rate was only twice the initial value and this change in the strain rate did not have any significant effect on the value of the yield stress. Therefore, the stress-strain curves at constant platen speeds, Figure (5.2), were considered to represent the yield stress of pure lead at constant strain rates.

To obtain the mean yield stress from the true stress-strain curves, the strain rate in the actual rolling process should be estimated. In the mandrel rolling process the strain rate varies from entry to exit and from point to

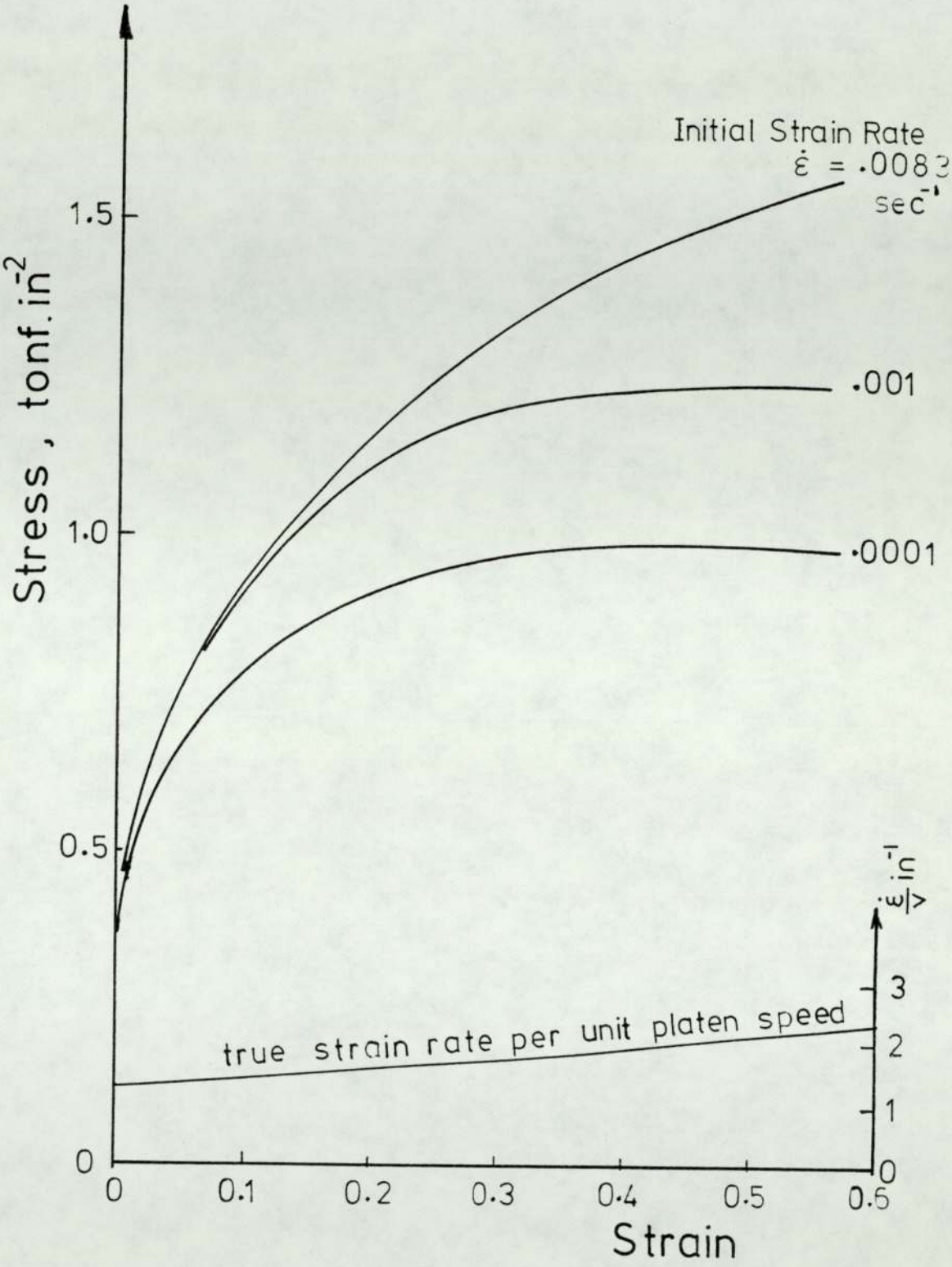

Fig.(5.2) True Stress v Strain for pure Lead in Uniaxial Compression

(From Ingham (20))

point on the surface of contact between tube and rolls. This variation coupled with the fact that contact between tube and rolls varies from entry to exit, made the estimation of a mean strain rate very complicated. However, it is possible to estimate the maximum mean strain rate $\bar{\lambda}_r$, which exists at the position corresponding to the root of the groove. By considering that the strain rate at a point outside the contact zone between tube and rolls is zero, it can be assumed that, at any section along the tube axis in the deformation zone, the strain rate varies from a maximum value at the root of the groove to zero at a point just outside the contact zone.

Following this argument, the total mean strain rate can be taken as the mean value between the maximum mean strain rate at the root of the groove and zero, i.e. $\bar{\lambda}_r/2$.

$$\lambda = \frac{1}{r} \frac{dr}{dt}$$

where r is the instantaneous tube radius.

From Figure (5.3), the strain rate at the root of the groove and at any point on the arc of contact is:

$$\lambda_r = \frac{1}{r} \frac{dr}{dt}$$

where $r = (R_s + e/2) - R_r \cos\Phi$, and $\frac{dr}{dt} = \omega R_r \sin\Phi$

$$\lambda_r = \frac{\omega R_r \sin\Phi}{(R_s + e/2) - R_r \cos\Phi}$$

The mean strain rate $\bar{\lambda}_r$ at the root of the groove can be written as:

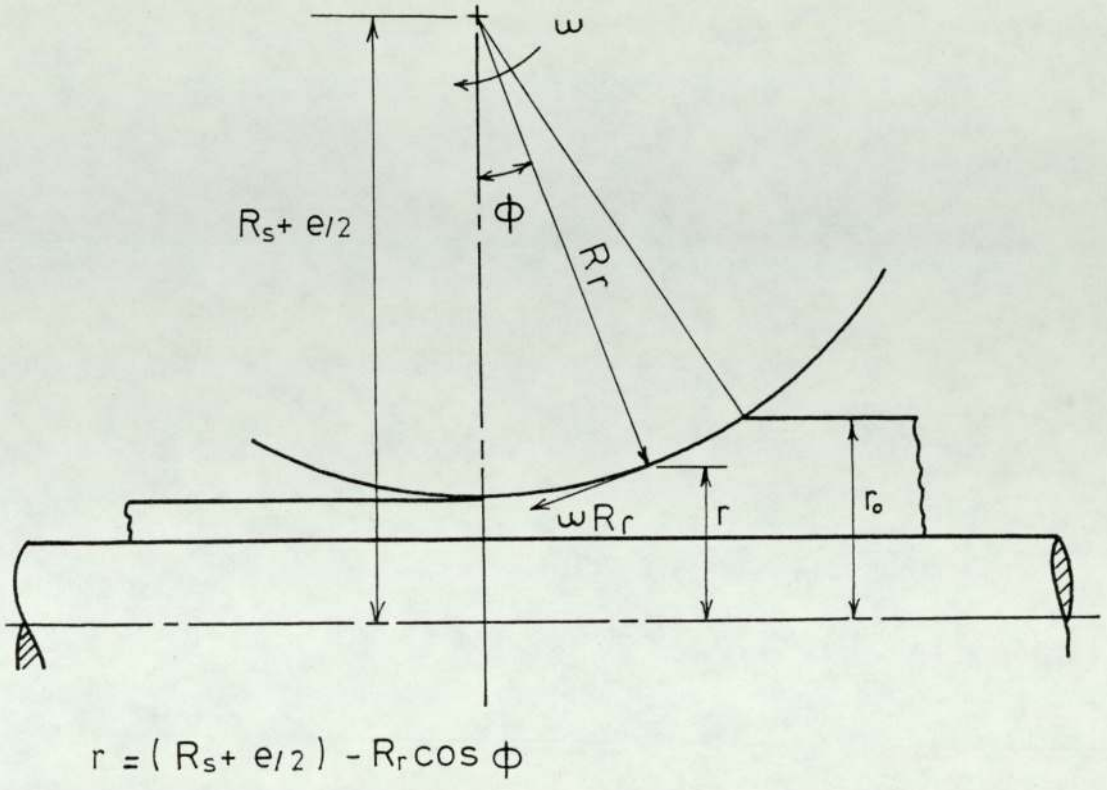

Fig.(5.3) Section at the root of the groove

$$\bar{\lambda}_r = \frac{\int_0^{\Phi_m} \lambda_r \, d\Phi}{\Phi_m} = \frac{1}{\Phi_m} \int_0^{\Phi_m} \frac{\omega R_r \sin\Phi}{(R_s + e/s) - R_r \cos\Phi} \, d\Phi$$

$$= \frac{\omega R_r}{\Phi_m} \int_0^{\Phi_m} \frac{\sin\Phi}{(R_s + e/2) - R_r \cos\Phi} \, d\Phi$$

$$= \frac{\omega}{\Phi_m} \left[\ln (R_s + e/2 - R_r \cos\Phi) \right]_0^{\Phi_m}$$

$$= \frac{\omega}{\Phi_m} \ln \frac{R_s + e/2 - R_r \cos\Phi_m}{R_s + e/2 - R_r} \qquad (5.5.1)$$

The total mean strain rate $\bar{\lambda} = \frac{\bar{\lambda}_r}{2}$ (5.5.2)

Having estimated the total mean strain rate, the corresponding stress-strain curve can be chosen from Figure (5.2). The mean yield stress $\bar{\sigma}_y$, is determined from that curve as the stress corresponding to the generalised strain $\bar{\varepsilon}_m$. It can be written that:

$$\bar{\varepsilon}_m = \varepsilon_h + \varepsilon_{red.} \qquad (5.5.3)$$

where ε_h is the generalized homogeneous strain

$\varepsilon_{red.}$ is the redundant strain corresponding to the redundant work W_r

$$\varepsilon_h = \sqrt{\frac{2}{3}} \sqrt{\varepsilon_1^2 + \varepsilon_r^2 + \varepsilon_\theta^2} \qquad (5.5.4)$$

where ε_1 is the longitudinal strain

ε_r is the radial strain

ε_θ is the circumferential strain

$$\varepsilon_l = \ln \frac{A_o}{A_l} \quad , \quad \varepsilon_r = \ln \frac{t_o}{t_l} \quad , \qquad \varepsilon_\theta = - (\varepsilon_l + \varepsilon_r)$$

where A_o and A_l are the tube cross-sectional areas before and after rolling respectively

t_o is the tube wall thickness before rolling

t_l is the mean tube wall thickness after rolling

CHAPTER (6)

RESULTS

Chapter (6) Results

Tables (6.1) - (6.5) contain the results of the rolling tests. The roll separating forces and rolling torques are listed in table (6.1), while the measurements taken from the pin-loadcells are given in table (6.2). Table (6.3) contains the tube measurements, roll gaps, percentage reductions of area and the peripheral contact angles between tube and rolls and between tube and mandrel.

The mean tube wall thickness, together with the different homogeneous and redundant strains and the mean yield stress are included in table (6.4). The tube cross-sectional areas were determined by the weighing technique and the corresponding values are given in table (6.5) as well as the calculated contact areas and the horizontal projection of the contact areas. Also, the inlet and outlet tube speeds and the mandrel speed are listed in table (6.5). In some of the tests the inlet or outlet tube speed measurement was not successful and therefore the corresponding value was calculated from the known outlet or inlet tube speed by applying the constant volume concept, i.e. A.U = const. When the tube was tight on the mandrel before rolling due to the drawing process which was performed on the tube, the mandrel speed was the same as the inlet tube speed.

The rolling tests were conducted under the following conditions:

1) Tests from 1 to 8 were initial tests to determine the range of loads, torques and pressures.
2) The rolling tests from 9 to 29 were performed using the 31.38 mm mandrel. These tests were free rolling

tests with a dry smooth mandrel. The roll gap and d/t ratio were varied during the tests.

3) Tubes in the tests 30 to 33 and 40 - 42 were rolled on the 37.6 mm mandrel which was dry. The roll gap and d/t ratio were changed in the tests.

4) Tests 34 - 36 and 43 - 45 were the same as the tests in (3), but with a lubricated mandrel.

5) The mandrel with the very rough surface was used in tests 37 - 39 and 46 - 48.

6) Tests 49 - 56 were similar to the tests in (2), but the mandrel was removed from the tubes and re-inserted back again before rolling commenced.

7) In tests 57 - 59, the 37.6 mm mandrel was pulled through the roll groove at a higher speed than that occurring in free rolling.

8) Oval tubes were rolled in tests 78 - 80 on the 37.6 mm mandrel.

All the above tests, i.e. tests 1 - 59 and 78 - 80, were made in groove (A).

9) Groove (B) was used in tests 60 - 77. In tests 60 - 61 and 63 - 65 the roll gap was changed.

10) The mandrel was removed and re-inserted back into the tube before rolling in tests 62 and 66 - 77. These tests were divided as follows:

a - Tests 62 and 66 - 68 were free rolling tests.

b - Front tension was applied to the tubes in tests 69 - 71.

c - Back tension was applied to the tubes in tests 72 - 74.

d - Front and back tensions were applied to the tubes in tests 75-77.

The following symbols are used in the tables of results:

RSF	Roll separating force
O.D.	Tube outer diameter
d/t	Tube diameter to thickness ratio
e	The actual roll gap
J	Reduction of area
q	Tube major axis after rolling
ψ_{c1}	Peripheral contact angle between tube and roll at the exit plane
γ_{c1}	Peripheral contact angle between tube and mandrel at the exit plane
t_1	Mean tube wall thickness after rolling
ε_r	Homogeneous radial strain
ε_l	Homogeneous longitudinal strain
ε_θ	Homogeneous circumferential strain
ε_h	Generalized homogeneous strain
$\varepsilon_{red.}$	Redundant strain
$\bar{\varepsilon}_m$	Total generalized strain
$\bar{\dot{\varepsilon}}$	Mean strain rate
$\bar{\sigma}_y$	Mean yield stress
A_1	Tube cross-sectional area after rolling
U_o	Tube inlet speed
U_1	Tube outlet speed
V_b	Mandrel speed

Table (6.1) Roll separating force and rolling torque.

Test No.	Front RSF, kN	Rear RSF, kN	Total RSF, kN	Upper Torque N.m	Lower Torque N.m	Total Torque N.m
1	14.753	15.333	30.09	393.449	377.973	771.422
2	19.832	20.373	40.2	536.798	513.595	1050.393
3	17.8	20.315	38.12	509.355	492.444	1001.799
4	18.767	20.896	39.66	537.782	492.444	1030.226
5	15.382	14.201	29.58	451.402	399.094	850.496
6	21.476	19.483	40.96	543.918	504.698	1048.616
7	21.186	19.406	40.59	543.918	475.797	1019.717
8	21.96	21.67	43.6	563.215	507.787	1071.002
9	2.676	3.032	5.708	62.037	60.03	122.067
10	4.237	4.14	8.377	89.670	83.376	173.046
11	2.07	1.838	3.908	26.230	41.354	67.584
12	10.293	9.771	20.064	262.3	229.448	491.748
13	11.048	11.299	22.343	295.85	277.472	573.322
14	11.575	11.547	23.122	309.105	270.135	579.14
15	16.987	15.594	32.581	445.3	425.546	870.846
16	13.769	13.092	26.761	391.418	354.622	746.04
17	16.091	16.542	32.633	480.883	424.656	905.539
18	16.852	16.291	33.143	538.02	394.864	932.884
19	4.295	4.063	8.358	88.817	81.908	170.725
20	6.443	5.882	12.325	154.94	131.4	286.34
21	6.125	5.947	12.072	150.25	137.402	287.652
22	9.035	8.997	18.032	230.580	196.766	427.346
23	9.229	9.539	18.768	239.120	171.420	410.54
24	11.628	10.622	22.250	289.14	272.698	561.838
25	5.611	5.321	10.932	128.710	120.727	249.437
26	7.004	6.733	13.737	174.460	151.41	325.87

Table (6.1) continued

Test No.	Front RSF, kN	Rear RSF, kN	Total RSF, kN	Upper Torque N.m	Lower Torque N.m	Total Torque N.m
27	7.35	7.573	14.923	175.294	154.744	330.038
28	9.345	8.821	18.226	236.679	202.768	439.447
29	9.829	9.848	19.677	257.42	236.118	493.538
30	14.67	14.15	28.82	-	-	-
31	23.38	23.2	46.5	527.363	480.24	1007.603
32	19.95	21.04	40.99	431.746	421.766	852.964
33	15.55	16.45	32	329.337	300.251	629.588
34	11.365	12.987	24.352	277.673	232.783	510.456
35	15.125	16.64	33.765	355.881	334.390	690.271
36	17.25	18.96	36.21	399.648	383.523	783.173
37	19.373	20.934	40.309	377.406	362.848	740.254
38	22.775	25.494	48.269	457.766	441.554	899.320
39	21.175	23.334	44.509	435.523	382.191	817.714
40	9.292	9.867	19.159	197.911	167.306	365.217
41	12.375	13.52	25.895	261.888	226.113	488.001
42	17.575	18.694	36.269	367.361	340.17	707.531
43	9.475	9.654	19.129	200.183	170.085	370.268
44	11.625	12.107	23.732	259.736	216.108	475.844
45	15.725	17.92	33.645	370.231	312.823	683.054
46	8.375	8.747	17.122	170.766	132.733	303.499
47	12.2	12.747	24.947	233.906	201.434	435.340
48	17.55	19.147	36.697	345.118	312.823	657.941
49	11.594	11.867	23.461	269.063	218.443	487.506
50	10.825	10.4	21.225	226.443	209.520	435.483
51	14.325	14.24	28.565	320.723	288.144	608.867
52	15.525	15.334	30.859	362.340	337.680	700.0 1

Table (6.1) continued

Test No.	Front RSF, kN	Rear RSF, kN	Total RSF, kN	Upper Torque N.m	Lower Torque N.m	Total Torque N.m
53	9.525	9.947	19.472	234.623	188.094	422.717
54	11.575	12.267	23.842	282.696	240.787	523.483
55	13.29	13.92	27.21	320.006	276.805	596.811
56	15.625	16.907	32.532	390.321	328.164	718.485
57	13.15	14.64	27.79	53.46	56.16	109.62
58	10.45	11.734	22.184	40.838	2.16	42.998
59	9.725	10.533	20.258	-16.335	-9.36	-25.695
60	8.30	10.907	19.207	301.95	191.763	494.713
61	11.9	14.667	26.567	253.996	281.474	535.470
62	12	15.867	27.867	321.441	276.805	598.246
63	15.75	16.907	32.657	381.424	316.158	697.582
64	16.525	17.867	34.392	443.416	342.838	786.254
65	16.95	18.347	35.297	449.156	355.311	804.667
66	10.15	11.12	21.27	195.161	199.433	394.894
67	15.7	17.12	32.82	353.011	300.817	653.828
68	18.875	20.374	39.249	420.456	369.518	789.974
69	10.95	12.507	23.457	190.856	145.406	336.262
70	16.475	18.214	34.689	293.458	241.454	534.912
71	17.05	18.48	35.53	320.005	298.149	618.155
72	10.675	11.44	22.115	280.543	225.447	505.990
73	12.9	14.24	27.14	350.858	268.801	619.659
74	18.525	19.627	38.152	440.547	392.196	832.743
75	17.325	18.307	35.832	397.496	371.519	769.015
76	14.75	15.822	30.572	343.204	265.689	608.893
77	11.271	11.889	23.160	249.929	206.214	456.143
78	11.650	11.974	23.624	259.731	213.745	473.476

Table (6.1) continued

Test No.	Front RSF, kN	Rear RSF, kN	Total RSF, kN	Upper Torque N.m	Lower Torque N.m	Total Torque N.m
79	11.5	11.627	23.127	259.731	233.45	493.181
80	11.85	12.214	24.064	283.345	242.121	525.466

Table (6.2) Average Pin Load, and Mean Pressure

Test No.	Average Pin Load, N			Mean pressure p_m, $N.mm^{-2}$
	Pin 1	Pin 2	Pin 3	
1	254.414	211.731	73.868	42.973
2	301.319	252.048	99.062	45.166
3	246.812	234.293	123.091	40.655
4	289 712	257.255	124.666	44.74
5	251.156	205.256	86.602	43.212
6	284.757	241.969	100.204	49.897
7	269.144	216.737	82.974	45.268
8	309.126	254.251	65.516	50.046
9	94.285	39.249	-	14.168
10	133.724	72.491	-	21.88
11	-	-	-	-
12	158.364	155.594	38.68	28.062
13	154.834	162.67	58.176	29.951
14	151.78	129.829	-	29.88
15	266.225	228.285	68.46	44.80
16	249.595	199.382	48.264	39.569
17	218.031	228.085	88.177	42.518
18	258.962	209.595	76.47	43.372
19	90.891	93.317	-	19.545
20	129.311	95.519	-	23.855
21	110.169	77.23	-	19.884
22	189.114	131.297	28.206	27.742
23	220.542	164.873	42.993	34.367
24	214.976	122.553	42.993	30.281
25	98.901	117.01	29.575	19.541
26	112.545	107.534	-	23.351

Table (6.2) continued

Test No.	Average Pin Load, N			Mean pressure p_m, $N.mm^{-2}$
	Pin 1	Pin 2	Pin 3	
27	127.275	110.338	-	25.212
28	157.006	148.452	40.39	27.522
29	187.485	156.262	41.418	30.65
30	370.489	238.364	7.188	49.023
31	577.15	341.58	20.661	75.906
32	509.915	280.231	20.121	64.816
33	430.902	230.688	-	53.078
34	274.778	220.208	17.868	40.812
35	373.001	240.53	16.088	47.674
36	418.955	250.42	14.24	54.367
37	492.673	275.344	15.54	62.354
38	560.282	346.833	20.196	73.793
39	496.067	283.821	19.58	63.621
40	295.142	95.052	-	41.401
41	348.360	141.11	-	51.934
42	481.201	220.809	22.523	57.657
43	265.139	121.085	-	40.980
44	344.830	140.976	5.956	39.135
45	404.972	261.794	12.597	54.062
46	280.684	67.618	-	36.956
47	366.552	111.606	-	50.734
48	489.347	192.841	20.743	55.938
49	334.988	188.102	7.941	42.258
50	293.717	169.946	23.961	38.804
51	356.913	181.56	12.323	43.831
52	282.856	186.099	12.254	38.293
53	210.767	156.128	-	38.929

Table (6.2) continued

Test No.	Average Pin Load, N			Mean pressure p_m, N.mm^{-2}
	Pin 1	Pin 2	Pin 3	
54	289.848	199.783	-	51.952
55	310.415	200.25	-	54.183
56	367.163	181.093	-	58.172
57	343.133	149.987	-	52.322
58	217.08	117.013	-	35.448
59	278.308	106.8	-	40.861
60	250.885	40.718	-	30.94
61	331.662	85.307	-	44.242
62	357.117	101.06	-	48.614
63	410.946	109.806	-	55.253
64	383.568	115.077	-	52.908
65	410.946	142.374	-	58.710
66	-	-	-	-
67	416.715	227.684	-	68.373
68	440.813	271.406	-	75.569
69	326.503	149.453	-	50.501
70	452.828	227.751	-	72.212
71	420.720	245.907	-	70.731
72	293.445	182.161	-	50.463
73	319.783	225.749	-	57.883
74	445.021	301.243	-	79.181
75	385.898	265.198	-	69.083
76	392.550	231.689	-	66.234
77	252.989	161.468	-	43.975
78	335.056	134.635	-	49.836
79	290.798	130.855	-	46.861

Table (6.3) Tube dimensions, roll gap, percentage reduction of area and peripheral contact angle.

Test No.	O.D. mm	d/t	e mm	J%	q mm	ψ_{c1}°	γ_{c1}° measured	γ_{c1}° calculated
1	41.98	7.92	1.23	12.09	44.08	64.5	55	55.79
2	42.52	7.64	1.42	17.55	44.47	69	58	59.77
3	42.75	7.5	1.38	19.14	44.6	69.5	64.5	62.2
4	42.76	7.5	1.41	18.83	44.68	71	61	62.13
5	41.55	8.17	1.22	13.31	43.93	63.5	52	51.48
6	42.58	7.61	1.43	17.96	44.69	70	60	60.3
7	42.44	7.68	1.43	16.95	44.54	69	57.51	59
8	42.39	7.7	1.48	15.54	44.68	70	56	58.16
9	39.19	10	0.52	0.69	40.12	32.75	28.75	28.901
10	39.18	10	0.38	1.33	40.5	35.5	27.5	30.75
11	39.14	10	0.82	0.42	39.14	21	21	22.53
12	41.99	7.9	2	5.31	44.64	63.5	50.5	50.09
13	41.97	7.9	1.65	7.87	44.64	67.5	54	52.7
14	42.01	7.9	1.67	8.72	44.56	67.25	54.25	52.94
15	41.97	7.9	1.34	10.74	44.24	65.5	54.5	54.98
16	41.9	7.9	0.92	12.4	44.52	73	57.5	57.04
17	41.98	7.9	1.03	13.21	44.24	67	55.5	57.08
18	41.95	7.9	0.7	14.89	44.46	73	57.5	58.81
19	40.39	9	1.39	1.2	41.70	-	-	35.47
20	40.38	9	0.95	2.09	42.76	48.5	40.5	40.47
21	41	8.5	1.71	2.76	42.58	44.5	38	40.323
22	40.36	9	0.88	4	43.34	58.5	48	40.95
23	40.36	9	0.85	5.29	41.97	47.5	47.5	41.23
24	40.37	9	0.3	5.84	44.20	66.4	48.9	46.38
25	40.99	8.5	1.68	2.17	42.9	-	-	40.48
26	41.01	8.5	1.49	3.46	43.10	51	43.5	42.92

Table (6.3) continued

Test No.	O.D. mm	d/t	e mm	J%	q mm	ψ_{C1}°	γ_{C1}° measured	γ_{C1}° calculated
27	40.98	8.5	1.51	3.59	42.92	49	43	42.48
28	41	8.5	1.06	5.07	43.94	63	46	46.75
29	41.03	8.5	1.1	5.32	44.14	65.75	47.25	46.80
30	41.02	24	2.02	5.21	44.54	65	40.5	36.70
31	40.99	24	1.6	12.08	45.44	79.5	44.75	41.47
32	40.99	24	1.826	8.57	44.92	71	41.5	38.87
33	41.00	24	2.085	4.94	44.92	66.5	38.5	35.6
34	41.001	24	1.94	5.7	45.22	72.75	39.5	37.56
35	41.00	24	1.87	7.68	44.8	67.5	43	38.498
36	40.99	24	1.62	10.44	44.98	72.5	42.75	41.249
37	41.00	24	2.24	0.46	45.7	77.5	40.5	33.272
38	40.995	24	2.11	0.63	46.2	79	42	35.105
39	41.014	24	2.19	-	46.12	79	43.5	34.255
40	40.28	30.4	1.71	2.9	41	45	31.5	28.801
41	40.25	30.4	1.54	4.09	41.66	47.5	34.5	31.025
42	40.25	30.4	1.36	5.39	43.24	57.13	38.5	33.732
43	40.26	30.4	1.69	1.81	40.78	42.63	31	28.892
44	40.26	30.4	1.5	4.38	41.1	46.75	35.25	31.905
45	40.23	30.4	1.34	8.55	42.16	54.5	38	33.796
46	40.24	30.4	1.89	-	40.50	36.5	27.5	26.51
47	40.24	30.4	1.6	0.502	41.08	41.25	28.25	29.927
48	40.25	30.4	1.57	-	43.38	51.63	33.75	30.51
49	41	24	1.92	6.07	44.66	67.25	39.75	37.76
50	41	24	1.88	7.06	44.3	65	39.5	38.27
51	40.99	24	1.77	8.81	45.38	75.5	41.5	39.52
52	41.05	24	1.52	11.21	45.52	74.5	44.5	43.1

Table (6.3) continued

Test No.	O.D. mm	d/t	e mm	J%	q mm	Ψ_{C1}°	θ_{C1}° measured	θ_{C1}° calculated
53	41.07	24	1.85	8.41	45	67	39	39.69
54	41.02	24	1.68	9.01	45.3	74	41	40.92
55	40.97	24	1.45	11.35	45.44	75	44	42.82
56	41	24	1.55	10.2	45.58	78	48	42.07
57	41.11	24	1.46	13.23	45.2	77.25	42.25	44.41
58	41.02	24	1.65	8.21	45.18	70.75	40.75	41.32
59	41.08	24	1.86	6.5	44.78	67.25	38.75	39.63
60	41.02	24	1.84	4.15	45.1	54.75	38.75	39.02
61	41.02	24	1.73	6.28	47.28	61.1	37.1	40.41
62	41.03	24	1.76	8.31	45.82	59	39	40.21
63	41.01	24	1.69	7.38	47.46	62.75	42.5	40.72
64	41.01	24	1.59	7.59	48.64	64	42.5	41.84
65	40.99	24	1.60	7.83	48.32	62	44	41.37
66	40.99	24	1.88	7.93	44.78	57.5	41	38.14
67	41.03	24	1.85	9.27	44	57	40	39.04
68	41.0	24	1.68	9.79	47.09	60	40.5	40.7
69	40.99	24	1.92	8.23	44.12	53	36.5	37.76
70	41.01	24	1.89	10.75	44.91	56.75	38.75	38.38
71	41.00	24	1.61	12.55	46.36	59.25	41.75	41.48
72	41.01	24	1.90	8.14	43.7	52.75	37.25	38.24
73	40.99	24	1.74	8.71	44.88	55	40	39.92
74	41.00	24	1.66	10.19	46.38	60	46	40.9
75	41.04	24	1.61	13.03	45.56	59	-	41.92
76	41.00	24	1.81	10.38	43.66	55	39	39.18
77	41.02	24	1.92	9.42	43.04	53	38	38.14
78	-	-	1.93	9.18	45.96	55	37.5	-

Table (6.3) continued

Test No.	O.D. mm	d/t	e mm	j%	q mm	Ψ°_{C1}	δ°_{C1} measured	δ°_{C1} calculated
79	-	-	1.67	11.78	46.20	57	43	-
80	-	-	1.39	13.75	46.59	57.25	41.25	-

Table (6.4) Strains, mean strain rate, yield stress and mean tube thickness after rolling

Test No.	t_1 mm	ε_r	ε_1	ε_θ	ε_h	$\varepsilon_{red.}$	$\bar{\varepsilon}_m$	$\bar{\lambda}$ sec^{-1}	$\bar{\sigma}_y$ $N.mm^{-2}$
12	4.99	0.061	0.055	0.007	0.067	0.004	0.071	0.007	10.01
13	4.86	0.087	0.082	0.005	0.098	0.005	0.102	0.008	11.16
14	4.82	0.096	0.091	0.005	0.108	0.004	0.113	0.007	11.5
15	4.72	0.114	0.114	0.001	0.132	0.006	0.138	0.009	12.21
16	4.60	0.134	0.132	0.001	0.154	0.006	0.159	0.007	12.74
17	4.59	0.144	0.142	0.003	0.165	0.006	0.171	0.009	13.03
18	4.50	0.161	0.161	0.000	0.186	0.006	0.192	0.009	13.47
19	4.45	0.013	0.012	0.001	0.014	0.002	0.016	0.005	6.45
20	4.36	0.033	0.021	0.012	0.033	0.003	0.036	0.006	8.16
21	4.69	0.032	0.028	0.004	0.035	0.002	0.037	0.006	8.25
22	4.22	0.063	0.041	0.002	0.064	0.004	0.068	0.007	9.87
23	4.22	0.061	0.054	0.007	0.067	0.003	0.071	0.007	10
24	4.15	0.08	0.06	0.02	0.08	0.005	0.088	0.008	10.68
25	4.67	0.029	0.022	0.007	0.031	0.002	0.033	0.006	7.97
26	4.61	0.044	0.035	0.009	0.047	0.003	0.049	0.006	8.99
27	4.59	0.044	0.037	0.008	0.047	0.003	0.05	0.006	9.01
28	4.51	0.065	0.052	0.013	0.07	0.004	0.072	0.007	10.07
29	4.5	0.07	0.055	0.015	0.072	0.004	0.077	0.007	10.27
30	1.58	0.08	0.054	0.026	0.081	0.003	0.085	0.007	10.56
31	1.45	0.155	0.129	0.027	0.166	0.005	0.171	0.008	13.02
32	1.51	0.117	0.09	0.027	0.122	0.004	0.126	0.007	11.89
33	1.57	0.08	0.051	0.029	0.081	0.003	0.084	0.007	10.54
34	1.56	0.087	0.059	0.029	0.089	0.003	0.092	0.007	10.83
35	1.53	0.106	0.08	0.026	0.111	0.004	0.115	0.008	11.57

Table(6.4) Cont.

Test No.	t_1 mm	ε_r	ε_1	ε_θ	ε_h	$\varepsilon_{red.}$	$\bar{\varepsilon}_m$	$\bar{\lambda}$ sec^{-1}	$\bar{\sigma}_y$ $N.mm^{-2}$
36	1.48	0.135	0.110	0.025	0.144	0.005	0.148	0.008	12.48
37	1.64	0.038	0.005	0.033	0.041	0.004	0.046	0.008	8.78
38	1.63	0.039	0.006	0.032	0.041	0.005	0.046	0.008	8.82
40	1.29	0.037	0.029	0.007	0.039	0.002	0.041	0.005	8.5
41	1.25	0.055	0.042	0.013	0.057	0.003	0.06	0.006	9.51
42	1.22	0.081	0.055	0.026	0.083	0.004	0.087	0.008	10.65
43	1.30	0.021	0.018	0.003	0.023	0.002	0.026	0.006	7.39
44	1.26	0.052	0.045	0.007	0.056	0.003	0.059	0.007	9.49
45	1.18	0.108	0.089	0.019	0.116	0.004	0.119	0.007	11.70
47	1.131	0.008	0.005	0.003	0.008	0.002	0.010	0.006	5.65
49	1.56	0.089	0.063	0.026	0.091	0.003	0.094	0.006	10.88
50	1.54	0.097	0.073	0.024	0.101	0.003	0.104	0.006	11.22
51	1.5	0.121	0.093	0.028	0.127	0.003	0.13	0.007	11.99
52	1.5	0.142	0.119	0.024	0.153	0.004	0.157	0.008	12.69
53	1.55	0.11	0.085	0.026	0.116	0.002	0.118	0.006	11.66
54	1.52	0.120	0.094	0.026	0.126	0.003	0.129	0.007	11.98
55	1.46	0.144	0.121	0.024	0.155	0.004	0.158	0.007	12.72
56	1.49	0.133	0.108	0.025	0.141	0.005	0.145	0.008	12.40
57	1.49	0.167	0.146	0.021	0.181	0.004	0.186	-	13.34
58	1.53	0.114	0.089	0.024	0.120	0.004	0.123	-	11.81
59	1.56	0.097	0.073	0.024	0.101	0.003	0.104	-	11.23
60	1.60	0.068	0.042	0.025	0.068	0.003	0.071	0.006	10.02
61	1.54	0.103	0.065	0.038	0.104	0.005	0.109	0.008	11.38
62	1.525	0.118	0.087	0.031	0.122	0.004	0.126	0.007	11.88
63	1.52	0.116	0.077	0.039	0.118	0.004	0.122	0.007	11.77
64	1.51	0.123	0.079	0.044	0.124	0.004	0.128	0.007	11.95
65	1.50	0.125	0.082	0.043	0.127	0.004	0.131	0.007	12.01

Table (6.4) Cont.

Test No.	t_1 mm	ε_r	ε_1	ε_θ	ε_h	ε_{red}	$\bar{\varepsilon}_m$	$\bar{\lambda}$ sec^{-1}	$\bar{\sigma}_y$ $N.mm^{-2}$
66	1.52	0.11	0.083	0.027	0.116	0.004	0.120	0.007	11.71
67	1.52	0.119	0.097	0.021	0.126	0.004	0.13	0.007	12
68	1.48	0.141	0.103	0.038	0.146	0.004	0.15	0.007	12.52
69	1.53	0.108	0.086	0.022	0.114	0.003	0.117	0.006	11.62
70	1.48	0.142	0.114	0.028	0.15	0.004	0.154	0.007	12.62
71	1.44	0.168	0.134	0.034	0.178	0.005	0.182	0.008	13.26
72	1.54	0.104	0.086	0.018	0.111	0.003	0.113	0.006	11.52
73	1.51	0.116	0.091	0.025	0.122	0.004	0.126	0.007	11.87
74	1.48	0.141	0.108	0.034	0.148	0.004	0.152	0.007	12.56
75	1.45	0.168	0.140	0.029	0.18	0.004	0.184	0.008	13.31
76	1.50	0.128	0.110	0.019	0.139	0.003	0.142	0.006	12.31
77	1.53	0.113	0.099	0.015	0.123	0.003	0.126	0.006	11.885
78	1.42	0.107	0.096	0.011	0.118	0.006	0.124	-	11.8
79	1.38	0.132	0.125	0.007	0.149	0.007	0.156	-	12.66
80	1.33	0.155	0.148	0.007	0.175	0.007	0.182	-	13.25

Table (6.5) Tube Cross-sectional area after rolling, contact area between tube and rolls, horizontal projection of the contact area, tube and mandrel speeds

Test No.	A_1 mm^2	Contact Area mm^2	Horizontal Projection mm^2	U_o $mm.\ sec^{-1}$	U_1 $mm.\ sec^{-1}$	V_b $mm.\ sec^{-1}$
12	578.98	1267.25	552.06	3.15	3.33	3.15
13	562.04	1384.38	605.68	3.07	3.34	3.07
14	558.77	1283.66	563.81	3.04	3.38	3.04
15	544.42	1518.12	674.32	3	3.45	3
16	530.20	1855.03	769.94	2.97	3.4	2.97
17	529.74	1897.93	787.68	2.95	3.4	2.95
18	518.02	1650.12	705.73	2.97	3.48	2.97
19	501.31	555.19	265.35	3.3	3.5	3.3
20	496.32	765.89	358.18	3.33	3.4	3.33
21	531.24	701.43	328.79	3.3	3.4	3.3
22	485.48	935.02	429.97	3.29	3.45	3.29
23	478.81	890.46	415.50	3.15	3.33	3.15
24	476.64	1334.77	592.71	3.15	3.35	3.15
25	534.12	754.69	353.71	3.3	3.37	3.3
26	528.61	797.59	371.42	3.19	3.3	3.19
27	525.72	822.10	380.94	3.29	3.41	3.29
28	518.74	1072.20	481.44	3.14	3.31	3.14
29	519.49	1160.34	517.60	3.14	3.33	3.14
30	200.05	1060.84	477.30	3.24	3.42	3.24
31	184.19	1550.67	649.87	2.97	3.4	2.97
32	191.49	1200.46	528.47	3.15	3.44	3.15

Table (6.5) Cont.

Test No.	A_1 mm^2	Contact Area mm^2	Horizontal Projection mm^2	U_o $mm.\ sec^{-1}$	U_1 $mm.\ sec^{-1}$	V_b $mm.\ sec^{-1}$
33	199.64	1036.90	463.45	3.25	3.42	3.25
34	197.99	1152.40	501.30	3.23	3.43	3.23
35	193.94	1278.52	568.30	3.2	3.5	3.2
36	187.57	1479.69	639.29	3.09	3.45	3.09
37	208.99	1411.67	600.96	3.34	3.35	3.34
38	208.25	1620.58	681.09	3.37	3.4	3.37
40	159.03	555.63	264.74	3.3	3.4	3.3
41	155.08	759.37	356.79	3.27	3.41	3.27
42	153.42	994.23	460.91	3.23	3.41	3.23
43	159.71	577.35	276.67	3.34	3.4	3.34
44	155.54	700.25	332.72	3.26	3.41	3.26
45	147.19	891.42	415.96	3.15	3.45	3.15
47	160.40	528.42	253.54	3.37	3.39	3.37
49	197.16	945.61	421.10	3.22	3.45	3.27
50	194.95	1001.67	446.07	3.19	3.41	3.25
51	190.74	1257.94	540.09	3.18	3.49	3.23
52	189.29	1451.56	616.61	3.07	3.46	3.2
53	196.84	952.56	423.48	3.16	3.53	3.26
54	192.04	1123.89	487.43	3.16	3.6	3.22
55	184.52	1242.81	536.13	3.05	3.6	3.1
56	188.32	1610.81	673.56	3.08	3.6	3.15
57	187.55	1299.57	599.8	3.31	-	4.09
58	193.25	1376.80	633.24	3.47	-	4.25
59	199.68	1603.42	724.69	3.50	-	4.12
60	202.10	934.17	426.01	3.18	3.51	3.18

Table (6.5) Cont.

Test No.	A_1 mm^2	Contact Area mm^2	Horizontal Projection mm^2	U_o mm. sec^{-1}	U_1 mm. sec^{-1}	V_b mm. sec^{-1}
61	198.10	1260.98	571.69	3.09	3.3	3.09
62	194.17	1144.13	519.09	3	3.4	3.01
63	195.24	1128.64	521.94	3.05	3.52	3.05
64	194.56	1131.47	512.24	3.03	3.65	3.03
65	192.74	1184.41	534.62	3.18	3.65	3.22
66	192.66	1128.80	514.37	3.09	3.65	3.16
67	191.89	1123.96	511.16	3.06	3.36	3.17
68	189.34	1085.42	495.39	3.01	3.37	3.18
69	192.56	828.99	385.59	3.25	3.57	3.28
70	187.91	1047.08	480.31	3.13	3.64	3.15
71	183.54	1189.95	542.42	3.07	3.57	3.12
72	193.29	856.97	395.25	3.04	3.25	-
73	191.49	942.14	436.76	3.03	3.2	-
74	189.95	1053.71	482.41	2.91	3.14	-
75	184.62	1079.67	495.43	2.86	3.34	-
76	188.11	972.62	445.74	2.96	3.58	-
77	191.22	874.90	402.53	3.18	3.36	-
78	181.35	910.01	399.13	3.12	3.43	-
79	176.47	1056.54	480.40	3.05	3.46	-
80	169.78	1131.35	484.82	3.02	3.5	-

CHAPTER (7)

DISCUSSION

The effect of changing the rolling conditions (e.g. reduction of area and tube diameter to thickness ratio) on roll separating force, rolling torque and pressure distribution round the groove will be discussed first, followed by a comparison between the proposed theory and the experimental results and other theoretical approaches.

7.1 Effect of changing the reduction of area, J, and d/t ratio

Figure (7.1) shows the effect of changing J and d/t ratio on the roll separating force. It was found that a linear equation in the form $y = A + Bx$ described accurately the relationship between the roll separating force, RSF, and the reduction of area, J, for the different d/t ratios. The equation of the best fitted line for each d/t ratio was obtained using the least square method.

The increase of roll separating force with the reduction of area, J, may be explained by observing that reducing the roll gap to achieve higher reductions increases both the work required to deform the tube and the work done against friction since the contact area between the tube and the rolls and between the tube and the mandrel is increased. Also, by reducing the roll gap the amount of redundant work is increased due to the increase in the amount of shear which the material suffers as it enters the deformation zone. This can be seen clearly from equation (3·2·29) which indicates that the redundant work is proportional to the maximum angle of contact, Φ_m. As Φ_m increases, when the roll gap is reduced, the redundant work will increase consequently.

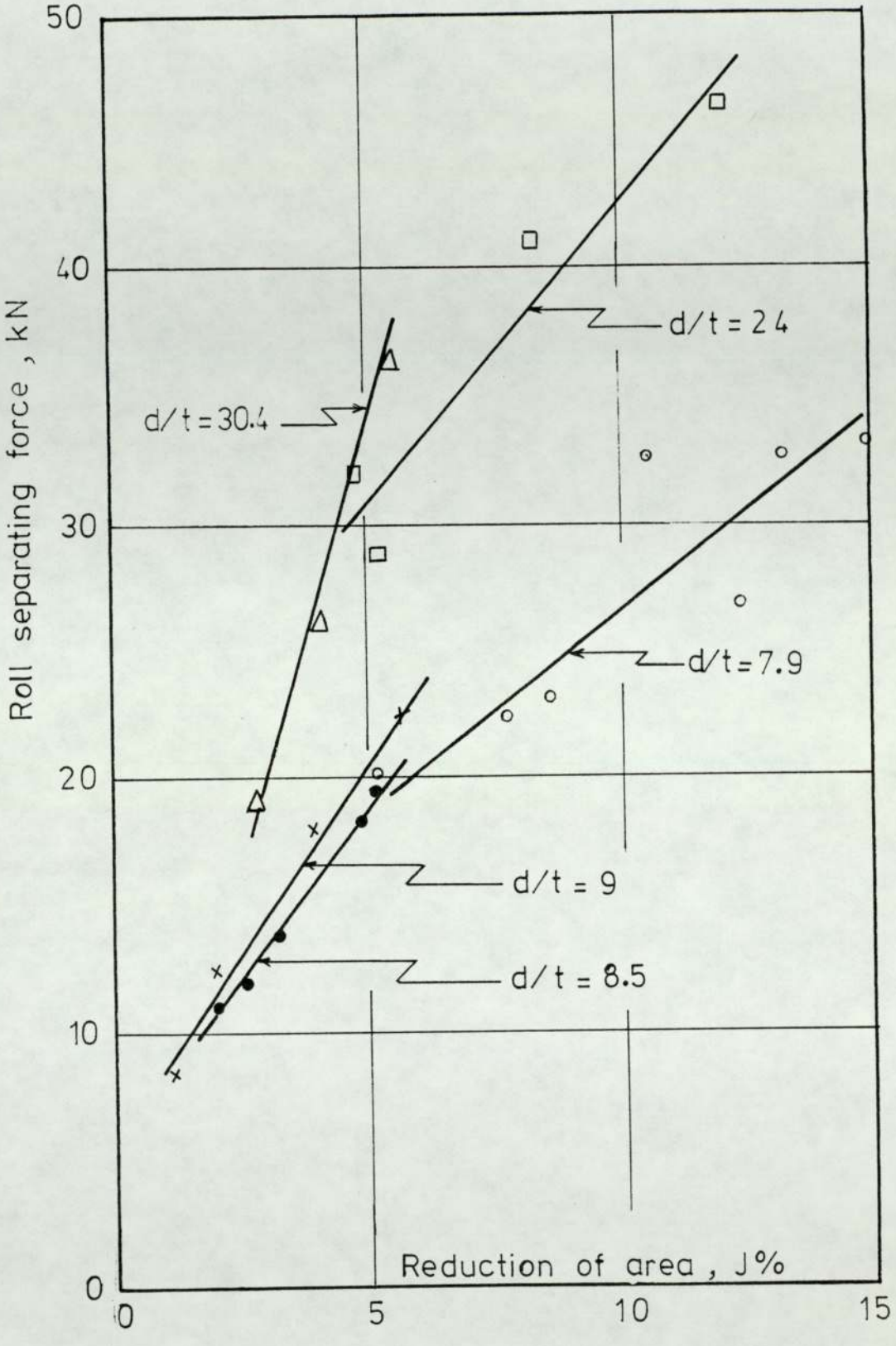

Fig.(7.1) Effect of changing the reduction of area and d/t on RSF

For each of the two mandrel sizes used in the experiments, the d/t ratio could not be changed by a substantially great amount. This was due to the fact that the tube outer diameter could not be reduced, to increase the d/t ratio, below a limit at which the tube would have passed through the groove without being rolled. The effect of changing the d/t ratio on roll separating force can be seen in Figure (7.1). For the same reduction of area, as the tubes were reduced in thickness, i.e. with increasing d/t ratios, the roll separating force became higher due to the increase in the proportion of the frictional work to the total work required in the rolling process. This is one reason why most of the tube reduction in an actual mill should be carried out in the first few stands where the d/t ratio is still fairly low compared with the ratio in later stands when the wall is thin.

It should be noted when comparing the two sets of experiments using the two mandrels, 31.38 mm and 37.6 mm in diameter, that three variables were involved in the experiments. The variables were the reduction of area, d/t ratio and mandrel diameter. It was very difficult to examine the two variables, mandrel diameter and d/t ratio separately, since they were interrelated. To examine the effect of changing the mandrel diameter at the same d/t ratio would entitle either having a large diameter tube on the 37.6 mm mandrel, which would be impossible to roll inside the groove, or having a small diameter tube on the 31.38 mm mandrel, which would pass through the groove without being rolled. Therefore, it was inevitable that when the mandrel diameter was changed, the d/t ratio was changed also and it is clear

from Figure (7.1) that increasing both increased the roll separating force.

The change in rolling torque with J and d/t ratio, Figure (7.2), followed exactly the same trend as for the variation of roll separating force. It may be reasoned that in the absence of front and back tensions and provided that the frictional conditions are constant, the rolling torque will be directly proportional to the roll separating force. The linear relationship between rolling load and torque, Figure (7.3), shows this to be true and is a measure of the accuracy of results.

The pressures round the groove perimeter were not uniformly distributed and the maximum pressure occurred in all the tests at the root of the groove. This result was expected, since due to the ovality of the pass, the maximum reduction occurred at the root of the groove. Figure (7.4) shows some typical examples of the pressure distribution curves obtained from pin-loadcell measurements. Pin number 4 which was situated near the roll shroud, did not touch the tube surface except in very few tests where the reduction of area was high. Since the reductions of area were chosen to be low to avoid exceeding the mill capacity and to prevent fin formation, the groove was not filled completely, and so the tube surface did not make contact with pin 4. The pressure on pin 3 was very small compared with the pressures on pins 1 and 2, and sometimes the pressure was too small to be registered by the pin-load cell. The low values of pressure associated with pin 3 were not due only to its situation in a low deformation zone, compared with pins 1 and 2, but also to the fact that at this part of the

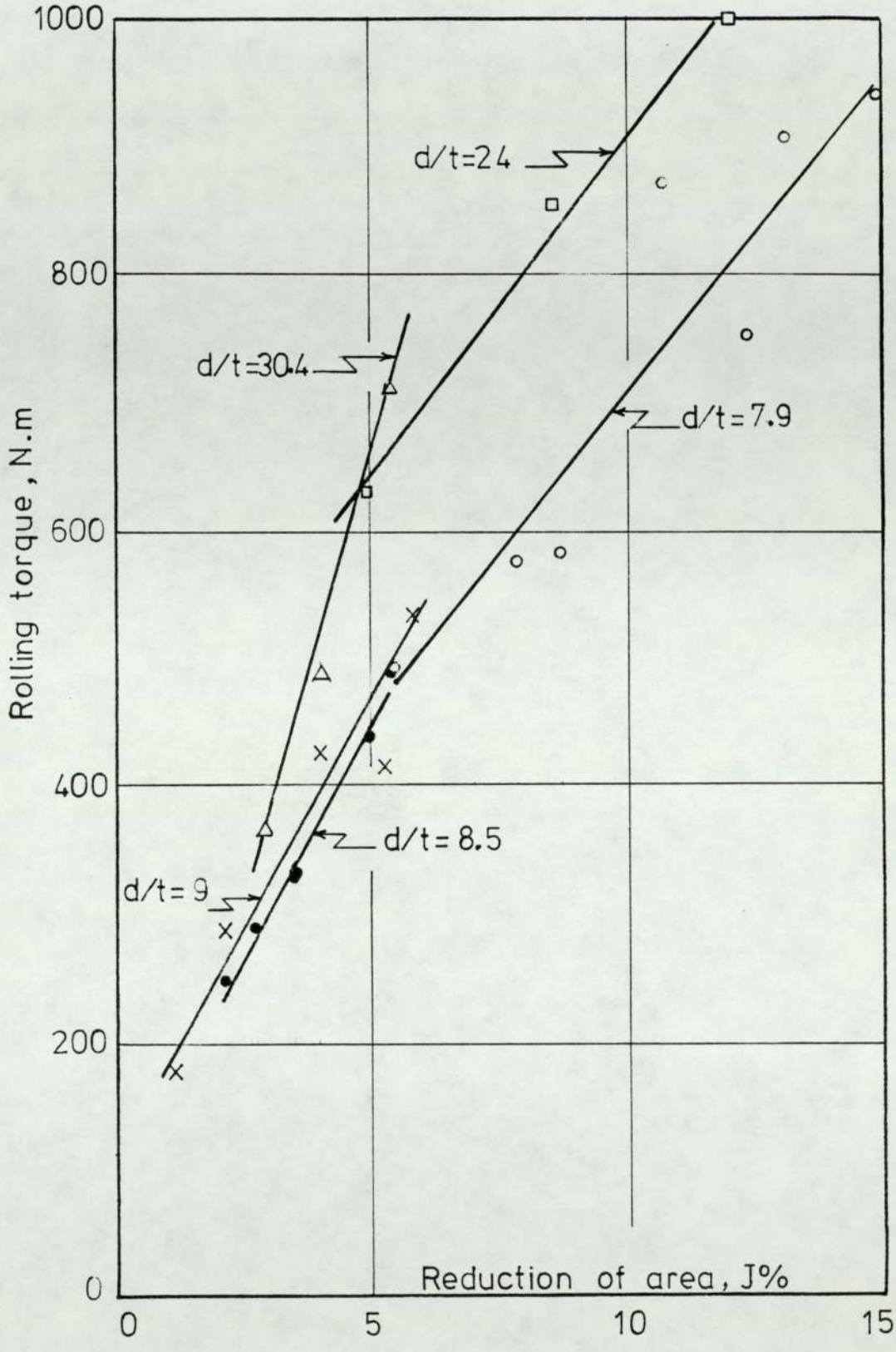

Fig.(7.2) Effect of changing the reduction of area and d/t on the rolling torque

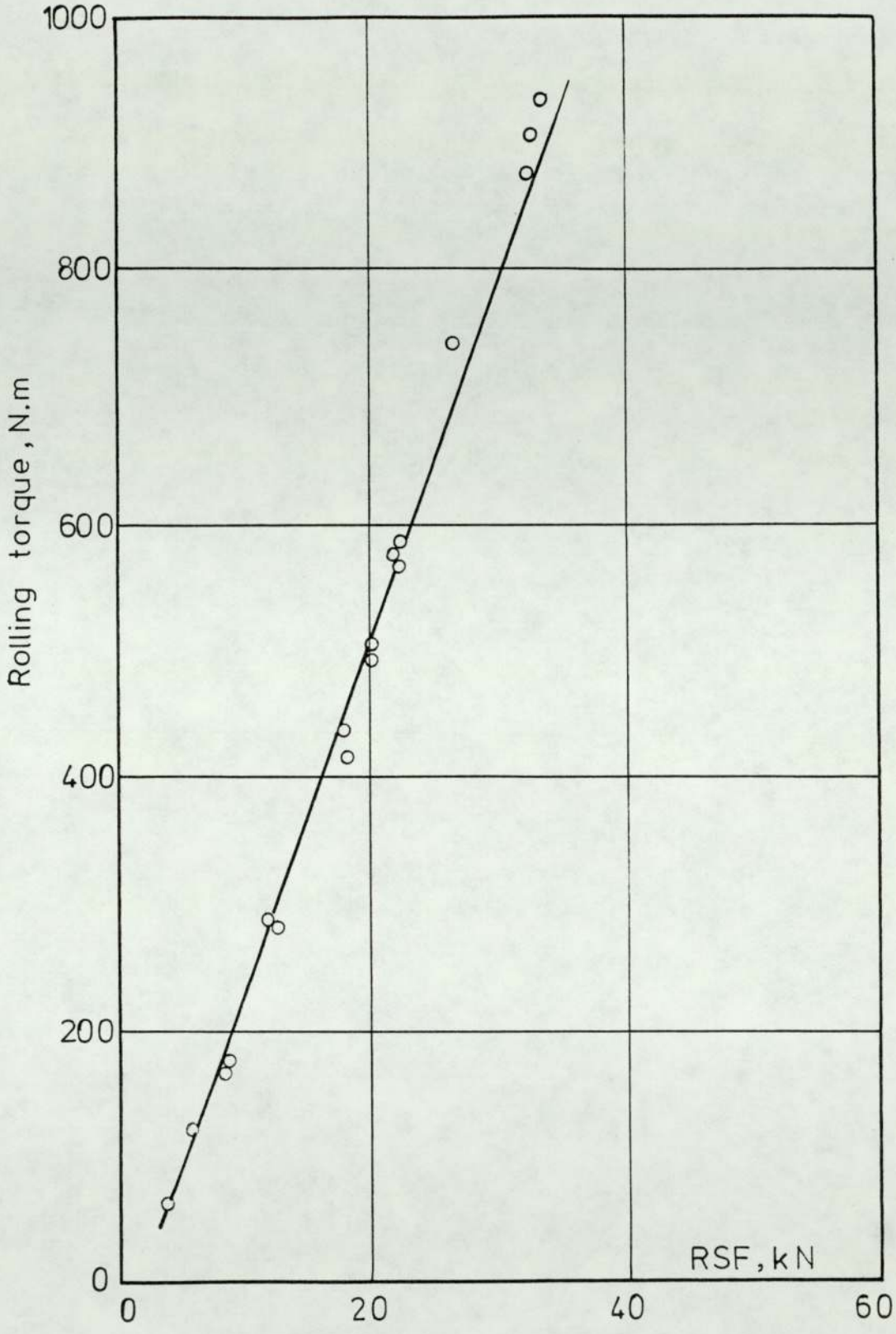

Fig.(7.3) Relationship between the rolling torque and RSF in free rolling tests.

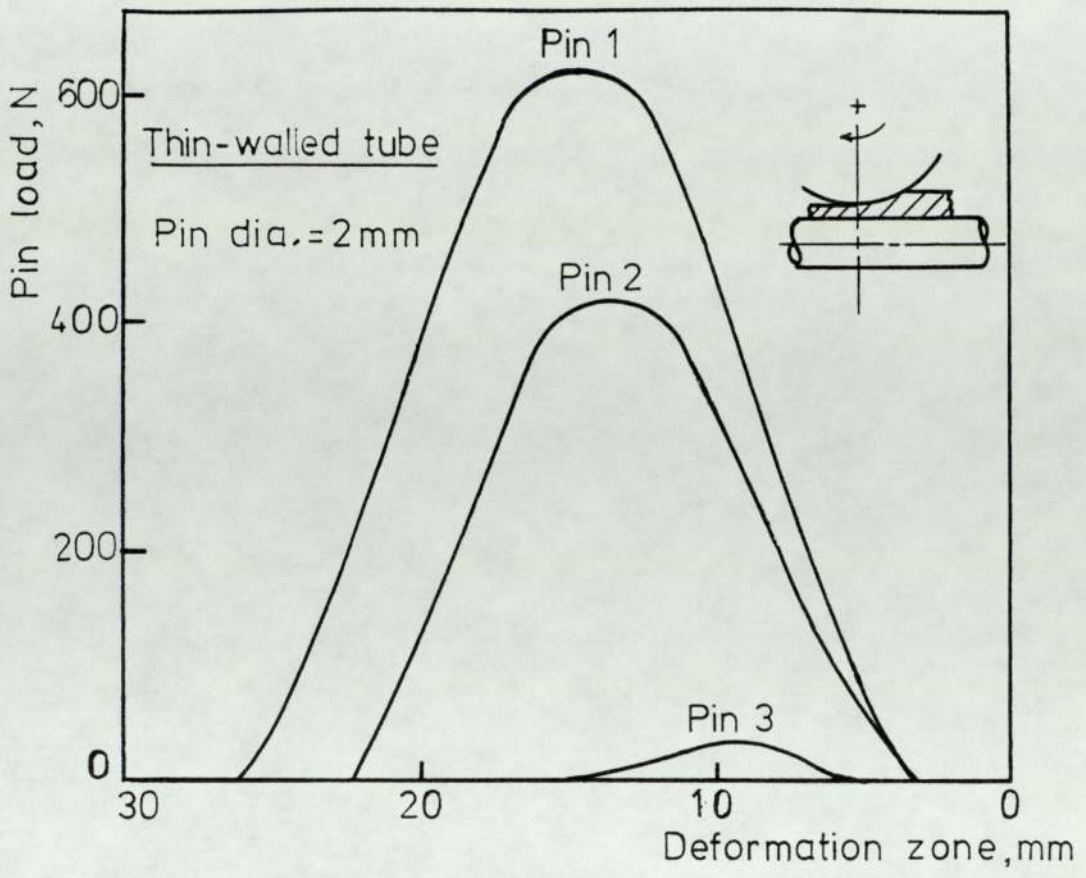

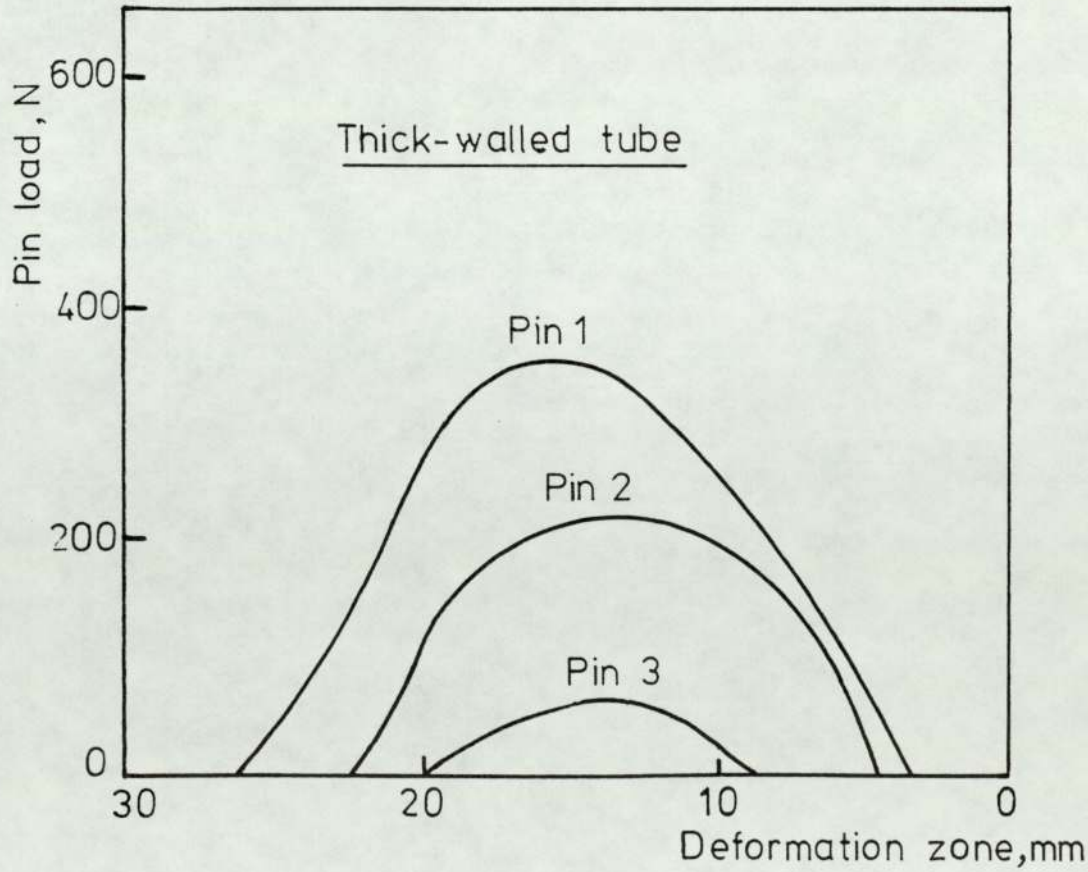

Fig.(7.4) Typical pressure curves

groove the tube inner surface was free. In other words, tube sinking occurred in the region of pin 3 while mandrel rolling occurred in the region of pins 1 and 2. By comparing the results of tube rolling on a mandrel with tube sinking (12), it was found that the pressures in the mandrel rolling process were much higher than those in the tube sinking process; this explains the very low values of pressure picked up by pin 3. The presence of pin 3 in the sinking region of the groove was verified from the clear markings on the tube inner surface which indicated the extent of contact between the tube and mandrel.

In order to assess the effect of changing J and the d/t ratio on the pressure distribution, the mean values for the pressures were calculated and compared with each other. A planimeter was used to trace the area under each pressure distribution curve and a mean value for the pressure corresponding to each pin position was thus obtained. The mean pressure for these mean values was calculated. Since it was known that near the roll shrouds the tube was touching the rolls very lightly and therefore the pressure was negligibly small, a zero value was included in the mean pressure calculation. This was thought to give a more representative value of the mean pressure in the groove. The mean pressure was plotted against J and d/t ratio in Figure (7.5). A trend similar to the roll separating force and the rolling torque can be detected for the mean pressure curves.

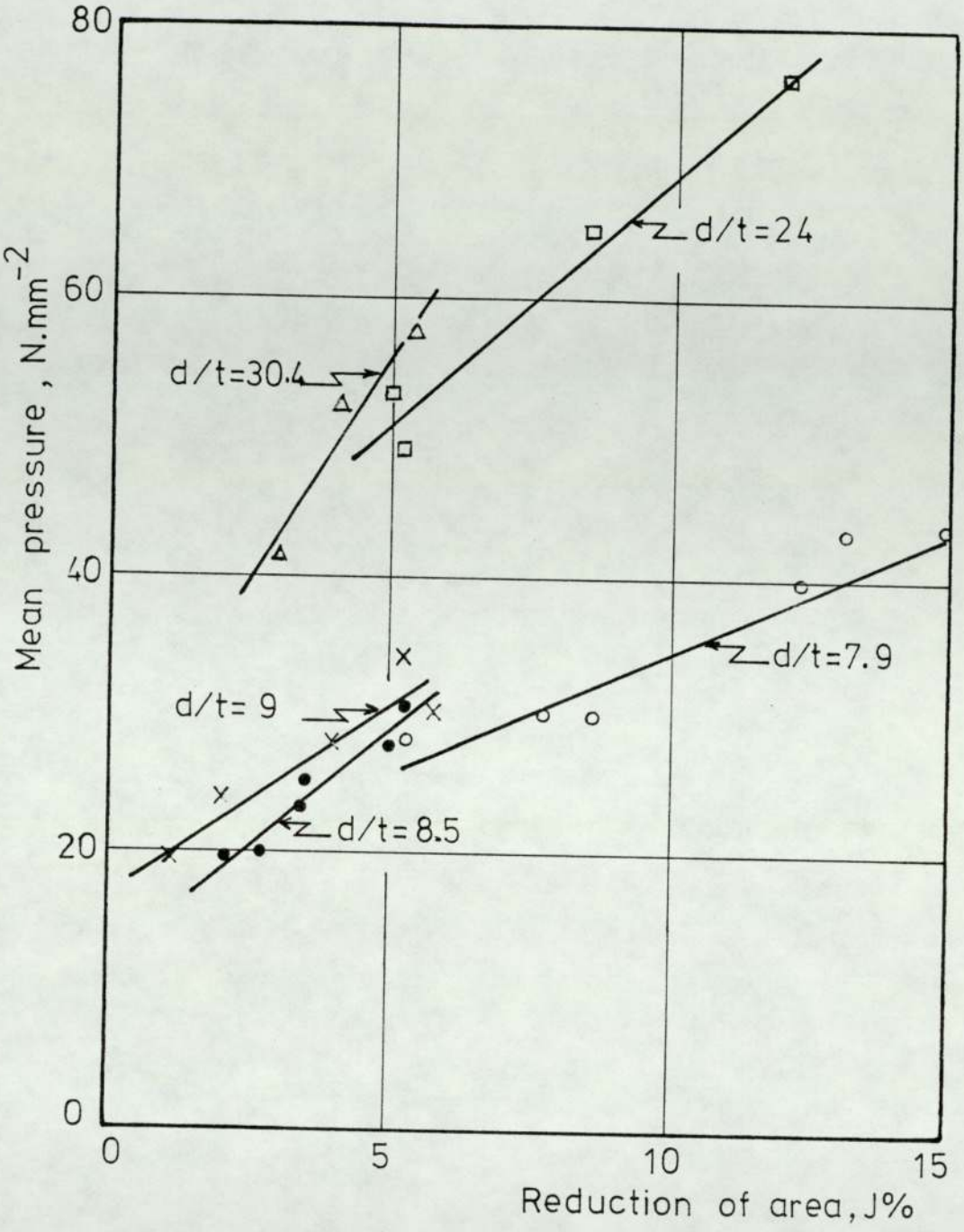

Fig.(7.5)Effect of changing the reduction of area and d/t on the mean pressure

7.2 Effect of changing the frictional conditions on the mandrel surface

Friction on the mandrel surface has a direct effect on the rolling loads and torques. The increase in frictional forces between the tube inner surface and the mandrel increases the work done by the rolls to overcome friction and subsequently leads to an increase in the rolling loads and torques.

Reducing friction between tube and rolls is as important as reducing friction between tube and mandrel, but in a production mill a lubricant is used only on the mandrel surface, i.e. the rolls are unlubricated since this helps to increase the angle of bite enabling higher reductions to be attempted.

Figure (7.6) shows the effect on roll separating force of lubricating the mandrel with graphite grease for two different d/t ratios. A considerable change in RSF could be detected as a result of lubricating the mandrel and the change was greater for the thinner walled tubes having a d/t ratio of 30.4 since the effect of friction on them was more critical than for the tubes with a d/t ratio of 24.

When a very rough mandrel was used in the experiments, very small reductions of area were observed, while the rolling loads and torques were very high. Sometimes the reductions of area were too small to be measured accurately. The results meant that due to the roughness of the mandrel surface, the tube material was prevented from flowing in the longitudinal direction and under the radial pressure from the rolls the material flowed circumferentially. The spread of the tube material in the circumferential direction

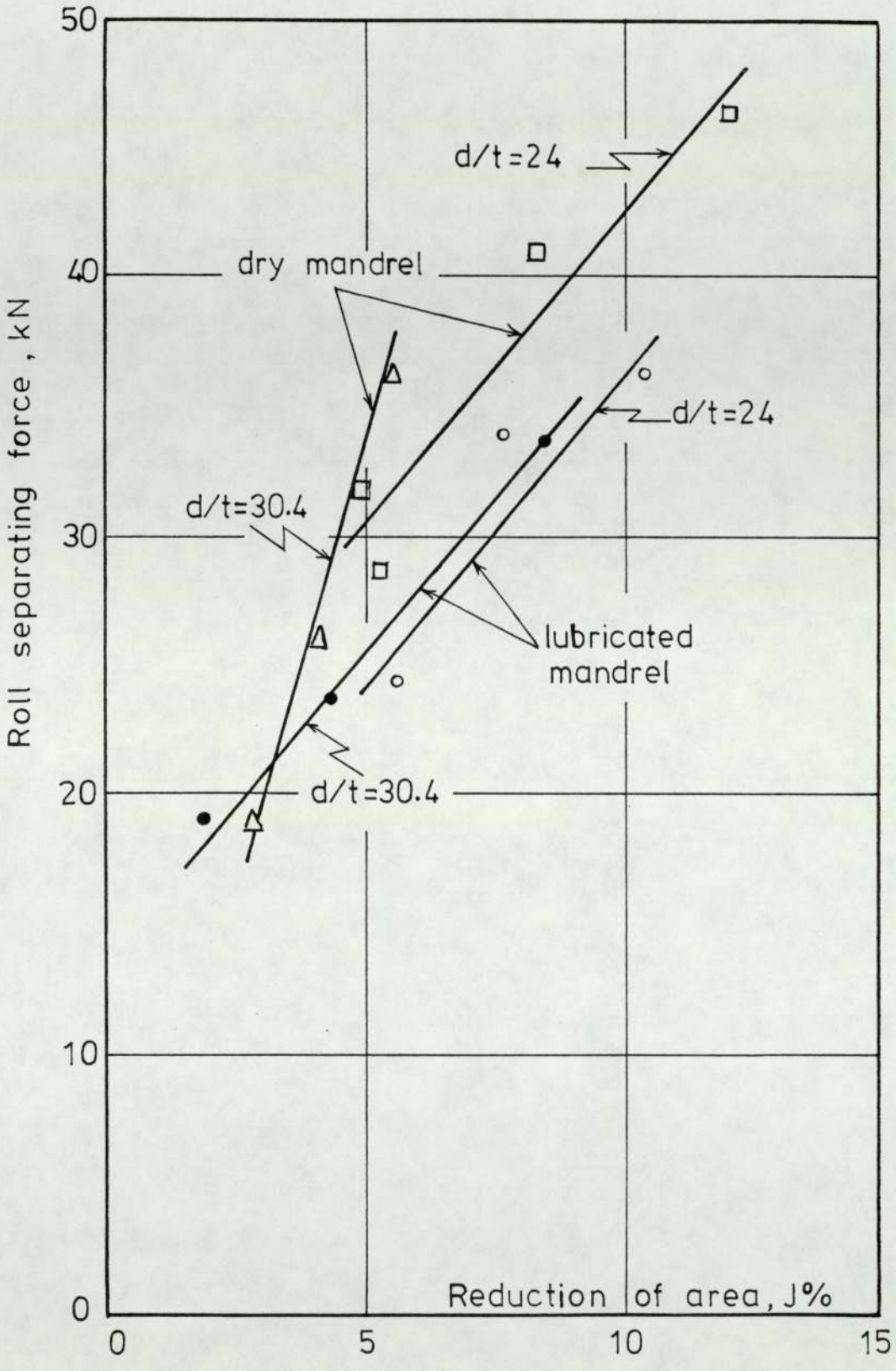

Fig.(7.6) Effect of lubricating the mandrel on RSF

is confirmed by considering table (6.3) of the results in which the peripheral contact angle between tube and rolls is shown for the different conditions on the mandrel surface. Also shown in this table are the different values of strain associated with each tube. It is clear that for the tubes which were rolled on the rough mandrel, the peripheral contact angles between tube and rolls were greater than those for the tubes which were rolled on a dry smooth mandrel although the roll gaps were greater in the case of a rough mandrel. Also, the circumferential strain, ε_θ , was greater than the longitudinal strain, ε_l , when a rough mandrel was used in the rolling tests. The opposite was true when a dry smooth mandrel was used. This indicates that if friction is high between tube and mandrel, the material will flow more in the circumferential direction than in the longitudinal direction.

The effect of changing the frictional conditions on the mandrel surface on rolling torque and the mean pressure is the same as for the effect on RSF as can be seen from tables (6.1) and (6.2) of the results.

7.3 Effect of pulling the mandrel through at a high speed

In a production mill, when the tube is situated in all stands the mandrel in most cases takes the mean velocity between the tube speeds in the first and last stands of the mill. In other words, the mandrel speed is higher than the tube speeds in the first stands, while its speed is lower than the tube speeds in the last stands of the mill.

To investigate the effect of increasing the mandrel speed on rolling loads and torques, the mandrel was attached to the

front tension device through the front tension loadcell and the mandrel was pulled through the roll groove at a higher speed than that occurring in free rolling. Since the mandrel was connected to the front tension device through the front tension loadcell, the horizontal force acting on the mandrel could be measured. The speed of the mandrel was measured so that the work supplied by the mandrel per unit time could be estimated by multiplying the horizontal force on the mandrel by its speed.

When the mandrel was pulled through the roll groove at a higher speed than that occurring in free rolling, only a small reduction was noticed in either the roll separating force or the mean pressure, but very substantial changes were observed in the values of rolling torques. Table (7.1) shows the reduction in torque for increasing values of reduction of area.

Table (7.1) Effect of pulling the mandrel through at a higher speed

Free Rolling			Pulling the mandrel through		
Test No	J%	Rolling Torque N.m	Test No	J%	Rolling Torque N.m
50	6.7	435.983	59	6.5	- 25.695*
51	8.6	609.975	58	8.2	42.998
52	11	700.02	57	13.2	109.62

* the negative sign indicates that the tube is driving the rolls, i.e. drawing takes place as well as rolling

Since the mandrel can be considered to be a roll of infinite diameter (8) , any change in its speed causes a corresponding change in the tube speed. The increase in tube speed leads to a re-distribution of friction between tube and rolls as can be seen from equation (3.2.32)for the calculation of frictional work per unit time between tube and rolls, i.e.

$$\dot{W}_f = \int_S \tau \cdot V_r \cdot dS \qquad (3.2.32)$$

where $\dot{W}_f$ is the frictional work per unit time between tube and rolls,

τ is the shear yield stress at the surface of contact,

V_r is the relative speed between tube and rolls,

S is the surface area of contact (or the contact area).

From table (7.2) it is obvious that the increase in mandrel speed led to an increase in tube speeds.

The work done by front tension, which was generated in the tube due to the increase in mandrel speed, reduced the work done by the torque so that the total power required by the rolls to deform the metal was reduced. To demonstrate this point, the powers supplied by the rolls and by the mandrel were calculated and compared with the power supplied by the rolls in the case of free rolling. Table (7.2) shows such comparison and it is clear that the reduction in the power required by the rolls to deform the tube was balanced by the power supplied through the mandrel so that the total power required in the process remained the same.

In the case of small reductions of area, i.e. test No 59 in table (7.1), where rolling loads were low, the power supplied through the mandrel became higher than the power

Table (7.2) Power supplied by the rolls and through the mandrel

Test No.	Total Torque N.m	Mandrel Speed mm/sec	Horizontal Force on the mandrel kN	Power supplied by the rolls N.m/sec	Power supplied through the mandrel N.m/sec
50	435.983	-	-	15.04	-
51	609.975	-	-	21.04	-
52	700.02	-	-	24.15	-
57	109.62	4.09	4.79	3.78	19.61
58	42.998	4.25	4.27	1.48	18.135
59	-25.695	4.12	4.2	-0.887	17.23

supplied by the rolls and this led to a negative torque being applied by the rolls. Consequently the process changed from one of rolling to one of drawing.

In a production mill the mandrel assumes a mean speed between the tube speeds in the first and last stands of the mill which means that the mandrel speed is higher than the tube speeds in the first stands. This leads to a reduction of the rolling power supplied by the first stands, while the power supplied by the last stands is increased so that the total rolling power in all stands remains unchanged.

It should be mentioned that the measurements of the horizontal force acting on the mandrel while pulling it, provided an approximate method for estimating the friction factor, m, between the tube and the mandrel. Since the only horizontal force opposing the mandrel results from the friction between tube and mandrel, the following relationship can be applied:

$$F = 2\mu P \qquad (7.3.1)$$

where F is the pulling force,

μ is the coefficient of friction between tube and mandrel, and

P is the roll separating force.

The factor 2 was used in the above equation to account for the two rolls.

To relate the coefficient of friction to the friction factor, m, Kudo (22) suggested that the shear stress of a Coulomb type of friction can be equated to that of a constant shear type of friction, i.e.

$$\mu_{av}\, p_{av} = m \frac{\sigma_y}{\sqrt{3}} \qquad (7.3.2)$$

where p_{av} is the average pressure.

Applying the above method to test No. (58) ,

where $F = 4.27$ kN, $P = 22.184$ kN, $p_{av} = 37$ N/mm^2 .

$\therefore \mu = 0.097$ and $m = 0.565$.

Therefore, a value of 0.6 for the friction factor was used in the theoretical predictions of the mean pressure and the RSF.

7.4 Effect of applying front and back tensions

Applying front and back tensions to the tubes presented a problem since because the tubes were thin, the yield stress of the tube material could be easily exceeded. Selecting an appropriate value of the back tension was not as difficult as for the front tension since the ingoing tube was relatively thicker than the outgoing tube. Very small changes in the speed of the carriage to which the front end of the tube was attached, brought a considerable change in the value of the applied front tension. After some trials, it was thought that the correct value of front tension was reached. Unfortunately, after a few tests it was discovered

from measurements of the tube cross-sectional area at different positions along the rolled tube axis, that the area was not the same. This indicated that the tube was extended outside the roll gap under the action of the applied front tension and necking of the tube wall took place. The front tension was adjusted and the trials were repeated again. To be able to draw curves of the effect of applying front and back tensions, the rolling tests were conducted under various degrees of reduction of area by changing the roll gap. However, it was impossible to maintain the same value of the applied tensions for all the tests. Varying the roll gap resulted in changes in tube speeds and the stresses in the tube. Due to these changes, the values of the applied tensions differed from one test to another in the same group, but since the differences were small, the curves in Figures (7.7) and (7.8) were drawn as if the applied tensions were the same for any one group of experiments.

As expected, both front and back tensions helped in reducing the RSF, but the effect was much more pronounced by the application of front tension as can be seen from Figure (7.7), which could be attributed to the value of the front tension being higher than the back tension. When quoting the values of the front and back tensions, it is common to associate them with the yield stress of the material being rolled. The ratio of the front tension or back tension to the load to cause yielding is called the stress coefficient or the stretch coefficient which is the term used in a production mill. Generally this ratio should not exceed 0.8, and if it exceeds unity deformation will take place outside the roll gap. Taking the yield

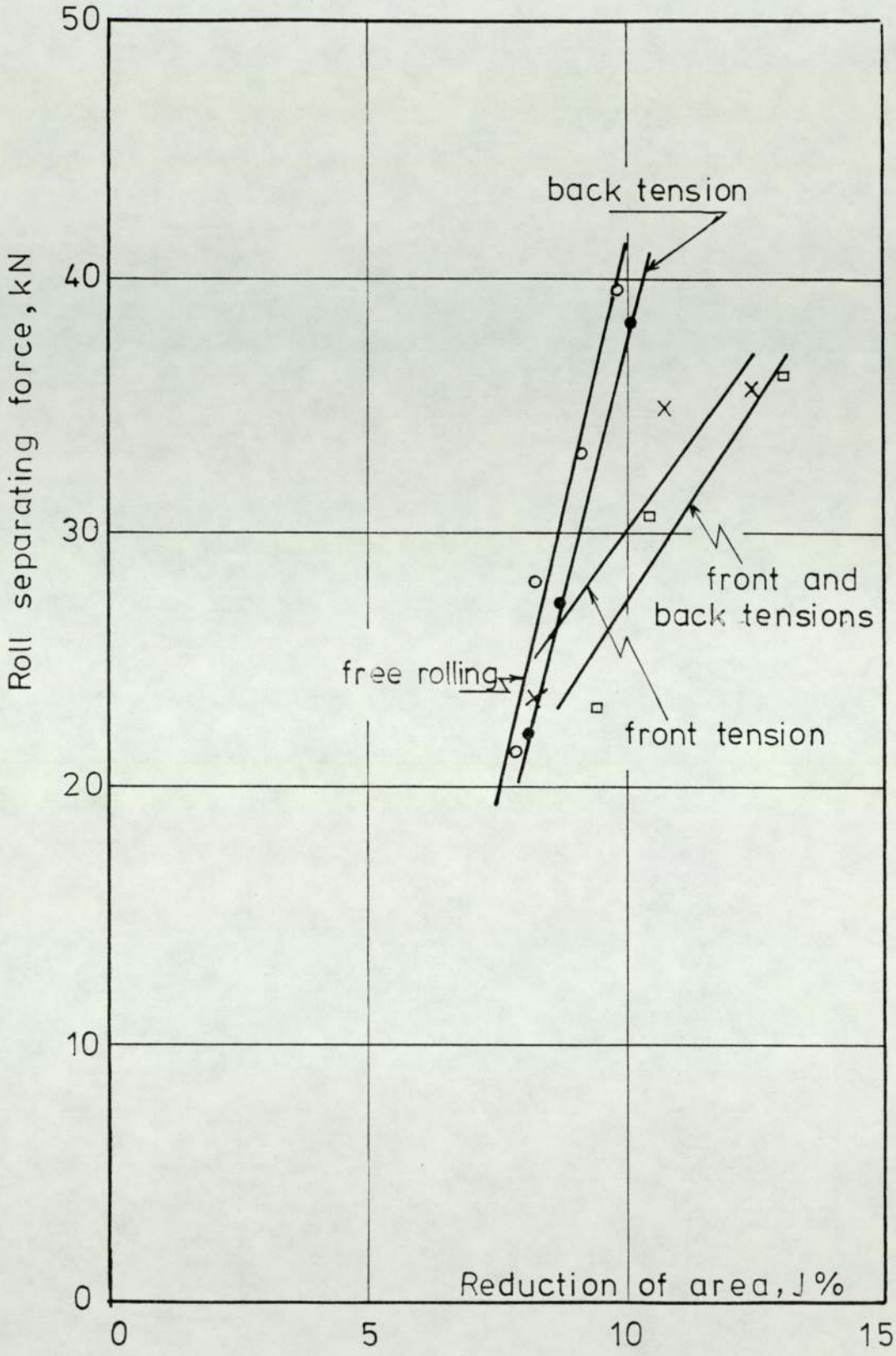

Fig.(7.7) Effect of applying front and back tensions on RSF

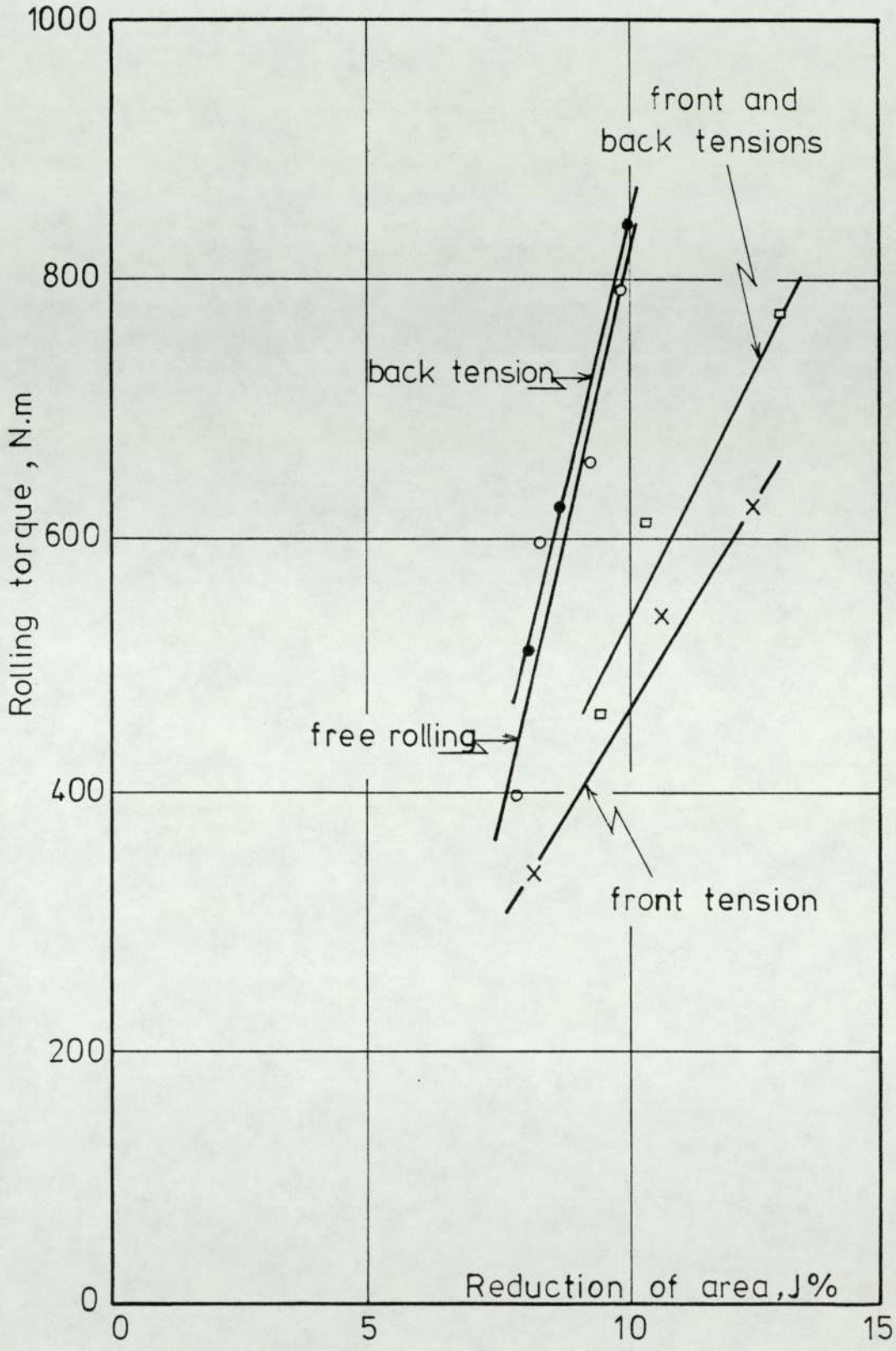

Fig.(7.8) Effect of applying front and back tensions on the rolling torque

stress of lead to be 10 $N.mm^{-2}$, the range of the stress coefficient when applying back tension was 0.29 to 0.34, and when applying front tension only the range was 0.71 to 0.82. The difference in the value of the stress coefficient between the back and front tensions was not due only to the difference in the applied tensions, but also to the difference in the inlet and outlet cross-sectional areas of the tube. The effect of front and back tensions on the rolling torque was great, but predictable, Figure(7.8). As expected, back tension increased the rolling torque while front tension reduced it. From consideration of table (7.3) which contains the values of the different powers associated with the process, it is clear that when back tension is applied to the tube more power is required by the rolls to overcome the added resistance due to the back tension. On the other hand, when front tension is applied, some power to help the rolls is associated with this tension which reduced the torque supplied by the rolls.

Figure (7.9) shows the effect of front and back tensions on the mean pressure which was similar to the effect on RSF.

7.5 Effect of changing the groove shape

Two groove shapes were investigated in the present work and these are shown in Figure (7.10). The only difference between the two grooves was that the sides of groove (B) were opened more than groove (A). The groove side opening is important especially in the first few stands of a production mill for the following reason:

Due to the groove ovality, which is defined as the distance between the centre of the circle forming the root of the groove and the centre of the pass, the tube

Table (7.3) Power values when rolling with front and back tensions

Test No.	Total Torque N.m	Front Tension, N	Back Tension, N	Power Supplied by the rolls N.m/sec	Power Supplied by front tension N.m/sec	Power Supplied by back tension N.m/sec
66	394.594	-	-	13.614	-	-
62	598.246	-	-	20.614	-	-
67	653.828	-	-	22.557	-	-
68	789.974	-	-	27.254	-	-
72	505.990	-	724.5	17.457	-	-2.2
73	619.659	-	598.5	21.378	-	-1.784
74	832.742	-	630	28.730	-	-1.833
69	336.262	1370	-	11.601	4.896	-
70	534.912	1548	-	18.455	5.635	-
71	618.155	1316	-	21.326	4.698	-
75	456.143	448.9	598.5	15.737	2.449	-2.269
76	608.893	503	787.5	21.007	1.801	-2.333
77	769.015	729	714	26.531	1.50	-1.711

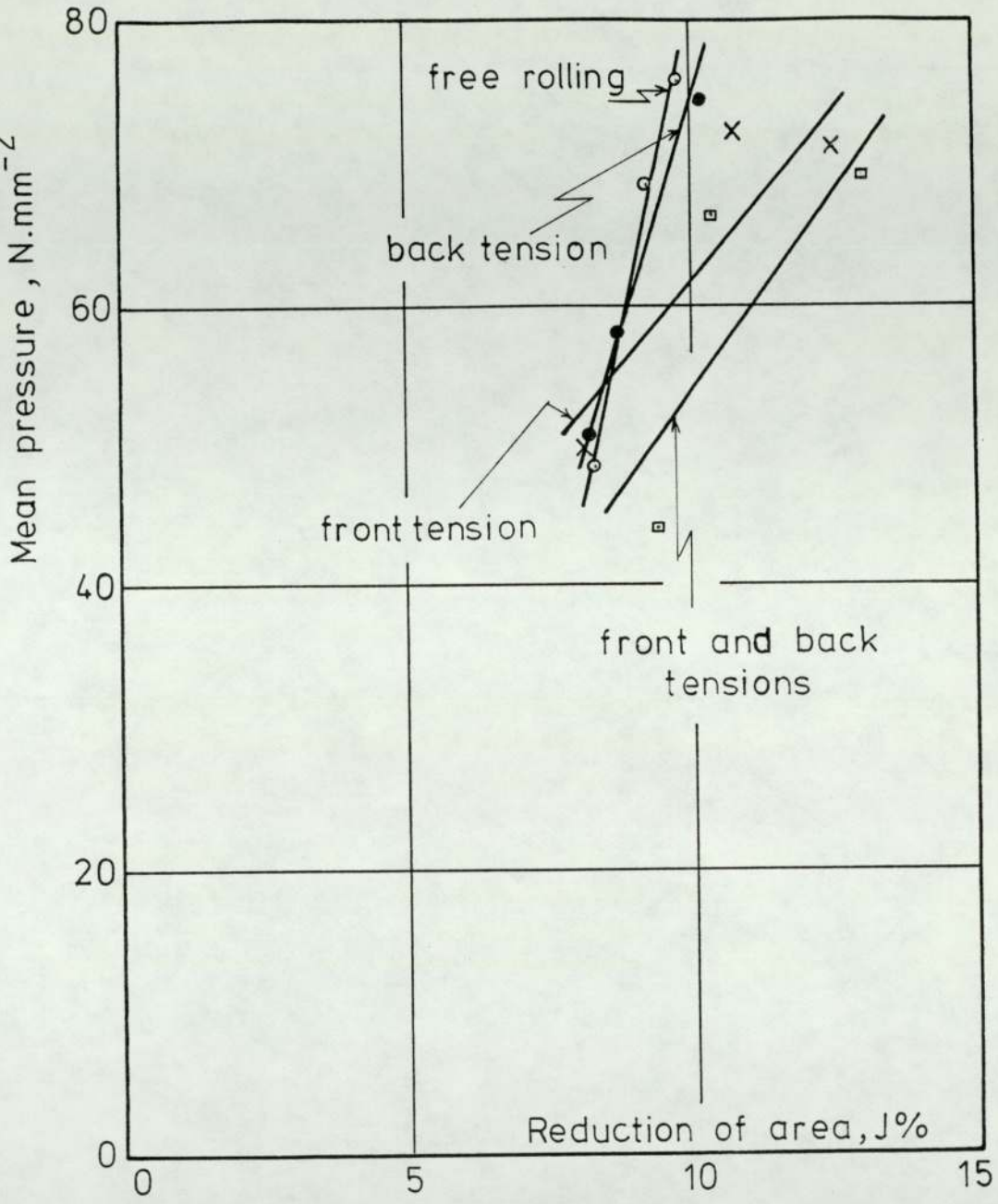

Fig.(7 .9) Effect of applying front and back tensions on the mean pressure

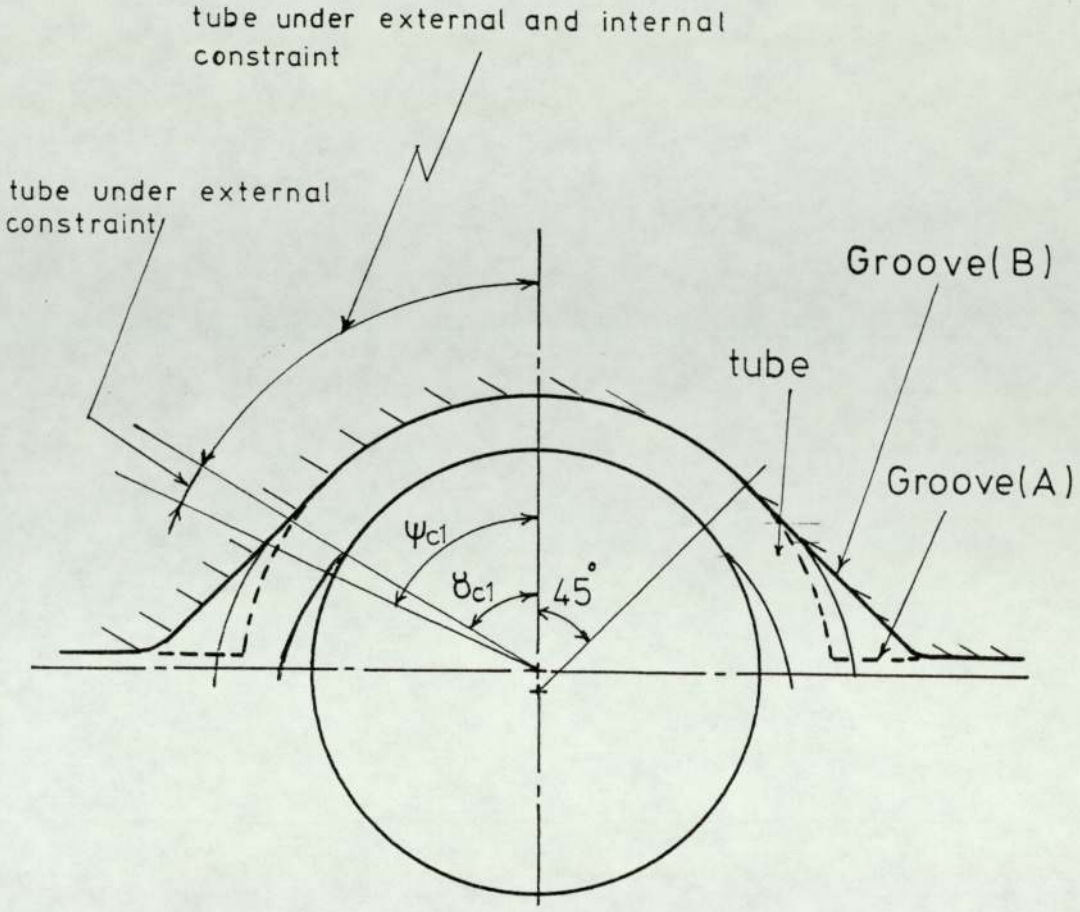

Fig.(7.10) Groove shapes

material at the root of the groove is deformed more in the radial direction than the material at the groove sides. The tube cross-section can be divided into two parts; the first part which is under external and internal constraints, and the second part which is without internal constraint, Figure (7.10). The radial deformation of the material in the first part causes the material to flow longitudinally and circumferentially. The circumferential flow of the material from the first part to the second part leads to an increase in the circumference of the tube in the second part. At low reductions of area, the increase in the circumference in the second part is achieved through an increase in the tube major axis which also means an increase in the peripheral contact angle between tube and groove surface, Figure (7.10). This is shown to be true from consideration of table (6.3) of the results which shows the peripheral contact angle between tube and groove surface and the length of the tube major axis at different reductions of area. By increasing the reduction of area, the peripheral contact angle and the tube major axis increase and this will continue until most of the tube surface is constrained by the groove surface, or in other words until the peripheral contact angle becomes nearly $\pi/2$. On further increase of the reduction of area, the circumferential flow of the material to the second part of the groove leads to a radial flow of the material and thickening of the tube wall and an increase of pressure on the groove sides take place. Consequently, overflow occurs in the groove which results in fin formation on the

tube surface. To avoid this happening to the tube in the first stands of a production mill where the reduction of area is great, the groove sides are opened. It is clear from Figure (7.10) that by using groove (B) more reduction of area can be achieved than by using groove (A) without overfilling the groove.

Figure (7.11) shows the effect on RSF of changing the groove shape. At lower reductions of area, the rolling loads in groove (B) were lower than those in groove (A) since the peripheral contact angles between tube and groove (B) were lower than the angles between tube and groove (A) as can be seen from table (6.3) of the results. This meant that at the same reduction of area, friction between tube and groove (A) was higher than the friction in groove (B). At higher reductions of area and as the contact area between tube and rolls was increased, it was expected that, since the circumference of groove (B) was greater than that of groove (A), friction between tube and rolls would increase more rapidly when rolling in groove (B) than when rolling in groove (A). This explains the higher values of RSF reached in groove (B) than that in groove (A) at higher reductions of area. But it should be emphasized that a limit on the reduction of area will be reached when rolling in groove (A) after which overfilling of the groove will take place. This limit on the reduction of area is higher for groove (B) than for groove (A).

The change in rolling torque and mean pressure with the groove shape followed the same trend as for the variation of RSF as can be seen from the tables of results.

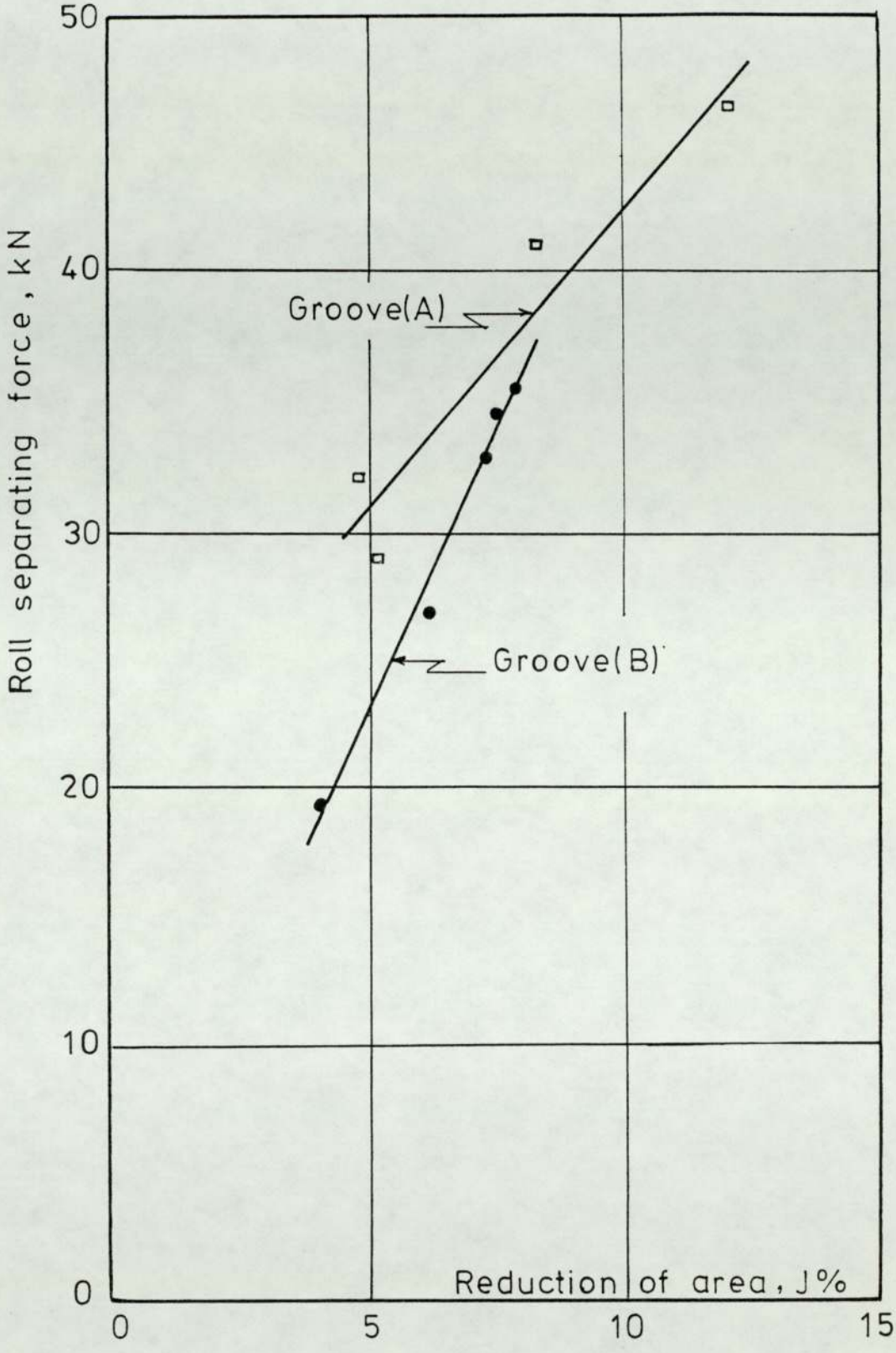

Fig.(7.11) Effect of changing the groove shape on RSF

7.6 Effect of removing the mandrel and re-inserting it again inside the tube before rolling

This point was not intended to be examined as a variable, but when the effect of front and back tensions was examined and the mandrel had been removed from the tube and re-inserted again inside the tube as explined in chapter (4), it was suspected that this might have an effect on the rolling loads and torques.

Free rolling tests, i.e. without front and back tensions, were performed after removing the mandrel and re-inserting it again inside the tube. The results were compared with the tests where the tubes were tight on the mandrel due to the drawing process as mentioned previously. Figure (7.12) shows such comparison for the two groove shapes (A) and (B). It is clear that when the tube was slightly loose on the mandrel, the RSF was lower than when the tube was tight on the mandrel. When the tube was tight on the mandrel, the mandrel travelled at a speed which was equal to or very close to inlet tube speed. This was because the mandrel was held back by the undeformed part of the tube. The slow speed of the mandrel opposed the longitudinal flow of the material and increased the work done by the rolls to over-come friction between tube and rolls since the work done against friction per unit time is proportional to the relative speed between tube and mandrel.

7.7 The arc of contact and the free zone

The use of pin-loadcells allowed measurements of the length of the arc of contact at different positions round the groove to be made. The maximum length of the arc of

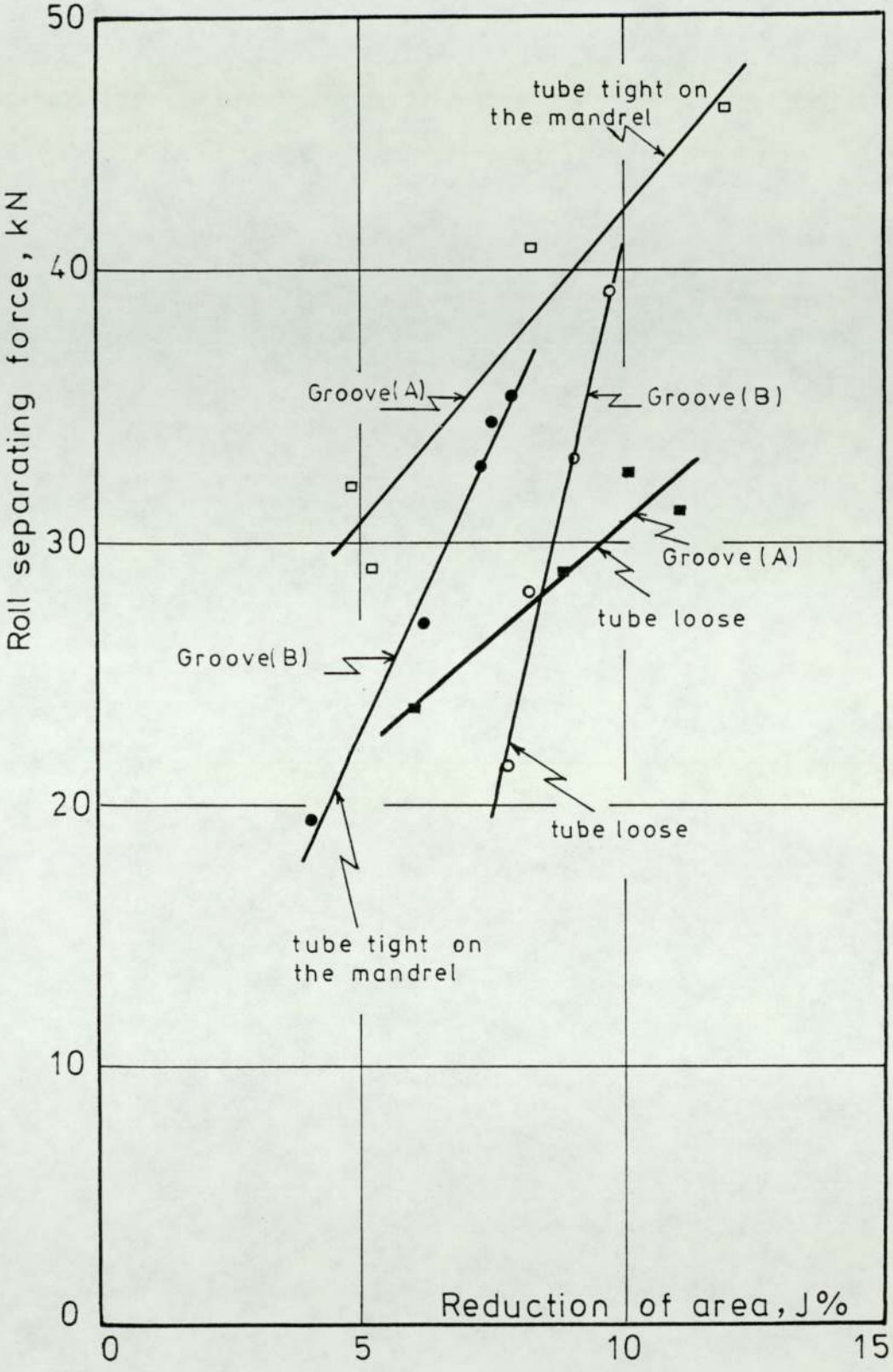

Fig.(7.12) Effect on RSF of removing the mandrel and re-inserting it again inside the tube before rolling.

contact occurred at the root of the groove as can be seen from plate (7.1). The two specimens in plate (7.1) were obtained by rolling two tubes to half their lengths and withdrawing them from the roll groove. The surface markings on the two tubes show clearly that the length of the arc of contact is not constant round the groove and the longest length occurs at the root of the groove. This was expected since as the groove surface narrows down from the inlet plane to the exit plane, more contact between tube and rolls occurs which also takes place due to the spread of the tube in the circumferential direction as the tube undergoes deformation.

When the length of the arc of contact at the root of the groove was estimated, it was found that the actual length obtained from pin-loadcell measurements was greater than the theoretical length calculated from the geometry of the tube and groove. The measured length of the arc of contact was corrected for the finite width of the pin by substracting twice the 2mm pin diameter from the measured length. The calculated angle of contact, Φ_m, at the root of the groove was obtained from equation (3.2.14):

$$\cos \Phi_m = 1 - \frac{r_o - (r_g - e_g) - e/2}{R_r} \qquad (3.2.14)$$

where r_o is the tube outside radius ,

r_g is the groove radius ,

e_g is the groove eccentricity, i.e. the distance between the centre of the circle forming the groove and the roll shrouds ,

e is the roll gap, and

R_r is the radius of the roll at the root of the groove .

Plate (7.1)

Contact zone between tube and roll

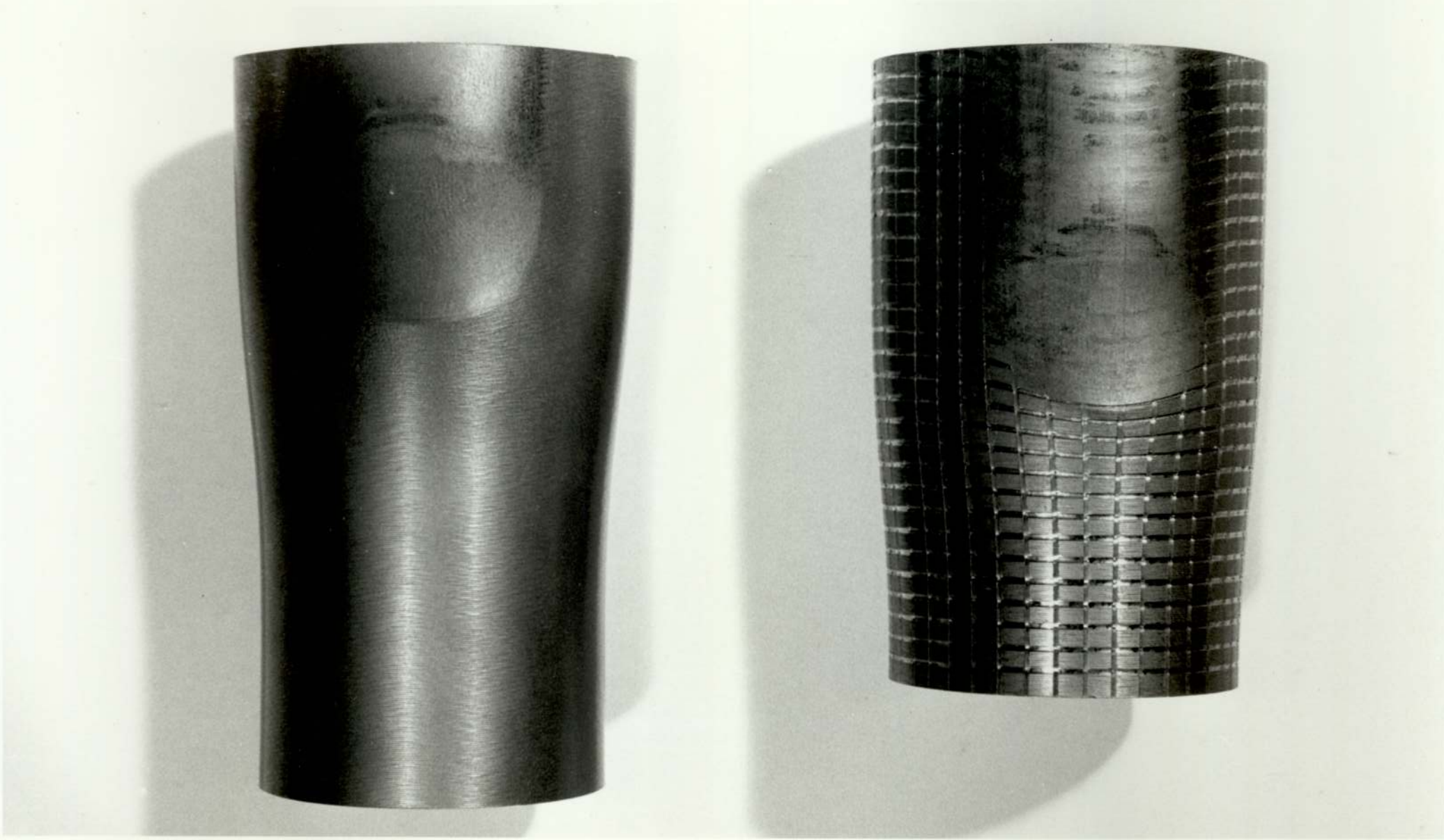

The calculated length of the arc of contact at the root of the groove is:

$$L_g = R_r \Phi_m \qquad (7.7.1)$$

where L_g is the calculated length of the arc of contact. The table in Appendix (B) shows a comparison between the calculated and measured values of the length of the arc of contact at the root of the groove. In all cases, except when rolling oval tubes, the measured value was greater than the calculated value. This might be due to the elastic compression of the rolls or the presence of a free zone, i.e. the tube might start to deform before entering the contact zone between tube and rolls. To investigate this point, measurements were taken of the change in height along each of the two specimen surfaces shown in plate (7.1). The measurements indicated that the outer surface of the tube rose gradually before the contact zone until it touched the roll surface at the start of the contact zone. Although this indicated the presence of a free zone, the possibility of elastic compression of the rolls occurring could not be discounted. An estimate was made roughly of roll flattening by considering a simple roll, i.e. a cylindrical roll, subjected to the loads measured during the tests. By applying Hitchcock's (24) equation for roll flattening, the change in the roll radius under the applied load could be determined. The equation can be written as:

$$\frac{R'}{R} = 1 + \frac{C}{\Delta h} \frac{P}{W} \qquad (7.7.2)$$

where R' is the roll radius under load

R is the initial roll radius

$C = 0.216 \times 10^{-4}$ mm^2/N for steel rolls

P/W is the roll separating force per unit width, and

Δh is the change in thickness between the ingoing and outgoing material.

W was taken as the groove width, while Δh was considered as being the difference between the inlet and outlet tube wall thicknesses. The maximum calculated value of R'/R was 1.06, while on average it was 1.03 for thin walled tubes and 1.01 for thicker tubes. As can be seen from these values, the change in roll radius was small and would account for a small change in the length of the arc of contact. Thus it is concluded that the presence of a free zone was the main reason for the increase in the length of the arc of contact.

The existence of a free zone has been observed in the drawing process by many investigators including Lloyd (25), Wistreich (26) and Hill (27). Johnson and Rowe (28) provided an interesting study of the bulge formation, which is the term frequently used for the free zone, in strip drawing with light reductions of area. They showed that a decrease in the reduction of area or an increase in the die angle enhanced bulge formation. Hill (27) related the bulge formation to the high value of die pressure at low reductions of area. He treated bulge formation by analogy with the pile-up round an indentation. The presence of a free zone was reported also in the redrawing process. In an extensive investigation by Walters (29) on the redrawing of cups, he showed that due to the bending of the cup as it enters the die, a system of tensile circumferential stresses will develop in the cup

wall outside the contact zone between cup and die. Under the action of the tensile stresses a bulge can develop just outside the contact zone. As the cup rim approaches the die, the length of the entering portion of the partially redrawn cup becomes shorter. As the redraw proceeds a stage is reached where this shortened length of the entering cup is unable to sustain the circumferential tensile stresses. The entering cup wall then proceeds to deform radially outwards causing the effect known as "splaying" shown in Figure (7.13).

The above discussion of the free zone in the drawing and redrawing processes led to the following two factors as being the likely causes of the free zone formation in the process of tube rolling on a mandrel:

(1) Bulging of the tube before the contact zone

Bulging can be explained by a similar mechanism as that occurring in the redrawing of cups process. At the start of contact between tube and roll, a bending moment is required to bend the tube along the arc of contact. This bending moment demands an opposing bending moment of equal magnitude to be supplied by the tube outside the contact zone, Figure (7.14.a). The opposing bending moment is supplied by circumferential tensile stresses in the tube outside the contact zone and is accompanied by shear stresses in the tube wall before the contact zone. The effect of the bending moment diminishes gradually away from the contact zone in the longitudinal direction so that the circumferential tensile stresses are generated over a short distance outside the contact zone.

The tensile stresses can lead to a small bulge forming in

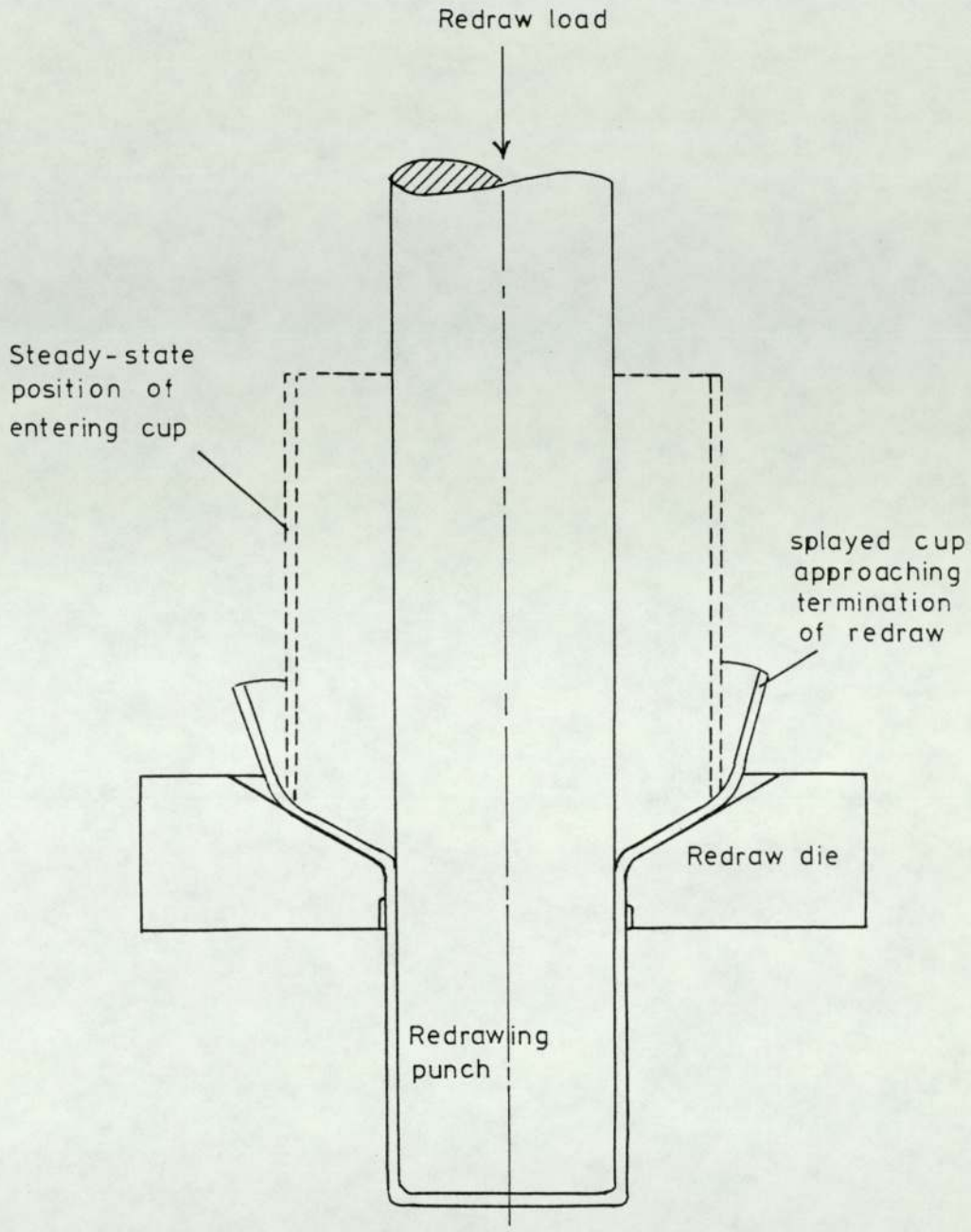

Fig (7.13) Splaying of a cup in Redrawing
(From Walters (29))

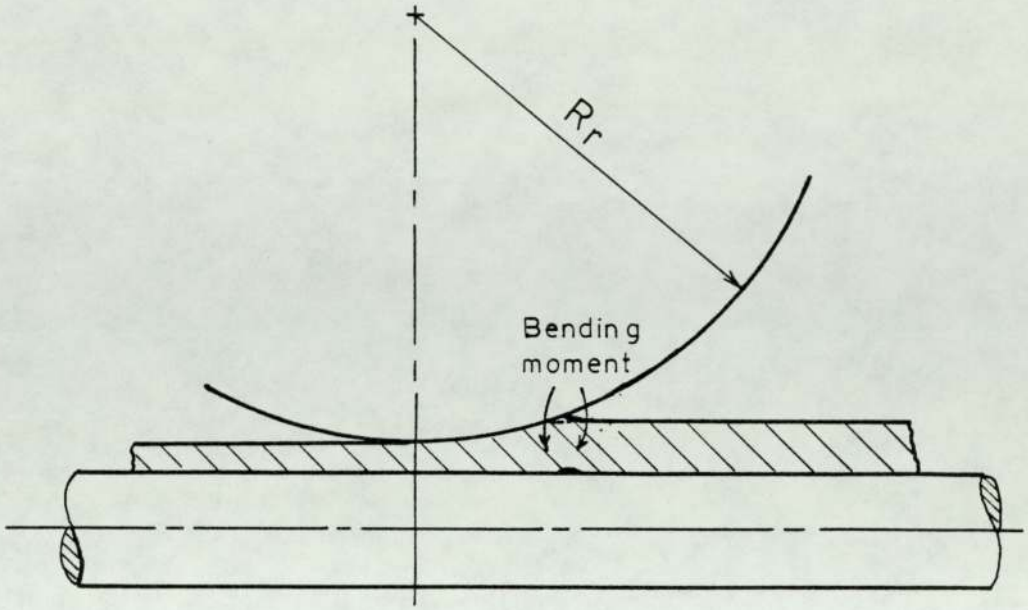

Fig.(7.14 a) Bulge formation

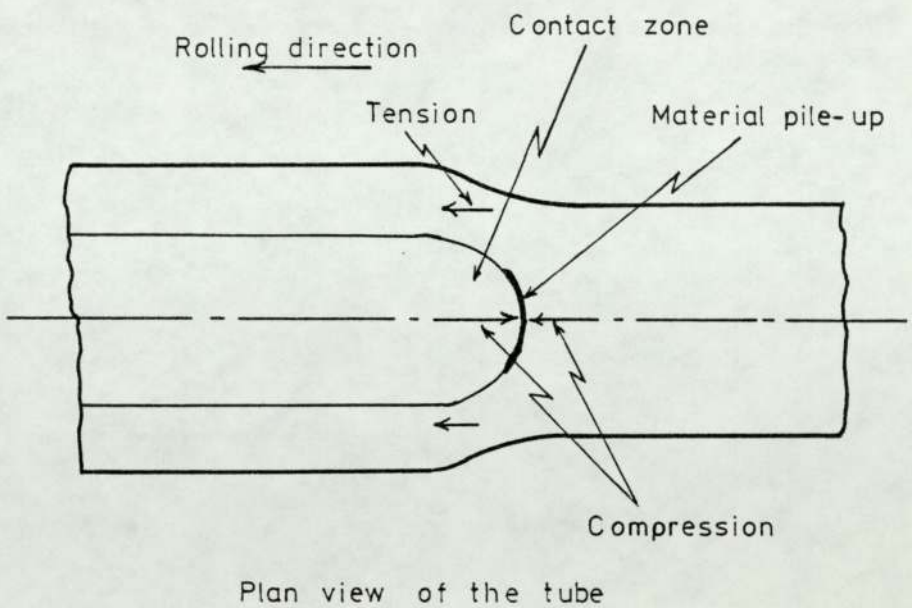

Fig.(7.14 b) Material pile-up in the free zone

the tube just outside the contact zone. When the tube end comes near the rolls, the tube material outside the contact zone will be insufficient to sustain the circumferential tensile stresses and the tube proceeds to deform radially outwards. This effect was observed in the rolling tests where the tube end at the end of rolling expanded before finally being rolled through the roll groove.

(2) Material pile-up due to longitudinal compression

At any section transverse to the rolling axis, the tube cross-section can be divided into two parts; the first part which is in contact with the groove surface and the mandrel, and the second part which is free from the inside. Since the tube material in the first part is rolled between the roll and the mandrel, which is similar to the case of flat rolling, it will be elongated in the longitudinal direction and will be subjected to longitudinal compression. The tube material in the second part will be elongated in the longitudinal direction by the elongation of the first part, which means that it will be subjected to longitudinal tension. Due to the groove ovality, the maximum deformation of the tube material occurs at the root of the groove, and it is expected, therefore, to find the maximum longitudinal compressive stress at the root of the groove.

Since different parts of the roll groove have different linear speeds according to their distances from the roll axis at any section along the tube axis, the tube material at the root of the groove tends to move slower than the tube material near the roll shrouds.

The longitudinal compressive stresses and the tendency of the tube to move slowly at and near the root of the groove,

lead to the material piling-up just outside the contact zone between tube and roll as shown in Figure (7.14.b). The amount of material pile-up in the free zone varies round the tube circumference. The maximum material pile-up can be found at a position corresponding to the root of the groove where the maximum longitudinal compressive stress exists and the roll speed is lowest. The variation of the material pile-up in the free zone round the tube circumference was confirmed from the measurements taken from the specimens in plate (7.1). It is clear also from plate (7.1), by considering the deformation of the grid which was engraved on the specimen surface, that longitudinal compressive stresses existed in the tube at and near the root of the groove. However, at the groove sides, the longitudinal tension in the tube tends to eliminate the occurrence of material pile-up. Similarly, if the mechanics of bulging are considered, it is concluded that the tendency to bulge formation is reduced by the longitudinal tension in the tube at the sides of the groove.

When oval tubes were rolled, with their major axes directed towards the root of the groove, no increase was detected in the length of the arc of contact. On the contrary, a decrease in the length of the arc of contact was observed and this result agreed with the work of Haleem (12). He reported that in tube sinking the measured length of the arc of contact is less than the calculated length. In tube sinking, since the tube is not internally supported, the tube in the pre-contact zone tends to bend downwards under the influence of the radial forces acting on the tube

at the start of contact between tube and roll. This results in the measured length of the arc of contact being less than the calculated length. In rolling oval tube on a mandrel with the tube major axis corresponding to the position of the root of the groove, a certain amount of sinking takes place before the tube inner surface comes into contact with the mandrel. Therefore, the measured length of the arc of contact was less than the calculated length.

7.8. Torque sharing and the arc of contact

From consideration of table (6.1) of the results, it is found that in most of the rolling tests, the upper torque was greater than the lower torque. Although the difference was not great, with the ratio of the upper torque to the total torque being 0.54 on average, this caused some concern.
It is known that the torque is affected by the frictional conditions on the roll and the contact area between tube and roll. Since great care was taken in preparing the tubes and in cleaning the rolls before each test, it is very unlikely that the difference between the upper and lower torques was caused by variation in friction between the top and bottom rolls. Even when the rolls were machined to change the groove shape, the difference between the upper and lower torques was similar to that prior to machining.
Having discounted friction as being the cause for the observed difference between the upper and lower torques, other factors, i.e. the contact area, have to be considered as being responsible for the difference. As the upper torque was greater than the lower torque, it may be deduced that the contact area between the tube and top roll was greater than that between the tube and bottom roll. Since the contact

area is proportional to the length of the arc of contact, the difference in torques indicates a difference in the length of the arc of contact between the two rolls. The increase in the length of the arc of contact on the top roll could have been caused either by a slight misalignment between the centres of the two rolls, or by a slight inclination of the tube and mandrel common axis to the pass axis as they travelled through the roll gap. The second cause is most likely to have occurred during rolling since there was no appreciable misalignment between the centres of the two rolls. To confirm this point, a tube was rolled for half of its length under normal conditions and, then, the mandrel was pushed downwards, from the entry side, to increase the area of contact between the tube and bottom roll. By comparing the torques in the two cases, it was found that as a result of pushing the mandrel downwards the lower torque became higher than the upper torque since the contact area between the tube and bottom roll was greater than that between the tube and top roll.

It was noticed that in some of the tests involving the application of front and back tensions the upper torque was very close to the lower torque since the tube and mandrel were forced to travel through the roll gap with their common axis coinciding with the pass axis.

The measured length of the arc of contact corresponded only to the top roll where the pin-load cells were situated. To determine an average value for the length of the arc of contact a correction factor should be applied to take account of the difference between the upper and lower torques. In his work, Haleem (12) used a torque sharing

factor T to correct the value of the measured length of the arc of contact. The torque sharing factor, T, was defined as;

$$T = \frac{\text{Total torque}}{2 \times \text{Upper torque}}$$

The corrected length of the arc of contact becomes:

$$L_{m.c} = L_m \times T$$

where L_m is the measured length of the arc of contact. Table (C1) in Appendix (C), shows the torque sharing factor T and the corrected length of the arc of contact for all the rolling tests.

The fact that the upper and lower torques can differ is an important factor when designing a rolling mill and an allowance should be made to account for more than half of the total torque being transmitted by either rolls, otherwise the variation of the upper and lower torques could lead to one of the rolls wearing more rapidly than the other.

In a production mill, the roll stands should be perfectly in line with each other, or variation between the upper and lower torques will occur in the individual stands and also the mandrel could be bent and subsequently damaged if the stands are not lined-up accurately.

7.9 The roll gap

It is well known that the loaded mill distorts elastically so that the initial roll gap changes during rolling according to the rolling loads and the rigidity of the mill. For every mill, depending on its rigidity, a relationship exists between the rolling load and the change in the roll gap. Sims (23)

examined this relationship and found that it could be graphically represented. The graph consists of a non-linear portion at low loads, and a portion which is essentially linear at high loads. The slope of the linear part is termed the mill modulus.

The relevance to the present work of determing the mill modulus was to evaluate accurately the actual roll gap from a knowledge of the initial roll gap and the rolling load. The mill springback, M, was determined from the following equation:

$$M = a - 2H - e_i$$

where a is the tube cross-section minor axis after rolling,

H is the groove height

e_i is the initial roll gap

The mill springback was evaluated for a wide range of rolling loads and the corresponding values are shown in Appendix (D). The values of the mill springback are plotted against the rolling load in Figure (7.15). A straight line in the following form could be fitted between the points:

$$P = 62.68 \times M - 1.47 \text{ kN}$$

where P is the roll separating force, and

M is the springback measured in mm

The correlation coefficient for this line is 0.98, which is considered a good standard of fit.

Since the linear relationship between the mill load and springback covered the whole range of rolling loads encountered in the rolling tests, the relationship was used to determine the actual roll gap in the tests.

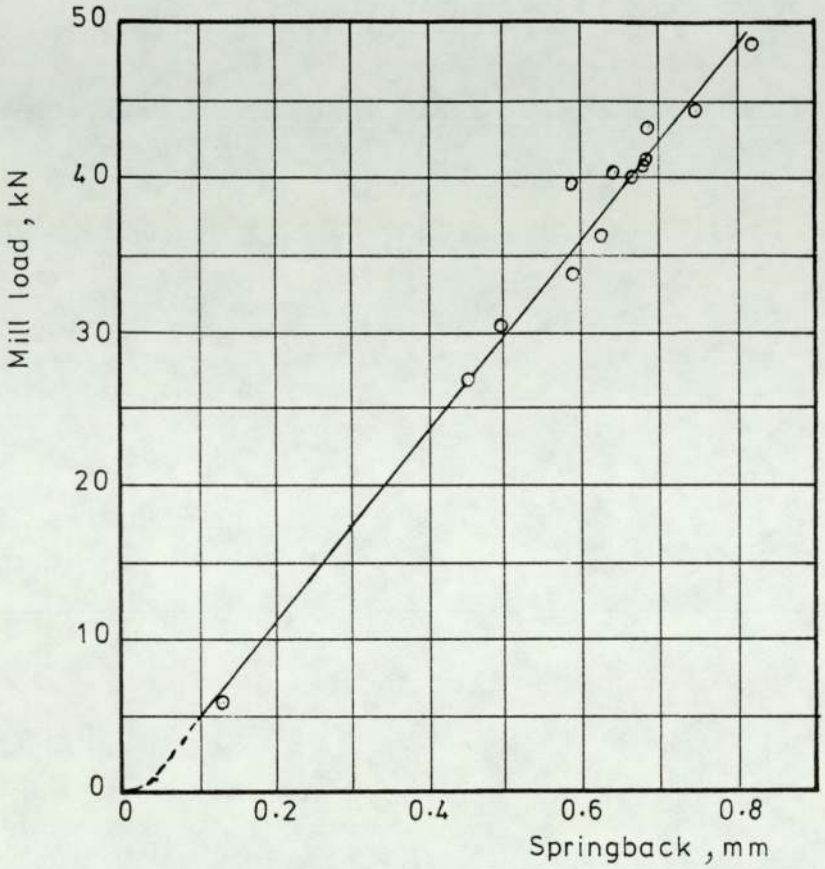

Fig.(7.15) The mill modulus

7.10 Mean tube thickness after rolling

Due to the irregular shape of the rolled tube cross-section, it was important to find means of calculating the mean tube thickness after rolling. Plate (7.2) shows some cross-sections of the rolled tubes. The mean tube thickness, t_1, was essential for the calculations of the radial strains and the work required in the rolling process. To calculate the mean thickness, the following method was adopted. Since most of the cross-section outer circumference was in contact with the groove surface at the exit plane, and the cross-section major axis could be measured easily, it was figured that the cross-section outer area could be calculated accurately. The cross-section outer surface was divided into two parts; the first part which was in contact with the groove surface and the second part which was free, Figure (7.16a). The peripheral angle of contact, ψ_{C1}, was measured by tracing the cross-section on a piece of paper and transferring the positions of the surface markings, which were found on the tube inner and outer surfaces, see figure (7.16b), to the traced cross-section. The angle ψ_{C1} determined the extent of the first part.

The first part had the same equation as the groove surface, i.e.

$$x^2 + \left[y + (e_g - e/2) \right]^2 = r_g^2 \qquad (7.10.1)$$

where e_g is the groove eccentricity, and

e is the roll gap. $y = \sqrt{r_g^2 - x^2} - (e_g - e/2)$

To determine the point of separation, $A(x_2, y_2)$, between the two parts, the instantaneous radius of the groove at an angle ψ_{C1} was estimated from the following equations:

Plate (7.2)

Some tube cross-sections

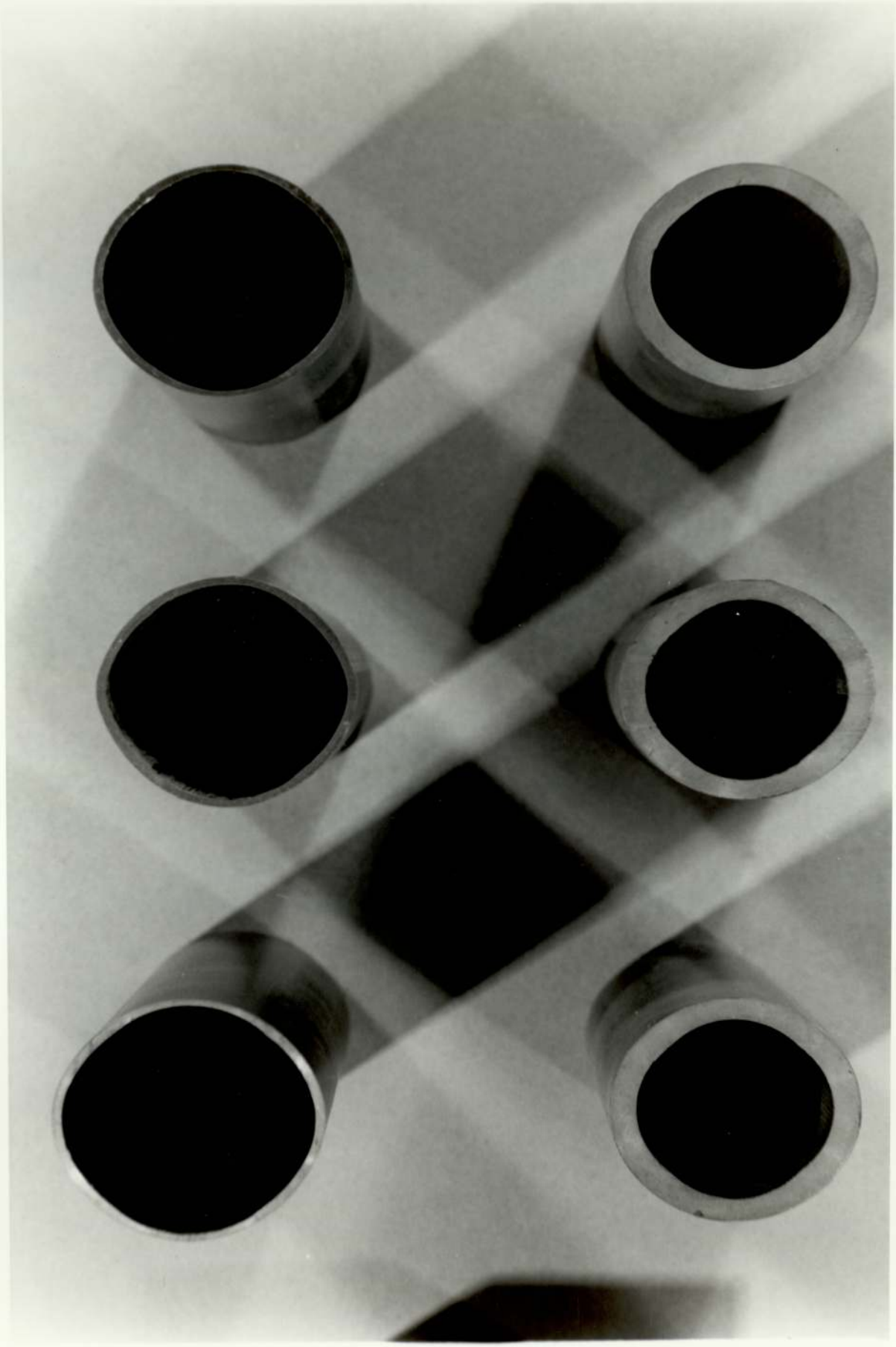

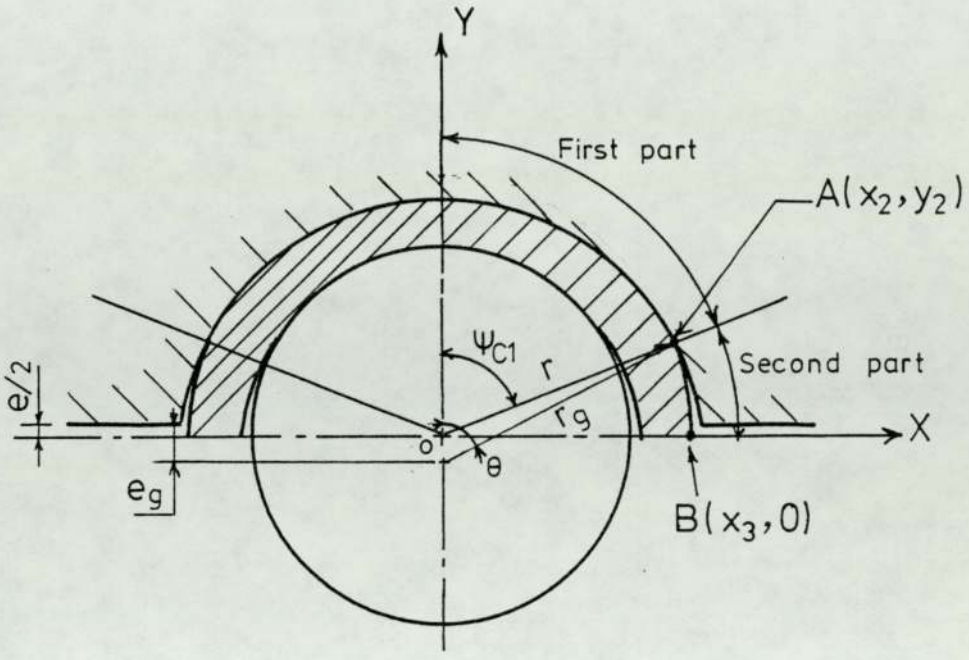

Fig.(7.16a) Tube cross-section at the exit plane.

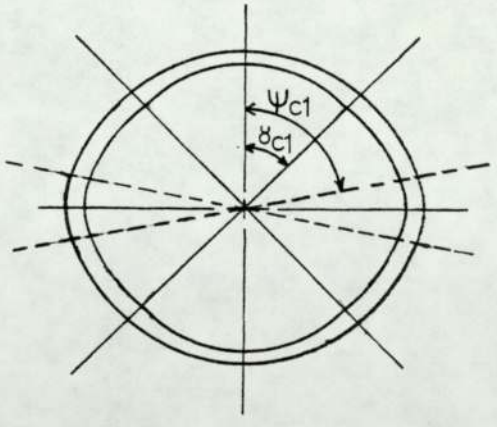

Fig.(7.16 b) Measuring the peripheral angles of contact from the tube cross-section.

$$r_g \sin\theta = r \sin\psi_{C1}$$

$$r_g^2 = r^2 \sin^2\psi_{C1} + [r \cos\psi_{C1} + e_g - e/2]^2$$

$$r_g^2 = r^2 \sin^2\psi_{C1} + r^2 \cos^2\psi_{C1} + 2r \cos\psi_{C1}(e_g - e/2) + (e_g - e/2)^2$$

$$r_g^2 = r^2 + 2r \cos\psi_{C1}(e_g - e/2) + (e_g - e/2)^2$$

$$r^2 + 2 \cos\psi_{C1}(e_g - e/2).\ r + (e_g - e/2)^2 - r_g^2 = 0$$

$$r = - \cos\psi_{C1}(e_g - e/2) \pm \sqrt{r_g^2 - (e_g - e/2)^2 \sin^2\psi_{C1}} \qquad (7.10.2)$$

The negative sign was not considered since it led to a negative value of r.

It can be written that:

$$x_2 = r \sin\psi_{C1}, \text{and } y_2 = r \cos\psi_{C1} \qquad (7.10.3)$$

From measurement of the cross-section major axis, the coordinate X_3 of point $B(X_3,0)$ is:

$$x_3 = \text{major axis}/2$$

The surface of the free part was assumed to be parabolic having the equation:

$$y^2 = - 4p\ (x - x_3) \qquad (7.10.4)$$

where p is a constant determined by substituting the coordinates of point A in the equation:

$$y_2^2 = - 4p\ (x_2 - x_3)$$

$$4p = \frac{y_2^2}{x_3 - x_2}$$

The equation of the free part becomes:

$$y^2 = - \frac{y_2^2}{(x_3 - x_2)}\ (x - x_3) \qquad (7.10.5)$$

$$\text{or} \quad y = \frac{y_2}{\sqrt{(x_3 - x_2)}} \left[-(x - x_3) \right]^{\frac{1}{2}}$$

The area of the outer surface of the cross-section was calculated as:

$$\text{Outside area} = 4 \int f(x).dx$$

$$= 4 \Big[\int_0^{x_2} \left(\sqrt{r_g^2 - x^2} - (e_g - e/2) \right) dx$$

$$+ \int_{x_2}^{x_3} \frac{y_2}{(x_3 - x_2)^{\frac{1}{2}}} \left(-(x - x_3)\right)^{\frac{1}{2}} dx \Big]$$

$$= 4 \Big[\frac{x_2}{2} \sqrt{r_g^2 - x_2^2} + \frac{r_g^2}{2} \sin^{-1} \frac{x_2}{r_g} - (e_g.e/2)x_2$$

$$+ \frac{2}{3} y_2 (x_3 - x_2) \Big] \qquad (7.10.6)$$

The area of the inside surface of the cross-section was determined by subtracting the tube cross-sectional area from the area of the outer surface.

Having estimated the outer and inner areas of the cross-section, the diameters of the circles corresponding to the two areas were determined and hence the mean tube thickness could be calculated.

7.11 Comparison between the proposed theory and the experimental results, and other theoretical approaches

In applying the proposed theory to the experimental results, modifications had to be made in the theory to account for the presence of the free zone which led to an increase in the length of the arc of contact. The modifications concerned mainly the calculations of the contact area between tube and rolls and between tube and mandrel. The modified theory

results in an increase in the work done against friction between tube and rolls and between tube and mandrel, since the contact areas are increased.

To calculate the modified areas of contact from knowledge of the maximum angle of contact $\Phi_{m.c}$, the peripheral contact angles between tube and roll and between tube and mandrel at any angle of contact Φ, should be estimated first. Having determined these angles, the contact area between tube and rolls, the horizontal projection of the contact area and the frictional work can be calculated as outlined in chapter (3). The following calculations of the peripheral contact angles are made for groove shape (A). The calculations for groove (A) and (B) are included in the computer programmes in Appendices (A-1)and (A-3).

At any section in the deformation zone having the contact angle Φ, Figure (7.17), the tube section can be divided into three parts; the first part which is under internal and external constraints, the second part which is under external constraint only, and the third part which is free. The peripheral angle of contact, γ_c, of the first part defines the contact angle between tube and mandrel, while contact between tube and roll is defined by the peripheral angle of contact ψ_c, see Figure (7.17). The third part is not used in the calculations since it is free. The angle γ_{c1} at the exit plane can be determined accurately from the following equations:

From Figure (7.17),

$$\cos\theta = \frac{1}{2\, r_g (e_g - e/2)} \left[r_g^2 - r_o^2 + (e_g - e/2)^2 \right] \qquad (7.11.1)$$

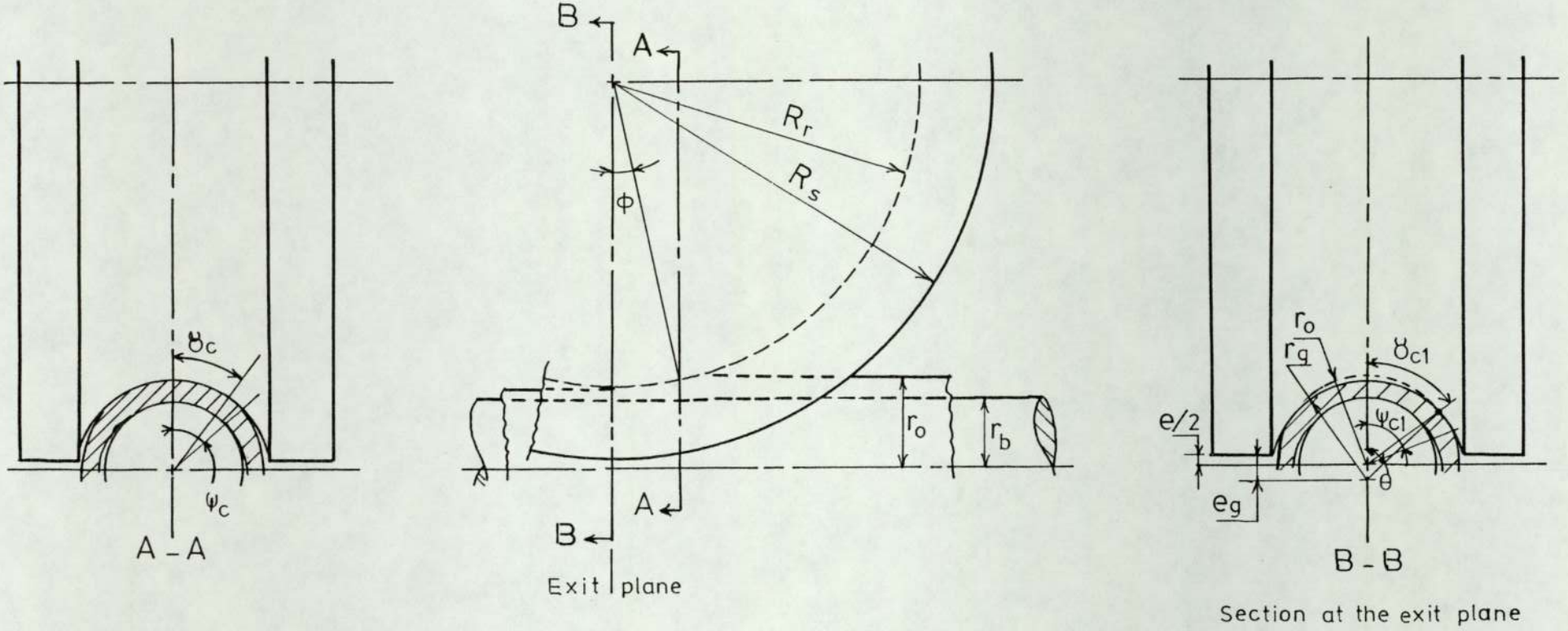

Fig.(7.17) Pass geometry

$$r_o \sin \gamma_{c1} = r_g \sin\theta$$

$$\gamma_{c1} = \sin^{-1} \left(\frac{r_g \sin\theta}{r_o}\right) \qquad (7.11.2)$$

where γ_{c1} is the peripheral angle of contact between tube and mandrel at the exit plane.

The calculated angle γ_{c1} at the exit plane agreed well with the measured value taken from the rolled tube cross-section. The calculated and measured values of γ_{C1} are shown in the tables of results, chapter (6).

From observation of the change in γ_c with ϕ, plate (7.1), the angle γ_c starts from zero at the entry plane and as ϕ decreases, γ_c increases sharply at first and then by a small amount until it reaches the value γ_{c1} at the exit plane.

It was noted when the original theory was applied, that the relationship between ϕ and γ_c can be represented by a curve in the form $\gamma_c = A.(\phi_{m.c} - \phi)^B$, where A and B are constants determined from a knowledge of any two points lying on the curve, and $\phi_{m.c}$ is the maximum measured and corrected angle of contact. This equation is used in the modified theory to obtain the relationship between γ_c and ϕ. Two points are chosen on the curve so that the constants A and B can be determined. The first point lies in the exit plane and has the co-ordinates $(0, \gamma_{C1})$. The second point is assumed to lie in a transverse plane making an angle ϕ of 1^o with the line joining the centres of the two rolls. The second point has the co-ordinates $(1, \gamma_{C2})$, where γ_{C2} is an assumed value close to γ_{C1}. The following expressions allow the constants A and B to be evaluated:

$$\gamma_C = A.(\phi_{m.c} - \phi)^B \qquad (7.11.3)$$

At $\phi = 0$, $\gamma_c = \gamma_{c1}$

$$\gamma_{c1} = A.(\phi_{m.c})^B \qquad (7.11.4)$$

Taking the natural logarithm of both sides:

$$\ln \gamma_{c1} = \ln A + B \ln \phi_{m.c}$$

$$\ln A = \ln \gamma_{c1} - B \ln \phi_{m.c} \qquad (7.11.5)$$

At $\phi = 1$, $\gamma_c = \gamma_{c2}$

$$\gamma_{c2} = A.(\phi_{m.c} - 1)^B$$

$$\ln \gamma_{c2} = \ln A + B \ln (\phi_{m.c} - 1) \qquad (7.11.6)$$

Substituting in (7.11.6) from (7.11.5):

$$\ln \gamma_{c2} = \ln \gamma_{c1} - B \ln \phi_{m.c} + B \ln (\phi_{m.c} - 1)$$

$$\ln \frac{\gamma_{c2}}{\gamma_{c1}} = B \ln \left(\frac{\phi_{m.c} - 1}{\phi_{m.c}}\right)$$

$$B = \ln\left(\frac{\gamma_{c2}}{\gamma_{c1}}\right) / \ln\left((\phi_{m.c} - 1)/\phi_{m.c}\right) \qquad (7.11.7)$$

Substituting from (7.11.7) in (7.11.4):

$$A = \gamma_{c1} / (\phi_{m.c})^B \qquad (7.11.8)$$

Equations (7.11.7) and (7.11.8) determine the constants A and B in equation (7.11.3), and hence the peripheral contact angle γ_c between tube and mandrel can be calculated at any angle ϕ.

The peripheral angle of contact, ψ_{c1}, between tube and rolls at the exit plane is measured from the rolled tube cross-section. Since the change of ψ_c with ϕ can be considered to follow the same trend as for the variation of γ_c with ϕ, it is reasonable to assume that the difference between the two angles, $(\psi_c - \gamma_c)$, is linearly related to the angle ϕ, i.e:

$$(\psi_c - \gamma_c) = C + F\phi \qquad (7.11.9)$$

where C and F are constants determined from a knowledge of any two points lying on the line. At the entry plane,

$(\psi_c - \delta_c) = 0$, since the contact between tube and rolls is just a point, while at the exit plane $\psi_c = \psi_{c1}$, and $\delta_c = \delta_{c1}$.

C and F are determined from the following calculations:

At $\Phi = \Phi_{m.c}$, $\psi_c - \delta_c = 0$

$$C + F\Phi_{m.c} = 0$$

$$F = -C/\Phi_{m.c} \qquad (7.11.10)$$

At $\Phi = 0$, $\psi_c = \psi_{c1}$, $\delta_c = \delta_{c1}$

$$\psi_{c1} - \delta_{c1} = C \qquad (7.11.11)$$

Substituting in (7.11.10),

$$F = -(\psi_{c1} - \delta_{c1})/\Phi_{m.c} \qquad (7.11.12)$$

The above calculations are included in the computer programme, Appendix (A-1)and are used in the evaluation of the surface or contact area, horizontal projection of the surface area and the frictional work. It should be mentioned that the modified theory can be used also in the absence of the free zone by substituting the appropriate value of the maximum angle of contact Φ_m in the calculations of mean pressure, RSF and total work done per unit volume. A complete example of the calculations is given in Appendix (E). Since the calculations are contained in the computer programme the example should clarify the construction of the computer programme.

The mean yield stress, $\bar{\sigma}_y$, was determined from Figure (5.2) according to the calculated mean strain-rate. The mean strain rates were found to lie between 0.005 and 0.009. It can be seen from Figure (5.2) , that between these limits of the strain rates and at low values of the total generalised strain, $\bar{\varepsilon}_m$, which did not exceed 0.19 in the rolling tests, the change in the shape of the stress-

strain curve with strain rate is very small and can be neglected. Therefore, it was decided to use the stress-strain curve corresponding to a strain rate of 0.008 in the estimation of the mean yield stress. Between zero and 0.2 strains, the equation of the chosen stress-strain curve can be described accurately by the following equation:

$$\sigma_y = 1.427\ (\varepsilon)^{0.298} \qquad (7.11.13)$$

where σ_y is the yield stress of lead in ton.in^{-2} corresponding to the strain ε .

The mean yield stress was calculated from equation (7.11.13). The values of the mean yield stress are shown in the tables of results, chapter (6).

In the theoretical calculations of the mean pressure and roll separating force, the friction factor, m_1 between tube and rolls was taken to be unity, i.e. sticking friction was assumed to exist between tube and rolls. This assumption is justified for a hot working process as the mandrel tube rolling process. A value of 0.6 was assigned to the friction factor, m_2 between tube and mandrel for the rolling tests with a dry mandrel. This value was taken from the experimental measurements as mentioned in section (7.3) of this chapter. For the case of a lubricated mandrel, m_2 was taken as 0.4, while for the mandrel with the very rough surface m_2 was unity. The mentioned figures of the friction factor are only rough approximations since determining the actual values with accuracy is extremely difficult.

Table (F1) in Appendix (F) shows the calculated total work done per unit volume of the material, together with a

comparison between the measured and calculated values of the mean pressure and the roll separating force. The relationship between the measured and calculated values are shown in Figures (7.18a) and (7.18b).

It can be seen from Figure (7.18) that there is, in most tests, a very good agreement between the measured and calculated values of the roll separating force and mean pressure. This shows clearly the advantage of using the energy method in the prediction of rolling loads.

Within acceptable limits, the calculated mean pressure was higher than the measured value, while the calculated RSF was lower than the measured one. The trend between the measured and calculated RSF should have existed also between the measured and calculated mean pressure. The departure from that ideal situation can be attributed to small differences between the calculated and actual values of the contact area and the horizontal projection of the contact area. If the calculated contact area is slightly lower than the actual value , this will lead to the calculated mean pressure being higher than the measured value while the calculated RSF will be lower than the measured value.

The calculated total work done per unit volume was most representative of the changes which occurred in the rolling conditions. By using the proposed theory, and minimizing the total work done the appropriate conditions which will increase the efficiency of the process can be chosen.

As mentioned in chapter (2), three different theories were examined in the present work, and all three involved the use of equilibrium approaches.

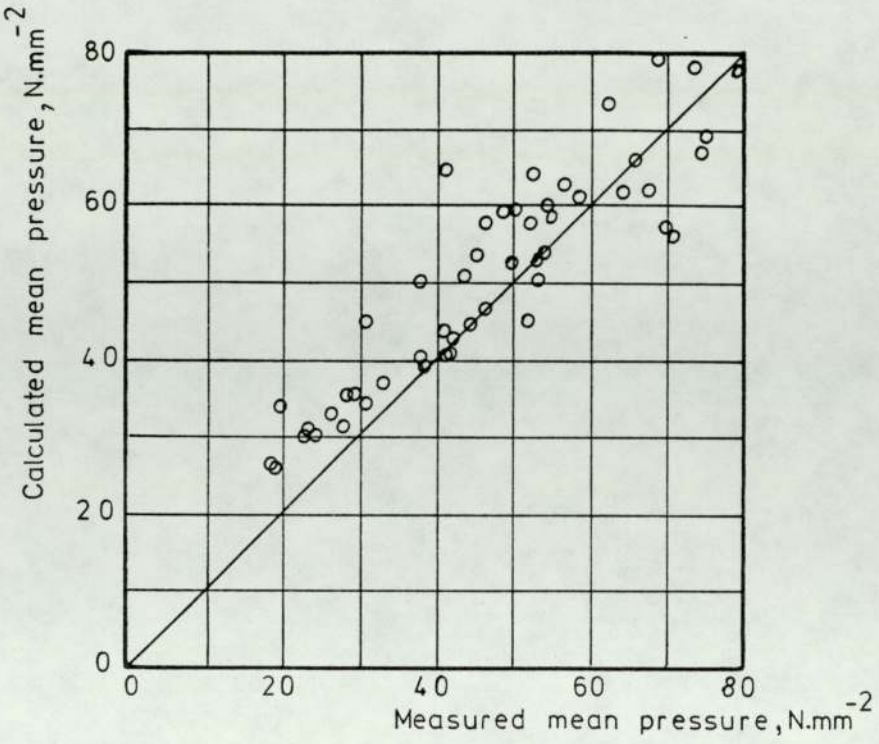

Fig.(7.18 a) Measured and calculated mean pressure

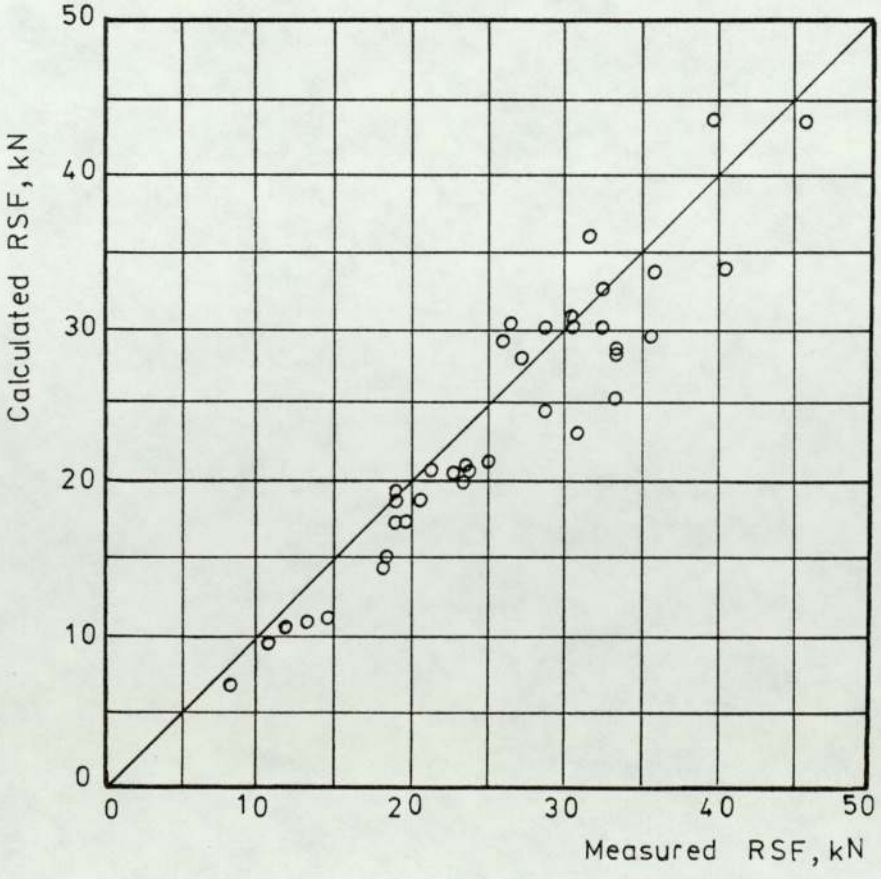

Fig.(7.18 b) Measured and calculated RSF

The theoretical analysis provided by Okamoto and Hayashi (10) is useful mainly in judging the filling of the groove perimeter. If overfilling or underfilling of the groove is predicted by their theory, the calculated values of stresses and strains, which are based on the assumption of complete filling of the groove, are not valid. Since, in the present work underfilling occurred in most tests, there was no point in carrying out the calculations for all the tests and the theory was applied to two test results. Okamoto and Hayashi neglected friction in their theory which is considered a serious drawback. Difficulty was experienced in applying the theory to the two test results, since the authors were not clear about the determination of some of the variables in the process. In both tests, the theory predicted that overfilling occurred and since it is known that underfilling occurred in both cases, this suggests that either the calculations were not carried out properly through misinterpretation of the theory, or the theory is not accurate.

The two Russian theories by Vatkin and Druyan (3) and Fomichev and Kirichenko (4) were applied to the results of free rolling tests. The same frictional conditions as applied in the present theory were used also in the two Russian theories. Vatkin and Druyan's predictions of the average pressure were compared with the measured mean pressures. Fomichev and Kirichenko did not provide calculations of the average pressure and, therefore, their theory was used to predict the pressure at the root of the groove and the results were compared with the measured pressure at the root of the groove. Table (G.1) in Appendix (G) shows the comparison between the measured

values of pressure and the predictions based on the two Russian theories.

Fomichev and Kirichenko's predictions underestimated the pressure while those of Vatkin and Druyan were better. It is believed that Vatkin and Druyan's predictions of the average pressure were not too inaccurate since the frictional conditions, the mean tube wall thickness after rolling, the yield stress and the length of the arc of contact were taken from the measurements and calculations performed in the present investigation. Although Vatkin and Druyan provided an equation for the estimation of the tube wall thickness, this equation was not accurate since it assumed that the whole of the tube inner surface was in contact with the mandrel at the exit plane which is not the case. Therefore, the mean wall thickness was taken from the present work. Finally, it should be mentioned that the dimensions of the equation for the average pressure provided by Vatkin and Druyan are not correct.

7.12 Calculation of the rolling torque

The lever arm method provided an easy way of assessing the rolling torques in the tests. In this method, the roll separating force is assumed to act at a distance (a) from the roll axis. In flat rolling, the distance (a) is usually taken to be some fraction ξ of the length of the arc of contact . The fraction ξ is called the lever arm and has the value of 0.5 for hot rolling.

Since in mandrel tube rolling, the length of the arc of contact is not constant round the groove as mentioned previously, the lever arm method was applied in the present

work in a slightly different manner. It was established that in the absence of front and back tensions, the rolling torque was linearly proportional to the rolling load as can be seen from Figure (7.3). The following relationship was obtained between the total rolling torque, T_t, and the rolling load, P (kN) :

$$T_t = 22.53 \times P \quad N.m \qquad (7.13.1)$$

If the value of the RSF is substituted in the above equation, the rolling torque can be estimated. Naturally, the calculated rolling torque will follow the same pattern as the calculated roll separating force.

CHAPTER (8)

CONCLUSIONS

Chapter (8) Conclusions

The following conclusions have been reached in the present investigation :

(1) The roll separating force, rolling torque and mean pressure have been shown to increase with the reduction of area and d/t ratio. The increase was dramatic when changing from thick tubes to thin tubes; this suggests that the higher reductions should be confined to the first stands in a production mill where the tube thickness is higher than the thickness in later stands. Also, when designing a new rolling mill, the calculations should be carried out with respect to rolling the thinnest tube where the worst conditions are known to exist.

(2) The pressure distribution round the groove perimeter is extremely irregular; the highest pressure occurs at the root of the groove.

(3) Friction on the mandrel surface greatly influences the rolling loads and torques. The effect is even greater as the tube gets thinner. Increasing friction between tube and mandrel hinders the flow of the material in the longitudinal direction and this leads to lower reductions of area at higher rolling loads and torques.

(4) In the absence of front and back tensions, the rolling torque varies linearly with the rolling load.

(5) Both front and back tensions reduce the rolling load. While front tension reduces the rolling torque, back tension increases it. Spread of the tube material is reduced by the application of front and back tensions, or alternatively, more of the radially displaced

material flows in the longitudinal direction. Consequently, higher reductions of area can be attempted with tension without increasing the rolling loads.

(6) Pulling the mandrel through the roll groove at a higher speed than that occurring in free folling produced a significant reduction in the rolling torque. This means that in a production mill the last stands reduce the rolling power supplied by the first stands so that it is preferable to shift most of the tube reduction to the first stands.

(7) Opening the groove sides allows the reduction of area to be increased and prevents overfilling of the groove, but the rolling loads will be higher.

(8) It has been shown that a free zone, where deformation takes place prior to the tube contacting the rolls can occur in mandrel tube rolling. Due to the presence of the free zone, the length of the arc of contact was higher than the theoretical length calculated from the geometry of the tube and the groove.

(9) The upper torque differed slightly from the lower torque, and corrections in the length of the arc of contact, measured by the pin-loadcells which were situated in the top roll, accounted for the difference in the torques.

(10) A good agreement has been shown to exist between the theoretical predictions based on an energy approach and the experimental results. Through the use of the developed computer programmes, it is possible to

arrive at the right combination of rolling parameters that will yield the minimum total work done per unit volume.

Three different theories were compared with the experimental results and only the Russian theory by Vatkin and Druyan (3) led to results which approached comparability.

CHAPTER (9)

SUGGESTIONS FOR FURTHER WORK

Chapter (9) Suggestions for Further Work

(1) The familiar method for determining the redundant work in a process by fitting together the stress-strain curves of the material before and after deformation, is suitable only for cold working processes where strain hardening is known to exist. This method was used, for example, by Blazynski and Cole (30), to determine the redundant work in tube drawing. In the mandrel rolling process, which is a hot working process, determination of the redundant work experimentally is difficult, especially because the material flow is quite complicated. It is suggested that the material flow can be assessed experimentally by the use of grids engraved on the tube surface. By rolling the tube for half of its length and withdrawing it from the roll groove, measurements taken from the deformed grid can lead to an accurate assessment of the material flow. Subsequently, the velocity field and the redundant deformation can be determined accurately. Since lead is very soft, the engraved grid after deformation is not clearly defined and is therefore of little use. Another material, possibly an aluminium alloy, which does not strain harden under deformation can be used instead of lead, but the RSF will be very much higher than when rolling lead. It should be mentioned that, since the grid is engraved on the tube surface, the information it reveals will be related to the tube surface. Therefore this method is suitable only for

analysing deformation of thin walled tubes where the deformation of an element on the tube surface can be assumed to be the same as that for an element near the mandrel surface.

(2) In a production mill, changing the conditions in one stand has an effect on all the stands. If the conditions are made favourable in one stand so that the work done in that stand is reduced, this does not mean that the total work done in all the stands is reduced also. Therefore, the proposed theory in the present investigation should be applied to all the stands to give the net effect on the total work done of changing any of the rolling conditions in a particular stand.

A computer programme will be most helpful in estimating the total work done in a multi-stand mill and subsequently the effect of changing the rolling conditions in one stand, on the total work done in all the stands can be evaluated.

(3) To simulate accurately the conditions existing in a production mill, a three stand experimental mill should be employed in the rolling tests. Such a mill can provide a clearer picture of the interaction between the rolling parameters in all the stands. More important, a 3-stand mill can assist in establishing the correct mandrel and tube speed pattern in a production mill. The mandrel speed changes on entry of the tube and mandrel to the mill and also during the run-out from the mill. The

change in mandrel speed could lead to the formation of a rear belly as suggested by Pfeiffer (13).
The phenomenon of belly formation and its origin can be investigated in a 3-stand experimental mill.
Also, the method suggested in the present work for the calculation of tube and mandrel speeds can be checked.
It was not possible to test this method in a single stand mill as the one used in the present investigation.

ACKNOWLEDGMENTS

The author wishes to express his sincere gratitude to Professor D.H.Sansome for his continued help and guidance throughout this investigation.

The helpful comments of Mr.P.Barrat, Mr.B.Jones and Mr.N.Price of the T I Weldless are most gratefully acknowledged.

The author would like to thank Mr G.M.Jones for his help with the experimental work.

Thanks are also due to Mrs.E.A.Copeland for her effort in typing the thesis.

Finally, the author wishes to thank his wife for her patience and encouragement.

References

(1) Matveev, Yu.M. and Lavrov, P.P.
"Effect of forward pressure and tension on the process of rolling tubes on a long mandrel".
Stahl (in English), 1964, Jan.,pp 51-55.

(2) Shevchenko, A.A. and Chekmarev, I.A.
"Complex investigation of the velocity and force parameters for the continuous mandrel rolling of tubes".
Proizvodstro Trub. Vypusk 13. Okrainskii. Nauchno-Issledovatel'skii Trubnyi Institut. 1964, Moscow, pp 28-37.

(3) Vatkin, Ya.L. and Druyan, V.M.
"Silovye usloviya pri opravochnoi prokatka trub"
(Force conditions in the mandrel rolling of tubes".)
Izvest. VUZ Chern. Met. 1966. No. 11, pp 72-77.

(4) Fomichev, I.A. and Kirichenko, A.N.
"The distribution of specific pressure in the zone of deformation for the rolling of tubes on a mandrel".
Izvest.VUZ Chern. Met. 1968, No. 4, pp 75-82.

(5) Neuhoff, K.W. and Pfeiffer, G.
"The technology of deformation in the operation of a continuous tube mill"
Stahl und Eisen, 90, 1970, No. 8, pp 406-412.

(6) Pfeiffer, G.
"Causes of irregularities of material flow in the continuous tube rolling process and measures to improve the rolling conditions"
Ph.D. thesis, Clausthal University, West Germany, 1974.

(7) Karman, Th.V.
"Contribution to the theory of rolling".
Applied mathematical mechanics,1925, Vol. 5, pp 139-142.

(8) Hoffman, O. and Sachs, G.
"Introduction to the theory of plasticity for engineers"
McGraw-Hill, 1953.

(9) Okamoto, T.
"The theory of deformation and stress of tubes by deformation factor".
Central Research Laboratories. Sumitomo Metal Industries Ltd., Japan.

(10) Okamoto, T. and Hayashi, C.
"Theory of plasticity on mandrel rolling".
The International Conference on the Science and Technology of Iron and Steel, Tokyo, 1970.

(11) Cole, I.M.
"An investigation of the rolling of cylindrical tube by grooved rolls".
Ph.D. thesis, 1969, University of Aston in Birmingham.

(12) Haleem, A.S.
"An investigation into the longitudinal rolling of tubes through two grooved rolls".
Ph.D. thesis, 1978, University of Aston in Birmingham.

(13) Pfeiffer, G.
"Systematic presentation of methods for the manufacture of seamless steel tube".
International Tube Association, International Conference on tube production and processing, April 1981, Aachen, West Germany.

(14) Vatkin, Ya. L. et al
"The specific pressure of the workpiece on the rolls and the mandrel for the rolling of tubes on a long mandrel".
Byull. TsIIN Ch M. No. 20, 48, 1965.

(15) Thompson, P.J. and Sansome, D.H.
"Apparent strain method for analysis of steady-state metal-working operations".
Metals Technology, November 1976, pp 497-502

(16) Blazynski, T.Z.
"Metal Forming: Tool Profiles and Flow".
McGraw-Hill.

(17) Johnson, W. and Mellor, P.B.
"Engineering Plasticity".
Van Nostrand Reinhold Company, 1973.

(18) Smith, C.L., Scott, F.H. Sylwestrowicz, W.
"Pressure distribution between stock and rolls in hot and cold flat rolling".
Journal of the Iron and Steel Institute, April 1952, pp 347-359.

(19) Loizou, N. and Sims, R.B.
"The yield stress of pure lead in compression".
Journal of Mechanics and Physics of Solids, 1953, Volume 1, pp 234-243.

(20) Ingham, P.
"The mechanics of thick slab rolling".
Ph.D. thesis, 1981, University of Aston in Birmingham.

(21) Haleem, A.S. and Sansome, D.H.
"Measurement of contact pressures in tube rolling".
Journal of Mechanical Working Technology, 1(1977), pp 153-168.

(22) Kudo, H.

"Some Analytical and Experimental Studies of Axi-symmetric Cold Forging and Extrusion".

Parts I and II, International Journal of Mechanical Sciences, Vol. 2, pp 102-127, 1960, Vol. 3, pp 91-177, 1961.

(23) Sims, R.B.

"Automatic gauge control in rolling mills".

Journal of the Institute of Metals, Vol. 86, 1957-1958, pp 289-302.

(24) Hitchcock, J.H.

"Elastic deformation of rolls during cold rolling".

ASME, Roll Neck Bearings, Appendix I, New York, 1935.

(25) Lloyd, D.H.

"Some principles of cold-working".

Metal Industry, Vol. 44, 1944, pp 71-73.

(26) Wistreich, J.G.

"Investigation of the mechanics of wire drawing"

Proceedings of the Institution of Mechanical Engineers, 169, 1955, pp 654-665.

(27) Hill, R. and Tupper, S.J.

"A new theory of the plastic deformation in wire-drawing".

Journal of the Iron and Steel Institute, 159, 1948, pp 353-359.

(28) Johnson, R.W. and Rowe, G.W.

"Bulge formation in strip drawing with light reduction in area".

Proceedings of the Institution of Mechanical Engineers, Vol. 182, Part 1, No. 22, 1967-1968, pp 521-526.

(29) Walters, J.A.
"An investigation of splaying in re-drawing".
Ph.D. thesis, University of Aston in Birmingham, 1971.

(30) Blazynski, T.Z. and Cole, I.M.
"An investigation of the plug-drawing process".
Proceedings of the Institution of Mechanical Engineers, 174, 1960, pp 797-804.

Appendix (A)

Computer Programmes

The computer programmes which were developed in the present investigation are given on the following pages. The language is BASIC and the correlation between labels used in the programmes and the nomenclature used elsewhere is given below:

Programme Label	Symbol	Programme Label	Symbol
RØ	r_o	M1	m_1
RR	R_r	M2	m_2
RS	R_s	ER	ε_r
EG	e_g	EL	ε_L
E	e	ET	ε_θ
R_B	r_b	ED	$\varepsilon_{red.}$
RG	r_g	EH	ε_h
TØ	t_o	EM	$\bar{\varepsilon}_m$
T1	t_1	EF	ε_f
AØ	A_o	AB	$\bar{\lambda}$
A1	A_1	MP	p_m
PM	$\Phi_{m.c}$	P	P
TH	Ψ_{C1}	YY	$\bar{\sigma}_y$
ØB	Ψ_C	BE	β
GA	γ_C	R1	R_1
ØM	ω	R2	R_2
UØ	U_o	H	H
VB	V_b	X3	x_3
LL	U	X7	x_7
LE	L	VW	V_w
Q1	μ_1	Q1	μ_1

In the case of rolling oval tubes in groove (c), the ingoing tube shape corresponds to a groove shape having the general dimensions R_1, R_2, H_1, e_1 and β_1. X7 is half the major axis of the ingoing tube cross-section, while X3 is half the major axis of the outgoing tube cross-section. The geometry of groove (c) is represented by the symbols R_3, R_4, H_2, e_2 and β_2.

The angles in the computer programmes are in degrees, while the rotational speed, ω, is in radians per second.

The symbol (∧) which appears in the computer programmes indicates a power calculation, i.e. (A)∧B means $(A)^B$.

The symbol (E) is an exponent, i.e. E 3 means 10^3.

The computer programmes are given in the Appendices from (A-1) to (A-7).

Appendix (A-1)

Computer programme for the case of rolling round tubes in groove (A)

```
  5 REM MEAN PRESSURE, RSF, TOTAL WORK - ROUND TO OVAL
    TUBE - GROOVE (A)
 10 INPUT RØ, R, ØM, E, VB, UØ, PM, M1, M2, X3, TH, RB
 20 RR = 94.55: RS = 113.45: EG = 4.49: RG = 23.39
 30 MA = 0: NA = 0: SA = 0: TA = 0
 45 REM OBTAIN THE RELATIONSHIP BETWEEN GAMMA, OBTHI
    AND PHI
 50 L = ACS ((RG*RG - RØ*RØ+(EG-E/2)^2)/(2*RG*(EG-E/2)))
 60 C1 = ASN(RG*SIN(L)/RØ): BS=(LN(C1/INT(C1))/LN
    (PM/(PM-1)))
 65 FØR I=0 TØ PM
 70 AS = C1/(PM)^BS: GA=AS*(PM-INT(PM)+I)^BS
 80 ØB = GA + (TH - C1)*(1-(INT(PM)-I)/PM)
 85 Z = RR*SIN(INT(PM)-I)
 88 REM CALCULATE THE X-COORDINATE OF THE CONTACT POINT
    AT OBTHI
 90 A = 0.001: C = RR*COS(INT(PM)-I)
100 X = C: GØSUB 800
110 Y  = B: X=A+C: GØSUB 800
120 D  = C: C = D-A*Y/(B-Y)
130 IF ABS (D-C)>= E-4 GØ TØ 100
140 XC = TAN(ØB)*(RS+E/2-C)
150 LL = UØ/(1-R)*(1-R*(INT(PM)-I)/PM)
160 D = 0
170 F = 5+2*I: B = (XC-D)/2/F
180 A = 0: X=D: GØ SUB 900
190 A = Y+A: X=X+B: GØSUB 900
```

```
200 A = Y*4+A: X=X+B: GØSUB 900
210 A = Y+A: F=F-1
220 IF F<>0 GØ TØ 190
230 LE = A*B/3
235 REM CALCULATE FRICTIONAL WORK, CONTACT AREA, HORZ.
    PROJECTION
240 HM = ABS(LL-VB)*RB*GA*π/180
250 D = 0
260 F = 5+2*I;  B = (XC-D)/2/F
270 A = 0: X=D: GØ SUB 1000
280 A = Y+A: X = X+B: GØ SUB 1000
290 A = Y*4+A: X = X+B: GØ SUB 1000
300 A = Y+A: F=F-1
310 IF F<>0 GØ TØ 280
320 FR = A*B/3
330 IF I > 0 GØ TØ 385
335 S1 = (SIN(PM)-SIN(INT(PM)))*RR
340 M = LE/2*S1
350 N = XC/2*S1
360 S = FR/2*S1
370 T = HM/2*S1
380 GØ TØ 430
385 S2 = (SIN(INT(PM)-I+1) - SIN(INT(PM)-I))* RR
390 M = (LE+LA)/2*S2
400 N = (XC+XA)/2*S2
410 S = (FR+FA)/2*S2
420 T = (HM+HA)/2*S2
430 MA = MA+M: NA = NA +N: SA=SA+S: TA = TA + T
440 LA = LE: XA = XC: FA = FR: HA = HM
```

```
450  NEXT I
455  REM CALCULATE THE MEAN TUBE THICKNESS AFTER ROLLING
460  RA = - CØS(TH)*(EG-E/2)+ √(RG*RG-((EG-E/2)*SIN(TH))∧2)
470  A = RA*SIN(TH)  :  B = RA*COS(TH)
480  W = A/2* √(RG*RG-A*A)+RG*RG/2*ASN(A/RG)*π/180
     - (EG-E/2)*A+2/3*B*(X3-A)
490  AØ =π* (RØ*RØ-RB*RB)
500  A1 = AØ*(1-R)  :  AI=4*W-A1
510  T1 = √(4* W/π) -√(AI/π)
515  REM CALCULATE RADIAL, LONGITUDINAL,CIRCUMFERENTIAL
     STRAINS
520  ER = LN ((RØ - RB)/T1)
530  EL = LN (1/(1-R))
540  ET = ER - EL
545  REM CALCULATE THE TOTAL GENERALIZED STRAIN
550  EH = √(2/3 * (ER*ER+EL*+ET*ET))
560  ED = (RØ-RB)/(12* √3*AØ*(1-R))*RR*(PM*π/180)∧2
     * (3-2*R)
570  EM=EH+ED
575  REM CALCULATE MEAN STRAIN RATE
580  AB=(ØM/(PM*π/180)*LN((RS+E/2-RR*COS(PM))/
     (RS+E/2-RR)))/2
590  PRINT "TOTAL GENERALIZED STRAIN =", EM
600  PRINT "MEAN STRAIN RATE =",AB
610  INPUT Y Y
620  EF = 4/√3 *(M1*SA + M2 * TA)/(AØ*UØ)
625  REM CALCULATE THE TOTAL WORK DONE PER UNIT VOLUME
630  WT = (EM+EF) * YY
635  REM CALCULATE THE MEAN PRESSURE AND RSF
640  MP = WT*AØ*UØ*PM*π/180/(4*MA*(RØ-RB-T1)*ØM)
```

```
650  P = 2 * NA * MP
660  PRINT "TOTAL WORK DONE =", WT
670  PRINT "MEAN PRESSURE =", MP
680  PRINT "RSF =", P
690  END


800  B = (TAN(ϕB)*(RS+E/2-X))∧2 + (RS+EG)∧2 - RG*RG
     - 2*(RS+EG)*(√(X*X+Z*Z))+X*X+Z*Z
810  RETURN


900  W1 = Z*Z/((RS+EG-√(RG*RG-X*X))∧2-Z*Z)
910  Y = √(X*X*(1+W1)/(RG*RG-X*X)+1)
920  RETURN


1000 W1=√(RG*RG-X*X)
1010 WA = √((X*X*(1+Z*Z/((RS+EG-W1)∧2-Z*Z))/(W1*W1))+1)
1020 Y = ABS(ϕM*√((RS+EG-W1)∧2-Z*Z)-LL)*WA
1030 RETURN
```

Appendix (A-2)

Computer programme for the case of rolling oval tubes in groove (A)

```
 5  REM MEAN PRESSURE, RSF, TOTAL WORK - OVAL TO OVAL
    TUBE -GROOVE (A)
10  INPUT R, ØM, E, UØ, VB, PM, M1, M2, X3, TH, RB, E1,
    A0, X7, TØ
20  RR = 94.55: RS= 113.45: EG = 4.49: RG = 23.39
30  MA = 0: NA=0: SA=0: TA=0: HA=0
42  REM OBTAIN THE RELATIONSHIP BETWEEN GAMMA. OBTHI AND
    PHI
44  A = EG-E1/2: B=RS+E/2: C=RS+EG
48  F = 4*(A*A+(C-B)^2)
50  G = 4*((B-C)*(C*C - A*A-B*B) - 2*C*A*A)
54  K = (C*C-A*A-B*B)^2 - 4*A*A*RG*RG+4*A*A*C*C
56  Y2 = (-G-√(G*G-4*F*K))/(2*F)
58  X2 =√(RG*RG-(C-Y2)^2)
60  C1 = ATN(X2/(RS+E/2-Y2)):BS=(LN(C1/INT(C1))/LN(P M/
    (PM-1)))
65  FØR I = 0 TØ PM
70  AS = C1/(PM)^BS:GA=AS*(PM-INT(PM)+I)^BS
80  ØB = GA+(TH-C1)*(1-(INT(PM)-I)/PM)
85  Z = RR*SIN(INT(PM)-I)
88  REM CALCULATE THE X- CO-ORDINATE OF THE CONTACT POINT
    AT OBTHI
90  A = 0.001: C = RR*COS(INT(PM)-I)
100 X = C: GØSUB 800
110 Y = B: X = A+C: GØSUB 800
```

```
120  D = C: C = D - A*Y/(B-Y)
130  IF ABS(D C) >= E - 4 GØ TØ 100
140  XC = TAN(ØB)*(RS+E/2-C)
150  LL = UØ/(1-R)*(1-R*(INT(PM)-I)/PM)
160  D = 0
170  F = 5+2*I: B=(XC-D)/2/F
180  A = 0: X = D: GØ SUB 900
190  A = Y + A: X = X+B: GØ SUB 900
200  A = Y*4+A: X = X+B: GØ SUB 900
210  A = Y+A: F F-1
220  IF F<>0 GØ TØ 190
230  LE = A*B/3
235  REM CALCULATE FRICTIONAL WORK, CONTACT AREA AND HORZ.
     PROJECTION
250  D = 0
260  F = F+2*I: B = (XC-D)/2/F
270  A = 0: X = D: GØ SUB 1000
280  A = Y+A: X = X+B: GØ SUB 1000
290  A = Y*4+A: X = X+B: GØ SUB 1000
300  A = Y +A: F = F-1
310  IF F<>0 GØ TØ 280
320  FR = A*B/3
330  IF I>0 GØ GØ 385
335  S1 = (SIN(PM) - SIN (INT(PM)) * RR
340  M = LE/2*S1
350  N = XC/2*S1
360  S = FR/2*S1
380  GØ TØ 430
385  S2 = (SIN(INT(PM)-I+1)-SIN(INT(PM)-I))*RR
390  M = (LE+LA)/2*S2
```

```
400  N = (XC+XA)/2*S2
410  S = (FR+FA)/2*S2
430  MA = MA+M: NA=NA+N: SA=SA+S
440  LA = LE: XA=XC :FA=FR
441  IF(INT(PM)-I)>(ACS(COS(PM) + (X7-RB)/RR))GØ TØ 450
443  HM = ABS(LL-VB)*RB*GA*π/180: T = (HM+HA)/2*S2
448  TA = TA+T: HA=HM
450  NEXT I
455  REM CALCULATE THE MEAN TUBE THICKNESS AFTER ROLLING
460  RA = -COS(TH)*(EG-E/2)+√(RG*RG-((EG-E/2)*SIN(TH))∧2)
470  A = RA*SIN(TH): B=RA*COS(TH)
480  W = A/2*√(RG*RG-A*A)+RG*RG/2*ASN(A/RG)*π/180
     - (EG-E/2)*A+2/3*B*  (X3-A)
500  A1 = AØ*(1-R): AI=4*W-A1
510  T1 =√(4*W/π) -√(AI/π)
515  REM CALCULATE THE RADIAL, LONGITUDINAL, CIRCUMFERENTIAL
     STRAINS
520  ER = LN(TØ/T1)
530  EL = LN(1/(1-R))
540  ET = ER-EL
545  REM CALCULATE THE TOTAL GENERALIZED STRAIN
550  EH =√(2/3*(ER*ER+EL*EL+ET*ET))
555  P1 = ACS(CØS(PM)+(X7-RB)/RR)
560  ED = (X3-X7)/(√3 * (1-R)*AØ)*RR*(LN(PM /P1)
     - R/PM*(PM-P1))
570  EM = EH+ED
575  REM CALCULATE THE MEAN STRAIN RATE
580  AB = (ØM/(PM*π/180)*LN((RS+E/2-RR*COS(PM))/
     (RS+E/2-RR)))/2
```

```
590  PRINT "TOTAL GENERALIZED STRAIN =", EM
600  PRINT "MEAN STRAIN RATE =", AB
610  INPUT YY
620  EF = 4/√3 * (M1*SA+M2*TA)/(AØ*UØ)
625  REM CALCULATE THE TOTAL WORK DONE PER UNIT VOLUME
630  WT = (EM+EF)*YY
635  REM CALCULATE THE MEAN PRESSURE AND RSF
640  MP = WT*AØ*UØ*PM*π/180/(4*MA*(TØ-T1)*ØM)
650  P = 2*NA*MP
660  PRINT "TOTAL WORK DONE =", WT
670  PRINT "MEAN PRESSURE =", MP
680  PRINT "RSF =", P
690  END

800  B = (TAN(ØB)*(RS+E/2-X))∧2 + (RS+EG)∧2-RG*RG
     - 2*(RS+EG)*(√(X*X+Z*Z))+X*X+Z*Z
810  RETURN

900  W1 = Z*Z/((RS+EG-√(RG*RG-X*X))∧2 - Z*Z)
910  Y = √(X*X*(1+W1)/(RG*RG-X*X)+1)
920  RETURN

1000 W1 = √(RG*RG-X*X)
1010 WA = √((X*X*(1+Z*Z/((RS+EG-W1)∧2-Z*Z))/(W1*W1))+1)
1020 Y  = ABS(ØM* √((RS+EG-W1)∧2 - Z*Z)-LL)*WA
1030 RETURN
```

Appendix (A-3)

Computer programme for the case of rolling round tubes in Groove (B)

```
  5 REM MEAN PRESSURE, RSF, TOTAL WORK- ROUND TO OVAL TUBE
    - GROOVE (B)
 10 INPUT RØ, R, ØM, E, UØ, VB, PM, M1, M2, X3, TH, PB
 20 RR = 94.55: RS = 113.45: EG = 4.49: RG = 23.39
 30 MA = 0: NA = 0: SA = 0: TA = 0
 45 REM OBTAIN THE RELATIONSHIP BETWEEN GAMMA, OBTHI AND
    PHI
 50 L = ACS ((RG*RG-RØ*RØ+(EG-E/2)^2)/(2*RG*(EG-E/2)))
 60 C1 = ASN(RG*SIN(L)/RØ): BS = (LN(C1/INT(C1))/LN(PM/(PM-1)))
 65 FØR I = 0 TØ PM
 70 AS = C1/(PM)^BS: GA = AS*(PM-INT(PM)+I)^BS
 80 ØB = GA+(TH-C1)*(1-(INT(PM)-1)/PM)
 85 Z = RR*SIN(INT(PM)-I)
 88 REM CALCULATE THE X-CO-ORDINATE OF THE CONTACT POINT AT
    OBTHI
 90 A = 0.001: C = RR*COS(INT(PM)-I)
100 X = C: GØ SUB 800
110 Y  = B: X = A+C: GØ SUB 800
120 D  = C: C = D-A*Y(B-Y)
130 IF ABS(D-C)>=  E-4 GØ TØ 100
140 XC = TAN(ØB)*(RS+E/2-C): XD=XC
144 IF XC < (RG* SIN45) GØ TØ 150
148 XD = RG*SIN45
150 LL = UØ/(1-R)*(1-R*(INT(PM)-I)/PM)
160 D = 0
170 F = 5+2*I: B = (XD-D)/2/F
```

```
180  A = 0: X = D: GØ SUB 900
190  A = Y+A: X = X+B: GØ SUB 900
200  A = Y*4+A: X = X+B: GØ SUB 900
210  A = Y+A: F=F-1
220  IF F<>0 GØ TØ 190
230  LE = A*B/3
250  D=0
260  F+5+2*I: B = (XD-D)/2/F
270  A = 0: X = D: GØ SUB 1000
280  A = Y +A: X=X+B: GØ SUB 1000
290  A = Y*4 +A: X = X+B: GØ SUB 1000
292  A = Y+A: F = F-1
294  IF F<>0 GØ TØ 280
296  FR = A*B/3
297  IF XC < (RG*SIN45) GØ TØ 329
298  BA = (((RS+EG)-RG*COS45)*TAN(90-45)-RG*SIN45)
299  B = ((BA*BA)-(RS+E/2)^2-Z*Z)*(1-1/((TAN(ØB))^2))
300  A = BA+(RS+E/2)/(TAN(ØB)): D = RG*SIN45
302  XD = (-A+√(A*A-B))/(1-1/(TAN(ØB))^2)
304  F = S+2*I: B =(XD-D)/2/F
306  A = 0: X=D: GØ SUB 1200
308  A = Y+A: X = X+B: GØ SUB 1200
310  A =Y*4+A :X = X+B: GØ SUB 1200
312  A = Y+A: F = F-1
314  IF F<>0 GØ TØ 308
315  L1 = A*B/3: LE=LE+L1
316  D = RG*SIN45
318  F = 5+2*I:  B=(XD-D)/2/F
320  A = 0: X = D: GØ SUB 1400
```

```
322  A = Y +A: X = X+B: GØ SUB 1400
324  A = Y*4+A: X = X+B: GØ SUB 1400
326  A = Y+A: F = F=F-1
327  IF F<>0  GØ TØ 322
328  F1 = A*B/3: FR = FR+F1
329  HM = ABS(LL-VB)*RB*GA*π/180
330  IF I>0 GØ TØ 385
335  S1 = (SIN(PM)-SIN(INT)PM)))*RR
340  M = LE/2*S1
350  N = XD/2*S1
360  S = FR/2*S1
370  T = HM/2*S1
380  GØ TØ 430
385  S2 = (SIN(INT(PM)-I+1)-SIN(INT(PM)-I))*RR
390  M = (LE+LA)/2*S2
400  N = (XD+XA)/2*S2
410  S = (FR+FA)/2*S2
420  T = (HM+HA)/2*S2
430  MA = MA+M: NA=NA+N: SA=SA+S: TA=TA+T
440  LA = LE: XA = XD: FA=FR: HA=HM
450  NEXT I
455  REM CALCULATE THE MEAN TUBE THICKNESS AFTER ROLLING
460  X1 = RG*SIN45: Y 1 = RG*COS45-(EG-E/2)
470  Y2 = (X1+Y1)/(1+TAN(ØB)): X2 = Y2*TAN(ØB)
480  WB = X1/2√(RG*RG-X1*X1) + RG*RG/2*ASN(X1/RG)*
     π/180-(EG-E/2)*X1+(X2-X1)*(Y1+X1/2-X2/2)
     + 2/3*Y2*(X3-X2)
490  AØ =  (RØ*RØ-RB*RB)
500  A1 = AØ*(1-R): AI = 4*WB-A1
```

```
510  T1 = √(4*WB/π) -  √(AI/π)
515  REM CALCULATE THE RADIAL, LONGITUDINAL, CIRCUMFERENT-
     IAL STRAINS
520  ER = LN((RØ-RB)/T1)
530  EL = LN(1/(1-R))
540  ET = ER-EL
545  REM CALCULATE THE TOTAL GENERALIZED STRAIN
550  EH = √(2/3*(ER*ER+EL*EL+ET*ET))
560  ED = (RØ-RB)/(12* √3*AØ*(1-R))*RR*(PM*π/180)∧2
     *(3-2*R)
570  EM=EH+ED
575  REM CALCULATE THE MEAN STRAIN RATE
580  AB=(ØM/(PM*π/180)*LN((RS+E/2-RR*COS(PM))/
     (RS+E/2-RR)))/2
590  PRINT "TOTAL GENERALIZED STRAIN =", EM
600  PRINT "MEAN STRAIN RATE =", AB
610  INPUT YY
620  EF = 4/√3 *(M1*SA+M2*TA)/(AØ*UØ)
625  REM CALCULATE THE TOTAL WORK DONE PER UNIT VOLUME
630  WT = (EM+EF)*YY
635  REM CALCULATE THE MEAN PRESSURE AND RSF
640  MP=WT*AØ*UØ*PM*π/180/(4*MA*(RØ-RB-T1)*ØM)
650  P = 2*NA*MP
660  PRINT "TOTAL WORK DONE =", WT
670  PRINT "MEAN Pressure =", MP
680  PRINT "RSF = ", P
690  END.

800  B = (TAN(ØB)*(RS+E/2-X)))∧2 + (RS+EG)∧2 - RG*RG
     -2*(RS+EG)*(√(X*X+Z*Z))+X*X+Z*Z
```

```
810  RETURN

900  W = Z*Z/((RS+EG-SQR(RG*RG-X*X))^2 - Z*Z)
910  Y = SQR(X*X*(1+W)/(RG*RG-X*X)+1)
920  RETURN

1000 W = SQR(RG*RG-X*X)
1010 WA = SQR((X*X*(1+Z*Z/((RS+EG-W)^2 - Z*Z)) W*W))+1)
1020 Y = ABS(ØM*SQR((RS+EG-W)^2-Z*Z)-L L)*WA
1030 RETURN

1200 Y = SQR(1+1/(1-(Z/(X+BA))^2))
1210 RETURN

1400 Y = ABS(ØM* ((X+BA)^2-(Z*Z))-LL)*SQR(1+1/(1-(Z/(X+BA))^2))
1410 RETURN
```

Appendix (A-4)

Computer programme for the case of rolling oval tubes in groove (B)

```
  5  REM MEAN PRESSURE, RSF, TOTAL WORK - OVAL TO OVAL
     TUBE - GROOVE (B)
 10  INPUT R, ØM, E, UØ, VB, PM, M1, M2, X3, TH, RB, E1,
     AØ, X7, TØ
 20  RR = 94.55: RS = 113.45: EG = 4.49: RG = 23.39
 30  MA = 0: NA = 0: SA = 0: TA = 0: HA = 0
 42  REM OBTAIN THE RELATIONSHIP BETWEEN GAMMA, OBTHI AND
     PHI
 45  C = RS-RR+E/2: A = 0.001
 50  X = C: GØ SUB 800
 55  Y = B: X=A+C: GØ SUB 800
 60  D = C: C=D-A*Y/(B-Y)
 65  IF ABS(D-C)>= E-4 GØ TØ 50
 70  XG = √(RG*RG-C*C) - (EG -E1/2)
 75  IF XG > (RG*SIN45)GØ TØ 95
 80  IF XG <(RG*COS45-(EG-E1/2)) GØ TØ 125
 85  C1 = ATN (XG/C)
 90  GØ TØ 150
 95  B = (EG-E1/2)-(2*RG*SIN45-(EG-E/2))
100  C = (EG-E1/2)^2 + (2*RG*SIN45-(EG-E/2))^2 - RG*RG
105  XG = (-B+√(B*B-2*C))/2
110  YG = (2*RG*SIN45-(EG-E/2))-XG
115  C1 = ATN(XG/YG)
120  GØ TØ 150
125  B = (EG-E/2)+(2*RG*SIN45-(EG-E1/2))
130  C = (2 *RG*SIN45-(EG-E1/2)+(EG-E/2))^2-RG*RG
135  XG = (B -√(B*B-2*C))/2
```

```
140  YG = (2*RG*SIN45-(EG-E1/2))-XG
145  C1 = ATN (XG/YG)
150  BS = (LN(C1/INT(C1))/LN(PM/(PM-1)))
155  FØR I = 0 TØ PM
160  AS = C1/(PM) ∧ BS: GA = AS*(PM-INT(PM) + I)∧BS
180  ØB = GA+(TH-C1)*(1-(INT(PM)-I)/PM)
185  Z = RR*SIN(INT(PM)-I)
188  REM CALCULATE THE X-CO-ORDINATE OF THE CONTACT POINT
     AT OBTHI
190  A = 0.001: C=RR*COS(INT(PM)-I)
200  X = C: GØ SUB 850
210  Y = B: X = A + C:  GØ SUB 850
220  D = C: C = D-A*Y/(B-Y)
230  IF ABS (D-C) >= .E-4 GØ TØ 200
240  XC = TAN(ØB)*(RS+E/2-C):XD=XC
244  IF XC (RG*SIN45) GØ TØ 250
248  XD=RG*SIN45
250  LL=UØ/(1-R)*(1-R*(INT(PM)-I)/PM)
260  D=0
270  F=5+2*I:  B=(XD-D)/2/F
280  A = 0: X = D: GØ SUB 900
290  A = Y+A: X=X+B: GØ SUB 900
300  A = Y*4+A: X=X+B: GØ SUB 900
310  A = Y+A: F = F-1
320  IF F<>0 GØ TØ 290
330  LE = A * B/3
350  D = 0
360  F = 5+2*I: B=(XD-D)/2/F
370  A=0: X=D: GØ SUB 1000
```

```
380  A=Y+A: X=X+B: GØ SUB 1000
390  A=Y*4+A: X=X+B: GØ SUB 1000
392  A=Y+A: F = F - 1
394  IF F<>0  GØ TØ 380
396  FR = A*B/3
397  IF XC < (RG*SIN45) GØ TØ 430
398  BA = (((RS+EG)-RG*COS45)*TAN(90-45)-RG*SIN45)
399  B = ((BA*BA)-(RS+E/2)^2-Z*Z)*(1-1/((TAN(ØB))^2))
400  A = BA+(RS+E/2)/(TAN(ØB)): D=RG*SIN45
402  XD=(-A+√(A*A-B))/(1-1/(TAN(ØB))^2)
404  F=5+2*I: B=(XD-D)/2/F
405  A=0: X=D: GØ SUB 1200
408  A=Y+A: X=X+B: GØ SUB 1200
410  A=Y*4+A: X=X+B: GØ SUB 1200
412  A=Y+A: F=F-1
414  IF F<>0 GØ TØ 408
415  L1=A*B/3: LE = LE + L1
416  D = RG*SIN45
418  F = 5+2*I:  B = (XD-D)/2/F
420  A = 0: X = D: GØ SUB 1400
422  A = Y+A: X = X+B: GØ SUB 1400
424  A = Y*4+A: X = X+B: GØ SUB 1400
426  A + Y+A: F=F-1
427  IF F<>0  GØ TØ 422
428  F1 = A*B/3: FR=FR+F1
430  IF I>0 GØ TØ 485
435  S1 = (SIN(PM) - SIN(INT(PM)))*RR
440  M=LE/2*S1
450  N=XD/2*S1
460  S=FR/2*S1
```

```
480  GØ TØ 530
485  S2 = (SIN(INT(PM)-I+1)-SIN(INT(PM)-I))*RR
490  M = (LE+LA)/2*S2
500  N = (XD+XA)2*S2
510  S = (FR+FA)/2*S2
530  MA = MA+M: NA = NA+N: SA=SA+S
540  LA = LE: XA = XD: FA = FR
541  IF (INT(PM)-I) > (ACS(COS(PM) + (X7-RB)/RR) GØ TØ 550
543  HM = ABS (LL-VB)*RB*GA*π/180
545  T = (HM+HA)/2*S2
548  TA = TA+T: HA=HM
550  NEXT I
555  REM CALCULATE THE MEAN TUBE THICKNESS AFTER ROLLING
560  X1=RG*SIN45: Y1 = RG*COS45-(EG-E/2)
570  Y2 = (X1+Y 1)/(1+TAN(ØB)): X2 = Y2 * TAN(ØB)
580  WB = X1/2 *√(RG*RG-X1*X1) + RG*RG/2*ASN(X1/RG)*
     π/180-   (E G-E/2)*X1 + (X2-X1)*(Y 1*X1/2-X2/2)
     + 2/3*(X3-X2)*Y2
600  A1 = AØ*(1-R): AI=4*WB-A1
610  T1=√(4*WB/π) -√(AI/π)
615  REM CALCULATE THE RADIAL, LONGITUDINAL,
     CIRCUMFERENTIAL STRAINS
620  ER = LN(TØ/T1)
630  EL = LN(1/(1-R))
640  ET = ER-EL
645  REM CALCULATE THE TOTAL GENERALIZED STRAIN
650  EH = √(2/3*(ER*ER+EL*EL+ET*ET))
655  P1 = ACS (COS(PM) + (X7-RB)/RR)
```

```
660  ED = (X3-X7/(√3*(1-R)*AØ)*RR*(LN(PM/P1)
     - R/PM*(RM-P1))
670  EM = EH+ED
675  REM CALCULATE THE MEAN STRAIN RATE
680  AB = (ØM/(PM*π/180)*LN((RS+E/2-RR*COS(PM))/
     (RS+E/2-RR)))/2
690  PRINT "TOTAL GENERALIZED STRAIN =", EM
700  PRINT "MEAN STRAIN RATE =", AB
710  INPUT YY
720  EF = 4/√3*(M1*SA+M2*TA)/(AØ*UØ)
730  WT = (EM+EF)*YY
735  REM CALCULATE THE MEAN PRESSURE AND RSF
740  MP = WT*AØ*UØ*PM*π/180/(4*MA*(TØ-T1)*ØM)
750  P = 2*NA*MP
760  PRINT "TOTAL WORK DONE =",WT
770  PRINT "MEAN PRESSURE =", MP
780  PRINT "RSF =", P
790  END

800  B = ((√(RG*RG-X*X)) - (EG-E1/2))∧2 + (X+EG-E/2)∧2
     - RG*RG
810  RETURN

850  B = (TAN(ØB)*(RS+E/2-X))∧2 + (RS+EG)∧2 - RG*RG
     - 2*(RS+EG)*(√(X*X+Z*Z))+X*X+Z*Z
860  RETURN

900  W = Z*Z/((RS+EG-√(RG*RG-X*X))∧2 -Z*Z)
910  Y = √(X*X*(1+W)/(RG*RG-X*X)+1)
920  RETURN
```

```
1000  W =  √(RG*RG-X*X)
1010  WA = √((X*X*(1+Z*Z/((RS+EG-W)∧2 -Z*Z))/(W*W))+1)
1020  Y = ABS(ØM* √((RS+EG-W)∧2-Z*Z)-LL)*WA
1030  RETURN

1200  Y = √(1+1/(1-(Z/(X+BA))∧2))
1210  RETURN

1400  Y  = ABS(ØM* √((X+BA)∧2 - (Z*Z))-LL)* √(1+1/(1-(Z/
      (X+BA))∧2))
1410  RETURN
```

Appendix (A-5)

Computer programme for the case of rolling round tubes in groove (C)

```
 5  REM MEAN PRESSURE, RSF, TOTAL WORK - ROUND TO OVAL
    TUBE - GROOVE (C)
10  INPUT RØ, R, ØM, E, ÜO, VB, PM, M1, M2, X3, TH, RB, RR,
    RS, BE, R1, R2, H
20  EG = R1 - H
30  MA = 0: NA = 0: SA = 0: TA = 0
40  REM OBTAIN THE RELATIONSHIP BETWEEN GAMMA, OBTHI AND
    PHI
42  L = ACS ((R1*R1-RØ*RØ+(EG-E/2)^2)/(2*R1*(EG-E/2)))
44  C1 = ASN(R1*SIN(L)/RØ)
45  X1 = RØ*SIN(C1)
47  AA = (R2-R1)*SIN(BE): BB = RS + EG + (R2-R1)*COS(BE)
48  B1 = RS + E/2
50  IF X1 <= (R1*SIN(BE)) GØ TØ 60
52  C = B1 - R1*COS(BE) - (EG-E/2): A = 0.001
54  X = C: GØ SUB 800
55  Y = B: X = A+C: GØ SUB 800
56  D = C: C = D-A*Y/(B-Y)
57  IF ABS(D-C) >= E-4 GØ TØ 54
58  X1 = (RØ*RØ - (B1-C)^2)
59  C1 = ATN(X1/(RS+E/2-C)
60  BS = (LN(C1/INT(C1))/LN(PM/(PM-1)))
65  FOR I = 0 TØ P M
70  AS = C1/(PM)^BS: GA = AS*(PM-INT(PM)+I)^BS
80  ØB = GA + (TH-C1)*(1-(INT(PM)-I/PM)
85  Z = RR*SIN(INT(PM)-I)
```

```
 88  REM CALCULATE THE X-CO-ORDINATE OF THE CONTACT POINT AT
     OBTHI
 90  A = 0.001:   C = RR*COS(INT(PM)-I)
100  X = C:  GØ SUB 850
110  Y = B:  X = A+C:  GØ SUB 850
120  D = C:  C = D-A*Y/(B-Y)
130  IF ABS(D-C) > = E-4 GØ TØ 100
140  XC = TAN(ØB)*(RS+E/2-C): XD = XC
144  IF XC < (R1*SIN(BE)) GØ TØ 150
148  XD = R1*SIN(BE)
150  LL = UØ/(1-R)*(1-R*(INT(PM)-I)/PM)
160  D = 0
170  F = 5+2*I: B = (XD-D)/2/F
180  A = 0:  X = D:  GØ SUB 900
190  A = Y+A: X = X + B:  GØ SUB 900
200  A = Y*4+A: X = X+B: GØ SUB 900
210  A = Y+A: F = F-1
220  IF F<>0 GØ TØ 190
230  LE = A*B/3
250  D = 0
260  F = 5+2*I: B = (XD-D)/2/F
270  A = 0: X = D: GØ SUB 1000
280  A = Y+A: X = X+B: GØ SUB 1000
290  A = Y*4+A: X = X+B: GØ SUB 1000
292  A = Y+A: F = F-1
294  IF F<>0 GØ TØ 280
295  FR = A*B/3
297  IF XC <(R1*SIN(BE)) GØ TØ 329
298  C = RR*CØS(INT(PM)-1): A = 0.001
299  X = C: GØ SUB 1100
```

```
300 Y = B: X = A+C: GØ SUB 1100
301  D = C:  C = D-A*Y/(B-Y)
302  IF ABS (D-C)>= E-4 GØ TØ 299
303  XD = (RS+E/2-C)*TAN(ØB): D = R1*SIN(BE)
304  F = 5+2*I:  B = (XD-D)/2/F
306  A = 0: X = D: GØ SUB 1200
308  A = Y+A:X=X+B:GØ SUB 1200
310  A = Y*4+A: X = X+B: GØ SUB 1200
312  A = Y+A: F = F-1
314  IF F<>0 GØ TØ 308
315  L1 = A*B/3: LE = LE + L1
316  D = R1*SIN(BE)
318  F = 5+2*I:  B = (XD-D)/2/F
320  A = 0:  X = D:  GØ SUB 1400
322  A = Y+A: X = X+B: GØ SUB 1400
324  A = Y*4+A: X = X+B: GO SUB 1400
326  A = Y+A: F = F - 1
327  IF F<>0 GØ TØ 322
328  F1 = A*B/3:  FR = FR + F1
329  HM = ABS(LL-VB)*RB*GA*π/180
330  IF I>0  GØ TØ 385
335  S1 = (SIN(PM) - SIN(INT(PM)))*RR
340  M = LE/2 * S1
350  N = XD/2*S1
360  S = FR/2*S1
370  T = HM/2*S1
380  GØ TØ 430
385  S2 = (SIN(INT(PM)-I+1) - SIN(INT(PM)-I))*RR
390  M = (LE+LA)/2*S2
400  N = (XD+XA)/2*S2
```

```
410  S = (FR+FA)/2*S2
420  T = (HM+HA)/2*S2
430  MA = MA + M: NA = NA+N: SA = SA+S: TA = TA+T
440  LA = LE: XA = XD: FA = FR: HA = HM
450  NEXT I
455  REM CALCULATE THE MEAN TUBE THICKNESS AFTER ROLLING
462  X1 = R1*SIN(BE)
464  X2 = XD: Y2 = X2/TAN(ØB)
466  Z2 = X2 + (R2-R1)*SIN(BE): Z3 = X3 + (R2 - R1)*SIN(BE)
468  W1 = X1/2*√(R1*R1-X1*X1) + R1*R1/2*ASN(X1/R1)*π/180
     - (EG - E/2)*X1+2/3*Y2*(X3-X2)
470  W2 = Z3/2*√(R2*R2-Z3*Z3)+R2*R2/2*ASN(Z3/R2)*π/180
     - Z2/2* √(R2*R2-Z2*Z2) - R2*R2*ASN(Z2/R2)
     * π/180 - ((R2-R1)*COS(BE) + (EG-E/2))*(X3-X2)
480  WB = W1 + W2
490  AØ = π*(RØ*RØ-RB*RB)
500  A1 = AØ *(1-R): AI = 4*WB-A1
510  T1 = √(4*WB/π) - √(AI/π)
515  REM CALCULATE THE RADIAL, LONGITUDINAL,
     CIRCUMFERENTIAL STRAIN
520  ER = LN((RØ-RB)/T1)
530  EL = LN(1/(1-R))
540  ET = ER-EL
545  REM CALCULATE THE TOTAL GENERALIZED STRAIN
550  EH = √2/3*(ER*ER+EL*EL+ET*ET))
560  ED = (RØ-RB)/(12*√3*A0*(1-R))*RR*(PM*π/180)∧2
     *(3-2*R)
570  EM = EH+ED
575  REM CALCULATE THE MEAN STRAIN RATE
```

```
580  AB = (ØM/(PM*π/180)*LN((RS+E/2-RR*COS(PM))/
     (RS+E/2-RR)))/2
590  PRINT "TOTAL GENERALIZED STRAIN =", EM
600  PRINT "MEAN STRAIN RATE =", AB
610  INPUT YY
620  EF = 4/√3*(M1*SA+M2*TA)/(AØ*UØ)
625  REM CALCULATE THE TOTAL WORK DONE PER UNIT VOLUME
630  WT = (EM+EF)*YY
635  REM CALCULATE THE MEAN PRESSURE AND RSF
640  MP = WT*AØ*UØ*PM*π/180/(4*MA*(RØ-RB-T1)*ØM)
650  P = 2*NA*MP
660  PRINT "TOTAL WORK DONE =", WT
670  PRINT "MEAN PRESSURE =", MP
680  PRINT "RSF =", P
690  END

800  B = (√(RØ*RØ-(B1-X)^2)+AA)^2+(BB-X)^2-R2*R2
810  RETURN

850  B = (TAN(ØB)*(RS+E/2-X))^2 +(RS+EG)^2 - R1*R1
     - 2*(RS+EG)*(√(X*X+Z*Z))+X*X + Z*Z
860  RETURN

900  W = Z*Z/((RS+EG-√(R1*R1 - XxX))^2 - Z*Z)
910  Y = √(X*X*(1+W)/(R1*R1-X*X)+1)
920  RETURN

1000 W = √(R1*R1-X*X)
1010 WA = √((X*X*(1+Z*Z/((RS+EG-W)^2 - Z*Z))/(W*W))+1)
```

```
1020  Y = ABS(ØM* √((RS+EG-W)∧2 - Z*Z)-LL)*WA
1030  RETURN

1100  B = ((RS+E/2-X)*TAN(ØB)+AA)∧2 + (BB - √(X*X+Z*Z))
       ∧2 - R2*R2
1110  RETURN

1200  W = R2*R2 - (X+AA)∧2
1210  Y = √(1+(1+Z*Z/((BB - √(W))∧2 - Z*Z))*((X+AA)∧2)/W)
1220  RETURN

1400  W = R2*R2-(X+AA)∧2
1410  WA = √((BB -  (W))∧2 - Z*Z)
1420  Y = ABS (ØM*WA-LL)*( √(1+(1+Z*Z/((BB-√(W))∧2
       - Z*Z))*((X+AA)∧2)/W))
1430  RETURN
```

Appendix (A-6)

Computer programme for the case of rolling oval tubes in groove (C)

```
 5  REM MEAN PRESSURE, RSF, TOTAL WORK - OVAL TO OVAL TUBE -
    GROOVE (C)
10  INPUT R, ØM, E2, UØ, VB, PM, M1, M2, X3, TH, RB, RR, RS,
    BE2, R3, R4, H2, E1, R1, R2, H1, BE1, X7, AØ, TØ
15  EG1 = R1 - H1: EG2 = R3 - H2
20  F1 = EG1 - E1/2: F2 = (R2-R1)*SIN(BE1): F3 = (R3 - R1)
    * COS (BE1) + (EG1-E1/2)
30  F4 = EG2 - E2/2: F5 = (R4-R3)*SIN(BE2): F6 =(R4-R3)
    * COS(BE2)+(EG2-E2/2)
35  MA = 0: NA = 0: SA = 0: TA = 0: HA = 0
40  REM OBTAIN THE RELATIONSHIP BETWEEN GAMMA, OBTHI AND PHI
42  B1 = RS + E2/2: BB = RS + EG2 + (R4 - R3) * COS (BE2)
45  C = R1*COS(BE1): A = 0.001
50  X = C: GØ SUB 800
55  Y  = B: X = A+C: GØ SUB 800
60  D = C: C = D-A*Y/(B-Y)
65  IF ABS(D-C) >=  E-4 GØ TØ 50
70  XG = C
75  IF XG > (R3*SIN(BE2)) GØ TØ 95
80  IF XG<(R1*COS(BE1) - (EG1-E1/2)) GØ TØ 135
85  C1 = ATN(XG/(√(R3*R3-XG*XG)-F4))
90  GØ TØ 168
95  C = R3*SIN(BE2): A = 0.001
100 X = C: GØ SUB 850
105 Y = B: X = A+C: GØ SUB 850
110 D = C: C = D-A*Y/(B-Y)
```

```
115  IF ABS(D-C)>= .E-4 GØ TØ 100
120  XG = C
125  C1 = ATN(XG/(√(R1*R1 - (XG+F1)∧2))
130  GØ TØ 168
135  C = 0: A = 0.001
140  X = C: GØ SUB 900
145  Y = B: X = A+C: GO SUB 900
150  D = C: C = D-A*Y/(B-Y)
155  IF ABS (D-C)>= E-4 GØ TØ 140
160  XG = C
165  C1 = ATN(XG/( (R3*R3-XG*XG)-F4))
168  FØR I = 0 TØ PM
170  BS = (LN(C1/INT(C1))/LN(PM/(PM-1)))
175  AS = C1/(PM)∧BS: GA = AS*(PM-INT(PM)+I)∧ BS
180  ØB = GA+(TH-C1)*(1-(INT(PM)-I)/PM)
185  Z = RR*SIN(INT(PM) -I)
188  REM CALCULATE THE X-CO-ORDINATE OF THE CONTACT POINT
     AT OBTHI
190  A = 0.001: C = RR*COS(INT(PM)-I)
200  X = C: GO SUB 950
210  Y = B: X = A+C: GØ SUB 950
220  D = C: C = D-A*Y/(B-Y)
230  IF ABS(D-C)>= E-4 GØ TØ 200
240  XC = TAN(ØB)*(RS+E2/2-C): XD=XC
244  IF XC <(R3*SIN(BE2)) GØ TØ 250
248  XD = R3*SIN(BE2)
250  LL = UØ/(1-R)*(1-R*(1-R*(INT(PM) - I)/PM)
260  D = 0
270  F = 5+2*I:  B = (XD-D/2/F
```

```
280  A = 0: X = D: GØ SUB 1000
290  A = Y+A: X = X+B: GØ SUB 1000
300  A = Y*4+A: X = X+B: GØ SUB 1000
310  A = Y+A: F = F-1
320  IF F<>0  GØ TØ 290
330  LE = A*B/3
350  D = 0
360  F = 5+2+I: B = (XD-D)/2/F
370  A = 0: X = D: GØ SUB 1050
380  A = Y+A: X = X+B: GØ SUB 1050
390  A = Y*4+A: X = X+B: GØ SUB 1050
392  A = Y+A: F = F-1
394  IF F<>0 GØ TØ 380
396  FR = A*B/3
397  IF XC <(R3*SIN(BE2)) GØ TØ 430
398  C   B1 - R3*COS(BE2)-(EG2-E2/2): A = 0.001
399  X = C: GØ SUB 1100
400  Y = B: X = A+C: GØ SUB 1100
401  D = C:C = D -A*Y/B-Y):  IF ABS(D-C)>=E-4 GØ TØ 399
403  XD = (RS + E2/2-C)*TAN(ØB): D = R3*SIN(BE2)
404  F = 5+2*I: B = (XD-D)/2/F
406  A = 0: X = D: GØ SUB 1200
408  A = Y+A: X = X+B: GØ SUB 1200
410  A = Y*4+A: X=X+B: GØ SUB 1200
412  A = Y+A: F = F-1 :  IF F<>0 GØ TØ 408
415  L1 = A*B/3: LE = LE+L1
416  D = R3*SIN(BE2)
418  F = 5+2*I: B = (XD-D)/2/F
420  A = 0: X = D: GØ SUB 1400
422  A = Y+A: X = X+B: GØ SUB 1400
```

```
424  A = Y*4+A: X = X+B: GØ SUB 1400
426  A = Y+A: F = F-1
427  IF F<>0 GØ TØ 422
428  F7 = A*B/3: FR = FR+F7
430  IF I > 0 GØ TØ 485
435  S1 = (SIN(PM) - SIN (INT(PM)))*RR
440  M = LE/2*S1
450  N = XD/2*S1
460  S = FR/2+xS1: GØ TØ 530
480  S2 = (SIN(INT(PM)-I+1) - SIN(INT(PM)-I))*RR
490  M = (LE+LA)/2*S2
500  N = (XD+XA)/2*S2
510  S = (FR+FA)/2*S2
530  MA = MA+M: NA = NA+N: SA = SA+S
540  LA = LE: XA = XD: FA = FR
541  IF (INT(PM)-I) > (ACS(COS(PM)+(X7-RB)/RR))GØ TØ 550
543  HM = ABS(LL-VB)*RB*GA*π/180
545  T = (HM+HA)/2*S2
548  TA = TA+T: HA=HM
550  NEXT I
555  REM CALCULATE THE MEAN TUBE THICKNESS AFTER ROLLING
562  X1 = R3*SIN(BE2): X2=R3*SIN(BE2): Y2 = X2/TAN(ØB)
564  Z2 = X2+(R4-R3)*SIN(BE2): Z3=X3+(R4-R3)*SIN(BE2)
568  W1 = X1/2* √(R3*R3-X1*X1) + R3*R3/2*ASN(X1/R3)* π/180
     - (EG2-E2/2)*X1+2/3*Y2*(X3-X2)
570  W2 = Z3/2* √(R4*R4-Z3*Z3) + R4*R4/2*ASN(Z3/R4)
     * π/180 - Z2/2* √(R4*R4-Z2*Z2)-R4*R4/2*ASN(Z2/R4)
     * π/180 - ((R4-R3)*COS(BE2)+(EG2-E2/2))*(X3-X2)
580  WB = W1 + W2
600  A1 = AØ*(1-R): AI = 4*WB-A1
```

```
610  T1 =√(4*WB/π) - √(AI/π)
615  REM CALCULATE THE RADIAL, LONGITUDINAL, CIRCUMFERENTIAL
     STRAINS
620  ER = LN(TØ/T1)
630  EL = LN(1/(1-R))
640  ET = ER-EL
645  REM CALCULATE THE TOTAL GENERALIZED STRAIN
650  EH = √(2/3*(ER*ER+EL*EL+ET*ET))
655  P1 = ACS(COS(PM) + (X7-RB)/RR)
660  ED = (X3-X7)/(√3*( 1-R)*AØ)RR*(LN(PM/P1) - R/PM*(PM-P1))
670  EM = EH - ED
675  REM CALCALCULATE THE MEAN STRAIN RATE
680  AB = (ØM/PM*π/180)*LN((RS+E2/2-RR*COS(PM))/
     (RS+E2/2-RR)))/2
690  PRINT "TOTAL GENERALIZED STRAIN =", EM
700  PRINT "MEAN STRAIN RATE =", AB
710  INPUT YY
720  EF = 4/√3*(M1*SA+M2*TA)/(AØ*UØ)
725  REM CALCULATE THE TOTAL WORK DONE PER UNIT VOLUME
730  WT = (EM+EF)*YY
735  REM CALCULATE THE MEAN PRESSURE AND RSF
740  MP = WT*AØ*UØ*PM*π/180/(4*MA*(TØ-T1)*ØM)
750  P = 2*NA*MP
760  PRINT "TOTAL WORK DONE =", WT
770  PRINT "MEAN PRESSURE =", MP
780  PRINT "RSF =",P
790  END

800  B =(√(R3*R3-X*X) - F4)^2 + (X+F1)^2 - R1*R1
810  RETURN
```

```
850  B = (X+F5)^2 + ( √(R1*R1-(X+F1)^2+F6)^2 - R4*R4
860  RETURN

900  B = ( √(R3*R3-X*X)-F4+F2)^2+(X+F3)^2 - R2*R2
910  RETURN

950  B = (TAN(ØB)*(RS+E2/2-X))^2 +(RS+EG2)^2 - R3*R3
     - 2*(RS+EG2)*( √(X*X+Z*Z))+X*X+ Z*Z
960  RETURN

1000 W = Z*Z/((RS+EG2- √(R3*R3-X*X))^2 - Z*Z)
1010 Y = √(X*X*(1+W)/(R3*R3-X*X)+1)
1020 RETURN

1050 W = √(R3*R3-X*X)
1060 WA =√((Z*X*(1+Z*Z/((RS+EG2-W)^2-Z*Z))/(W*W))+1)
1070 Y = ABS(ØM*√((RS+EG2-W)^2 - Z*Z)-LL)*WA
1080 RETURN

1100 B = ((RS+E2/2-X)*TAN(ØB)+F5)^2 + (BB-√(X*X + Z*Z))^2
     - R4*R4
1110 RETURN

1200 W = R4*R4-(X+F5)^2
1210 Y =√(1+(1+Z*Z/((BB- √(W))^2 - Z*Z))*((X+F5)^2)/W)
1220 RETURN

1400 W = R4*R4 - (X+F5)^2
1410 WA =√((BB- (w))^2 -Z*Z)
```

```
1420  Y = ABS(ØM*WA-LL)*(√(1+(1+Z*Z/((BB-√(W))∧2
      - Z*Z))*((X+F5)∧2/W))
1430  RETURN
```

Appendix (A-7)

Computer Programme for the calculation of Tube and Mandrel speeds in a multi-stand mill

```
 10  REM CALCULATIONS OF TUBE AND MANDREL SPEEDS
 20  DIM P(8) DIM U(8): DIM X(8): DIM Y(8)
 30  DIM Q1(8): DIM Q2(8): DIM VW(8)
 40  REM READ ROLL SEPARATING FORCES AND ROLL SPEEDS
 50  FØR I = 1 TØ 8
 60  INPUT P(I), VW(I), Q1(I), Q2(I)
 70  NEXT I
 80  REM LET THE INITIAL TUBE SPEEDS EQUAL ROLL SPEEDS
 90  FØR I = 1 TØ 8
100  U(I) = VW(I)
110  NEXT I
120  REM CALCULATE MANDREL AND TUBE SPEEDS
130  FØR N = 1 TØ 20
140  SX = 0.0: SY  = 0.0
150  FØR I = 1 TØ 8
160  X(I) = P(I)*Q2(I)
170  SX = SX + X(I)
180  Y(I) = P(I)*Q2(I)*U(I)
190  SY = SY+Y(I)
200  NEXT I
210  REM CALCULATE MANDREL SPEED
220  VB = SY/SX
230  REM COMPARE VB WITH PREVIOUS VALUE
240  V1 = VB
250  IF N = 1 GØ TØ 270
260  IF (ABS(V1-V2) < 0.001) GØ TØ 320
```

```
270  V2 = V1
280  FØR J = 1 TØ 8
290  U(J) = ((VW(J)*Q1(J))+(VB*Q2(J)))/(Q1(J)+Q2(J))
300  NEXT J
310  NEXT N
320  PRINT "VB =", VB
330  PRINT U(J)
340  END
```

Appendix (B)

Table (B1) Comparison between the measured and calculated length of the arc of contact

Test No	L_m mm	L_g mm	Φ_m^o measured	Φ_m^o calculated
12	17.58	14.42	10.65	8.74
13	18.86	15.46	11.43	9.37
14	18.86	15.52	11.43	9.40
15	22.20	16.40	13.45	9.95
16	21.43	17.38	12.99	10.53
17	22.71	17.29	13.76	10.48
18	23.7	18.10	14.39	10.97
19	12.31	10.66	7.4	6.46
20	14.88	12.42	9.02	7.53
21	13.72	11.88	8.32	7.20
22	17.58	12.61	10.65	7.64
23	18.22	12.71	11.04	7.70
24	19.12	14.66	11.59	8.88
25	13.98	11.94	8.47	7.26
26	15.25	12.79	9.24	7.75
27	14.49	12.57	8.78	7.62
28	17.32	14.22	10.50	8.62
29	17.58	14.21	10.65	8.61
30	17.32	10.63	10.50	6.44
31	20.40	12.29	12.36	7.45
32	18.09	11.38	10.96	6.89
33	16.68	10.26	10.11	6.22
34	17.58	10.92	10.65	6.62

Table (B1) Cont.

Test No	L_m mm	L_g mm	Φ_m^o measured	Φ_m^o calculated
35	19.37	11.24	11.74	6.81
36	19.89	12.20	12.05	7.40
37	18.86	9.54	11.43	5.78
38	20.27	10.11	12.29	6.13
39	19.37	9.82	11.74	5.9
40	13.72	8.53	8.32	5.17
41	15.52	9.25	9.41	5.61
42	19.12	10.17	11.59	6.16
43	15.14	8.56	9.17	5.19
44	16.93	9.55	10.26	5.79
45	18.60	10.19	11.27	6.18
46	13.08	7.79	7.93	4.72
47	13.98	8.90	8.47	5.39
48	18.09	9.09	10.96	5.51
49	15.78	11.00	9.56	6.67
50	15.65	11.17	9.48	6.77
51	17.45	11.60	10.57	7.03
52	19.12	12.81	11.59	7.77
53	15.52	11.60	9.41	7.03
54	16.93	12.07	10.26	7.32
55	17.96	12.78	10.88	7.75
56	20.79	12.49	12.60	7.57
57	19.37	13.24	11.74	8.02
58	18.09	12.21	10.96	7.40
59	16.55	11.58	10.03	7.01
60	17.96	11.41	10.88	6.91

Table (B1) Cont.

Test No	L_m mm	L_g mm	Φ_m^o measured	Φ_m^o calculated
61	18.60	11.89	11.27	7.21
62	18.60	11.81	11.27	7.16
63	19.63	12.00	11.90	7.27
64	20.14	12.41	12.21	7.52
65	19.89	12.26	12.05	7.43
66	17.45	11.14	10.57	6.75
67	18.22	11.41	11.04	6.92
68	18.86	12.01	11.43	7.28
69	16.93	10.99	10.22	6.67
70	18.60	11.2	11.27	6.79
71	19.37	12.29	11.74	7.45
72	15.91	11.15	9.64	6.76
73	19.12	11.74	11.59	7.12
74	19.12	12.09	11.59	7.33
75	18.86	12.41	11.43	7.52
76	17.32	11.48	10.50	6.96
77	15.78	11.11	9.56	6.73
78*	16.04	21.92	9.72	13.28
79*	17.70	23.66	10.73	14.34

* Rolling Oval Tubes

Appendix (C)

Table (C1) Torque sharing and the corrected length of the arc of contact

Test No	Torque Sharing T	L_m mm	$L_{m.c}$ mm	$\Phi^\circ_{m.c}$
12	0.94	17.58	16.47	8.74
13	0.97	18.86	18.28	11.07
14	0.94	18.86	17.67	10.71
15	0.98	22.20	21.71	13.16
16	0.95	21.43	20.42	12.38
17	0.94	22.71	21.40	13.00
18	0.87	23.74	20.58	12.47
19	0.96	12.31	11.83	7.17
20	0.92	14.88	13.75	8.33
21	0.96	13.72	13.13	7.95
22	0.93	17.58	16.29	9.87
23	0.86	18.22	15.63	9.47
24	0.97	19.12	18.58	11.26
25	0.97	13.98	13.55	8.21
26	0.93	15.52	14.50	8.79
27	0.94	14.49	13.64	8.27
28	0.93	17.32	16.07	9.74
29	0.96	17.58	16.86	10.21
31	0.96	20.40	19.48	11.81
32	0.99	18.09	17.89	10.84
33	0.96	16.68	15.94	9.66
34	0.92	17.58	16.15	9.79

Table (C1) Continued

Test No	Torque Sharing T	L_m mm	$L_{m.c}$ mm	$\phi^{\circ}_{m.c}$
35	0.97	19.37	18.79	11.39
36	0.98	19.89	19.49	11.81
37	0.98	18.86	18.50	11.21
38	0.98	20.27	19.91	12.06
39	0.94	19.37	18.19	11.02
40	0.92	13.72	12.67	7.68
41	0.93	15.52	14.47	8.77
42	0.96	19.12	18.41	11.15
43	0.93	15.14	14.00	8.48
44	0.92	16.93	15.51	9.4
45	0.92	18.60	17.17	10.41
46	0.89	13.08	11.63	7.05
47	0.93	13.98	13.02	7.89
48	0.95	18.09	17.2	10.45
49	0.91	15.78	14.30	8.66
50	0.94	15.65	14.68	8.90
51	0.95	17.45	16.56	10.03
52	0.94	19.12	18.03	10.92
53	0.90	15.52	13.98	8.47
54	0.93	16.93	15.68	9.50
55	0.93	17.96	16.76	10.16
56	0.92	20.79	19.12	11.59
60	0.82	17.96	14.73	8.93
61	1.05	18.60	19.61	11.88
62	0.93	18.60	17.32	10.50
63	0.91	19.63	17.94	10.87

Table (C1) Continued

Test No	Torque Sharing T	L_m mm	$L_{m.c}$ mm	$\phi^\circ_{m.c}$
64	0.89	20.14	17.87	10.83
65	0.90	19.89	17.82	10.80
66	1.01	17.45	17.62	10.68
67	0.93	18.22	16.87	10.22
68	0.94	18.86	17.71	10.73
69	0.88	16.93	14.92	9.04
70	0.91	18.60	16.95	10.27
71	0.97	19.37	18.72	11.34
72	0.90	15.91	14.35	8.69
73	0.88	19.12	16.88	10.23
74	0.93	19.12	17.86	10.82
75	0.97	18.86	18.24	11.05
76	0.89	17.32	15.36	9.31
77	0.91	15.78	14.41	8.73
78	0.91	16.04	14.62	8.86
79	0.95	17.70	16.82	10.19

Appendix (D)

Table (D1) RSF and roll springback

Test No	RSF, kN	Initial Roll gap mm	Tube Minor Axis mm	Springback mm
1	30.09	0.76	39.06	0.5
2	40.2	0.76	39.20	0.64
4	39.66	0.76	39.15	0.59
6	40.96	0.76	39.24	0.68
7	40.59	0.76	39.24	0.68
8	43.6	0.76	39.25	0.69
9	5.71	0.76	38.44	0.13
16	26.761	0.51	38.76	0.45
35	33.765	1.33	39.72	0.59
36	36.21	1.035	39.46	0.625
37	40.31	1.58	40.05	0.67
38	48.27	1.3	39.92	0.82
39	44.51	1.45	40	0.75

Appendix (E)

An example of the calculations of mean pressure, RSF and work done per unit volume

The calculations are carried out on test No (31). The following data are known:

r_o = 20.50 mm J = 0.12

e = 1.6 mm ω = 0.0345 rad. sec^{-1}

U_o = 2.97 mm.sec^{-1} V_b = 2.97 mm sec^{-1}

$\Phi_{m.c}$ = 11.81° Ψ_{C1} = 79.5°

X_3 = 22.7 2 mm r_b = 18.8 mm

r_g = 23.39 mm e_g = 4.49

R_r = 94.55 mm R_s = 113.45 mm

m_1 = 1 m_2 = 0.6

The sequence of the calculations is as follows:

(1) The peripheral angle of contact between tube and mandrel γ_{C1} at the exit plane is determined from equation (7.11.1) and (7.11.2),

$$\cos\theta = \frac{1}{2r_g(e_g - e/2)}\left[r_g^2 - r_o^2 + (e_g - e/2)^2\right] \qquad (7.11.1)$$

$$= 0.814$$

$$\gamma_{C1} = \sin^{-1}\left(\frac{r_g \sin\theta}{r_o}\right) \qquad (7.11.2)$$

$$= 41.55^\circ$$

(2) The relationship between γ_C and Φ is determined from equation (7.11.3)

$$\gamma_C = A(\Phi_{m.c} - \Phi)^B \qquad (7.11.3)$$

where $B = \left(\ln \frac{\gamma_{c1}}{\text{Integer}(\gamma_{c1})}\right) / \left(\ln \frac{\Phi_{m.c}}{(\Phi_{m.c} - 1)}\right) = 0.15$

and $A = \gamma_{c1} / (\Phi_{m.c})^B = 28.69$

$$\gamma_c = 28.69(11.81 - \Phi)^{0.15} \qquad \text{(E.1)}$$

(3) The deformation zone from $\Phi = 0$ to $\Phi = \Phi_{m.c}$, is divided into transverse sections. At any section having a contact angle Φ, γ_c and ψ_c are evaluated from equations (E.1) and (7.11.9).

$$\gamma_c = 28.69\ (11.81 - \Phi)^{0.15} \qquad \text{(E.1)}$$

$$\psi_c = \gamma_c + (\psi_{c1} - \gamma_{c1})\ \left(1 - \frac{\Phi}{\Phi_{m.c}}\right) \qquad \text{(7.11.9)}$$

$$= \gamma_c + (79.5 - 41.55)\ \left(1 - \frac{\Phi}{11.81}\right)$$

If, as an example, an angle of contact Φ of 11° is chosen,

$\gamma_c = 27.8^\circ$

$\psi_c = 30.4^\circ$

The section at $\Phi = 11^\circ$ will be used in steps (4) to (8)

(4) The y co-ordinates of the contact point corresponding to a peripheral angle of contact ψ_c of 30.4°, is determined from equation (3.2.8) of the groove surface:

$$x^2 + \left[b - (y^2 + Z^2)^{\frac{1}{2}}\right]^2 = r_g^2 \qquad \text{(3.2.8)}$$

where $b = R_s + e_g$ and $Z = R_r \sin\Phi$

Having determined ψ_c in step (3), it can be written:

$$\tan\psi_c = \frac{x}{R_s + e/2 - y}$$

$$X = (R_s + e/2 - y) \tan \psi_c \qquad (E.2)$$

By substituting equation (E.2) in equation (3.2.8)

$$[(\tan(\psi_c))(R_s + e/2 - y)]^2 + (R_s + e_g)^2 - r_g^2 -$$

$$2(R_s + e_g)\sqrt{(y^2 + z^2)} + y^2 + z^2 = 0 \qquad (E.3)$$

By trial and error y corresponding to $\psi_c = 30.4^o$ is determined as being equal to 95.59 mm

$$X = 10.95 \text{ mm}$$

(5) The tube speed U is determined from equation (3.2.2 3)

$$U = \frac{U_o}{1-J}\left(1 - \frac{J\Phi}{\Phi_{m.c}}\right) = 3 \text{ mm.sec}^{-1}$$

(6) The length of the peripheral arc of contact between tube and roll at $\Phi = 11^o$ is determined by integrating equation (3.2.13) between $X = 0$ to $X = 10.95$

$$dL = \left(\frac{x^2\left[1 + \frac{Z^2}{b-(r_g^2 - x^2)^{\frac{1}{2}} - Z^2}\right]}{r_g^2 - x^2} + 1\right)^{\frac{1}{2}} dx \qquad (3.2.13)$$

The integration is solved by approximate numerical methods. Using Simpson's method:

$$L = 11.41\text{mm at } \Phi = 11^o$$

(7) The work done per unit time against friction between tube and roll at $\Phi = 11^o$ is calculated by:

$$d\dot{W}_{fa} = \tau_a [\omega y - U]\, dL$$

$$= \tau_a \left[\omega \sqrt{[b - (r_g^2 - x^2)^{\frac{1}{2}}]^2 - Z^2} - U\right] dL \qquad (3.2.36)$$

Again, the integration is solved by applying Simpson's method, which gives: $\dot{W}_{fa} = 2.67\, \tau_a$ at $\Phi = 11^o$.

(8) The work done per unit time against friction between tube and mandrel at $\Phi = 11^{\circ}$ is:

$$\dot{W}_{fb} = \tau_b \cdot (U - V_b)\, r_b \cdot \delta_c \cdot \pi/180 = 0.27\,\tau_b$$

(9) To calculate the contact area, horizontal projection of the contact area and work done per unit time against friction, from the entry plane where $\delta_c = \psi_c = 0$ to the plane at $\Phi = 11^{\circ}$, the following expressions are used:

From $\Phi = \Phi_{m.c} = 11.81^{\circ}$ to $\Phi = 11^{\circ}$

$$S_1 = (\sin\Phi_{m.c} - \sin\Phi)\, 94.55 = 1.31$$

$$\text{Contact area} = \frac{L}{2} S_1 = 7.47 \text{ mm}^2$$

$$\text{Horizontal projection} = \frac{x}{2} S_1 = 7.17 \text{ mm}^2$$

$$\dot{W}_{fa} = \frac{2.67\tau_a}{2} \cdot S_1 = 1.75\,\tau_a \text{ N.mm.sec}^{-1}$$

$$\dot{W}_{fb} = \frac{0.27\tau_b}{2} S_1 = 0.18\,\tau_b \text{ N.mm.sec}^{-1}$$

(10) Steps from (3) to (9) are repeated while decreasing Φ until $\Phi = 0$. The final results are:

Contact area = $4 \times 387.668 \text{ mm}^2$

Horizontal projection per roll = $2 \times 324.93 \text{ mm}^2$

$$\dot{W}_{fa} = 4 \times 65.4\,\tau_a \text{ N.mmsec}^{-1}$$

$$\dot{W}_{fb} = 4 \times 50.73\,\tau_b \text{ N.mm.sec}^{-1}$$

Since the calculations are performed using only a quarter of the groove, the above expressions are multiplied by 4 to account for the whole groove.

$$\tau_a = m_1 \frac{\sigma_y}{\sqrt{3}}, \qquad \tau_b = m_2 \frac{\sigma_y}{\sqrt{3}}$$

(11) To determine the mean tube thickness after rolling, the outside area of the tube cross-section is calculated from equations (7.10.6) and (7.10.2):

$$\text{Outside area} = 4\left[\frac{x_2}{2}\sqrt{r_g^2 - x^2} + \frac{r_g^2}{2}\sin^{-1}\frac{x_2}{r_g} - (e_g - e/2)x_2 + \frac{2}{3}y_2(x_3 - x_2)\right] \qquad (7.10.6)$$

$$r = -\cos\psi_{c1}(e_g - e/2) + \sqrt{r_g^2 - (e_g - e/2)^2\sin^2\psi_{c1}} \qquad (7.10.2)$$

$$= 22.43 \text{ mm}$$

$x_2 = r\sin\psi_{c1} = 22.05$ mm, $y_2 = r\cos\psi_{c1} = 4.09$ mm

Outside area = 1372 mm^2

Inside area = Outside area - cross-sectional area

= 1188 mm^2

$$t_1 = \sqrt{1372/\pi} - \sqrt{1188/\pi} = 1.45 \text{ mm}$$

(12) The radial, longitudinal and tangential strains are evaluated from the following expressions:

$$\varepsilon_r = \ln\frac{t_o}{t_1} = 0.155$$

$$\varepsilon_l = \ln\frac{A_o}{A_1} = 0.129$$

$$\varepsilon_\theta = \varepsilon_r - \varepsilon_l = 0.027$$

The generalized homogeneous strain, ε_h, is determined from equation (3.2.18)

$$\varepsilon_h = \sqrt{\frac{2}{3}(\varepsilon_r^2 + \varepsilon_l^2 + \varepsilon_\theta^2)} = 0.166$$

The redundant strain, $\varepsilon_{red.}$, is calculated from equation (3.2.29):

$$\varepsilon_{red.} = \frac{(r_o - r_b)}{12\sqrt{3}\, A_o(1-J)} \cdot R_r \cdot \Phi_{m.c}^{\,2} \quad (3\text{-}2J) \qquad (3.2.29)$$

$$= 0.005$$

The total generalized strain, $\bar{\varepsilon}_m$, is:

$$\bar{\varepsilon}_m = \varepsilon_h + \varepsilon_{red.} = 0.171$$

(13) The mean strain rate is evaluated from equation (5.5.1)

$$\bar{\lambda} = \frac{\omega}{2\Phi_{m.c}} \ln \left(\frac{R_s + e/2 - R_r \cos \Phi_{m.c}}{R_s + e/2 - R_r}\right)$$

$$= 0.008 \text{ sec}^{-1}$$

The mean yield stres, $\bar{\sigma}_y$, is determined from the appropriate stress-strain curve corresponding to $\bar{\lambda}$ and $\bar{\varepsilon}_m$.

$$\bar{\sigma}_y = 13.02 \text{ N.mm}^{-2}$$

(14) The frictional strain, ε_f is determined as follows:

$$\varepsilon_f = \frac{4}{\sqrt{3}} (65.4\, m_1 + 50.73\, m_2)/(A_o\, U_o)$$

where m_1 and m_2 are the friction factors between tube and roll and between tube and mandrel respectively. m_1 is taken as unity, while m_2 is 0.6

$$\varepsilon_f = 0.355$$

(15) The total work done by the rolls per unit volume is:

$$W_t = (\bar{\varepsilon}_m + \varepsilon_f)\bar{\sigma}_y = 6.85 \text{ N.mm.mm}^{-3}$$

The mean pressure, p_m, is determined from the following expression:

$$p_m = \frac{W_t \cdot A_o U_o \cdot \Phi_{m.c}}{\text{contact area } (t_o - t_1)\omega}$$

$= 67.29\ N.mm^{-2}$

The roll separating force, RSF is:

RSF = 2 x 324.93 x 67.29 = 43.73 kN

where 2 x 324.93 is the horizontal projection of the contact area.

Appendix (F)

Table (F1) The total work done by the rolls per unit volume and the comparison between the measured and calculated values of the mean pressure and roll separating force

Test No	W_t N.mm.mm^{-3}	Mean Pressure, N.mm^{-2}		RSF, kN	
		Measured	Calculated	Measured	Calculated
12	1.314	28.062	31.77	20.064	17.539
13	2.057	29.951	35.315	22.347	21.39
14	2.225	29.88	35.815	23.122	20.193
15	3.231	44.80	44.551	32.581	30·042
16	4.274	39.569	39.168	26.761	30.157
17	4.714	42.518	40.803	32.633	32.14
18	4.747	43.372	40.715	33.143	28.734
19	0.145	19.545	27.402	8.358	7.272
20	0.491	23.855	31.49	12.325	11.279
21	0.48	19.884	33.108	12.072	10.886
22	0.994	27.742	32.052	18.032	13.781
23	1.197	34.367	37.816	18.768	14.466
24	1.816	30.281	35.261	22.250	20.9
25	0.380	19.541	26.488	10.932	9.369
26	0.640	23.351	30.083	13.737	11.173
27	0.678	25.212	29.655	14.923	11.297
28	1.2	27.522	31.195	18.226	15.019
29	1.486	30.65	34.666	19.677	17.943
31	6.858	75.906	67.29	46.5	43.729
32	3.942	64.816	61.474	40.99	32.487

Table (F1) Cont.

Test No	$N.mm.mm^{-3}$	Mean Pressure, $N.mm^{-2}$		RSF , kN	
		Measured	Calculated	Measured	Calculated
33	2.108	53.078	50.093	32	23.215
34	1.975	40.812	43.093	24.352	21.603
35	2.5	47.674	47.775	33.765	27.151
36	3.948	54.367	53.168	36.21	33.99
37	1.628	62.354	73.168	40.309	43.971
38	1.888	73.793	77.962	48.269	53.099
40	0.841	41.401	65.402	19.159	17.315
41	1.339	51.934	58.797	25.895	21
42	2.186	57.657	62.84	36.269	29
43	0.457	40.980	62.54	19.129	17.303
44	1.141	39.135	60.857	23.732	20.248
45	2.807	54.062	60.127	33.645	25.01
49	2.021	42.258	43.763	23.461	18.429
50	2.187	38.804	41.636	21.225	18.573
51	3.273	43.831	44.85	28.565	24.223
52	4.628	38.293	50.533	30.859	31.097
53	2.413	38.929	40.575	19.472	17.183
54	3.06	51.952	44.804	23.842	21.839
55	4.599	54.183	53.459	27.21	28.661
56	4.805	58.172	53.923	32.532	36.321
60	1.563	30.94	45.155	19.207	19.237
61	2.679	44.242	50.757	26.567	29.017
62	3.757	48.614	59.223	27.867	30.742
63	3.510	55.253	58.737	32.657	30.07
64	4.08	52.908	64.01	34.392	32.789

Table (F1) Cont.

Test No	$N.mm.mm^{-3}$	Mean Pressure, $N.mm^{-2}$		RSF , kN	
		Measured	Calculated	Measured	Calculated
65	3.035	58.710	61.03	35.297	32.628
66	2.9	-	50.958	21.27	26.211
67	4.09	68.373	62.403	32.82	31.898
68	4.911	75.569	68.00	39.249	33.686
69	2.75	50.501	59.593	23.457	22.979
70	3.872	72.212	56.03	34.689	26.912
71	4.895	70.731	57.718	35.53	31.307
72	3.043	50.463	59.339	22.115	23.454
73	3.356	57.883	62.994	27.14	27.513
74	5.561	79.181	78.666	38.152	37.949
75	6.753	69.083	79.627	35.832	39.45
76	4.548	66.234	66.835	30.572	29.791
77	2.974	43.975	54.906	23.160	22.1
78	2.746	49.836	52.581	23.624	20.987
79	3.852	46.861	58.606	23.127	28.154

Appendix (G)

Table (G1) Comparison between the measured and calculated values based on the two Russian theories

Test No	Mean Pressure, $N.mm^{-2}$		Pressure at the root of the groove, $N.mm^{-2}$	
	Measured	Vatkin and Druyan	Measured	Fomichev
12	28.062	18.927	50.408	20.619
13	29.951	22.193	49.285	26.849
14	29.88	22.381	48.313	27.715
15	44.80	26.654	84.742	34.337
16	39.569	26.819	79.448	43.979
17	42.518	28.06	69.401	43.012
18	43.372	28.324	82.430	53.273
19	19.545	10.937	28.932	9.408
20	23.855	14.785	41.160	26.059
21	19.884	14.415	35.067	19.813
22	27.742	19.5	60.198	26.547
23	34.367	19.322	70.20	27.565
24	30.281	22.67	68.428	50.439
25	19.541	14.116	31.481	12.331
26	23.351	16.402	35.824	24.671
27	25.212	15.976	40.512	19.755
28	27.522	19.304	49.976	29.695
29	30.65	20.166	59.678	29.875
31	75.906	58.232	183.712	27.727
32	64.816	49.479	162.310	21.422
33	53.078	39.892	137.16	19.954
34	40.812	40.047	87.464	22.464

Table (G1) Cont.

Test No	Mean Pressure, $N.mm^{-2}$		Pressure at the root of the groove, $N.mm^{-2}$	
	Measured	Vatkin and Druyan	Measured	Fomichev
35	47.674	48.146	118.729	25.080
36	54.367	53.728	133.357	27.138
37	62.354	50.029	156.823	22.566
38	73.793	53.578	178.343	24.871
40	41.401	31.737	93.946	16.042
41	51.934	39.774	110.886	21.142
42	57.657	53.177	153.171	23.913
43	40.980	28.843	84.396	14.091
44	39.135	40.283	109.762	18.531
45	54.062	54.639	128.906	26.528
49	42.258	37.99	106.629	19.537
50	38.804	40.00	93.493	24.904
51	43.831	47.02	113.608	23.643
52	38.293	52.615	90.035	28.399
53	38.929	39.564	67.089	27.151
54	51.952	44.797	92.261	26.809
55	54.183	50.658	98.808	28.819
56	58.172	54.591	116.871	26.523
60	30.94	33.354	79.859	20.145
61	44.242	47.370	105.571	21.767
62	48.614	44.811	113.673	22.389
63	55.253	45.826	130.808	23.023
64	52.908	46.438	122.093	25.096
65	58.710	46.797	130.808	24.785
67	68.373	44.385	132.644	21.464
68	75.569	48.499	140.315	24.816

THE UNIVERSITY OF ASTON IN BIRMINGHAM

DEPARTMENT OF PRODUCTION TECHNOLOGY & PRODUCTION MANAGEMENT

MECHANICS OF ROLLING TUBE ON A MANDREL THROUGH TWO GROOVED ROLLS

Submitted in fulfilment of the requirements
for the degree of Doctor of Philosophy

Author: OSAMA MOSTAFA LABIB Year: 1982

Paper presented at the International Conference
on tube production and processing,
International Tube Association, April 1981,
Aachen, West Germany.

UNIVERSITY OF ASTON IN BIRMINGHAM

DEPARTMENT OF PRODUCTION TECHNOLOGY AND PRODUCTION MANAGEMENT

Experimental investigation of the mandrel tube-rolling process using two grooved rolls

O.M. Labib and D.H. Sansome

THE UNIVERSITY OF ASTON IN BIRMINGHAM

DEPARTMENT OF PRODUCTION TECHNOLOGY AND PRODUCTION MANAGEMENT

Experimental investigation of the mandrel tube-rolling process using two grooved rolls

O.M. Labib and D.H. Sansome

SUMMARY

An experimental investigation of the process of tube rolling on a mandrel through two grooved rolls was undertaken to provide an understanding of the mechanics of the process. Lead tubes with various diameter to thickness ratios were rolled in an experimental mill for different reductions of area, and the effect of changing these parameters on the roll separating force, rolling torque and pressure distribution round the groove were ascertained. The existence of a free deformation zone, wherein deformation takes place prior to the contact zone was established. Rolling torques were shewn to be significantly reduced with increasing mandrel speed. Since great care was taken in the preparation of the lead tubes and in controlling the various rolling parameters, it has been concluded that there is a linear relationship obtained between rolling load and torque.

THE UNIVERSITY OF ASTON IN BIRMINGHAM

DEPARTMENT OF PRODUCTION TECHNOLOGY AND PRODUCTION MANAGEMENT

Experimental investigation of the mandrel tube-rolling process using two grooved rolls

O.M. Labib and D.H. Sansome

INTRODUCTION

The complexity of deformation in the rolling of tubes on a mandrel through two grooved rolls makes it one of the more difficult metal forming processes to analyse and consequently the process has been neglected by comparison with flat rolling. The present paper attempts to provide some understanding of the factors affecting the process and their practical aspects.

Investigations have been made of the way in which roll separating force, rolling torque and pressure distribution round the groove vary for different reductions and tube diameter to thickness ratios. Rolling tests have been performed under the same conditions of friction between tube and rolls and between tube and mandrel. In the work reported here back tension has not been applied to the tubes, but in order to simulate conditions in a production mill, the mandrel speed was increased in some of the tests. The use of pin load cells, apart from providing the pressure distribution round the groove and along the arc of contact, allowed an accurate measurement of the arc of contact length to be made.

Lead was selected in the rolling tests as an analogue material to hot steel. Lead, which is hot worked at room temperature,

has the further advantage of being able to deform at lower stresses than hot steel and this assisted in reducing the mill loads. The use of lead as a model material will be discussed in more detail later on.

EXPERIMENTAL MILL

The rolling tests were made in a stand formed by adding two grooved rolls to a milling machine as shewn in Fig.(1) and Plate (1). Since the bottom shaft was suspended from the top shaft by two load cells, the roll gap could be altered by the adjustment of the screws holding the load cells to the top shaft. Pin load cells, which were originally employed in a previous investigation by Haleem, Cole and Sansome (1), were used also, when re-calibrated, in the present work to provide the pressure distribution round the groove and along the arc of contact. The roll separating force and rolling torque were measured by means of strain gauges bonded respectively to the two load cell elements and to the top and bottom shafts. Inlet and outlet tube speeds and the mandrel speed were recorded by the use of photo-electric cells.

Preparation of the tubes

To avoid the occurrence of eccentricity in the unrolled tubes the following procedure was adopted. Lead tubes in the as-extruded form were drawn on a mandrel through a ring die and then turned in a lathe to the required size. The mandrel which was used in drawing was used also in rolling and this procedure therefore eliminated eccentricity and ensured a close pass tube rolling process. Lead tubes with diameter to thickness ratios, (d/t), of 8.5 and 9 were rolled on the same mandrel having a

diameter of 31.38 mm. Thinner walled tubes, with d/t ratios of 24 and 30.4, were rolled on a 37.60 mm mandrel. Both mandrels were ground in exactly the same way to ensure that they had the same surface finish.

Process Parameters

The tubes were rolled in an oval groove the shape of which is shewn in Fig.(2). For each d/t ratio, a series of experiments was carried out, by changing the rollgap, to determine the effect of varying the reduction ratio r, on the roll separating force, the rolling torque and the pressure distribution. To assess the reduction in tube cross-sectional area after rolling, a weighing technique was employed in which a specimen was cut from the rolled tube and faced in a lathe. From measurements of specimen length and weight in air and water, the density of lead and the tube cross-sectional area were obtained. In all rolling tests, measurements of roll separating force (RSF), rolling torque and pressure distribution were noted when steady state conditions had been attained.

The use of lead as a model material

A model material should satisfy the following conditions:

1. simulates as closely as possible the stress-strain characteristics of the hot steel used in the production mill, i.e. a material which does not strain harden and which has a stress-strain curve of the same shape as steel,
2. deforms under lower stresses than hot steel - to minimise the rolling loads.

Lead is frequently used as an analogue material for hot steel since it is hot worked at room temperature and deforms at low stresses. Experiments carried out by Loizou and Sims (2), for

the determination of yield stress of pure lead in uniaxial compression under different conditions, led to the now well known conclusions that, like steel, the yield stress of lead depends on the temperature, strain rate and magnitude of the current strain especially at high strain rates. Ingham (3) obtained the yield stress of the same pure lead as that used in these tests at different strain rates and the curves in Fig.(3), plotted for the true stress strain relationship, are reproduced from some of his tests. At low strain rates, like those used in the present investigation, the yield stress of lead remains nearly constant with strain and this feature is representative of the behaviour of hot steels.

RESULTS AND DISCUSSION

Fig.(4) shews the effect of changing the reduction ratio, r, and d/t on the roll separating force. The increase of roll separating force with r, which approximates to a straight line but which is concave downwards near the lower reductions, may be explained by observing that reducing the roll gap, to achieve higher reductions increases both the work required to deform the tube and the work done against friction; i.e. the contact area between the tube and the rolls and between the tube and the mandrel is increased. Also, by reducing the roll gap the amount of redundant work is increased.

Varying the d/t ratio had a marked effect on rolling loads. For the same reduction, as the tubes were reduced in thickness i.e. with increasing d/t ratios, the roll separating force became higher due to the increase in the proportion of frictional work to the total work required in the rolling process. This is one reason why most of the tube reduction in an actual mill is carried out

in the first few stands when the d/t ratio is still fairly low compared with the ratio in later stands when the wall is thin.

The change in rolling torque with r and d/t, Fig.(5), followed exactly the same trend as for the variation of roll separating force; this is indicative of a linear relationship between the rolling loads and the torques and is a measure of the accuracy of results, since in the absence of front and back tensions, the torque should be proportional to the roll force.

The pressure distribution round the groove perimeter is not uniform as the greatest pressure occurs at the root of the groove, Fig.(6a). In order to assess the effect of changing r and d/t on pressure distribution, mean values for the pressures were calculated and compared with each other. A planimeter was used to trace the area under each pressure distribution curve and a mean value for the pressure corresponding to each pin position was thus obtained. The mean pressure for these mean values was calculated and plotted against r and d/t in Fig.(6b). A trend similar to the roll separating force and the roll torque curves can be detected for the mean pressure distribution curves.

When the length of the arc of contact was estimated, it was found that the actual length, obtained from pin load cell measurements, was greater than the theoretical length calculated from the geometry of the tube and the groove. This might be due to the presence of a free zone; i.e. the tube may start to deform before entering the contact area between tube and rolls.

The presence of such a free zone was reported previously in the tube sinking process by Haleem (4). To establish the presence of a free zone a grid was engraved on the tube surface and subsequently the tube was rolled for half of its length and withdrawn from the roll groove. Examination of the tube surface

just before the contact zone revealed that the outer surface of the tube expanded gradually, i.e. the tube diameter increased until it touched the roll surface at the start of the contact zone. Thus, when rolling on a mandrel the material in the free zone deformed in a direction opposite to that recorded by Haleem (4), who found that the diameter decreased when rolling tube without a mandrel.

Measurements of mandrel and tube speeds indicated that the mandrel speed was close to the inlet tube speed, i.e. the no-slip point on the mandrel surface was closest to the entry plane.

When the mandrel was pulled through the roll groove at a higher speed than that occurring in free rolling, very little reduction was noticed in either the roll separating force or the average pressure, but very substantial changes were observed in the values of rolling torques. Table I shews the reduction in torque for increasing values of reduction of area.

TABLE I Effect of pulling the mandrel through at a higher speed

Free Rolling		Pulling the mandrel through	
r%	Rolling torque kN. mm	r%	Rolling torque kN. mm
6.732	435.983	6.481	-25.695 *
8.555	609.975	8.214	42.998
10.89	700.02	13.233	109.62

* the negative sign indicates that the tube is driving the rolls i.e. drawing takes place as well as rolling.

Since the mandrel can be considered to be a roll of infinite diameter, any change in its speed causes a corresponding change in the tube speed. The increase in tube speed leads to a redistribution of friction between the tube and the roll; also the work done by front tension reduces the work done by the torque so that the total power required by the rolls to deform the metal is reduced. In the case of small reductions in area, where rolling loads are low, slip occurs between the tube and the roll over the whole of the contact zone and this leads to a negative torque being applied by the rolls. Consequently, the process changes from one of rolling to one of drawing. Thus in a production mill where several stands operate in tension, the last stands reduce the rolling power supplied by the first stands.

CONCLUSIONS

(1) The changes in roll separating force, rolling torque and average pressure distribution which occur in tube rolling on a mandrel have been shewn, experimentally, to increase with r and d/t.

(2) The pressures round the groove perimeter are not uniformly distributed; the greatest pressure occurs at the root of the groove.

(3) In the absence of front and back tensions, the rolling load varies in proportion to the rolling torque.

(4) An increase in mandrel speed generated front tension which produced a significant reduction in the rolling torque.

(5) It has been shewn that the deformation zone can be divided into two zones: a free zone where deformation takes place prior to the tube contacting the rolls, and a contact zone,

in which deformation takes place between the rolls and the mandrel.

REFERENCES

1. Haleem, A.S., Cole, I.M. and Sansome, D.H. " Measurement of contact pressures in tube rolling" Journal of Mechanical Working Technology, Volume 1, (1977), pp. 153 - 168

2. Loizou, N. and Sims, R.B. "The yield stress of pure lead in compression" Journal of Mechanics and Physics of Solids, 1953, Volume 1, pp. 234 - 243

3. Ingham, P. "The mechanics of thick slab rolling" Ph.D. thesis, 1981, Aston University in Birmingham.

4. Haleem, A.S. "An investigation into the longitudinal rolling of tubes through two grooved rolls" Ph.D. thesis, Aston University in Birmingham, February 1978.

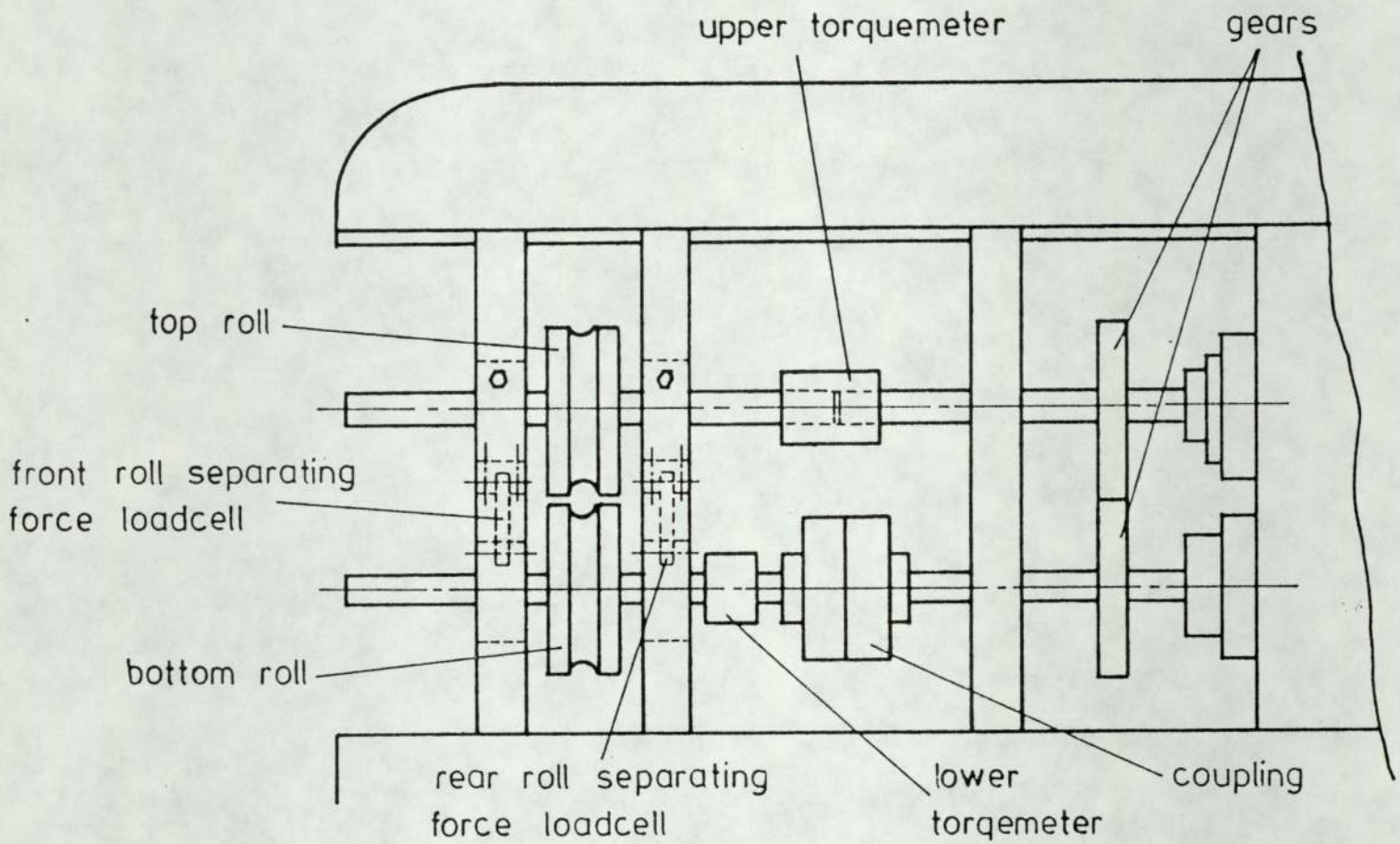

Fig.(1) General Assembly of the Rolling Stand

PLATE (1)

Géneral View of the Roll Stand

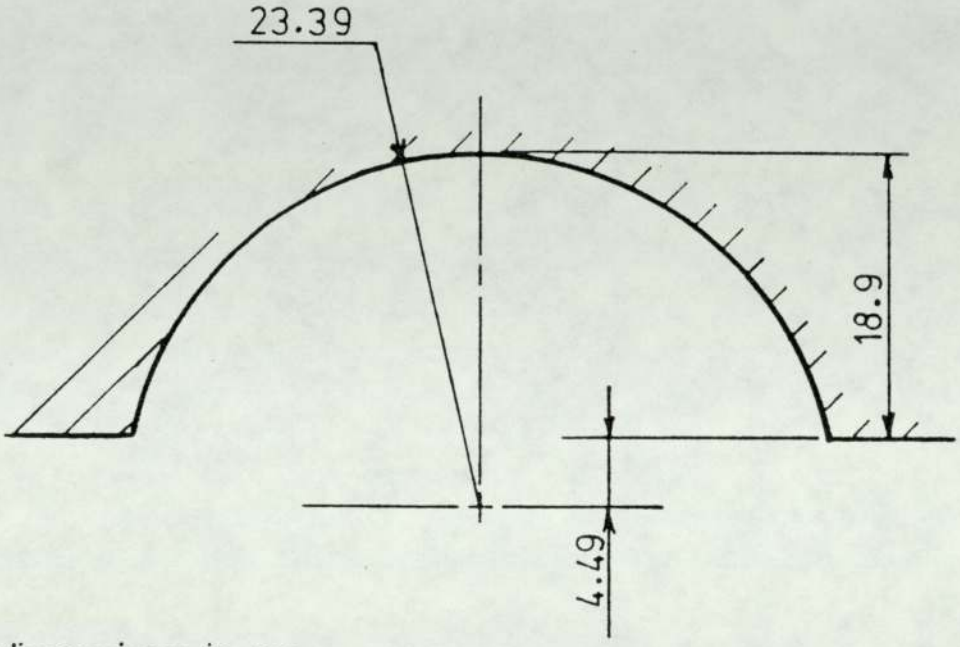

all dimensions in mm

Fig.(2) Groove Shape

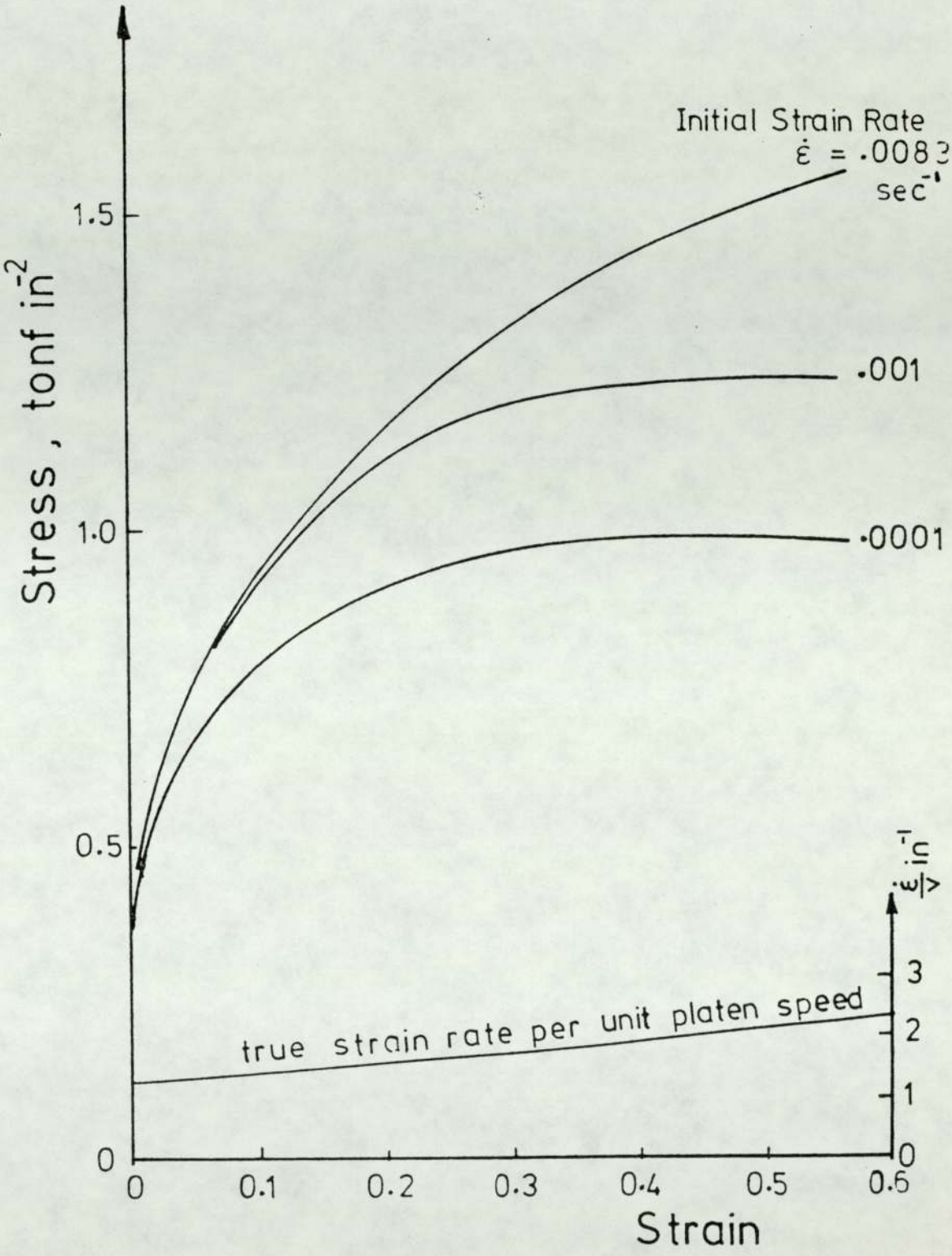

Fig.(3) True Stress v Strain for pure Lead in Uniaxial Compression

(From Ingham(3))

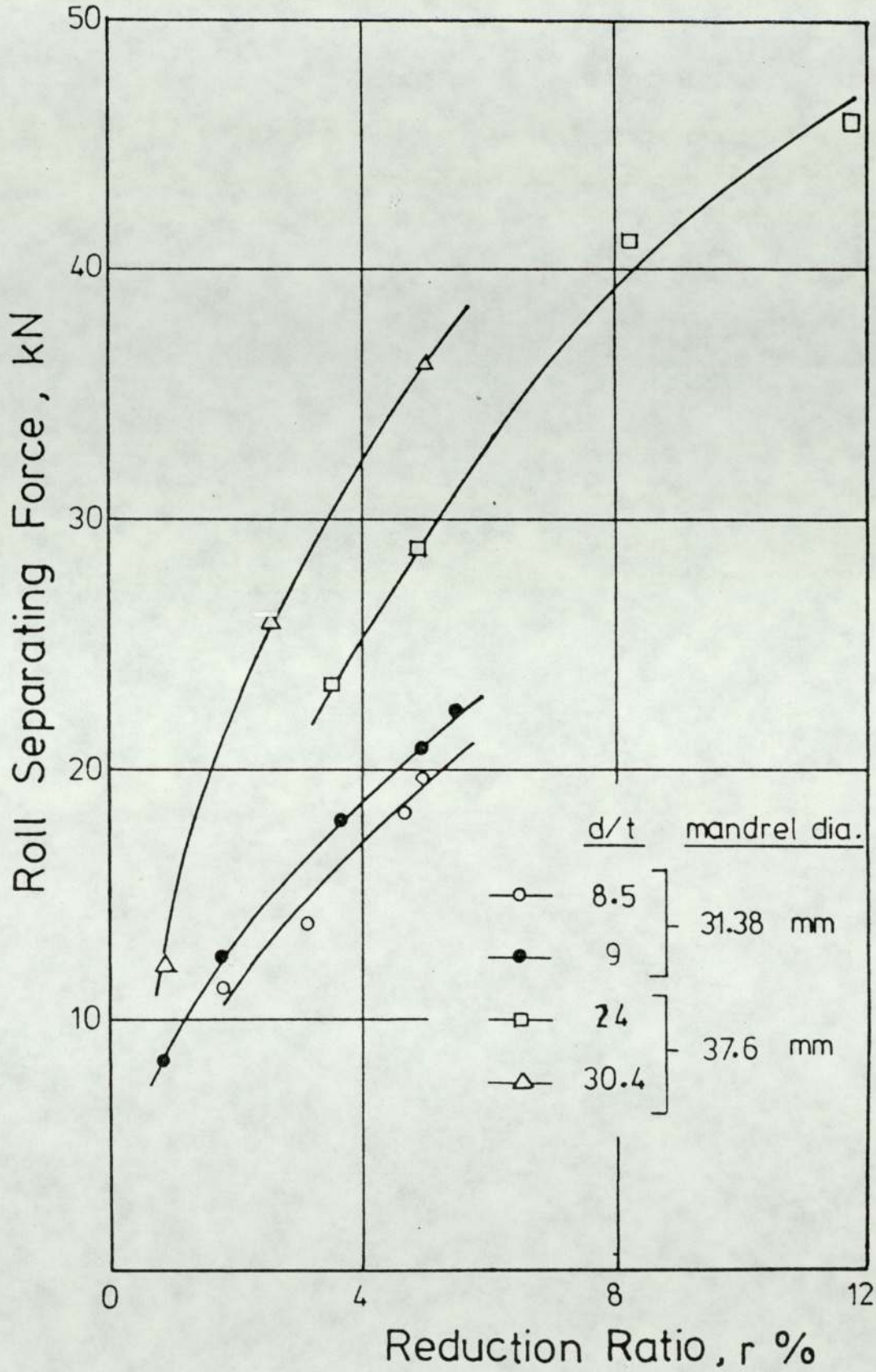

Fig.(4) Variation of RSF with r and d/t

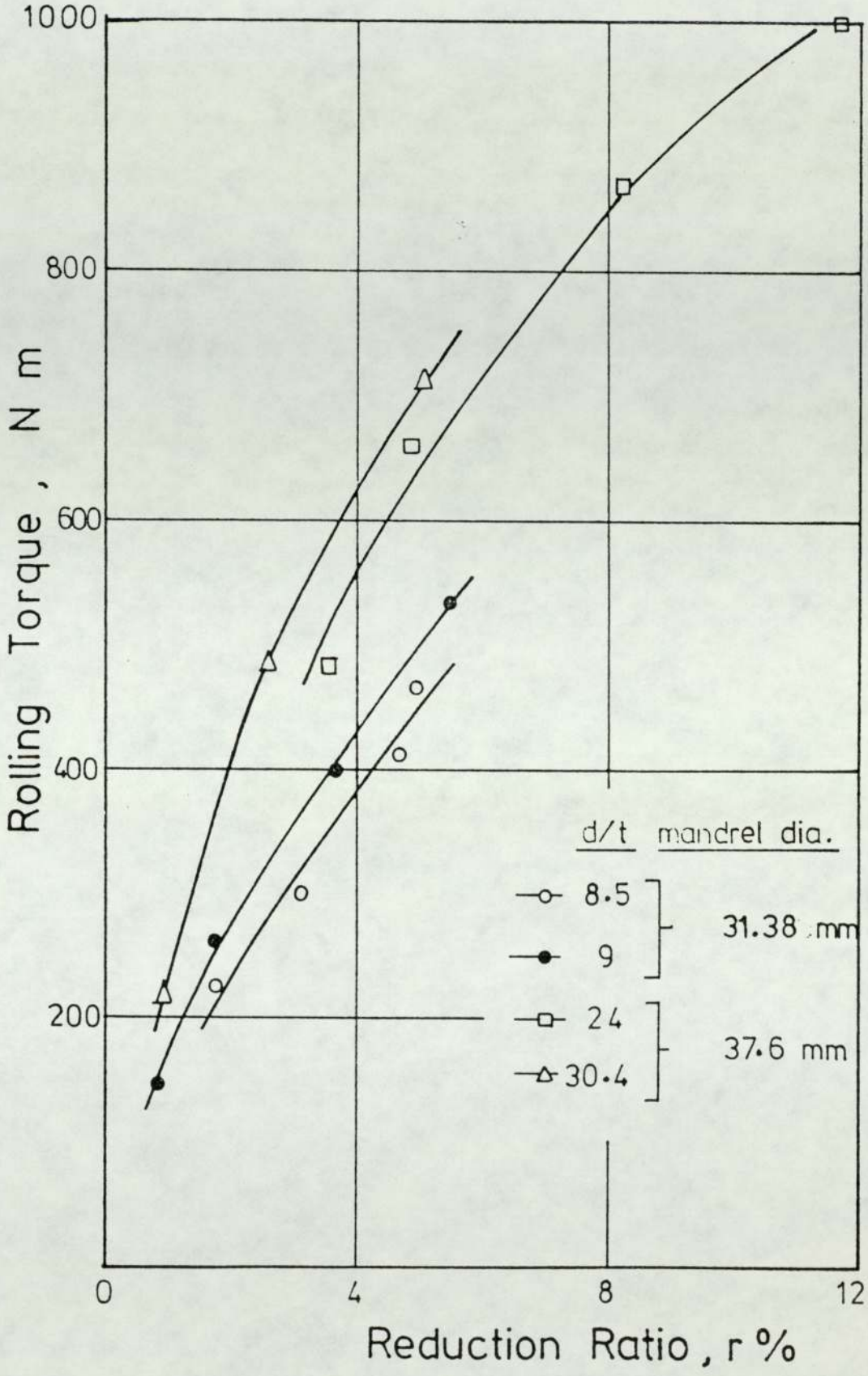

Fig.(5) Variation of Rolling Torque with r and d/t

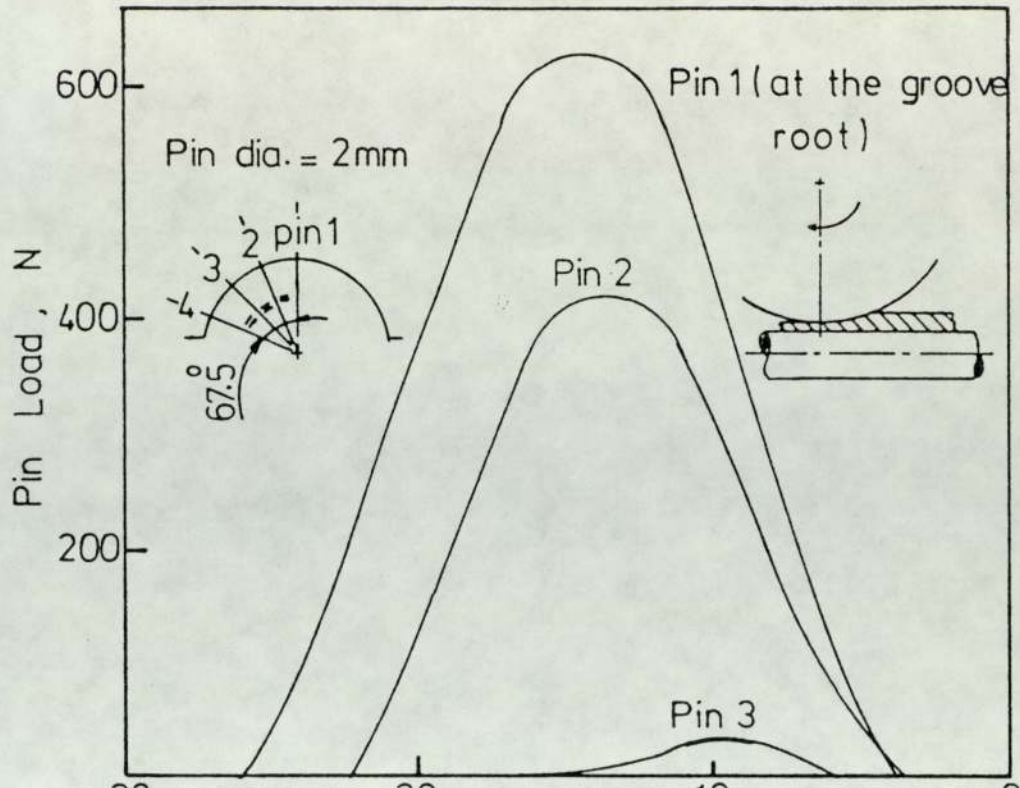

(a) Typical Pressure Curves

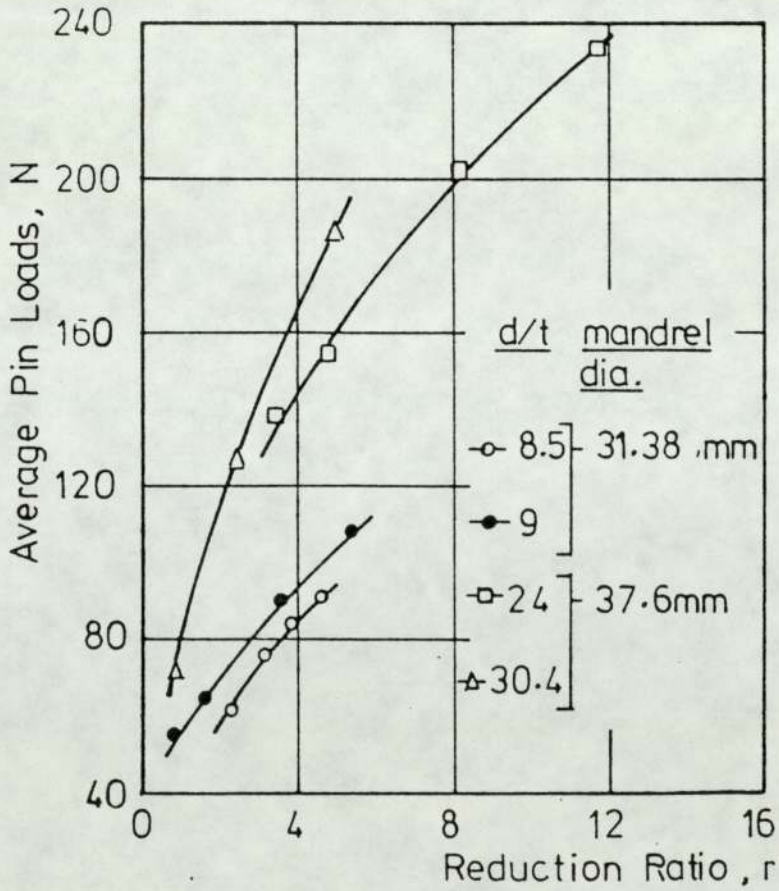

(b) Variation of the average pin loads with r and d/t

Fig.(6) Pin Load Cell Measurements